The interactions between arsenic, iron and organic mater in anoxic environment

Charlotte Catrouillet

ANNÉE 2015

THÈSE / UNIVERSITÉ DE RENNES 1
sous le sceau de l'Université Européenne de Bretagne

pour le grade de

DOCTEUR DE L'UNIVERSITÉ DE RENNES 1

Mention : Sciences de la Terre

Ecole doctorale Sciences de la Matière

présentée par

Charlotte Catrouillet

Préparée à l'unité de recherche Géosciences Rennes
(UMR CNRS 6118)
OSUR Observatoire des Sciences de l'Univers de Rennes

Les interactions entre l'arsenic, le fer et la matière organique en milieu anoxique

Thèse soutenue à Rennes
le 9 octobre 2015

devant le jury composé de :

Marc BENEDETTI
Professeur, Université Paris Diderot / rapporteur

Jose-Paulo PINHEIRO
Professeur, Université de Lorraine/ *rapporteur*

Christian MIKUTTA
Docteur, ETH / *examinateur*

Gérard GRUAU
Directeur de recherche, Université de Rennes 1 / *Président du jury*

Mélanie DAVRANCHE
Maître de conférences, Université de Rennes 1 / *directrice de thèse*

Aline DIA
Directeur de recherche, CNRS / *directrice de thèse*

Avant-propos

Ce travail de thèse a été réalisé au sein de l'université de Rennes 1, à Géosciences Rennes (UMR 6118) dans l'équipe de Géochimie des eaux et des interfaces. Il a été encadré par Mélanie Davranche et Aline Dia, en collaboration avec Gérard Gruau. L'ensemble du travail expérimental a été réalisé au sein de l'atelier de Géochimie analytique de Géosciences Rennes avec le soutien de Martine Bouhnik-Le Coz et Patrice Petitjean. Cette thèse a entièrement été financée par le programme ANR Jeunes Chercheurs ARSENORG.

Remerciements

- Je tiens tout d'abord à remercier mon jury d'avoir accepté de juger mon travail. Merci aux Pr Pinheiro, Benedetti et Mikutta. Merci pour la discussion scientifique que nous avons eu mais également pour vos rapports et questions. *(First of all, I would like to thank my jury for accepting to evaluate my work. Thank you very much to Professors Pinheiro, Benedetti and Mikutta for the scientific discussion and for your reports and questions)*.

- Bien entendu, un grand merci à mes deux directrices de thèse :
Merci **Mélanie** de m'avoir fait confiance pendant ces trois années de thèse, malgré les difficultés rencontrées. Un grand merci de m'avoir soutenue en toute circonstance, d'avoir toujours été disponible et pour toutes ces nombreuses conversations scientifiques !! Merci de m'avoir autant appris au cours de ces trois (même quatre) années ! J'espère que nous garderons toujours ces bons rapports. En conclusion, merci pour tout !
Merci **Aline** pour nos conversations scientifiques, pour ta disponibilité mais aussi d'avoir réussi dans ton rôle de double co-directrice. Merci d'avoir été ma traductrice au conseil de l'unité et d'avoir toujours essayé de soutenir les étudiants au sein du comité de suivi des doctorants !

- Merci aux membres de mon équipe :
Merci **Gérard** pour vos corrections sur les articles et les conversations scientifiques qui en ont découlées. Merci également de m'avoir rassurée au moment opportun concernant mon travail de thèse.
Merci **Mathieu** de m'avoir donné ta carte de visite il y a de cela quelques années et envoyé les sujets de stage de l'équipe qui ont abouti à cette thèse. Merci également pour ton aide au cours de cette thèse et de m'avoir défendue pour ce poste d'A.T.E.R..
Merci **Martine** pour tous ces échantillons passés à l'ICP en si peu de temps et avec autant de pression ! Merci pour toutes nos conversations scientifiques, d'être aussi investie dans ton travail dont nous dépendons beaucoup ! Merci aussi pour toutes nos conversations personnelles dont cinématographiques :).
Merci **Patrice** pour ton aide sur l'UV, le TOC mais aussi la chambre anaérobie. Merci de m'avoir pardonnée ces erreurs sur la chambre malgré les pressions de planning.
Merci **Anne-Catherine** pour nos conversations concernant les A.T.E.R., les post-docs, les concours de maitres de conf, mais aussi pour nos conversations un peu plus personnelles.
Merci **Rémi**, dans un 1er temps pour avoir discuté recherche et thèse avec moi à la Goldschmidt. Merci également pour les "coups de pattes" comme tu dis en modélisation et les conversations scientifiques que nous avons eu !
Un grand merci aux gestionnaires/secrétaires pour leur aide précieuse pour toutes les tâches administratives. Merci à vous pour votre bonne humeur et tous les mots sympathiques échangés : **Stéphanie**, **Chantal**, **Aline**, etc.

Merci aux doctorants (ou anciens doctorants) de l'unité :
*En premier, **mes co-bureaux**, merci à vous tous de m'avoir supportée pendant les bons mais aussi les moins bons moments de stress. Merci pour votre soutien lors des difficultés de la thèse mais aussi personnelles !!*
Je tiens à remercier **Hélène** d'être arrivée dans notre équipe lors de ma 2ème année de thèse. Merci pour toutes nos conversations (dois-je préciser, pas forcément scientifiques?), nos sorties (ciné, resto...), l'entraide scientifique ou non-scientifique... En fait, merci pour tous les bons moments passés ensemble ! Je voudrais en particulier te dire merci pour avoir un jour haussé le ton pour que je descende dans le Sud faire un peu bronzette !
Merci à **Marie**, arrivée il y a un an mais qui semble être là depuis bien plus longtemps (une très bonne intégration tout ça !!) ! Merci pour cette ambiance détendue, pour tous ces fous rires (les voisins ne disent peut-être pas la même chose ^^)!!! Merci pour ces si belles expressions françaises (du français, vraiment?) apprises ces deux dernières années...

Merci **Sandra**, oui, tu ne fais pas partie du bureau 321 mais bon, on était souvent dans le bureau de l'une ou l'autre, alors c'est comme si ! Ton passage, même s'il a été rapide à Rennes, a été très appréciable ! Merci pour les nombreuses conversations personnelles que nous avons eues et qui m'ont remontées le moral. La boîte de mouchoirs a également servi de mon côté ;) !
Merci **Edwige**, qui fut auparavant ma stagiaire dans ma dernière année de thèse. Merci pour ta présence et pour tes messages et carte. Merci d'avoir réussi à supporter la pression non négligeable sans jamais te plaindre et d'avoir aussi bien travaillé ! Bienvenue parmi nous dans ce bureau !!
Thank you **Sen** and I am sorry if I do not speak in English very often. I do not have as much vocabulary in English than in French, and as you might have heard, I speak a lot, but in French.

Merci aux joueurs de tarot réguliers ou non :
Merci **Sylvia** de m'avoir accueillie dans la bande des doctorants. Un grand merci de m'avoir écoutée et conseillée si souvent en 1ère et 2ème année ! Je n'aurais sans doute pas réussi à tenir autant sans ton soutien ! J'espère te revoir bien vite !
Merci **Caro** (et non carreau ! Non ne fais pas la blague, qui n'en est pas une !!), toujours en pleine forme (mais tu manges quoi le matin??) ! Merci pour cette semaine de rando sur le GR 441 fort sympathique et pour tous ces concerts, pièces de théâtre, opéra partagés ensemble !
Anthony, alias Pochon merci pour ta bonne humeur, de toujours être partant pour une (seulement?) petite partie de tarot et pour tous les bons moments du midi !
Merci **Roman** de toujours nous allécher avec tes bons petits plats et ta générosité culinaire, même si les odeurs qui arrivent jusqu'en haut sont peut-être moins appréciées par tout le monde ^^ !
Christian, plus vraiment doctorant mais inconditionnel joueur de tarot ! Merci pour ta constante bonne humeur, pour tes blagues misogynes (oui, oui mais bon, il ne le pense pas !) ou contre les géochimistes, et non, je n'ai pas fait de log(log()), tu peux vérifier ! Et puis, je n'ai pas fait de droite avec un seul point, tu peux vérifier aussi :) !
Merci également à **Laurie**, plus parmi nous mais qui m'a accueillie également dans le laboratoire. Nos conversations me manquent ! J'espère que nous nous reverrons bientôt !
Merci à tous les autres doctorants que je n'ai pas cités, avec qui j'ai passé quelques repas, soirées, etc. : Alain, Bob, Camille, Gemma, Hugo, Jérôme, Justine*2, Loic, Luc, Marie, Nico, Olivier, Paul, Pierre-Louis, Sarah, Tristan, Youss,etc.

Merci à mes amis de la 072*, amis fidèles qui me connaissent depuis de nombreuses années maintenant et qui m'ont soutenue pendant ces trois années de thèse. Ca y est c'est fini, vous pouvez maintenant me surnommer Dr Cat' (mais vous n'êtes vraiment pas obligés) sans que je puisse dire quelque chose !*
Merci à ma binôme, également surnommée ma jumelle **Christelle**. Merci d'avoir toujours été présente, de m'avoir envoyé ces nombreux mails, d'avoir fait l'effort de monter à Paris, Rennes ou autres villes pour que nous puissions nous revoir. Un grand merci d'avoir répondu oui quand je t'ai demandé si je pouvais débarquer le lendemain chez toi...
Merci **Olivier** (P.), tu ne fais pas partie de la 072 mais à la fois de LaSalle et ancien de Rennes. Je voulais te dire un grand merci car je sais que sans toi, je ne serai pas allée à la Goldschmidt, n'aurai pas rencontré Mathieu et Rémi, 1ère étape avant le stage puis la thèse. Merci de m'avoir soutenue auprès de Mélanie, je sais qu'il y a eu des coups de téléphone ! Et puis merci pour tes cours de géochimie !
Merci **Marie** et **Rémy** de m'avoir accueillie à de nombreuses occasions à Paris pour un week-end de retrouvailles. Merci pour votre soutien psychologique pendant ces trois années et d'être venus également à Rennes malgré la petitesse de mon appart.
Merci **Flavie** pour tous ces coups de téléphone. Nous sommes chacune à un bout de la France mais le téléphone fonctionne bien (ou pas d'ailleurs !) ! Merci d'avoir appelé pour

raconter les bons moments, les news et bien sur également lorsque les mouchoirs étaient au rendez-vous.
Merci **Amélie**, **Damien**, **Marie** (T.) et **Sophie** pour ces moments passés ensemble à Paris, Le Mans, Beauvais et de m'avoir accueillie quelques fois chez vous. Merci pour votre soutien régulier à travers les sms, mails, conversations téléphoniques, mais aussi lors de mes passages à Paris, de m'avoir écoutée parler de mes petits soucis et de m'avoir rassurée !
Merci **Gotgot**, très loin d'ici mais près à faire des kilomètres pour passer voir les amis ! Merci pour tes messages par mail, Facebook... et ne refais pas le coup de la panne la prochaine fois ;) (non, non pas d'idées mal placées) !
Merci **Nath**, également très loin d'ici. Le nombre de fois où je me suis dit qu'il fallait que je t'envoie un message... Désolée si j'ai donné si peu de nouvelles !

Je voudrais également remercier la **chorale**, oui, car la thèse c'est aussi savoir se détendre à côté. Merci pour la bonne humeur, pour ces moments détente et tous les fous rires avec les sopranes ou autres : désolée pour les chefs de chœur, je ne suis pas la plus disciplinée des chanteuses... Je voudrais remercier les chefs de chœur qui donnent cette ambiance fraternelle : **Marie-Amélie**, **Thibaud** et avant eux Joseph et Pauline ! Merci aux personnes participant aux after : notre pianiste préférée **Thérèse** (merci pour ton sourire chaleureux !), **Morgane**, **Clémence** (nous sommes les plus anciennes de la chorale, toujours présentes !!), **Leslie** (ouiiiii une autre thésarde !), **Laura**, **Romane** (snif, partie loin), **Lucile**, **Johann** et tous les autres !

Merci à **Lucile** d'être toujours présente à mes côtés malgré le nombre d'années. Non, je ne vais pas compter, sinon ça va faire mal mais quand même, nous nous connaissons depuis... ouch le lycée ! Au final, nous nous sommes toujours suivie: Le Mans, Angers puis maintenant Rennes ! Merci pour tous les moments passés ensemble : les soirées, les repas, les discussions, les cinés, livres etc.

Merci à **ma marraine**, son mari et ses enfants d'avoir toujours été présents tout près, de m'avoir invitée à ces repas, de m'avoir soutenue et m'avoir fait rencontré tes assistantes ! Merci également à **tous les membres** (nombreux !) **de ma famille**, en particulier Manu, Sonia, Ellyn, Evan, Danièle, Ophélie, Yannick, Régine et tous les autres !

Merci enfin à **ma boulangère** et à toutes les vendeuses ! Merci pour les discussions, les sourires échangés et pour tous les cadeaux de fin de service !!

Merci à toutes les personnes non citées ici que j'ai pu oublier et qui ont contribué de près ou de loin à cette thèse !

Enfin, je voudrais dédier ce manuscrit de thèse aux personnes suivantes :

Ma tante et mon oncle de Cesson. Merci d'avoir été présents tout le long de cette thèse et auparavant au cours de mon stage. Malgré les aléas de la vie, vous avez toujours été présents pour moi (les réparations de vélo, les viennoiseries...) mais aussi et surtout merci pour toutes les fois où vous m'avez accueillie chez vous pour un repas, pour les nombreuses discussions que nous avons eues. J'aurais tellement voulu que vous soyez présents à ma soutenance, en particulier toi Marie-Jo, pour que je puisse te dire merci... mais la vie en a malheureusement décidé autrement ! Merci pour tout Marie-Jo et j'espère que tu savais combien tu m'as apporté et combien tu me manques aujourd'hui ! Merci bien évidemment à toi aussi Roland, avec toutes ces difficultés, tu as été et tu es toujours là pour moi !

Mes parents qui m'ont soutenue tout le long de ma scolarité ! Merci de m'avoir fait confiance notamment en seconde pour le choix de spécialité, pour mon choix un peu farfelu de vouloir faire une prépa puis une école d'ingé en géologie (ma passion depuis toute petite !). Merci de m'avoir soutenue moralement et financièrement toutes ces années et d'avoir toujours cru en moi !!

Enfin, merci à **mon frère**, compagnon de jeux depuis 26 ans (et de chamailleries) ! Merci de m'avoir supportée depuis toutes ces années et merci d'avoir toujours répondu oui aux toc toc à ta porte pour m'aider sur un exo, un concept... Si j'aime la chimie, je crois que c'est grâce à toi et à tes explications "tu vois c'est simple, quand tu prends ça et puis tu mets ça en plus, eh ben hop ça donne ça" (avec les bras qui gesticulent, sinon, ce n'est pas une explication à la Sylvain !).

Finalement, je voudrais vous remercier vous **lecteur** d'avoir été au bout de ces remerciements et de vous intéresser à ce sujet de thèse qui m'a passionnée pendant toutes ces années ! Aucune frayeur à avoir, je ne fais pas de pudding à l'arsenic ;) !

Bonne lecture !!

Sommaire

Résumé

L'arsenic est un élément toxique présent naturellement dans l'environnement. Parfois en fortes concentrations dans les eaux souterraines, utilisées comme eaux de boisson, il est responsable de l'une des plus grandes mortalités au monde. Il est donc important de mieux comprendre les interactions de l'As avec l'environnement et son mode de transfert jusqu'aux aquifères. Cette thèse a pour objectif de comprendre les mécanismes de complexation direct et indirect de l'As(III) par la matière organique (MO) en milieu anoxique, notamment via les groupements thiols de la MO et sous forme de complexes ternaires faisant intervenir le Fe ionique.

La première partie de ce travail a été consacrée à la complexation de l'As(III) par les groupements thiols de la MO. Des expériences de complexation d'As(III) par un acide humique (AH) naturel greffé ou non en sites thiols ont été réalisées. L'As(III) se complexe à la MO directement mais les concentrations complexées sont faibles et dépendantes de la densité en sites thiols. La modélisation, à l'aide de PHREEPLOT-PHREEQC-Model VI modifié afin de tenir compte des sites thiols de la MO, a mis en évidence que l'As était complexé à la MO sous forme de complexes monodentates. Il existe, cependant, un autre mécanisme qui propose une complexation indirecte via la formation d'un pont cationique. Nous nous sommes intéressés ici, en conditions anoxiques, à la possibilité que ce pont soit un pont de Fe(II). Il n'existe cependant que très peu d'information sur la complexation du Fe(II) par la MO. Des expériences de complexation du Fe(II) par des substances humiques (SH) ont donc été réalisées. Les résultats expérimentaux ont montré que le Fe(II) est faiblement complexé aux SH lorsque le pH était acide et les groupements fonctionnels protonés. Au contraire à pH neutres à basiques, 100% du Fe(II) est complexé aux SH. La modélisation a montré que le Fe(II) forme majoritairement des complexes bidentates carboxyliques à pH acides et des complexes bidentates carboxy-phénoliques et phénoliques à pH basiques.

Dans la dernière partie, la complexation de l'As(III) par des complexes ternaires As(III)-Fe(II, III) ionique-MO a été testée. Les résultats expérimentaux ont montré que des complexes ternaires As(III)-Fe(II)-MO pouvaient se former en milieu anoxique. La modélisation a permis de tester différentes conformations structurales de complexes ternaires. Le complexe le plus probable est un complexe bidentate mononucléaire d'As(III) sur un complexe bidentate de Fe(II)-AH. Cependant, PHREEPLOT-PHREEQC-Model VI doit être amélioré car la distribution des sites bidentates n'est pas réaliste en comparaison des données spectroscopiques. Au contraire, pour de faibles concentrations en Fe(III), lorsque les espèces oxydantes et réduites coexistent, l'As(III) ne forme pas de complexes ternaires As(III)-Fe(III) ionique-MO.

La spéciation de l'As et du Fe est particulièrement importante dans l'étude du transfert de l'As. Si l'As(III) est complexé à la MO, comme c'est le cas dans les complexes ternaires, son transfert dépendra totalement des mécanismes de transfert de la MO. Cependant, ces travaux ont montré que, tant que les conditions du milieu restent anoxiques, une partie majoritaire de l'As(III) reste sous forme libre et pourrait atteindre et contaminer les aquifères sous-jacents.

Mots clés : arsenic(III), fer(II), matière organique, acide humique, complexation, spéciation, thiol, pont cationique, modélisation, PHREEPLOT-PHREEQC-Model VI

Abstract

Arsenic occurs naturally in groundwater used as drinking water. It is thus responsible of a great mortality in the world. Understand the As interactions with its environment and its transfer mode to the aquifers is therefore crucial. This work was focused on the direct and indirect binding mechanisms of As(III) by organic matter (OM) in anoxic environments, in particular via OM thiol groups and as ternary complexes involving ionic Fe.

The first part of this work was dedicated to the complexation of As(III) by the OM thiol. Binding experiments of As(III) by a humic acid (HA) grafted or not by thiol were thus

performed. Grafted or not OM were able to bind As(III) but bound As(III) concentrations were low and dependant on the thiol site density. Modeling with PHREEPLOT-PHREEQC-Model VI modified to take into account thiol site demonstrated that As(III) was bound as monodentate complexes to OM thiol sites. Another indirect binding mechanism involving ternary complex via cationic bridge was however described to explain larger binding of As(III, V) to natural OM. Here under anoxic conditions, we speculated that this bridge was an ionic Fe(II) bridge. However, little information exists about the binding of Fe(II) by OM. Complexation experiments of Fe(II) by humic substances (HS) were thus conducted. The experimental results showed that Fe(II) was weakly complexed to HS at acidic pH, when the functional groups were protonated. By contrast, at basic pH, 100% of Fe(II) were complexed to HS. Modeling calculations demonstrated that Fe(II) formed mainly carboxylic bidentate at acidic pH and carboxy-phenolic and phenolic bidentate at basic pH. In the last part, the complexation of As(III) as As(III)-ionic Fe(II, III)-OM ternary complexes was tested. Experimental results showed that As(III)-Fe(II)-OM ternary complexes could form in anoxic environments. Modeling allowed to test several ternary complexes conformations. The most potential was the binding of As(III) as mononuclear bidentate complex onto a bidentate Fe(II)-HA complex. However, another definition of the model that should be constrained by XAS data is required. By contrast, at low concentrations of Fe(III), when the oxidizing and reduced species coexist, As(III) does not form As(III)-ionic Fe(III)-OM ternary complexes.

Speciation of As and Fe is particularly important in the study of the As(III) transfer. When As(III) is bound to OM as ternary complexes, its transfer is entirely controlled by the own OM transfer mechanisms. Here, we calculated, however, that much of As(III) remains as labile species and can therefore reach underlying aquifers as long as anoxic conditions exist.

Keywords : arsenic(III), fer(II), organic matter, humic acid, complexation, speciation, thiol, cationic bridge, modelising, PHREEPLOT-PHREEQC-Model VI

Introduction

L'arsenic est un élément chimique omniprésent dans la nature et retrouvé non seulement, dans l'atmosphère, les sols, les roches, les eaux naturelles mais également, dans certains organismes vivants (Bowell et al., 2014). C'est un métalloïde dont les propriétés chimiques sont intermédiaires entre les métaux et les non-métaux. Son symbole est As, sa masse molaire est de 74.92 g mol^{-1} et son numéro atomique est 33. Dans le tableau périodique de Mendeleïev, l'As est donc situé entre le phosphore et l'antimoine. Le comportement chimique de l'As est souvent comparé à celui de l'antimoine (les deux éléments chimiques présentent les deux états redox V et III) et l'As(V) au phosphore. L'As est retrouvé sous cinq états rédox, organiques ou non: l'arsine, As(-III), retrouvé dans les milieux très fortement réduits; l'arsenopyrite (FeAsS) et la löllingite (FeAs2), As(-I); l'As élémentaire, As(0), très rarement présent dans les environnements naturels, et les deux formes les plus abondantes, l'arsénite, As(III) et l'arséniate, As(V). Deux formes méthylées sont également synthétisées par les organismes vivants telles que le diméthylarséniate (DMA), le monométhylarséniate (MMA(V)) et le monométhylarsénite (MMA(III)). Toutefois, ces formes organiques sont peu concentrées dans les eaux, sauf aux abords de fortes pollutions industrielles (Smedley and Kinniburgh, 2002). L'arséniate est présent sous quatre formes en fonction du pH : $As(OH)_3O$, $As(OH)_2O_2^-$, $As(OH)O_3^{2-}$ et AsO_4^{3-} des pH acides aux pH basiques (Figure Intr. 1). L'arsénite est présent sous trois formes différentes : $As(OH)_3$, neutre, la plus courante, $As(OH)_2O^-$, négatif, retrouvé à des pH basiques et $AsOHO_2^{2-}$, présent seulement à des pH très basiques et très peu répandu (Figure Intr. 1).

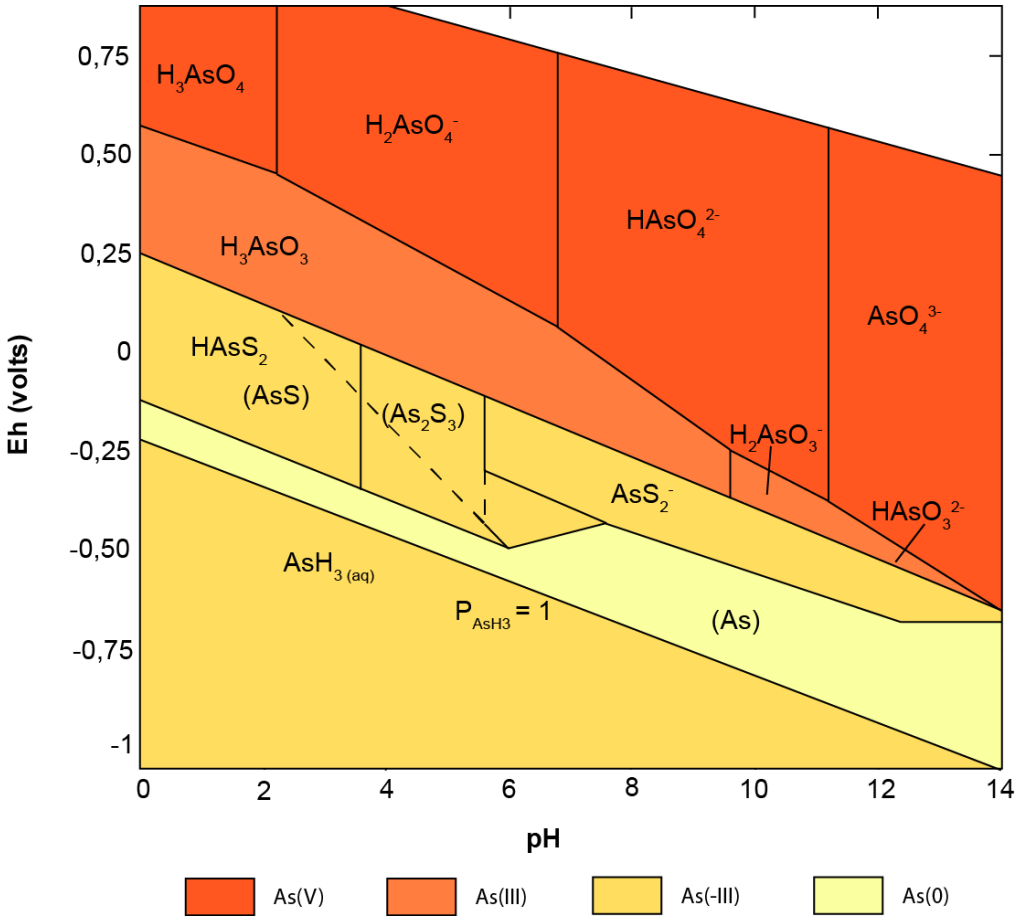

Figure Intr. 1 : Diagramme Eh-pH de l'arsenic (Wang and Mulligan, 2006) à 25°C, 101.3 kPa avec une concentration en As de 10^{-5} mol L^{-1} et une concentration en soufre de 10^{-3} mol L^{-1}

L'As est classé 47ème sur 88 en abondance parmi les éléments chimiques terrestres. Cependant sa concentration dans les eaux et les sols dépend fortement de la géologie et des activités humaines environnantes (Tableau Intr. 1). Dans les minéraux des roches, la chimie de l'As est généralement liée à celle du S, présent sous forme de sulfures. Le minéral d'As majoritaire est l'arsénopyrite : FeAsS. Dans les dépôts provenant des mines, la source la plus importante d'As est la pyrite arséniée : $Fe(S,As)_2$. La pyrite est formée à faible température dans des environnements sédimentaires sous conditions réductrices. Elle est retrouvée dans les sédiments des rivières, lacs et océans mais aussi dans de nombreux aquifères où elle joue un rôle prépondérant pour de nombreux éléments chimiques (Bowell et al., 2014). La pyrite n'est cependant pas stable dans les systèmes aérobies où elle s'oxyde en produisant des oxydes de fer (Fe) et en libérant les éléments traces associés, dont l'As. De fortes concentrations en As sont ainsi été retrouvées associées non seulement,

aux oxydes de Fe et Mn mais aussi, aux argiles et à la surface de la calcite ou dans les minéraux de phosphate (exemple l'apatite) (Smedley and Kinniburgh, 2002). Dans les sols, la concentration en As dépend fortement des minéraux présents et de leur structure. Généralement, la concentration en As dans les sols varie de 5 à 10 mg kg^{-1} (Smedley and Kinniburgh, 2002). Les tourbières et marécages sont des milieux réducteurs qui peuvent également présenter de fortes concentrations en As (13 mg kg^{-1}), dues à la présence de sulfures, piégeurs d'As (Tableau Intr. 2). Les concentrations en As dans les principales roches, sédiments et sols sont présentées dans le Tableau Intr. 2. De plus, les apports anthropiques, peuvent augmenter les concentrations en As dans l'environnement. Ainsi, l'utilisation de pesticides et herbicides contenant de l'As a été interdite en 1968 et ce n'est seulement qu'en 2004 que l'utilisation de composés de l'As pour traiter le bois a été interdite (décret du 19 novembre 2004). Ces utilisations ont laissé des traces dans les sols et eaux, présentant parfois des concentrations non négligeables en As. Aux abords des mines, de fortes concentrations en métaux lourds et en As peuvent également être retrouvées (Tableau Intr. 1 et Tableau Intr. 2). Enfin, de fortes concentrations en As sont également retrouvées dans les eaux géothermales et les émissions volcaniques qui présentent également de fortes concentrations en sulfures (Tableau Intr. 1). Les sources d'As sont diverses à travers le monde mais, les sources naturelles restent les plus nombreuses.

Tableau Intr. 1 : Concentrations en As dans les eaux (Smedley and Kinniburgh, 2002)

Type d'eau et localisation	[As] (µg L^{-1})	Références
Eau de pluie		
Référence		
Marine	0.02	Andreae, 1980
Terrestre (W USA)	0.013-0.032	Andreae, 1980
Côte (Milieu-Atlantique, USA)	0.1 (<0.005-1.1)	Scudlark and Church, 1988
Eau de rivière		
Référence		
Variable	0.83 (0.13-2.1)	Andreae et al., 1983; Froelich et al., 1985; Seyler and Martin, 1991
USA	0.15-2.1	Sonderegger and Ohguchi, 1988; Waslenchuk, 1979
Dordogne, France	0.7	Seyler and Martin, 1991
Rivières polluées européennes	4.5-45	Seyler and Martin, 1991
Bassin versant de Schelde, Belgique	0.75-3.8 (jusqu'à 30)	Andreae and Andreae, 1989
Influencée par de fortes concentrations en As dans les eaux souterraines		
Chili du Nord	190-21800	Caceres et al., 1992
Córdoba, Argentine	7-114	Lerda and Prosperi, 1996
Influence géothermale		
Waikato, Nouvelle Zélande	32 (28-36)	McLaren and Kim, 1995
Rivières Madison et Missouri, USA	10-370	Nimick et al., 1998; Robinson et al., 1995
Influence minière		
Ron Phibun, Thaïlande	218 (4.8-583)	Williams et al., 1996
Ashanti, Ghana	284 (<2-7900)	Smedley, 1996
Lac		
Référence		
Colombie britannique	0.28 (<0.2-0.42)	Azcue et al., 1994; Azcue and Nriagu, 1995
France	0.73-9.2 (fortes [Fe])	Seyler and Martin, 1989
Japon	0.38-1.9	Baur and Onishi, 1969
Influence géothermale		
USA de l'Ouest	0.38-1000	Benson and Spencer, 1983
Influence minière		
Territoires du Nord-Ouest, Canada	270 (64-530)	Bright et al., 1996
Ontario, Canada	35-100	Azcue and Nriagu, 1995
Estuaire		
Oslofjord, Norvège	0.7-2.0	Abdullah et al., 1995
Estuaire du Rhône, France	2.2 (1.1-3.8)	Seyler and Martin, 1990
Influences minière et industrielle		
Estuaire de la Loire, France	Jusqu'à 16	Seyler and Martin, 1990
Estuaire Tamar, UK	2.7-8.8	Howard et al., 1988
Estuaire Schelde, Belgique	1.8-4.9	Andreae and Andreae, 1989
Eau de mer		
Pacifique profond et Atlantique	1.0-1.8	Cullen and Reimer, 1989
Côte de l'Espagne	1.5 (0.5-3.7)	Navarro et al., 1993
Eau souterraine		
Référence UK	<0.5-10	Edmunds et al., 1989
Provinces riches en As (Bengale, Argentine, Mexique, Nord du Chili, Taiwan, Hongrie)	10-5000	BGS and DPHE, 2001; Das et al., 1995; Delrazo et al., 1990; Hsu et al., 1997; Luo et al., 1997; Nicolli et al., 1989; Smedley et al., 2001; Varsanyi et al., 1991
Eaux souterraines contaminées par les produits miniers	50-10000	Welch et al., 1988; Williams et al., 1996; Wilson and Hawkins, 1978
Eau géothermale	<10-50000	Baur and Onishi, 1969; Ellis and Mahon, 1977; White et al., 1963
Drainage minier		
Variables, USA	<1-34000	Plumlee et al., 1999
Montagne de fer	Jusqu'à 850000	Nordstrom and Alpers, 1999
Montagne Ural	400000	Gelova, 1977
Eaux interstitielles des sédiments		
Référence, estuaire suédois	1.3-166	Widerlund and Ingri, 1995
Référence, sédiments de plateforme continentale	>300	Sullivan and Aller, 1996
Contamination minière, Colombie britannique	30-360	Azcue et al., 1994
Résidus miniers, Ontario, Canada	300-100000	McCreadie and Blowes, 2000

Tableau Intr. 2 : Concentrations en As dans les roches, sédiments ou autres dépôts (Smedley and Kinniburgh, 2002)

Type de roche/sédiment	Concentration en As moyenne et/ou gamme (mg kg^{-1})	Références
Roches ignées		
Roches ultrabasiques (péridotite, dunite, kimberlite)	1.5 (0.03-15.8)	
Roches basiques (basalte)	2.3 (0.18-113)	
Roches basiques (gabbro, dolérite)	1.5 (0.06-28)	Onishi and Sandell, 1955
Intermédiaires (andésite, trachyte, latite)	2.7 (0.5-5.8)	Baur and Onishi, 1969
Intermédiaires (diorite, granodiorite, syenite)	1 (0.09-13.4)	Boyle and Jonasson, 1973
Roches acides (rhyolite)	4.3 (3.2-5.4)	Ure and Berrow, 1982
Roches acides (granite, aplite)	1.3 (0.2-15)	Riedel and Eikmann, 1986
Roches acides (pechstein)	1.7 (0.5-3.3)	
Verres volcaniques	5.9 (2.2-12.2)	
Roches métamorphiques		
Quartzite	5.5 (2.2-7.6)	
Cornéenne	5.5 (0.7-11)	
Phyllade/ardoise	18 (0.5-143)	Boyle and Jonasson, 1973
Schiste/gneiss	1.1 (<0.1-18.5)	
Amphibolite et roche verte	6.3 (0.4-45)	
Roches sédimentaires		
Schiste argileux marin/pélite	3-15 (plus de 490)	
Schiste argileux (dorsale Atlantique)	174 (48-361)	
Schiste argileux non marin/pélite	3-12	
Grès	4.1 (0.6-120)	Onishi and Sandell, 1955
Calcaire/dolomite	2.6 (0.1-20.1)	Baur and Onishi, 1969
Phosphorite	21 (0.4-188)	Boyle and Jonasson, 1973
Formations de Fe et sédiments riches en Fe	1-2900	Belkin et al., 2000; Cronan, 1972; Riedel and Eikmann, 1986; Welch et al., 1988
Evaporites (gypse/anhydrite)	3.5 (0.1-10)	
Charbons	0.3-35000	
Schiste argileux bitumineux (Kupferschiefer, Allemagne)	100-900	
Sédiments non consolidés		
Variables	3 (0.6-50)	Azcue and Nriagu, 1995
Sables alluviaux (Bengladesh)	2.9 (1.0-6.2)	BGS and DPHE, 2001
Boue alluviale/argile (Bengladesh)	6.5 (2.7-14.7)	BGS and DPHE, 2001
Sédiments de lit de rivière (Bengladesh)	1.2-5.9	Datta and Subramanian, 1997
Sédiments de lac (lac supérieur)	2 (0.5-8)	Allan and Ball, 1990
Sédiments de lac (Colombie anglaise)	5.5 (0.9-44)	Cook et al., 1995
Moraine glaciaire (Colombie anglaise)	9.2 (1.9-170)	Cook et al., 1995
Sédiments de rivière moyens à travers le monde	5	Martin and Whitfield, 1983
Limon de cours d'eau et lac (Canada)	6 (<1-72)	Boyle and Jonasson, 1973
Limon lœss (Argentine)	5.4-18	Arribére et al., 1997; Smedley et al., 2002
Sédiments de marge continentale (argileux, quelques uns anoxiques)	2.3-8.2	Legeleux et al., 1994
Sols		
Variables	7.2 (0.1-55)	Boyle and Jonasson, 1973
Sols tourbeux et marécages	13 (2-36)	Ure and Berrow, 1982
Sols sulfatés acides (Vietnam)	6-41	Gustafsson and Tin, 1994
Sols sulfatés acides (Canada)	1.5-45	Dudas, 1984; Dudas et al., 1988
Sols proches des dépôts sulfureux	126 (2-8000)	Boyle and Jonasson, 1973
Dépôts superficiels contaminés		
Sédiment de lac contaminé par les mines (Colombie anglaise)	342 (80-1104)	Azcue et al., 1994; Azcue and Nriagu, 1995
Sédiment du réservoir contaminé par les mines (Montana)	100-800	Moore et al., 1988
Sols contaminés par les résidus de mine (Colombie anglaise)	903 (396-2000)	Azcue and Nriagu, 1995
Sols contaminés par les résidus de mine (Grande-Bretagne)	120-52600	Kavanagh et al., 1997
Sols contaminés par les résidus de mine (Montana)	Plus de 1100	Nagorski and Moore, 1999
Sédiments intertidaux pollués par pollution industrielle	0.38-1260	Davis et al., 1997
Sols en dessous d'une usine chimique (USA)	1.3-4770	Hale et al., 1997
Boue de station d'épuration	9.8 (2.4-39.6)	Zhu and Tabatabai, 1995

1. Contamination et toxicité de l'As

Souvent confondu avec le cyanure (CN), l'As est tristement connu pour être un poison pour l'Homme. En revanche, il est moins su que l'As est responsable de l'une des plus grandes mortalités dans le monde (Smith et al., 2000). Il a ainsi été classé par l'organisation mondiale de la santé (OMS) comme un poison majeur à travers le monde. Lorsqu'il est consommé à faibles concentrations et à long terme, l'As peut provoquer des lésions de la peau (maladie du pied noir), des cancers de la peau, de la vessie, des poumons, des maladies cardiovasculaires, des problèmes respiratoires et du diabète.

Figure Intr. 2 : Lésions de la peau : maladie du pied noir (http://www.betterlifelabs.org)

Cette contamination se produit généralement via la consommation d'eau contaminée en As. L'ingestion d'aliments contenant de l'As peut également renforcer le problème (animaux contaminés et irrigation du riz par de l'eau contaminée). Cette contamination de l'eau touche de nombreux pays à travers le monde tels que l'Argentine, le Bengladesh, le Chili, la Chine, les Etats-Unis, l'Inde, le Mexique (Figure Intr. 3). Smedley et Kinniburgh (2002) estiment ainsi qu'environ 40 millions de personnes sont concernées par la contamination de l'eau à l'As. La concentration à partir de laquelle l'As peut être consommé sans risque n'est pas clairement établie. L'OMS a ainsi abaissé la concentration maximale d'As dans l'eau pouvant être consommée de 50 à 10 µg L^{-1} en 1993. Cette valeur est fonction de la taille de l'individu et de la quantité d'eau bue au cours d'une journée (dans les pays très chauds, cette valeur peut encore être abaissée). Cette valeur est généralement la

valeur respectée dans les pays développés mais, dans les pays en voie de développement les concentrations ne sont parfois pas connues (aucune mesure possible) ou les mesures effectuées n'atteignent pas les limites de quantification de 10 µg L^{-1}.

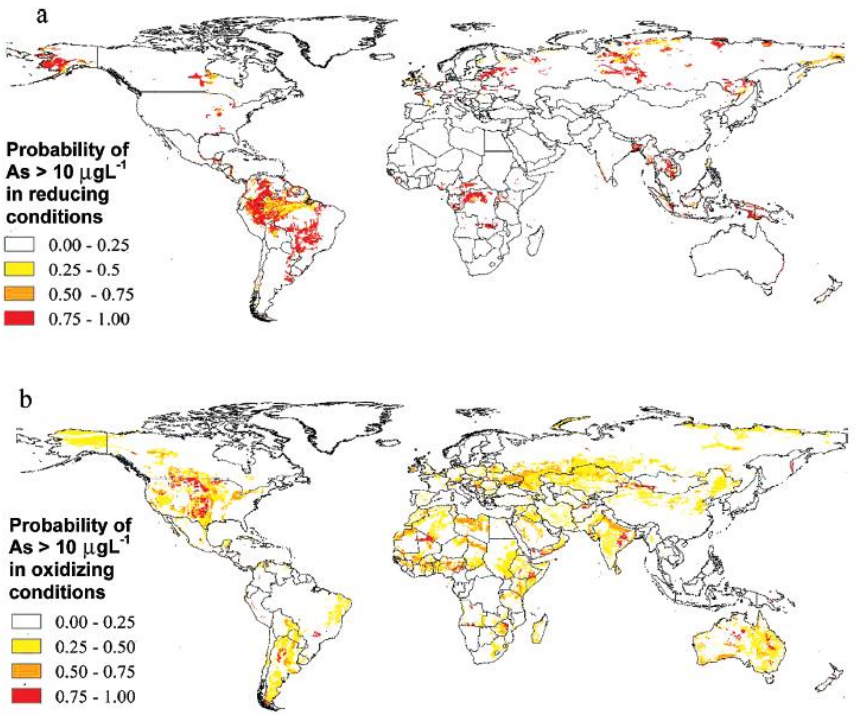

Figure Intr. 3 : Carte de probabilité de contamination en As dans les eaux souterraines a - en conditions réductrices et b - en conditions oxydantes (Amini et al., 2008)

La forme non organique la plus dangereuse pour l'Homme est l'arsénite - As(III). En effet, l'arsénite est connu pour être capable de former des complexes avec des sites thiols (SH) présents dans la cystéine (Figure Intr. 4a), un acide aminé constitutif de nombreuses protéines et peptides comme le glutathion (Figure Intr. 4b). L'arsenite se lie à un ou plusieurs de ces sites thiols provoquant une modification de la conformation des protéines et des peptides et empêchant leur utilisation par d'autres éléments chimiques du corps (Figure Intr. 4c). Les protéines et peptides complexant ainsi As(III) ne peuvent remplir le rôle qui leur est attribué dans le corps humain, provoquant ainsi des cancers et maladies. L'arséniate, reconnu moins dangereux pour l'Homme, est capable de remplacer le phosphore dans les chaines d'ADN, provoquant ainsi également des cancers.

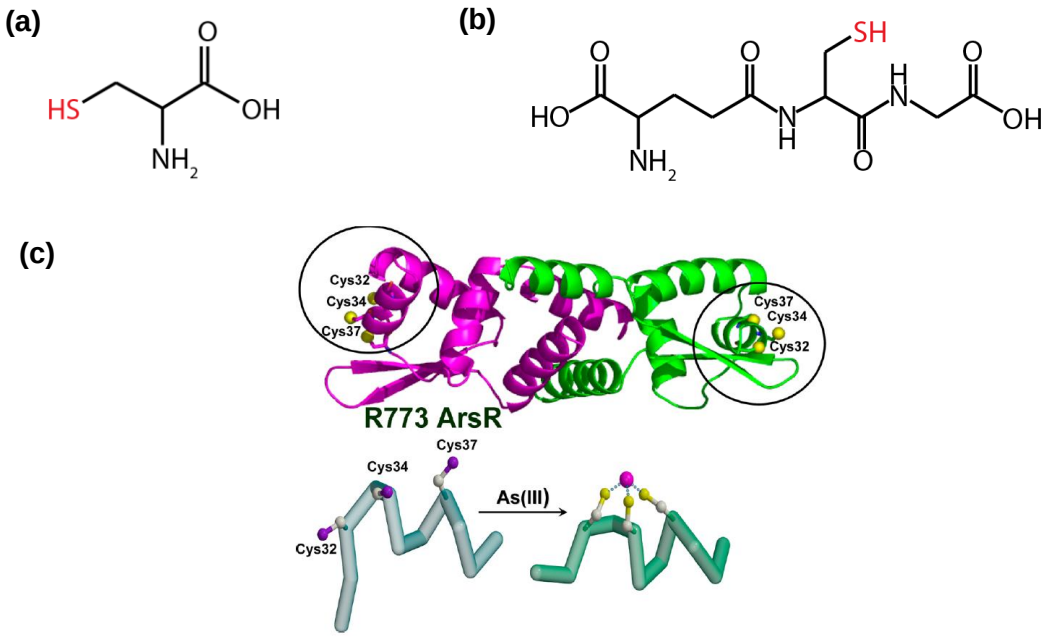

Figure Intr. 4 : Représentations de (a) la cystéine et (b) du glutathion. Les sites thiols sont représentés en rouge. (c) Changements conformationnels après complexation de l'As(III) sur les sites thiols des cystéines de la protéine ArsR de E. coli (Shen et al., 2013)

2. Origine des contaminations naturelles des aquifères en As

Différents mécanismes ont été présentés concernant la contamination en As des eaux souterraines. Le premier mécanisme a été largement étudié au Bengladesh, pays où de nombreux cas de maladie du pied noir ont été répertoriés. Ils sont dus à la contamination en As des eaux souterraines consommées comme eaux de boisson et/ou dans l'irrigation des cultures. Cette large contamination en As est un phénomène qui n'est apparu que récemment. Auparavant, l'eau était captée dans le réseau hydrographique de surface mais avec l'accroissement des problèmes sanitaires, tels que la présence de matières fécales, des puits ont dus être creusés afin d'utiliser les eaux souterraines. Or, les concentrations en As dans les sédiments des aquifères, qu'ils soient sous forme de sulfures et/ou complexés aux oxydes de Fe, sont naturellement extrêmement importantes. L'exploitation des aquifères en abaissant les niveaux piézométriques des aquifères a permis l'introduction d'O_2 et la dissolution des sulfures riches en As, alors libérés en solution. Lorsque celui-ci est lié aux oxydes de Fe, sa solubilisation intervient par le biais de bactéries ferro-réductrices capables de dissoudre les oxydes de Fe. Cette dissolution réductrice par les bactéries nécessite un

apport de matière organique. Les bactéries pour croitre utilise le carbone de la matière organique qu'elles oxydent par le biais des oxydes de Fe présents dans le milieu. En contre partie, ces derniers sont réduits et se dissolvent. Le Fe(III) solide se transforme en Fe(II) soluble, libérant ainsi dans le milieu la charge en métaux et métalloïdes associés tels que l'As. Plusieurs hypothèses ont été avancées concernant la source de matière organique, celle-ci pourrait être allochtone ou autochtone. Dans la cas de la source allochtone, la matière organique proviendrait de la surface, c'est-à-dire des sols, qui déstockeraient le carbone organique en raison de l'irrigation intensive nécessitée par la culture du riz (Harvey et al., 2006). L'eau d'irrigation enrichie en matière organique diffuserait ensuite jusqu'aux aquifères sous-jacents. Ne détectant pas de matières fécales dans les puits, McArthur et al. (2004) ont proposé un autre mécanisme où la matière organique aurait une source autochtone. Cette matière organique proviendrait de strates tourbeuses juxtaposées aux sables de certains aquifères dont la solubilisation serait exacerbée par l'augmentation des flux dus au pompage. Meharg et al. (2006) suggèrent, quant à eux, que l'As s'est déposé en même temps que du carbone organique dans les sédiments deltaïques du Bengale (corrélations entre les concentrations en As et en carbone organique).

Un autre mécanisme de contamination des aquifères met en jeu les zones humides et plaines d'inondation, comme révélé notamment dans la plaine d'inondation du Mékong. L'altération de l'Himalaya produit de grandes quantités de sédiments riches en oxydes de Fe porteurs d'As. Lors des crues du Mékong, ces sédiments sont déposés dans les zones humides et les plaines d'inondation bordant les fleuves (Figure Intr. 5). Ces milieux, par définition, sont des milieux très riches en matière organique particulaire, colloïdale ou dissoute et présentent des alternances redox qui contrôlent le cycle des éléments. Ainsi, en période de crues, c'est-à-dire de hautes eaux, ils sont saturés en eaux. Des conditions réductrices se développent alors, et les bactéries ferro-réductrices réduisent les oxydes de Fe déposés par les crues, solubilisant ainsi l'As qu'ils comprenaient, sous forme d'As(III). Celui-ci, sous forme soluble, aurait alors la possibilité de transiter jusque dans l'aquifère sous-jacent (Fendorf and Kocar, 2009; Kocar, 2008; Polizzotto et al., 2008) (Figure Intr. 5).

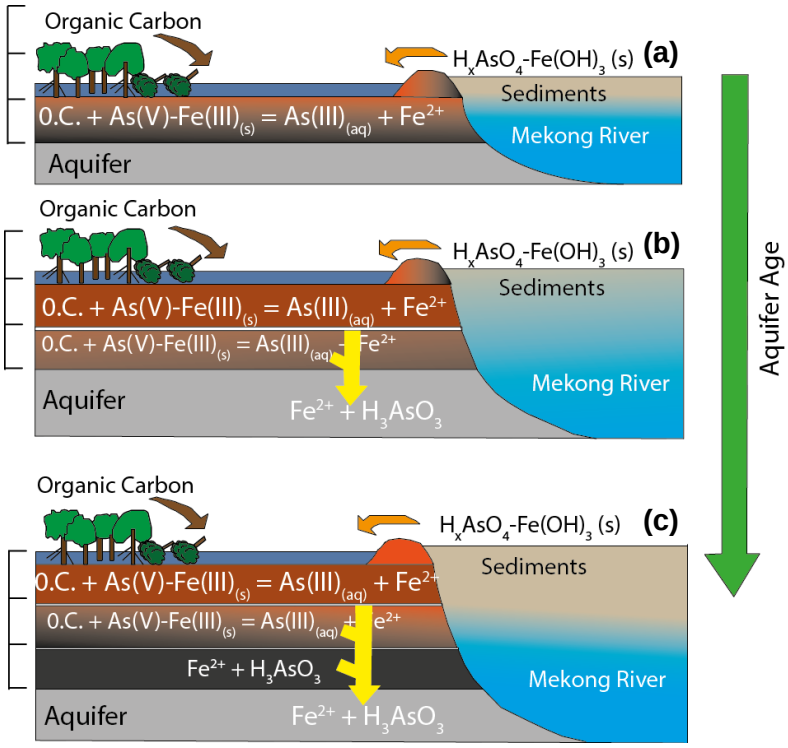

Figure Intr. 5 : (a) Lors des crues du Mékong, les oxydes de Fe porteurs d'As sont déposés dans les zones humides, l'apport de matière organique favorise la dissolution des oxydes de Fe, libère le Fe(II) et l'As(III). (b) Les apports du Mékong sont permanents et l'As(III) et le Fe(II) préalablement libérés migrent jusque dans les aquifères sous-jacents. (c) Continuité des phénomènes précédents avec les apports continus provenant du Mékong (Kocar, 2008)

Néanmoins, il est important de noter qu'ici la matière organique n'est considérée que comme une source de carbone pour les bactéries ferro-réductrices. Pourtant de nombreux travaux ont montré qu'une partie de cette matière organique, c'est-à-dire les acides humiques et fulviques, était capable de complexer des métaux mais aussi des métalloïdes (Fukushima et al., 1996; Mota et al., 1994; Pinheiro et al., 1994; Tipping et al., 2002; Town and Powell, 1993). Il est donc légitime de se poser la question de l'influence que les fortes concentrations en matière organique (particulaire ou colloïdale) pourraient avoir sur le transfert de l'As. Il ne faut pas oublier non plus, ici, le rôle du Fe. Dans ces conditions réduites les oxydes de Fe sont détruits, dissous et transformés en Fe(II) dont les concentrations dans le milieu sont importantes. De même que les oxydes de Fe(III), ce Fe(II) pourrait-il, avoir une influence sur la dynamique de l'As(III)?

3. Que sait-on des interactions entre l'As, le Fe et la matière organique?

La matière organique, et plus spécifiquement les acides humiques et fulviques, sont capables de complexer de nombreux éléments chimiques comme les terres rares (REE), le Fe, le Cu, le Mg... via leurs groupements fonctionnels (carboxyliques, phénoliques, thiols, amines...) (Buffle et al., 1998; Sposito, 1986; Tipping et al., 2002). En se déprotonant, ces groupements fonctionnels confèrent à la matière organique une charge globalement négative (Kim et al., 1990; Leenheer et al., 1995; Milne et al., 2001; Tipping, 1998). Contrairement aux métaux électropositifs lorsqu'ils sont sous forme d'espèces libres, l'As est un oxyanion qui peut être neutre ou chargé négativement. La complexation de l'As par la matière organique globalement négative n'est donc pas favorisée. Pourtant, plusieurs études se sont intéressées aux interactions entre l'As et la matière organique. Elles ont alors montré que l'As était capable de se lier à la matière organique (Buschmann et al., 2006; Fakour and Lin, 2014; Kappeler, 2006; Lenoble et al., 2015; Liu and Cai, 2010; Thanabalasingam and Pickering, 1986; Warwick et al., 2005). Des mécanismes directs ou indirects de complexation de l'As par la matière organique ont ainsi été proposés.

Dans le cas des complexations directes, Buschmann et al. (2006) et Lenoble et al. (2015) suggèrent que la complexation de l'As(III, V) se réalise via les groupements carboxyliques et phénoliques ; sites les plus nombreux au sein de la matière organique. Ces deux types de groupements fonctionnels sont reconnus comme étant capables de complexer de nombreux métaux (Atalay et al., 2009; Avena et al., 1999; Gustafsson, 2001; Milne et al., 2003, 2001; Ritchie and Perdue, 2003; Tipping, 1998; Tipping and Hurley, 1992). Buschmann et al. (2006) propose la complexation de l'As(III) sur les groupements phénoliques forts et peu abondants de la matière organique par perte d'un OH^- d'$As(OH)_3$ (Figure Intr. 6). Les groupements carboxyliques, plus abondants mais moins réactifs, ne peuvent vraisemblablement pas entrainer la perte d'un groupement OH^- mais, la présence d'un oxygène (C=O) dans l'environnement de l'As peut stabiliser le complexe par la formation d'une liaison hydrogène (Figure Intr. 7).

Figure Intr. 6 : Complexation de l'As(III) sur les groupements phénoliques de la matière organique (Buschmann et al., 2006)

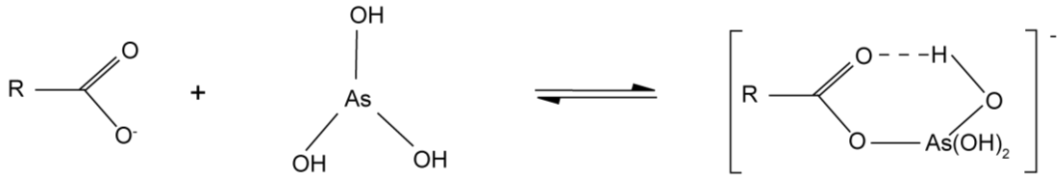

Figure Intr. 7 : Complexation de l'As(III) sur les groupements carboxyliques de la matière organique (Buschmann et al., 2006)

L'As(III) aurait également la possibilité de se lier aux sites thiols présents à la surface de la matière organique (Hoffmann et al., 2012; Langner et al., 2011a). Deux processus, l'un actif (découlant de l'absorption), et l'autre passif (adsorption) ont été proposés. Le processus actif concerne des environnements naturellement très riches en As. Dans ces milieux, les êtres vivants, bactéries ou végétaux, se sont adaptés aux fortes concentrations en As. Ils ont développé des systèmes de détoxification ou de protection. La biomasse produite est donc riche en As. Ce dernier est complexé notamment aux protéines sous forme de complexes tridentates (Figure Intr. 4). Une fois, cette biomasse transformée, notamment en tourbe, il semblerait que les complexes ainsi formés soient conservés comme cela a été démontré pour la tourbière de Gola di Lago en Suisse (Hoffmann et al., 2013; Langner et al., 2011a). Les mécanismes de complexation de l'As par les groupements thiols de la matière organique sont analogues aux mécanismes de complexation entre l'As(III) et la cystéine des protéines et peptides (Figure Intr. 4 et Figure Intr. 8a). L'As(III) perd ses groupements OH^- pour former une (ou des) molécule(s) d'eau avec le proton du groupement thiol :

$3H_3Cys + As(OH)_3 \rightleftharpoons (H_2Cys)_3As + 3H_2O$ log k = 29.8 (Rey et al., 2004).

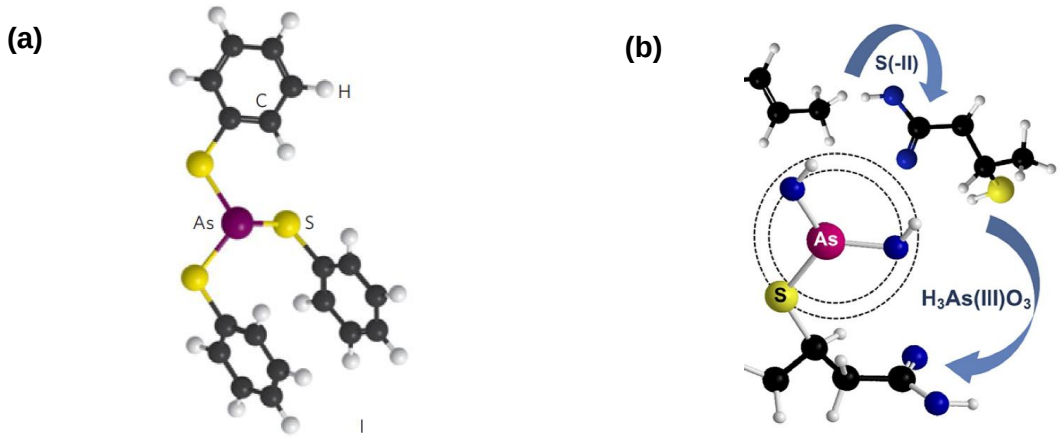

Figure Intr. 8 : Complexation de l'As(III) par (a) trois groupements thiols dans la matière organique et (b) un groupement thiol (Hoffmann et al., 2012; Langner et al., 2011a)

Le processus passif repose sur l'adsorption de l'As présent en solution sur les sites thiols présents à la surface de la matière organique. Dans ce cas, l'adsorption aboutirait à la formation d'un complexe monodentate entre un As(III) et un site SH (Figure Intr. 8b).

Les mécanismes indirects font intervenir soit, un cation, soit, un minéral (le plus souvent colloïdal) qui joue ici un rôle de pont entre l'As et la matière organique (Figure Intr. 9).

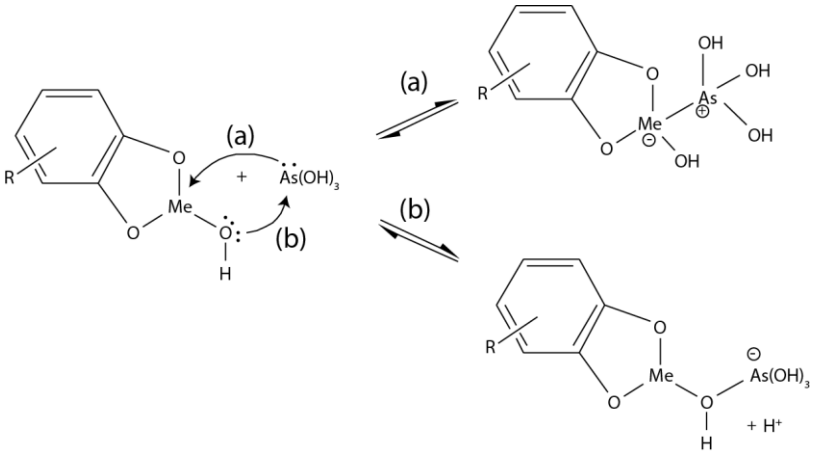

Figure Intr. 9 : Exemple de complexes ternaires entre l'As(III, V), un métal Me et la matière organique (Buschmann et al., 2006)

Ainsi, la présence de Fe(III) ionique ou sous forme d'oxydes augmente la complexation de l'As(V, III) par la matière organique, mettant en évidence la formation de complexes ternaires. Redman et al. (2002) et Bauer and Blodau (2006) ont montré que la concentration en As(V) complexé à la matière organique était fonction de la concentration en Fe présent dans la matière organique. Redman et al. (2002) ont également montré ces

résultats pour l'As(III) mais, celui-ci a fortement été réoxydé au cours des expériences rendant l'analyse des résultats plus difficile. En réalisant des expériences cinétiques entre l'As, l'hématite et les acides humiques, Ko et al. (2004) ont montré que l'As et la matière organique étaient en compétition pour leur complexation à la surface de l'hématite, confirmant les résultats précédents (Redman et al., 2002). Au contraire, en réalisant des expériences de complexation de l'As(III) par la matière organique en présence de Fe(III), Sharma et al. (2010) ont montré que 95% du Fe(III) et 94% de l'As(V) étaient présents dans la phase colloïdale contre 5% du Fe(III) et 6% de l'As(V) dans la phase dissoute. Mikutta and Kretzschmar (2011) ont observé que 25 à 70% de l'As(V) étaient liés aux complexes Fe(III)-MO par des complexes de sphère interne. De plus, les données spectroscopiques XAS (X-ray absorption spectroscopy) ont montré que l'As(V) était complexé sous forme de monodentate binucléaire dans lequel l'As(V) partageait deux atomes d'O avec deux octaèdres de Fe $Fe(O,OH)_6$; ce qui est en accord avec les données spectroscopiques de complexation de l'As(V) sur des oxyhydroxides de Fe. Des complexes mononucléaires stabilisés par une liaison hydrogène avec un groupe OH d'un octahèdre de $Fe(O,OH)_6$ adjacent ont également été observés dans ces échantillons, comme proposé pour la complexation de l'As(V) sur la goethite. De plus, il a été montré que l'As(III) était complexé à hauteur de 70 à 90 % au Fe sous forme oligomérique plutôt qu'à la ferrihydrite. Seulement deux études ont étudié la complexation de l'As(III) sous forme de complexes ternaires As-Fe-MO. Hoffmann et al. (2013) ont montré que l'As(III) était capable de former des complexes ternaires avec de la tourbe via du Fe(III) sous forme ionique. L'As(III) y est complexé sous forme de complexes bidentates mononucléaires avec le Fe(III) pour de faibles concentrations en Fe(III) et de bidentates mononucléaires et monodentates binucléaires pour de fortes concentrations en Fe(III). Ils ont par ailleurs calculé que les constantes de stabilité de ces complexes étaient plus faibles que celles des complexes formés entre l'As(III) et les sites thiols de la même tourbe. Par voix analytique, à l'aide d'un couplage SEC (chromatographie d'exclusion stérique)-UV-ICP-MS, Liu et al. (2011) ont mis en évidence

l'existence de complexes ternaires entre l'As(III), le Fe(III), probablement sous forme de ferrihydrite, et la matière organique (Figure Intr. 10).

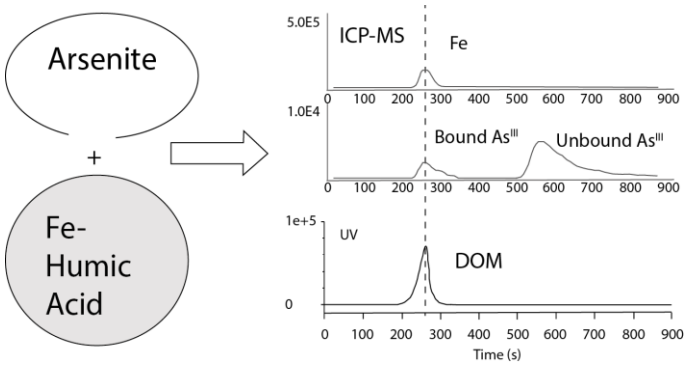

Figure Intr. 10 : Sortie concomitante de l'As(III), du Fe(III) et de la matière organique en sortie de colonne SEC-UV-ICP-MS attestant de la formation de complexes ternaires

Lenoble et al. (2015) ont expérimentalement observé que l'As(V) pouvait former des complexes ternaires avec le Ca et la matière organique alors que l'As(III) n'en formait pas. Enfin, Buschmann et al. (2006) ont montré que l'As et l'Al étaient en compétition pour leur complexation par la matière organique. Aucun complexe ternaire entre l'As(III, V) et l'Al(III)-MO ne semble donc possible.

A la vue, de toutes ces données de la littérature, il apparait donc que peu d'informations existent sur des relations possibles entre As(III), Fe(II) et matière organique qui sont les espèces majoritairement retrouvées dans les eaux anoxiques.

4. Objectifs et plan de la thèse

Considérant les problèmes engendrés par la contamination en As à travers le monde, il est important de mieux appréhender les processus responsables de sa dynamique, notamment dans les milieux riches en matière organique tels que les zones humides qui sont des sources potentielles d'As pour les eaux souterraines. Dans les zones humides, la réduction des oxydes de Fe porteurs d'As en période de saturation en eaux, entraine la solubilisation concomitante de Fe(II), d'As(III) et de matière organique. Si de nombreuses études se sont intéressées aux mécanismes de complexation de l'As(V) par la matière organique notamment, via des ponts ioniques ou sous forme colloïdale de Fe(III), peu

d'études ont été réalisées sur les interactions possibles entre l'As(III), le Fe(II) et la matière organique. Les objectifs de ce travail sont donc de mieux comprendre et d'expliquer les mécanismes de liaisons possibles entre l'As(III), le Fe(II) et la matière organique. L'As(III) a t-il la possibilité de se lier directement à la surface de la matière organique? Quel pourrait être le rôle du Fe(II)? La formation de complexes ternaires entre l'As(III), le Fe(II) et la matière organique, est-elle possible? Autant de questions dont les réponses permettront de mieux évaluer le rôle exact des zones humides dans la libération ou le piégeage de l'As.

Afin de répondre à ces questions, ce travail de thèse s'est organisé en trois parties. La première partie s'intéresse à la complexation directe de l'As(III) sur la matière organique. Elle repose principalement sur une étude expérimentale et de modélisation de la complexation de l'As(III) via les sites thiols de la matière organique. Elle visait à déterminer les mécanismes et les constantes de complexation entre l'As(III) et les groupements thiols de la matière organique. La deuxième partie s'intéresse à la complexation du Fe(II) par les acides humiques et fulviques. En effet, il n'existait que très peu de données dans la littérature, notamment quantitatives, concernant la complexation du Fe(II) par la matière organique.

Enfin, la dernière partie de ce travail porte sur la possibilité de former ou non des complexes ternaires entre l'As(III) et la matière organique via des ponts ioniques de Fe(II) mais aussi de Fe(III). Ces trois parties reposent sur un travail de laboratoire avec une approche méthodologique, expérimentale, qui a consisté à produire des jeux de données de complexation concernant non seulement, l'As(III) mais aussi, le Fe(II) par des acides humiques purifiés en présence ou non de Fe(II) et de Fe(III) en ce qui concerne l'As(III). Ces jeux de données ont ensuite été utilisés afin de déterminer les paramètres de complexation afin de tester différents mécanismes réactionnels à l'aide du modèle couplé PHREEQC/Model VI qu'il a fallu modifier pour certaines des études menées

Chapitre I : Complexation de l'arsenite par les groupements thiols de la matière organique

Ce chapitre correspond à un article publié dans la revue "Journal of Colloid and Interface Science": Thiol groups controls on arsenite binding by organic matter: new experimental and modeling evidence, Charlotte Catrouillet, Mélanie Davranche, Aline Dia, Martine Bouhnik-Le Coz, Rémi Marsac, Gérard Gruau (Journal of Colloid and Interface Science, Elsevier, 2015, 460, pp 310-320, doi:10.1016/j.jcis.2015.08.045)

Thiol groups controls on arsenite binding by organic matter:

new experimental and modeling evidence

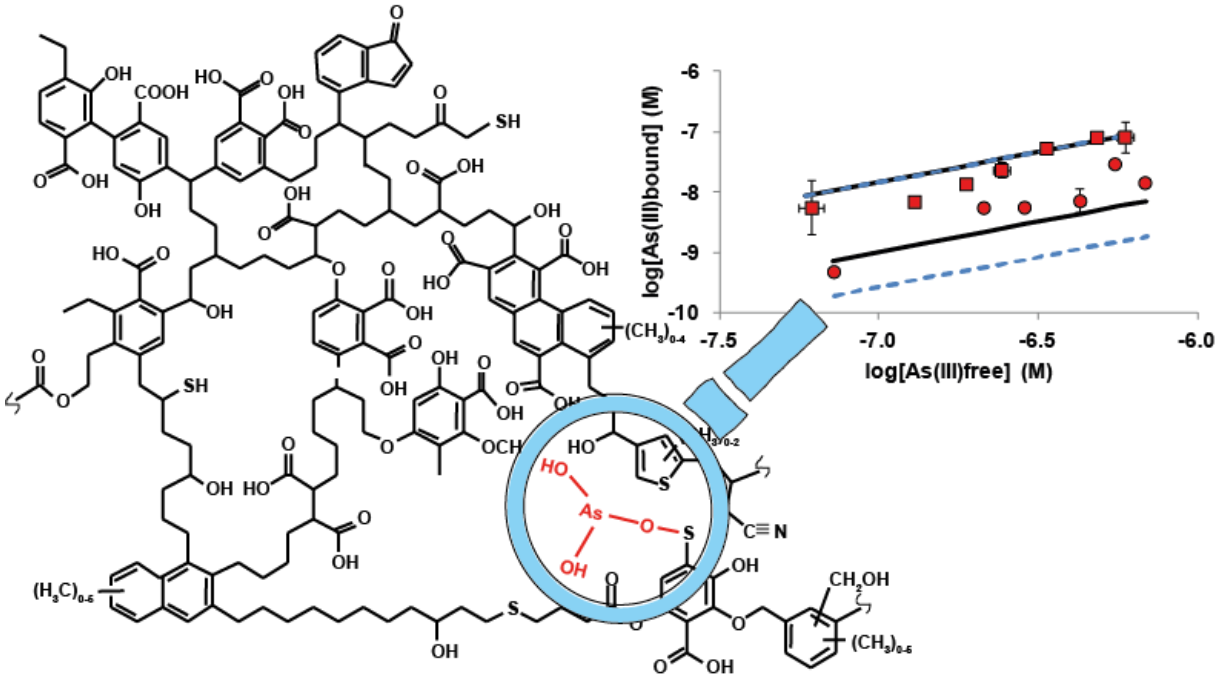

Complexation de l'As(III) par les sites thiols de la matière organique - As(III) complexation through thiol groups of organic matter

RESUME

Bien que plusieurs mécanismes aient été proposés pour la complexation directe de l'As(III) par la matière organique (MO), les groupements fonctionnels thiols des acides humiques (AHs) sont apparus récemment comme des ligands potentiels. Pour tester cette hypothèse, des isothermes d'adsorption d'As(III) sur des AHs, greffés ou non de sites thiols, ont été réalisées. Les concentrations d'As(III) complexées aux AHs sont faibles et dépendent de la densité en sites thiols. Les jeux de données expérimentales ont ensuite été utilisés afin de développer un nouveau modèle (PHREEQC-Model VI modifié), qui définit les AHs comme un ensemble de sites discrets carboxyliques, phénoliques et thiols. Dans un premier temps, il a fallu déterminer les constantes de protonation/déprotonation pour chaque groupe de sites à partir des AHs greffés ou non. La constante de protonation/deprotonation des sites thiols, $pK_{S,}$ correspond à celles des ligands organiques simples contenant des fonctions thiols. Deux modèles de complexation ont été testés, le modèle Mono, qui considère que l'As(III) est lié aux sites thiols des AHs sous forme de complexes monodentates, et le modèle Tri qui considère que l'As(III) est lié aux sites thiols des AHs sous forme de complexes tridentates. Les jeux de données disponibles dans la littérature ont été utilisés pour valider ou non les modèles. C'est, finalement, le modèle Mono, c'est-à-dire l'hypothèse de complexes monodentates qui permet de reproduire au mieux les données qui a donc été validé. Cette étude a mis en évidence l'importance des groupements thiols dans la réactivité de la MO et a permis de développer un modèle capable de déterminer les concentrations en As(III) directement liées à la MO.

ABSTRACT

Although it has been suggested that several mechanisms can describe the direct binding of As(III) to organic matter (OM), more recently, the thiol functional group of humic acid (HA) was shown to be an important potential binding site for As(III). Isotherm experiments on As(III) sorption to HAs, that have either been grafted with thiol or not, were thus conducted to investigate the preferential As(III) binding sites. There was a low level of binding of As(III) to

HA, which was strongly dependent on the abundance of the thiols. Experimental datasets were used to develop a new model (the modified PHREEQC-Model VI), which defines HA as a group of discrete carboxylic, phenolic and thiol sites. Protonation/deprotonation constants were determined for each group of sites (pK_A = 4.28 ± 0.03; ΔpK_A = 2.13 ± 0.10; pK_B = 7.11 ± 0.26; ΔpK_B = 3.52 ± 0.49; pK_S = 5.82 ± 0.052; ΔpK_S = 6.12 ± 0.12 for the carboxylic, phenolic and thiols sites, respectively) from HAs that were either grafted with thiol or not. The pK_S value corresponds to that of single thiol-containing organic ligands. Two binding models were tested: the Mono model, which considered that As(III) is bound to the HA thiol site as monodentate complexes, and the Tri model, which considered that As(III) is bound as tridentate complexes. A simulation of the available literature datasets was used to validate the Mono model, with log K_{MS} = 2.91 ± 0.04, i.e. the monodentate hypothesis. This study highlighted the importance of thiol groups in OM reactivity and, notably, determined the As(III) concentration bound to OM (considering that Fe is lacking or at least negligible) and was used to develop a model that is able to determine the As(III) concentrations bound to OM.

1 Introduction

According to the World Health Organization (WHO), arsenic (As) is known to be a major poison in the world. Even at low concentrations, As causes serious damage to human health such as cutaneous lesions (black foot disease), cancers (skin, lung, bladder, etc.), cardiovascular diseases, respiratory problems, etc. The main contamination process occurs through the consumption of As-contaminated water and the ingestion of contaminated crops (such as rice). Arsenic-contaminated water affects millions of people in Argentina, Bangladesh, Chili, China, United States, India, Mexico, etc. The abundance of As in the soil and water primarily depends on the geology and human activity (historic or current). As(III) is the most toxic inorganic form. Many studies have been performed to understand the mechanisms responsible for the contamination of water by As (Bauer and Blodau, 2009, 2006; Guo et al., 2011; Plant et al., 2004; Ritter et al., 2006). Wetlands and floodplains have

been highlighted as a source of As for the surrounding environments (Fendorf, 2010; Kocar, 2008; Polizzotto et al., 2005). Arsenic-rich sediments, in which As is bound to Fe-oxyhydroxides, are deposited in riparian wetlands and floodplains during flooding events. In the anoxic, organic-rich environments that characterize these zones, Fe-oxyhydroxides are reductively dissolved and the associated As is released into the soil solutions, and are then available for transfer in the underlying aquifers. However, there is a lack of information regarding the fate of As in this type of Fe(II), OM-rich solution. In such environments, OM is often discussed as a source of carbon for the heterotrophic bacteria able to reductively dissolve Fe-oxyhydroxides and solubilize the associated elements, such as As, or to directly reduce As(V) to As(III) in their detoxification metabolism (Akai et al., 2004; Islam et al., 2004; McArthur et al., 2004, 2001; Tufano et al., 2008). Organic matter is also shown to be a competitor of anions, such as arsenite, for their binding to the functional sites of Fe-oxyhydroxides (Bauer and Blodau, 2009; Grafe et al., 2001; Ko et al., 2004; Redman et al., 2002). Several studies present OM as a possible ligand for As(III), but no consensus exists about the nature of the exact direct or indirect mechanisms involved. Thanabalasingam and Pickering (1986) and Warwick et al. (2005) proposed that As(III) is bound to humic acid (HA) through cationic bridges involving Al, Fe and Ca impurities occurring in HA or by direct binding through HA amino groups. Using Suwannee River HA (SRHA), Buschmann et al. (2006) and Lenoble et al. (2015) hypothesized that As(III) could be bound to HA through its carboxyl and phenolic functional groups. Alcohols are able to bind As(III) by losing an OH^- (Holleman and Wiberg, 1995), suggesting that As(III) could be bound to phenolic groups of OM. Regarding the weaker and more abundant carboxylic groups, Buschmann et al. (2006) suggested that binding could occur through the formation of H-bridges between the OH^- group of $As(OH)_3$ and the =O part of the group without any OH loss. In their study, these authors also proposed that Fe might act as a bridge between As(III) and HA (Buschmann et al., 2006). Fakour and Lin (2014) and Liu and Cai (2010), through experimental and modeling approaches, hypothesized that As(III) was bound to HA by two kinds of binding sites, one strong and one weak.

More recently, spectroscopic and experimental studies have suggested that thiols (SH^-) could play an important role in As(III) binding to peat and HA (Hoffmann et al., 2012; Langner et al., 2011a). These authors demonstrated that As(III) is bound to tridentate or monodentate complexes via thiol groups, depending on the selected peat and HA. By spiking HA and peat with bisulfides, Hoffmann et al. (2012) showed that As(III) binding increased with increasing bisulfide concentrations. Using EXAFS, they provided evidence of the formation of a monodentate thiol-As(III) complex on S(-II)-spiked HA and peat. Conversely, Langner et al. (2011a) used EXAFS data to show that As(III) is bound to three S in peat from Gola di Lago (Switzerland). The different complexes might be explained by differences in the origin of the organic matter (OM). In the Gola di Lago peatland, peat was formed in an As-enriched environmental context. Arsenic was absorbed by plants and/or microorganisms, which were the precursors of the peat. In these precursors, As was bound to proteins, enzymes, etc., mainly as tridentate complexes with the SH^- group of cystein; a configuration that seems to be conserved in the peat structure (Hoffmann et al., 2012). The binding of As(III) with thiol is not surprising considering that As(III) is bound to dithiol and trithiol sites in many proteins and peptides (Cavanillas et al., 2012; Gaber and Fluharty, 1972; Kitchin and Wallace, 2008; Rey et al., 2004; Spuches et al., 2005a; Starý and Růzicka, 1968; Zahler and Cleland, 1968; Zhao et al., 2012), either completely or partly inhibiting their specific actions in the body.

Here, we present a new contribution to evaluate the role of thiol sites in the binding of As(III) to OM. More specifically, considering the recent spectroscopic studies, we tried to determine the mechanisms of complexation between As(III) and the thiol groups in HA (the formation of mono- or tridentate complexes), using experimental and modeling approaches. Arsenic(III) was reacted with three samples of HA containing different concentrations of thiol sites. The experimental dataset was subsequently used to test the hypothesis of As(III)-HA binding through mono or tridentate complexes via HA thiol groups, using a combination of the PHREEPLOT (fitting program) and PHREEQC-Model VI programs. No model is currently available in the literature to describe the interactions between As(III) and organic matter. In a

first step, the thiol groups had to be described and their binding parameter was introduced in PHREEQC-Model VI. Finally, the extrapolated binding parameters from the hypothesis of mono- or tridentate As(III)-thiol (HA) complexes were tested using the whole datasets available in the literature to identify the more valuable binding mechanisms. The goal of the model developed in the present study is to determine the speciation of As(III) in OM-rich water.

2 Experimental, analytical and modeling methods

2.1 Reagents and materials

All aqueous solutions were prepared with analytical grade Milli-Q water (Millipore). The As(III) solutions were prepared with sodium arsenite ($NaAsO_2$) from Sigma Aldrich. The S(-II) solution was prepared with sodium sulfide nonahydrate ($Na_2S.9H_2O$) from Sigma Aldrich. NaOH, HCl and HNO_3, all sub-boiling ultrapure grade, came from Fisher Chemical, Merck and VWR, respectively.

Humic acids corresponded to the standard HA purified Leonardite from the International Humic Substance Society (IHSS) and the Aldrich HA (AHA) from Sigma Aldrich, which have different concentrations of S. To remove humins from the humic and fulvic acids, AHA was purified (PAHA) using the method described by Vermeer et al. (1998). Prior to the experiments, molecules < 10 kDa were removed using a Labscale TFF system equipped with a Pellicon XL membrane (PGCGC10, Millipore^{TM}) for the two standard solutions used (Leonardite and AHA).

All materials were soaked in 10% HNO_3 and then rinsed with deionized water twice overnight.

2.2 Experimental setup

Thiol grafting experiment. To obtain HA with different concentrations of thiol groups (S(-II)), S(-II) were sorbed to Leonardite using a dialysis bag (pore size = 12-14 kDa) at a ratio [S(-II)]/[DOC] ≈ 6 mmolS/molC, as was done previously in a precedent study (Hoffmann

et al., 2012). No grafting was performed for PAHA because of its natural high concentration in S. Humic acids and the S(-II) solutions were placed inside the membrane, whereas S(-II) was outside. The pH was maintained at 6 and the ionic strength (IS) was fixed at 0.05 M with NaCl. The Leonardite grafted with thiol groups will be noted S(-II)-Leonardite hereafter. To prevent any oxidation of S(-II), the experiments were performed in a Jacomex isolator glove box. The concentration of S(-II) outside of the membrane was monitored using an ionometric method. Ten mL of solution was sampled and mixed with SAOB (Sulphide AntiOxidant Buffer) at a 1:1 ratio. The concentration of S(-II) was measured outside of the glove box using a sulfide combined electrode (9616BNWP from Thermo Scientific). The grafting experiment continued until all S(-II) had disappeared from the solution outside of the membrane.

Humic acid titrations. Acid-base potentiometric titrations of the Leonardite and S(-II)-Leonardite were performed using an automatic pH stat titrator (Titrino 194, Metrohm) equipped with burettes of 0.1 M NaOH and HCl solutions. The detailed method is described elsewhere (Avena et al., 1999). Fifty mL of 1 g L^{-1}(DOC) was titrated at three IS, 0.001, 0.01 and 0.1 M NaCl with 0.1 M of the NaOH and HCl solutions. Because the addition of NaOH/HCl continuously modified the IS, this latter was re-calculated for each titration point and used to calculate the H^+ and OH^- concentrations. To avoid any oxidation and carbonate addition, the solutions were continuously bubbled with nitrogen (N_2). To prevent any hysteresis, three titrations were performed, one after another. Only the second titration was used for the modeling calculations. The HA charge was calculated as follows:

$$Q = [\text{Acid}] - [\text{Base}] - ([H^+]-[OH^-]) \quad \text{(Eq. 1)}$$

with [Acid], [Base], $[H^+]$ and $[OH^-]$ equal to the concentration of HCl and NaOH added, and where free H^+ is calculated as $[\mathrm{H}^+] = \frac{10^{-\mathrm{pH}}}{\gamma(\mathrm{H}^+)}$ and free OH^- is calculated as $[\mathrm{OH}^-] = \frac{10^{(-14+\mathrm{pH})}}{\gamma(\mathrm{OH}^-)}$.

As(III)-HA binding experiments. A standard batch equilibrium method was used. Three adsorption isotherm experiments were carried out with 5 to 50 µg L^{-1} of As(III) and 55.76, 50.12 and 56.02 mg L^{-1} of average dissolved organic carbon (DOC) for Leonardite, S(-

II)-Leonardite and PAHA, respectively. To ensure anoxic conditions, experiments were performed in a Jacomex isolator glove box. The pH was fixed at 6 with ultrapure HCl and NaOH. The pH was monitored with a multi-parameter Consort C830 analyzer equipped with a combined electrode from Bioblock Scientific (combined Mettler InLab electrode). Calibrations were performed with WTW standard solutions (pH = 4.01 and 7.00 at 25°C). The accuracy of the pH measurements was ± 0.05 pH units. The $[As(III)]_{tot}$, pH and DOC values used in these experiments corresponded to values that can be encountered in reduced wetland water (Bauer and Blodau, 2009; Fakih et al., 2009). The IS of all experiments was fixed at 0.05 M with NaCl electrolyte solution. Experimental solutions were stirred for 48h to reach equilibrium (determined from preliminary kinetic experiments). Then, 15 mL of solution was sampled and ultrafiltrated at 5 kDa (Vivaspin VS15RH12, Sartorius) by centrifugation at 2970 g for 30 min under N_2 atmosphere. Ultracentrifugation cells were previously washed with Milli-Q water to obtain a DOC concentration < 1 mg L^{-1} in the ulltrafiltrate. Each isotherm experiment was conducted in triplicate.

2.3 Chemical analyses

All measurements were performed at Géosciences Rennes, University of Rennes I, France. DOC concentrations were determined using an organic carbon analyzer (Shimadzu TOC-V CSH). The accuracy of the DOC measurements was estimated at ± 5% for all samples using a standard solution of potassium hydrogen phtalate. Arsenic concentrations were determined by ICP-MS using an Agilent Technologies 7700x at Géosciences Rennes. All samples were previously digested twice with 14.6 N HNO_3 and H_2O_2 ultra-pure grade at 90°C, then evaporated to complete dryness and finally resolubilized with HNO_3 at 0.37 mol L^{-1} to avoid any interference with DOC during the analysis. ICP-MS analyses were carried out using a He gas collision cell to reduce the $^{40}Ar^{35}Cl/^{75}As$ ratio, allowing a low detection limit to be reached for the As analysis (LD As: 0.003 µg L^{-1}). Instrumental and data acquisition parameters can be found in the ANNEXE 1. Quantitative analyses were performed using a conventional external calibration procedure (seven external standard multi-element solutions

- Inorganic Venture, USA). A mixed solution of rhodium-rhenium at 300 ppb was used as an internal standard for all measured samples to correct any instrumental drift and matrix effects. Calibration curves were calculated from the intensity ratios between the internal standard and the analyzed elements. A SLRS-5 water standard was used to check the accuracy of the measurement procedure, and the instrumental error on the As analysis was established as below 5%. Chemical blanks of As were below the detection limit (0.003 µg L^{-1}), and were thus considered as negligible.

To ensure that no oxidation occurred during the experiments, the concentrations of As(III) and As(V) were checked. The As species were separated and the As(III) concentrations were determined in the ultrafiltrate ($[As(III)]_{UF}$) through High Performance Liquid Chromatography (HPLC-Agilent 1260 Infinity) equipped with an anion exchange resin column (Agilent G3154-65001) coupled with ICP-MS. Quantitative analyses were performed using an injection of mixed standard solutions As(III, V) (Inorganic venture, USA) to determine the calibration curves. The total As concentrations in the mixed As(III)-HA solutions were only measured by ICP-MS using the above described procedure (with no estimation of the speciation). The HPLC column retains OM, which prevents any quantitative measurement of As(III) in this fraction from being taken. The accuracy of the $[As(III)]_{UF}$ and $[As(III)]_{tot}$ measurements was estimated at less than 5% above a concentration of As(III) of 1 µg L^{-1} (all samples). The As(III) concentrations in the ultrafiltrates were assumed to be inorganic As(III), whereas As(III) bound to HA (As(III)-HA) was considered to be in the retentate fraction > 5 kDa. The fraction of As(III) bound to HA ([As(III)-HA]) was calculated as $[As(III)\text{-}HA] = [As(III)]_{tot} - [As(III)]_{UF}$, with $[As(III)]_{tot}$, the As concentration in the HA-As(III) solutions prior to ultrafiltration and $[As(III)]_{UF}$, the As concentration in the ultrafiltrate as determined with the ICP-MS.

The amounts of S and organic C in Leonardite and S(-II)-Leonardite and PAHA were determined at the "Laboratoire d'analyses des Sols d'Arras" (INRA, Arras, France) by dry combustion (ISO 10694) and ICP-AES (ISO 22036), respectively.

2.4 Determination of the PHREEQC-Model VI binding parameters

2.4.1 Thiol implementation in PHREEQC-Model VI and the models used

A new model was developed to implement the thiol groups in PHREEQC-Model VI. PHREEQC-Model VI described humic substances as a set of discrete functional sites that can be divided into groups of weak and strong sites (Tipping, 1998). Weak sites are usually assumed to be carboxyl groups, whereas strong sites are generally assumed to consist of phenolic and N-containing sites. In the original Model VI, the binding of metals by humic substances occurs through eight discrete sites: four weak sites, named A sites and four strong sites, named B sites. In the present study, to implement the thiol group, we added four thiol groups, named S sites. The abundances of the type A, B and S sites are named n_A, n_B and n_S (mol g^{-1}), respectively. The intrinsic proton dissociation constants for the type A, B and S sites and their distribution terms are pK_A, pK_B, pK_S, ΔpK_A, ΔpK_B and ΔpK_S, respectively. The fractions of sites that can make bidentate sites and tridentate sites are named f_B and f_T and are equal to 0.5 and 0.065, respectively (Tipping, 1998). The abundances calculated for the 84 sites (monodentates, bidentates and tridentates) are given in Annexe II 1 and 2.

The proton association/dissociation equations and calculations of pK (equilibrium constant) for the 12 groups (carboxylic, phenolic and thiol) are described in the Annexe II 2. The protonation/deprotonation of the bidentates and tridentates are described as the decomposition of both protonation/deprotonation of the monodentates and the associated pK. For example, for the bidentate Ha_ab, the reaction and pK are:

$Ha\_abH_2 = Ha\_abH^- + H^+ \qquad pK = pK(a) = pK_A - \frac{\Delta pK_A}{2}$ (Eq. 2)

$Ha\_abH^- = Ha\_ab^{2-} + H^+ \qquad pK = pK(b) = pK_A - \frac{\Delta pK_A}{6}$ (Eq. 3)

Ion sorption by humic substances is described by the specific complexation parameters log K_{MA}, log K_{MB} and log K_{MS} for the carboxylic, phenolic and thiol sites, respectively. In this study, only the binding of the As(III)-thiol groups was studied, and therefore, only the binding parameter log K_{MS} was determined. It is important to note that the binding reaction of each thiol with As(III) is characterized by a stability constant log K, where

log K_{MS} is the binding parameter for all the HA thiol sites defined in the modified PHREEQC-Model VI. Two models of As(III) binding by HA were tested. They consisted of $As(OH)_3$ binding by HA: (i) as monodentate complexes via one HA thiol site (Mono Model) and (ii) as tridentate complexes via three HA thiol sites (Tri Model). The Mono model is based on the spectroscopic results obtained elsewhere (Hoffmann et al., 2012), showing 0.5 to 1.5 S in the first neighbor shell of As(III) bound to HA. The Tri model is based on the 1:3 complexes evidenced in the binding of As(III) with proteins (Cavanillas et al., 2012; Gaber and Fluharty, 1972; Kitchin and Wallace, 2008; McSweeney and Forbes, 2014; Rey et al., 2004; Spuches et al., 2005a; Starý and Růzicka, 1968; Zahler and Cleland, 1968; Zhao et al., 2012). The binding of As(III) with proteins is described as a deprotonation of three thiol groups in the cystein units and the loss of the three OH^- in $As(OH)_3$. The same mechanism was used in a study on $As(OH)_3$ complexation to thiol grafted amberlite resin (Hoffmann et al., 2014). In the Mono model, only monodentates with thiol sites are defined, therefore, only four log K were fitted. The binding mechanism of $As(OH)_3$ by monodentate complexes with HA was adapted for the binding of a neutral species and was described by the following reaction for the binding of $As(OH)_3$ by the site i:

$$Ha\_iH + As(OH)_3 = Ha\_iAs(OH)_2 + H_2O \qquad \log K(i) = \log K_{MS} - \frac{\Delta LK_{1S}}{2} \quad \text{(Eq. 4)}$$

The other reactions describing the binding of $As(OH)_3$ by monodentate complexes are described in the Annexe II 1. In the Tri model, As is bound as tridentate with only three thiol groups (i.e. no tridentate with a combination of thiol, carboxylic and phenolic sites), therefore, only four log K were fitted. The binding mechanism between the ijk site and $As(OH)_3$ is written as:

$$Ha\_ijkH_3 + As(OH)_3 = Ha\_ijkAs + 3\ H_2O \qquad \log K(ijk) = 3 * \log K_{MS} - \frac{\Delta LK_{1S}}{2} \text{ (Eq. 5)}$$

The other reactions concerning the binding mechanisms between the tridentate sites and $As(OH)_3$ are described in Annexe II 2.

2.4.2 Electrostatic model

Previous studies, where Models V, VI or VII were coupled to PHREEQC, attempted to convert this empirical electrostatic humic ion-binding model into the diffuse layer model (DLM) formalism (Appelo and Postma, 2005; Catrouillet et al., 2014; Liu et al., 2008; Marsac et al., 2014, 2011). This type of conversion requires the calculation of a surface area (A) that depends on the ionic strength similar to the calculations made for polyelectrolytes such as polyacrylic acid (Lützenkirchen et al., 2011). However, these approaches usually lead to surface areas that are physically unrealistic (e.g. $A_{HA} > 10^4$ m² g^{-1}) for HA (Appelo and Postma, 2005; Catrouillet et al., 2014; Liu et al., 2008; Lützenkirchen et al., 2011; Marsac et al., 2014, 2011). Therefore, it may not be appropriate to use the DLM to implement the humic ion-binding models of Tipping and coworkers in PHREEQC. Instead, the constant capacitance model (CCM) was used. The CCM is a very simple electrostatic model in which the capacitance (C, in F m^{-2}) is an adjustable parameter that varies with the IS (Lützenkirchen, 1999). Specifically, the CCM employs a linear relationship between the surface charge density (σ_0, in C m^{-2}) and the surface potential (Ψ_0, in V), $\sigma_0 = C \times \Psi_0$.

However, the CCM is not defined in PHREEQC and had therefore to be implemented in PHREEQC-Model VI. To do this, we modified the TLM (triple layer model) in PHREEQC to only consider the capacitance of the 1-plane, C_1 (F m^{-2}). In the TLM model, the capacitance of the 2-plane C_2 was set to a very large value ($C_2 \approx \infty$) to be annulled. In the resulting model (i.e. a basic Stern model), if the surface area A (m^2 g^{-1}) is multiplied by a large factor X (e.g. $X = 10^7$), the double layer is suppressed. The new surface area is A' = (A×X) and the surface charge density at the 0-plane is $\sigma_0' = (\sigma_0 / X) = (C_1 \times X) \times \Psi_0$ (C m^{-2}). The charge at the 0-plane (in eq g^{-1}) is $Z_0 = A \times \sigma_0 / F = A' \times \sigma_0' / F$, where F is Faraday's constant (in C mol^{-1}). At the 0-plane, then: $Z_0 = A' \times (C_1/X) \times \Psi_0 / F$. By setting the new capacitance in PHREEQC as $C_1' = C_1/X$, the charge-potential relationship remains unchanged for the 0-plane, whereas the diffuse layer is suppressed by the high A' value. This approach results in the CCM.

In Model VI (Tipping, 1998), the electrostatic term $F\times\Psi/(R\times T)$ is replaced by $2\times P\times Z\times \log I$, where I is the IS (mol L^{-1}) and P is an adjustable parameter (generally $-400 < P < -100$) that only depends on the humic substance considered (e.g. composition, origin). Then, the charge-potential relationship is: $Z = F\times(2\times R\times T\times P\times \log I)^{-1}\times\Psi$. In fact, the latter Z-Ψ relationship is similar to the CCM in which the capacitance $C_1 = F^2\times(2\times R\times T\times P\times A\times \log I)^{-1}$. As the parameter P is negative, C_1 is a function of -1/log I. The capacitance C_1 thus increases with I (IS). According to the molar mass and the radius of HA (15000 g mol^{-1}; 1.72 nm) in Model VI, the surface area of HA (A_{HA}) is 1500 $m^2\ g^{-1}$. C_1 can therefore vary from 0.6 F m^{-2} (for P = -400, I = 10^{-4} M) to 9.4 F m^{-2} (for P = -100, I = 10^{-1} M), within the same order of magnitude as the minerals (Lützenkirchen, 1999).

Ion accumulation in the vicinity of HA is calculated with a Donnan model. The Donnan volume (V_D) is the surface area multiplied by the thickness of the accumulation layer. This thickness is approximated by the Debye-Hückel parameter κ, where $\kappa^{-1} = (3.29x10^9xI^{1/2})^{-1}$. Because working with the CCM in PHREEQC/Model VI requires an unrealistic surface area value, a thickness $L = \kappa^{-1}/X$ must be used in PHREEQC/Model VI to keep a realistic V_D value. For HA: $V_D = A_{HA} \times \kappa^{-1} = A' \times L$. Here, A = 10^7 $m^2\ g^{-1}$, therefore $L = 1.5 \times 10^{-4} \times (3.29\times10^9\times I^{1/2})^{-1} = 1.44 \times 10^{-12}$ m for I = 10^{-3} M. V_D is therefore equal to 1.44×10^{-5} $m^3\ g^{-1}$ (or 14.4 L kg^{-1}). V_D is within the same magnitude order as V_D in NICA-Donnan, which varied from 1 to 80 L kg^{-1} (Kinniburgh et al., 1999). Table I. 1 summarizes the parameters defined for the CCM model in the modified PHREEQC-Model VI.

Table I. 1: Summary of the different parameters of the model.

Electrostatic model			
C_1	**C_2**	**A (m²/g)**	**L (m)**
$F^2 \times (2 \times R \times T \times P \times A \times \log I)^{-1}$	∞	∞	$A_{HA} \times \kappa^{-1} \times A^{-1}$
Model of fit			
	Leonardite		**S(-II)-Leonardite**
n_A	Fitted		
n_B	$\frac{n_A}{2}$		
n_S	fixed from $3.22\ 10^{-5}$ to $1.61\ 10^{-4}$		fixed from $1.96\ 10^{-3}$ to $2.09\ 10^{-3}$
pK_A	Fitted		
ΔpK_A	Fitted		
pK_B	Fitted		
ΔpK_B	Fitted		
pK_S	Fitted		
ΔpK_S	Fitted		

2.4.3 Fitting the binding parameters

The PHREEQC-Model VI binding parameters were fitted using the program PHREEPLOT (Catrouillet et al., 2014) using the experimental datasets recovered from the titrations and isotherm experiments. The 84 types of sites defined in PHREEQC-Model VI as well as the 84 complexation reactions with H^+ were added in the "minteq.v4" database. Humic acids were defined as SOLUTION_MASTER_SPECIES, SOLUTION_SPECIES and PHASES. The modeling procedure was designed to determine: (i) the intrinsic proton dissociation constants, the distribution terms and the abundance (n) of the A, B and S type sites (Leonardite and S(-II)-Leonardite), and (ii) the specific binding parameters of the thiol groups for As(III), (Leonardite, S(-II)-Leonardite). The binding parameters were determined for Mono and Tri models, respectively. However, this set of parameters was large and had to be decreased to better constrain the model. The abundance parameter for the phenolic groups (n_B) was set to half of the abundance parameter (n_A) for the carboxylic groups, as proposed by Tipping (1998). This assumption is in agreement with the proportion determined in the literature (Thurman, 1985) and in several ion-OM binding models (Gustafsson, 2001; Tipping and Hurley, 1992). The parameter n_S was considered to be minor compared to n_A and n_B and regards to the total concentration of S (S_{tot}) in humic acids (0.76% of S in IHSS Leonardite). Only a part of S_{tot} occurs as thiol sites, which were supposed to be the more

reactive groups regards to As(III) binding. The concentration of thiol groups, namely n_S, could be estimated from S_{tot} and from the % thiol, as :

$$n_S = \text{thiol \%} * S_{tot} \quad \text{(Eq. 6)}$$

If the thiol % was not determined for the used Leonardite HA, a range of thiol % was available in the literature for various HA (Dong et al., 2010; Haitzer et al., 2003; Jiang et al., 2015; Manceau and Nagy, 2012; Qian et al., 2002; Rao et al., 2014; Xia et al., 1998), mainly determined from XAS records. This range varied from 10 to 50 % of S_{tot} as thiol groups. Therefore, to estimate the H^+ dissociation constant and binding parameters of As(III) with Leonardite, 5 fits were performed on this range, namely with n_S = 10, 20, 30, 40 and 50% * S_{tot}. For this 5 fits, n_S parameter for Leonardite and n_S' for S(-II)-Leonardite were calculated as:

$$n_S = \text{thiol \%} * S_{tot}(\text{Leonardite}) \quad \text{(Eq. 7)}$$

$$n_S' = S_{tot}(\text{S(-II)-Leonardite}) - S_{tot}(\text{Leonardite}) + n_S$$

$$n_S' = S_{tot}(\text{S(-II)-Leonardite}) - S_{tot}(\text{Leonardite}) + \text{thiol \%} * S_{tot}(\text{Leonardite}) \quad \text{(Eq. 8)}$$

The binding parameter log K_{MS} was fitted from isotherm datasets using the combination of PHREEPLOT/PHREEQC-Model VI for the various thiol % (n_S = 10, 20, 30, 40 or 50% * S_{tot}). In the model's hypothesis, no strong bidentates and tridentates are possible, and the strong site parameter of the thiol groups, ΔLK_2 did not need to be fitted. However, we had to attribute a value to the ΔLK_1 of thiol (ΔLK_{1S}). We chose to fix ΔLK_{1S} to the ΔLK_1 of the strong site used by Tipping (1998): $\Delta LK_{1B} = \Delta LK_{1S} = 0.8$. Arsenic(III) log K_{MS} was optimized using the weighted sum of squares of the residuals, RMSE (Root Mean Square Error). The stability constants of the four thiol sites - log K (monodentates or tridentates) - defined in PHREEQC-Model VI were calculated from log K_{MS} and ΔLK_{1B} (see Annexe II 6).

2.4.4 Dataset from the literature

Seven literature datasets were used to compare both tested models (Fakour and Lin, 2014; Hoffmann et al., 2012; Kappeler, 2006; Lenoble et al., 2015; Liu and Cai, 2010; Thanabalasingam and Pickering, 1986; Warwick et al., 2005). The abundance of the thiol

sites, n_s, had to be determined for each dataset. Manceau and Nagy (2012) determined, from XANES fitting, that 23.6% of S is as exocyclic form in SRHA. We supposed here that this % corresponds to the thiol %. For Hoffmann et al. (2012), the thiol concentrations were determined by the authors. However, since no XANES data were available for PAHA and AHA, modeling calculations were thus performed on a thiol % range (n_S = 10, 20, 30, 40 and 50% * S_{tot}) with S_{tot} equal to 2.33%, 4.2% and 0.54% for PAHA (Kim et al., 1990), AHA (Arnold et al., 1998) and SRHA (value from IHSS), respectively.

3 Results

3.1 S(-II) grafting and titration

After S(-II) addition, the concentration of [S(-II)] outside of the dialysis membrane decreased and reached 0 after about 20h (Figure I. 1). For the titration and isotherm experiments, the S(-II)-Leonardite stock solution was sampled after 24h of grafting and was used immediately.

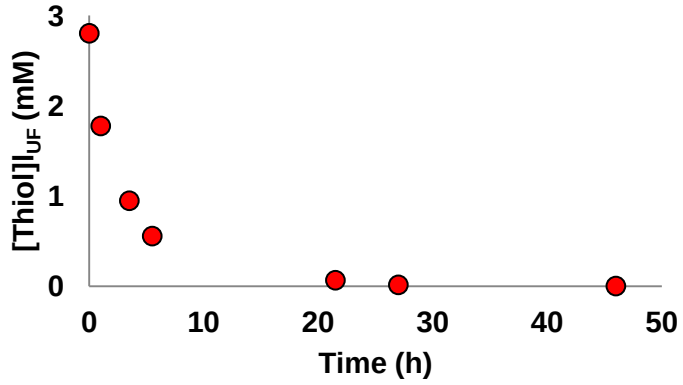

Figure I. 1: Thiol group grafting (mmol L^{-1}) over time expressed in hours

The titrations of Leonardite and S(-II)-Leonardite for three IS are plotted in Figure I. 2. The global charge decreased with increasing pH. At basic pH, the charge Q was more negative for S(-II)-Leonardite than for Leonardite (at pH = 10, Q(S(-II)-Leonardite) = -4.32 meq g^{-1} versus Q(Leonardite) = -2.98 meq g^{-1}). This difference in charge, Q(S(-II)-Leonardite) - Q(Leonardite) = -4.32 + 2.98 = -1.34 meq g^{-1}, corresponds to the charge developed by the thiol groups added to the Leonardite during the grafting.

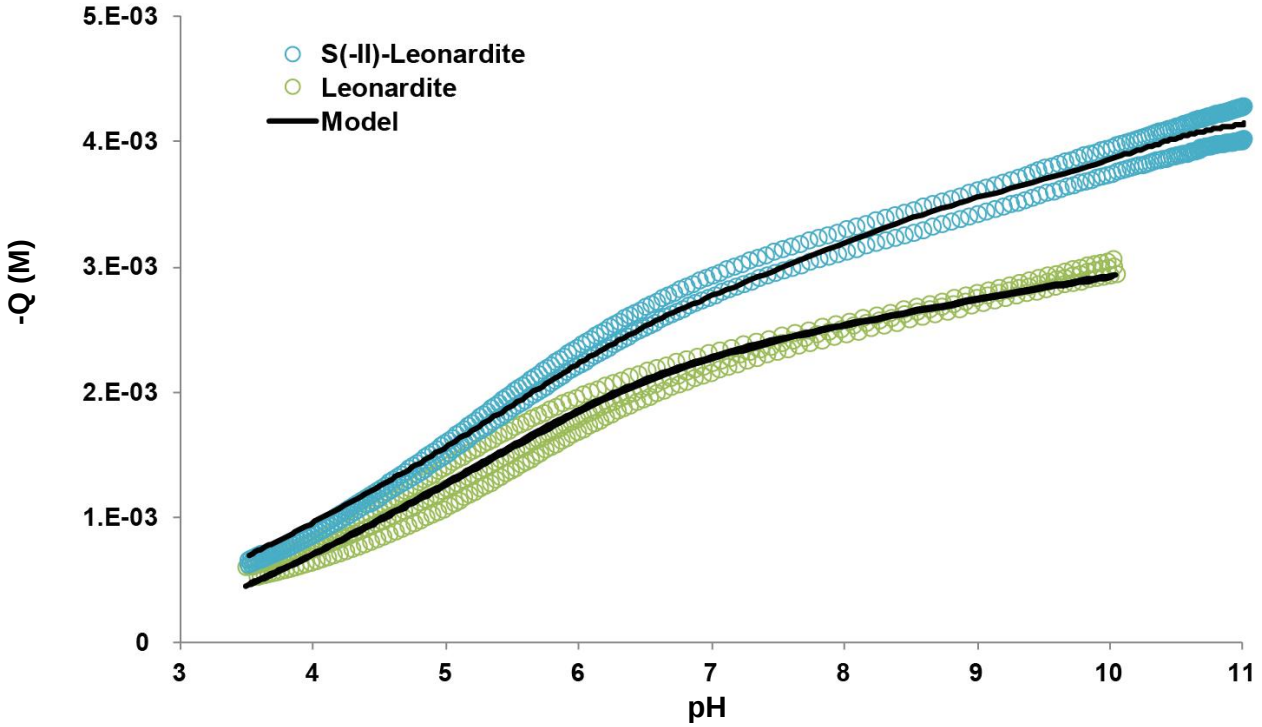

Figure I. 2: Titrations of Leonardite (shown as green symbols) and S(-II)-Leonardite (shown as blue symbols) as compared to the modeling (shown as black lines).

3.2 Adsorption isotherms

From the As(III) and As(V) concentrations measured in the ultrafiltrate, it can be observed that no oxidation occurred in any of the samples. Figure I. 3 presents the adsorption isotherms of As(III) by Leonardite and S(-II)-Leonardite (log[As(III)-HA] relative to log [As(III)]). No plateau was reached for either HA. The percentage of As(III) bound to the Leonardite was below 5%, and between 5 and 15% for the S(-II)-Leonardite. The adsorption of As(III) was clearly stronger for S(-II)-Leonardite than for Leonardite. The highest concentration of bound As to S(-II)-Leonardite confirmed that the addition of thiols to HA increased its binding capacity with regards to As(III).

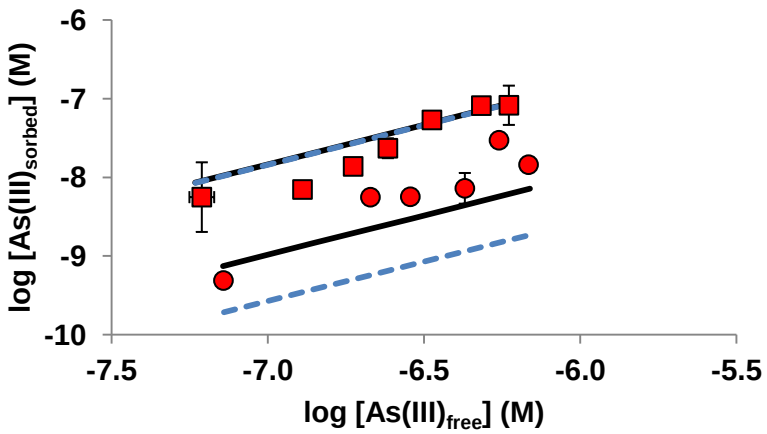

Figure I. 3: Experimental and modeled datasets of Leonardite and S(-II)-Leonardite

3.3 H-HA model

To determine the quality of the fit between the measured and modeled data using PHREEQC/Model VI, RMSE values were calculated according to RMSE = $\sqrt{\text{mean}((\log\mu(\text{exp}) - \log\mu(\text{cal}))^2}$, with logμ(exp) and logμ(cal) representing the logarithm of the charge (or concentration) of the experimental data and modeled data, respectively. For the titration dataset, the RMSE was 0.03 for all calculated n_S, indicating that the fitted H^+ binding parameters were able to reproduce the experimental dataset. The protonation/deprotonation parameters for the carboxylic and phenolic groups are listed in Table I. 2 for the various thiol %. The protonation/deprotonation parameters were in the range of the standard deviation (±) of the model. They were within the same range as the parameters given by Tipping (1998) for Model VI, except for n_A and pK_B, the reasons for which are discussed below in the discussion section.

Table I. 2: Values of the protonation/deprotonation parameters of the three sites (A: carboxylic groups, B phenolic groups and S thiol groups). Values in bold are fixed.

	n_S = 10%*S_{tot}	n_S = 20%*S_{tot}	n_S = 30%*S_{tot}	n_S = 40%*S_{tot}	n_S = 50%*S_{tot}	Tipping (1998) (Table V)
n_A	$2.01\ 10^{-3} \pm 3\ 10^{-5}$	$1.99\ 10^{-3} \pm 2\ 10^{-4}$	$1.97\ 10^{-3} \pm 3\ 10^{-5}$	$1.96\ 10^{-3} \pm 8\ 10^{-5}$	$1.94\ 10^{-3} \pm 3\ 10^{-5}$	$2.5\ 10^{-3}$ - $4.3\ 10^{-3}$
pK_A	4.26 ± 0.02	4.26 ± 0.03	4.26 ± 0.02	4.28 ± 0.03	4.28 ± 0.03	3.8 - 4.3
ΔpK_A	2.11 ± 0.08	2.12 ± 0.09	2.10 ± 0.09	2.13 ± 0.10	2.14 ± 0.11	0.1 - 3.4
n_B	**0.5 n_A**	**0.5 n_A**	**0.5 n_A**	**0.5 n_A**	**0.5 n_A**	**0.5 nA**
pK_B	7.12 ± 0.15	7.10 ± 0.15	7.07 ± 0.16	7.11 ± 0.26	7.10 ± 0.16	8.3 - 8.9
ΔpK_B	3.33 ± 0.23	3.41 ± 0.12	3.36 ± 0.23	3.52 ± 0.49	3.57 ± 0.10	3 - 4.6
n_S	**$3.22\ 10^{-5}$**	**$6.44\ 10^{-5}$**	**$9.66\ 10^{-5}$**	**$1.29\ 10^{-4}$**	**$1.61\ 10^{-4}$**	Not determined
n_S'	**$1.96\ 10^{-3}$**	**$2.00\ 10^{-3}$**	**$2.03\ 10^{-3}$**	**$2.06\ 10^{-3}$**	**$2.09\ 10^{-3}$**	
pK_S	5.82 ± 0.04	5.84 ± 0.04	5.84 ± 0.04	5.82 ± 0.05	5.82 ± 0.04	
ΔpK_S	6.14 ± 0.14	6.12 ± 0.14	6.15 ± 0.14	6.12 ± 0.12	6.12 ± 0.14	
RMSE	0.03	0.03	0.03	0.03	0.03	

3.4 As-HA model

Using the protonation/deprotonation constants of the 12 (carboxylic, phenolic and thiol) binding sites of HA for each thiol abundance, the binding parameter for the thiol groups (log K_{MS}) was determined using the dataset from the Leonardite and S(-II)-Leonardite isotherm experiment. The log K_{MS} calculated with the Mono model, which hypothesizes the complexation of As(III) by HA through monodentate complexes only, was equal to 2.93 (n_S = 10% * S_{tot}), 2.92 (n_S = 20 and 30% * S_{tot}) and 2.91 (n_S = 40 and 50% * S_{tot}) whereas it varied from 2.93 (n_S = 10% * S_{tot}) to 2.12 (n_S = 50% * S_{tot}) for the Tri model, in which complexation is assumed to occur through the tridendate complexes. The simulation of As(III) binding by Leonardite and S(-II)-Leonardite with the Mono and Tri models is displayed in Figure I. 3. For the Mono model, the binding parameter, log K_{MS}, did not vary significantly with the thiol %. However, the corresponding RMSE decreased from 0.72 to 0.33 with the increasing n_S (Table I. 3). By contrast, for the Tri model, log K_{MS} increased strongly with the decreasing thiol %, log K_{MS} = 2.93 to 2.12. It is important to note that these differences were multiplied by a factor of 3 for the corresponding log K (see part 2.4), which thus varied from 2.12*3 = 6.36 to 3*2.93 = 8.79. Regards to the smallest RMSE, for all the following calculations, log K_{MS} was fixed at 2.91 and 2.12 for the Mono and Tri models, respectively. The modeling

performed with both the Mono and Tri models was very similar, as demonstrated by the RMSE values of 0.33 and 0.27, respectively. The standard deviations calculated for the log K_{MS} values were small (0.03 and 0.02 for the Mono and Tri models, respectively). Therefore, these two simulations alone could not be used to validate either one of the models in particular. To further validate the modeling approach, the fitted binding parameters therefore had to be tested using other experimental datasets.

Table I. 3: Log K_{MS} determined from the Mono and Tri models.

	Monodentates		**Tridentates**	
	log K_{MS}	**RMSE**	**log K_{MS}**	**RMSE**
n_S = 10%*S_{tot}	2.93 ± 0.04	0.72	2.93 ± 0.11	0.46
n_S = 20%*S_{tot}	2.92 ± 0.04	0.54	2.35 ± 0.06	0.33
n_S = 30%*S_{tot}	2.92 ± 0.04	0.43	2.24 ± 0.04	0.30
n_S = 40%*S_{tot}	2.91 ± 0.04	0.37	2.17 ± 0.03	0.28
n_S = 50%*S_{tot}	2.91 ± 0.03	0.33	2.12 ± 0.02	0.27

3.5 Simulations with the Mono and Tri models

The RMSE fits were averaged and weighted by all available data (Table I. 3) to compare Mono and Tri models.

PAHA. Three studies used this HA (Thanabalasingam and Pickering, 1986; Warwick et al., 2005). The first used dataset was produced in the present study and corresponded to the As(III) adsorption isotherm on purified Aldrich humic acid (PAHA) (Figure I. 4a). Between 7 and 16% of As(III) were bound to PAHA in the performed experiments. The present produced datasets were better fitted with the Tri model than with the Mono model (mean RMSE = 0.86 and 0.62 for the Mono and Tri models, respectively). By contrast, both other datasets (Thanabalasingam and Pickering, 1986; Warwick et al., 2005) were less simulated (mean RMSE = 0.73 and 0.53 against 1.24 and 0.82 for the Mono and Tri models, respectively). The weighted RMSE was lower for the Mono than for the Tri models (RMSE = 0.67 and 0.90 for the Mono and Tri models, respectively) (Table I. 4 and Figure I. 4b and c).

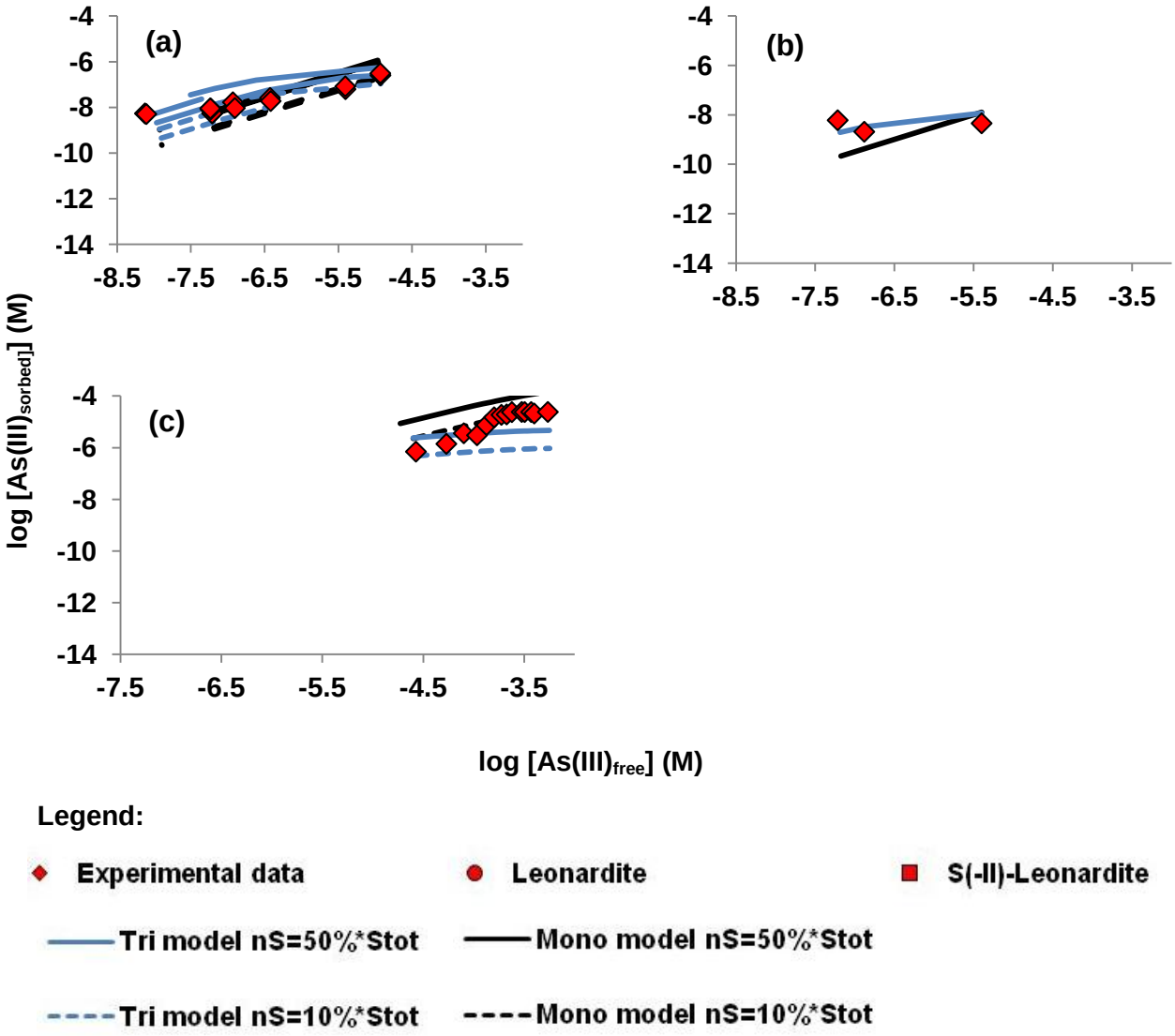

Figure I. 4: Experimental and modeled data (Mono = with monodentates only; Tri = with tridentates only) (a) the present purified Aldrich HA, (b) PAHA from Thanabalasingam & Pickering (1986), (c) PAHA from Warwick et al. (2005)

AHA. Several studies used this HA (Fakour and Lin, 2014; Kappeler, 2006; Liu and Cai, 2010; Thanabalasingam and Pickering, 1986) at various pH and HA concentrations. Note that this humic acid was not purified with the IHSS protocol and contained probably humin, humic and fulvic acids and impurities (silica, metals, etc.). The experimental datasets from Kappeler (2006) and Liu and Cai (2010) at pH 5.2 were better fitted with the Tri than the Mono models (RMSE mean = 0.4, 0.3 and 0.51 and 0.52, respectively) (Figure I. 5a and b and Table I. 4). However, Liu and Cai (2010) datasets at pH 7 and 9, Fakour and Lin (2014)

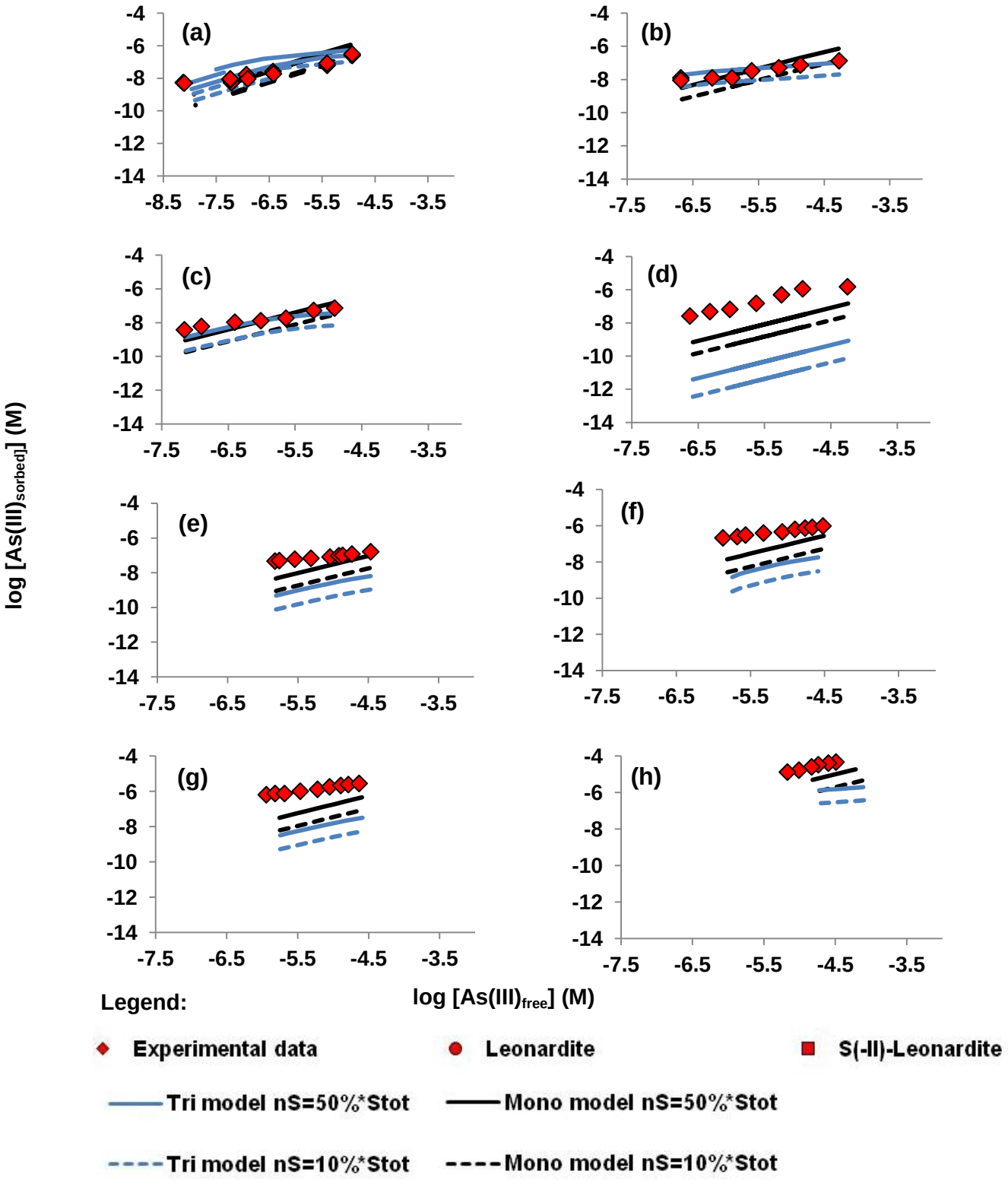

Figure I. 5: Experimental and modeled data (Mono = with monodentates only; Tri = with tridentates only) (a) AHA experimental data from Kappeler (2006), (b) AHA at pH 5.2 from Liu and Cai (2010), (c) AHA at pH 7 from Liu and Cai (2010), (d) AHA at pH 9.3 from Liu and Cai (2010), (e) AHA at DOC = 5 mg L^{-1} from Fakour and Lin (2014), (f) AHA at DOC = 15 mg L^{-1} from Fakour and Lin (2014), (g) AHA at DOC = 30 mg L^{-1} from Fakour and Lin (2014), (h) AHA from Thanabalasingam and Pickering (1986)

and Thanabalasingam and Pickering (1986) were better fitted with the Mono than with the Tri models (Table I. 4 and Figure I. 5c-h). For all datasets, the lower weighted RMSE was obtained for the Mono model (Table I. 4). The datasets at high pH were lesser fitted by both models which was probably account for the presence of $H_2AsO_3^-$ specie that was bound to HA with a mechanism not described in both models.

SRHA. Only two datasets used this HA (Kappeler, 2006; Lenoble et al., 2015). The used thiol % of SRHA was determined as $n_S = 23.6\% * S_{tot}$ (Manceau and Nagy, 2012). Regards to the experimental pH range, the fitting calculations used only 3 and 2 data points for Kappeler (2006) and Lenoble et al. (2015) datasets, respectively. The best fits were obtained with the Tri model (Table I. 4, Figure I. 6a and b). However, regards to the small number of data, RMSE should be considered carefully (see Discussion section).

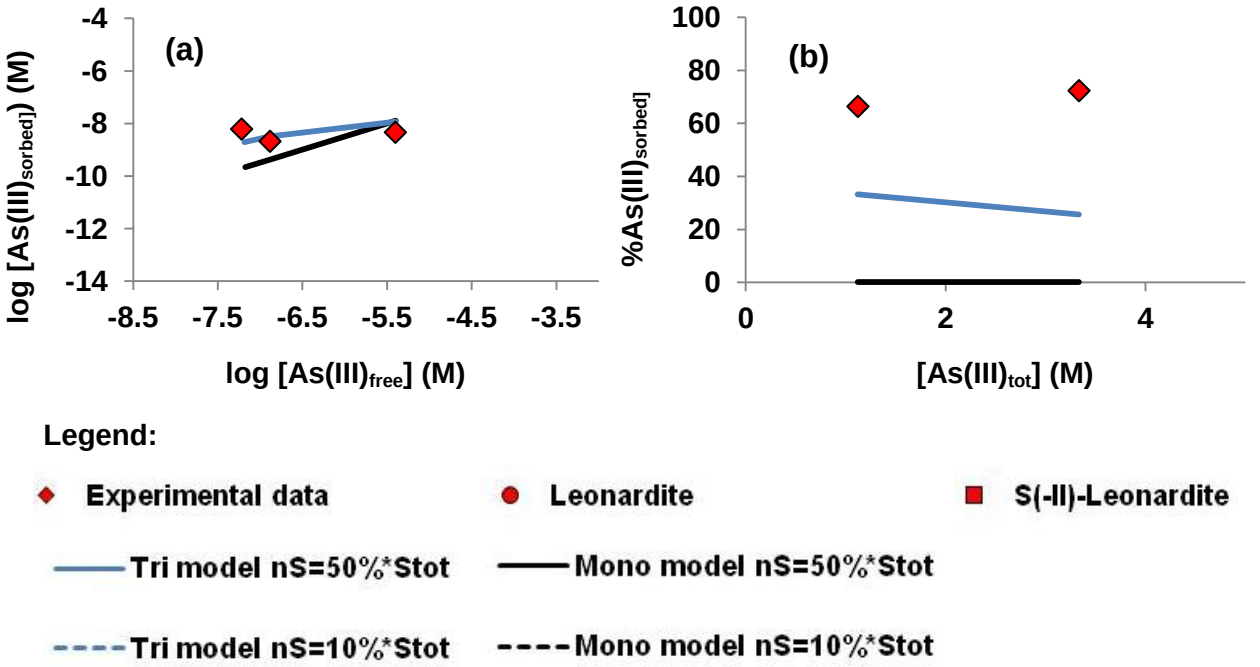

Figure I. 6: Experimental and modeled data (Mono = with monodentates only; Tri = with tridentates only) (a) SRHA experimental data from Kappeler (2006), (b) SRHA experimental data from Figure 1 of Lenoble et al. (2015)

Elliot Soil HA and Peat. For both datasets, thiols were grafted to HA and their % were estimated using XRF spectroscopy. The Hoffmann et al. (2012) HA dataset was lesser reproduced by the Mono than the Tri models (Figure I. 7a and Table I. 4) (RMSE = 0.74 for

the Mono model versus 0.19 for the Tri model). By contrast, neither the Mono nor the Tri model reproduced the peat dataset of Hoffmann et al. (2012), over the entire thiol % range (Figure I. 7b, Table I. 4). More precisely, the Tri model could simulate the experimental dataset at low thiol %, but the Mono model better simulated the dataset at high thiol %. The weighted RMSE calculated for both datasets was better for the Tri than for the Mono model. However, the spectroscopic data obtained by Hoffmann et al. (2012) clearly allowed to reject the Tri model, since only one S was determined in the vicinity of the As(III) (Hoffmann et al., 2012).

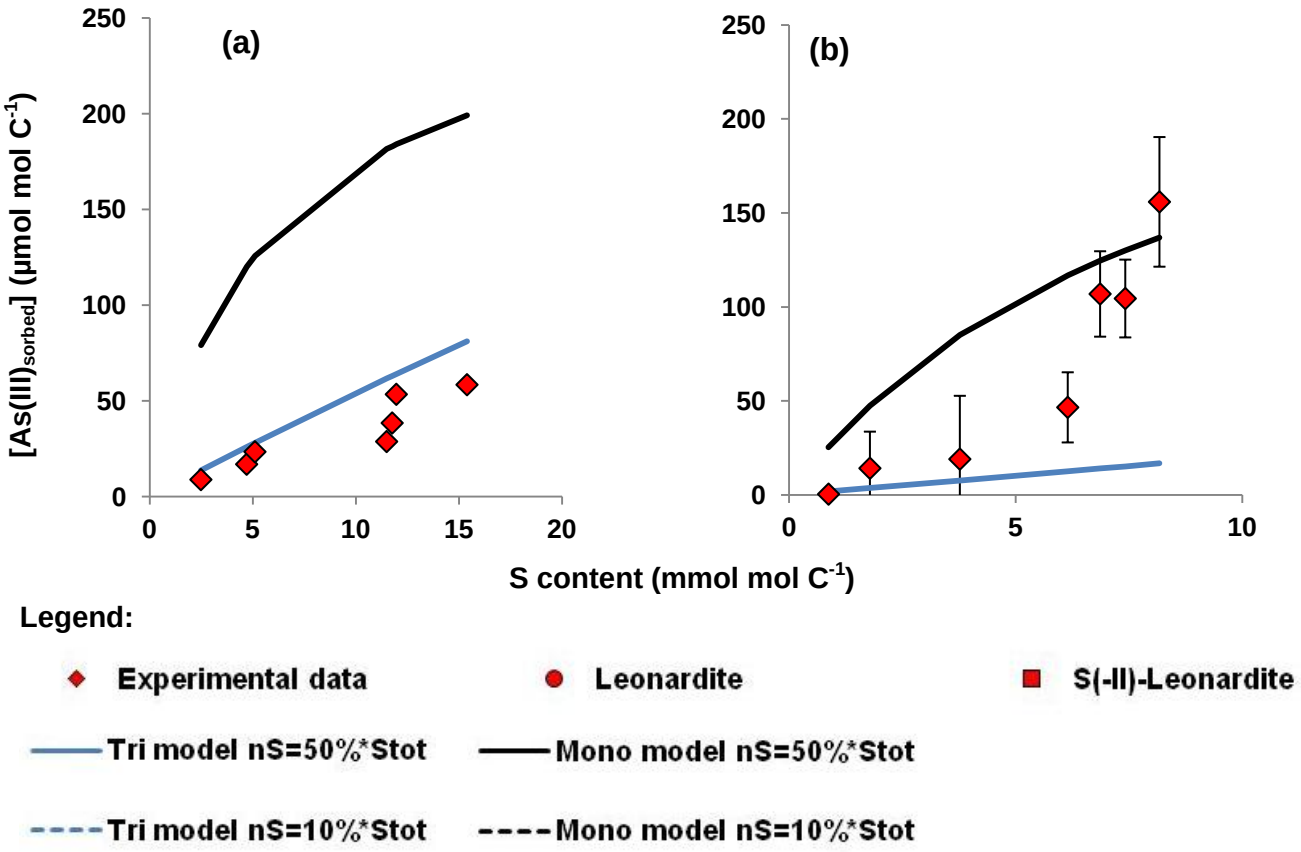

Figure I. 7: Experimental and modeled datasets of (a) HA experimental data from Hoffmann et al. (2012), (b) peat experimental data from Hoffmann et al. (2012).

Based on the weighted RMSE calculated for all datasets, it appears that the Mono model better simulated the experimental datasets than the Tri model, notably regards to the data from PAHA and AHA (Table I. 4). Moreover, as specified before, for the datasets at pH > 7 (Fakour and Lin, 2014; Liu and Cai, 2010 at pH 7 and 9.3) the potential presence of

$H_2AsO_3^-$ species decreased the fit quality. Using the datasets for AHA and PAHA at pH < 7, namely without $H_2AsO_3^-$, the weighted RMSE decreased to 0.60 and 0.75 for Mono and Tri models, respectively (Table I. 4) indicating that the Mono model simulated more datasets than the Tri model. Note that the high RMSE were due to the large range of thiol % used for AHA and PAHA (n_S = 10-50% * S_{tot}).

Table I. 4: Abundances calculated for the datasets from the literature and RMSE calculated using the Mono and Tri models.

	n_S (mol g^{-1})	Number of data	Mono model	Tri model
PAHA		**30**	**0.67**	**0.90**
Present study	$7.28\ 10^{-5}$ to $3.64\ 10^{-4}$	7	0.86	0.62
Thanabalasingam and Pickering (1986)		9	0.73	1.24
Warwick et al. (2005)		14	0.53	0.82
AHA		**71**	**0.90**	**1.56**
Kappeler (2006)	$1.31\ 10^{-4}$ to $6.56\ 10^{-4}$	16	0.51	0.40
Liu and Cai (2010) pH = 5.2		8	0.52	0.31
Liu and Cai (2010) pH = 7		7	0.56	0.57
Liu and Cai (2010) pH = 9		7	1.73	4.12
Fakour and Lin (2014) pH = 7.5		27	1.16	2.22
Thanabalasingam and Pickering (1986)		6	0.67	1.52
SRHA		**5**	**1.71**	**0.45**
Kappeler (2006)	$3.98\ 10^{-5}$	3	0.96	0.39
Lenoble et al. (2015)		2	2.83	0.54
Others		**14**	**0.75**	**0.46**
Hoffmann et al. (2012) Elliot Soil	$1.14\ 10^{-4}$ to $7.06\ 10^{-4}$	7	0.74	0.19
Hoffmann et al. (2012) Peat	$3.86\ 10^{-5}$ to $3.61\ 10^{-4}$	7	0.77	0.72
Weighted RMSE		**120**	**0.86**	**1.22**
PAHA and AHA weighted RMSE without basic pH		**60**	**0.60**	**0.75**

4 Discussion

4.1 H-HA parameters

The protonation/deprotonation parameters for the A, B and S sites are presented and compared to Tipping's parameters (Tipping, 1998) for Model VI (Table I. 2). The variation in the carboxylic and phenolic abundances might be explained by the implementation of thiol groups (n_S). For a same total abundance of site (dependent only on the type of humic

substance), three different abundances (n_A, n_B and n_S) are defined here versus two abundances (n_A and n_B) in Model VI. Figure I. 2 showed that the HA titrations performed in this study are within the range of the HA titration values compiled by Milne et al. (2001); notably, the obtained pK_A and ΔpK_A are close to those of Tipping's parameters (Tipping, 1998). The most noticeable difference occurred for pK_B which was explained by the fact that in Model VI, the thiol and phenol groups were grouped together and considered as site B. Data from the literature showed that the pK of the phenol ligands seems to depend on the carbon radical to which the hydroxyl (OH) is bound. For example, the pK of hydroxybenzene, (OH^- bound to one benzoic cycle) is 9.98 (at 25°C and IS = 0 mol L^{-1}) versus 7.21 for nitrophenol (OH bound to one benzoic cycle, which is itself bound to NO_2) (at 25°C and IS = 0 mol L^{-1}). As the molecular structure of OM is complex and heterogeneous, the form/structure of the carbon radical of phenol cannot be identified. However, the fitted pK_B of 7.11 obtained in this study was consistent with the pK_A of phenol.

The H^+ dissociation constant for the thiol groups, pK_S = 5.82 ± 0.05, was lower than pK_B, suggesting that thiol groups are more deprotonated at acidic pH than phenolic groups. For a simple organic ligand (aliphatic or aromatic) containing thiol groups, the pK varied from 5.2 to 13.24 (Figure I. 8). This pK_A range correlates with the molecular weight of the molecules: pK_A decreases with increasing molecular weights (Figure I. 8). Moreover, for aromatic molecules containing one thiobenzene, the increasing molecular weight of the radical associated with the aromatic ring is correlated with the decreasing pK_A. Based on this dataset, the low pK_S (5.82) obtained for the deprotonation of the thiol sites can therefore be justified by the high molecular weight and aromaticity of HA (Figure I. 8). The distribution term of pK_S, ΔpK_S, was high (6.12 ± 0.12), suggesting that the thiol pK were distributed over a large pK range. Humic acids are not only macromolecular but also supramolecular moieties (Pédrot et al., 2009), i.e. not only formed with high weight aromatic molecules but also lower weight molecules. The correlation between pK for the thiol group and the molecular weight of thiol-containing organic molecules might therefore explain this high distribution (ΔpK_S). Several simulations were performed to test the influence of ΔpK_S on the fitting of the As(III)-

HA binding parameters. Variations in ΔpK_S did not produce any variation for the As(III) concentrations bound to HA (Table I. 5).

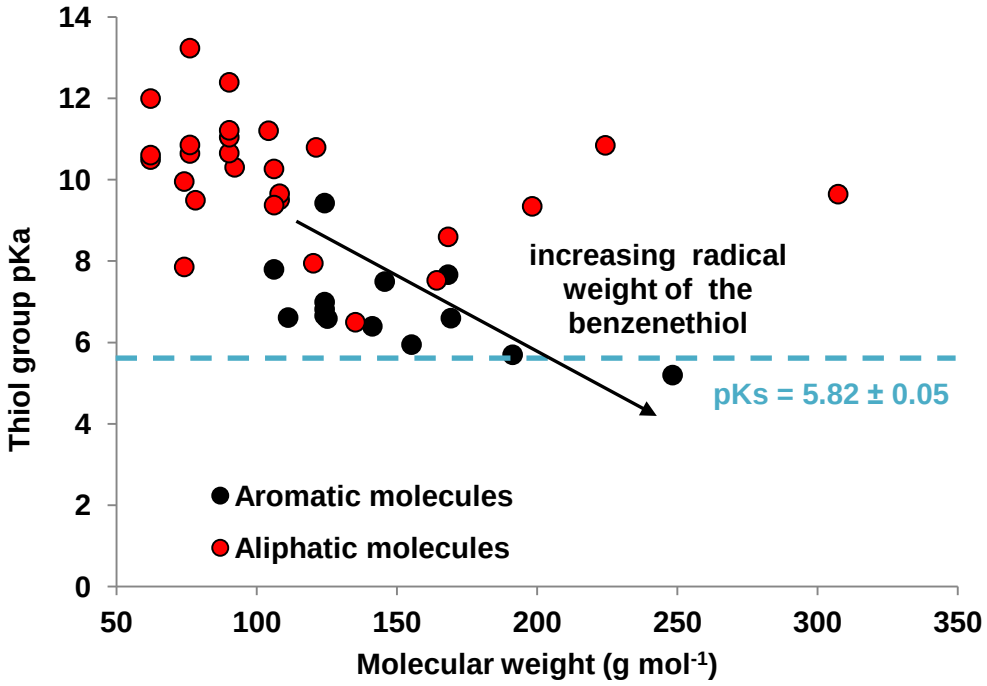

Figure I. 8: Compilation of the pKa of the thiol function of thiol-containing organic molecules according to their molecular weight (Edsall and Wyman, 1958; Gough et al., 2003; Martell and Smith, 1989; Williams, n.d.). The distinction was made between aliphatic (red symbols) and aromatic ring-containing molecules (black symbols).

Table I. 5: Concentrations of bound As(III) calculated using different ΔLK_{1S} values.

$[As(III)]_{tot}$ (mol L^{-1})	$[As(III)]_{bound}$ (mol L^{-1})		
	$\Delta pK_S = 2$	$\Delta pK_S = 6.12$	$\Delta pK_S = 8$
7.2610-08	7.33E-10	7.33E-10	7.33E-10
1.41E-07	1.43E-09	1.43E-09	1.43E-09
2.19E-07	2.22E-09	2.22E-09	2.22E-09
2.92E-07	2.95E-09	2.95E-09	2.95E-09
4.34E-07	4.42E-09	4.42E-09	4.42E-09
5.79E-07	5.90E-09	5.90E-09	5.90E-09
6.98E-07	7.09E-09	7.09E-09	7.09E-09
9.77E-08	1.24E-08	1.24E-08	1.24E-08
1.41E-07	1.78E-08	1.78E-08	1.78E-08
2.12E-07	2.68E-08	2.68E-08	2.68E-08
2.92E-07	3.72E-08	3.72E-08	3.72E-08
4.34E-07	5.53E-08	5.53E-08	5.53E-08
6.02E-07	7.68E-08	7.68E-08	7.68E-08
8.54E-07	1.09E-07	1.09E-07	1.09E-07

4.2 As(III)-HA binding parameters

There is no consensus regarding the mechanisms involved in the binding of As(III) by HA. Buschmann et al. (2006) and Lenoble et al. (2015) proposed that this binding occurs through the complexation of As(III) by carboxylic and phenolic groups. These functional groups are the most abundant in OM and they are able to complex many cations such as Fe(II, III), REE, Al, Mg, etc. (Buffle et al., 1998; Milne et al., 2003; Sposito, 1986; Tipping and Hurley, 1992). However, the direct complexation of As(III) species by HA carboxylic groups has not been supported so far by any spectroscopic data. At any rate, the log K of As(III) binding to simple organic ligands is low - As(III)-catechol with log K = -6.89 and As(III)-pyrogallol with log K = -6.32 (Martell and Smith, 1989), indicating that this complexation, if any, should be of minor importance. By contrast, recent spectroscopic studies suggested two new binding mechanisms. The first one consists of an indirect mechanism in which As(III) is bound to OM via Fe (Buschmann et al., 2006; Hoffmann et al., 2013; Ko et al., 2004; Lin et al., 2004; Liu and Cai, 2010; Warwick et al., 2005). The second consists of a direct mechanism in which As(III) is bound to OM via thiol functional groups (Hoffmann et al., 2014; Langner et al., 2011b). Arsenic(III) has high affinity for S containing-ligands. The stoechiometry of the formed As-thiol organic molecules are either 1:1 (i.e. thiol in peat and HA, Hoffmann et al., 2012) or 1:3 (i.e. cystein Spuches et al., 2005a) depending on the ligand involved. In this study, two models were designed to test the reality of these complexes, i.e. the monodentate (1:1) model, the so-called Mono model, and the tridentate (1:3) model, the Tri model. Simulations of published datasets with the binding parameters established using the experimental data of this study demonstrated that the Mono model well reproduced more datasets than the Tri model (weighted RMSE = 0.86 and 1.22 for the Mono and Tri models, respectively). Considering the datasets of PAHA and AHA without $H_2AsO_3^-$ species, the mean RMSE was lower with the Mono than the Tri model. The Mono model is in accordance with the binding mechanisms proposed by Hoffmann et al. (2012), i.e. the formation of monodentate complexes. Hoffmann et al.'s (2012) spectroscopic study

demonstrated that only one S is located in the vicinity of As(III) in their HA sample (0.5 < CN (coordination number) < 1.5 at 2.29 - 2.34 Å). The fact that neither the Mono model nor the Tri model was successful in fitting these experimental data (Hoffmann et al., 2012) could be explained by the experimental conditions used by the authors. In order to meet the requirement for the spectroscopic analyses, high As(III) and HA concentrations had to be used in the experiments. These high amounts of As(III) could promote the formation of arsenite polymers. This hypothesis is supported by the presence of As in the vicinity of the bound As(III) in the EXAFS fitting of HA data by Hoffmann et al. (2012) (0.3 < CN < 0.5 at 2.63 - 2.67 Å). This model, which only considered As(III), therefore overestimated the bound As(III) concentrations. The same overestimation was obtained for Warwick et al.'s (2005) dataset. The experimental conditions of this dataset ([As(III)] = 2 - 42 mg L^{-1} and [HA] = 1.5 g L^{-1}) were within the same range as those of Hoffmann et al. (2012) ([As(III)] = 4.1 mg L^{-1} and [peat] = 4.5 g L^{-1}) and it is likely that As(III) polymers were formed during these experiments. Moreover, the sorption isotherm of Warwick et al. (2005) exhibited two sorption increase/decrease steps (Figure I. 4c), a feature that could not be explained. The differences between the experimental and modeled data for the peat dataset of Hoffmann et al. (2012) can be explained by the nature of the peat used, as it is a specific OM formed in very specific conditions and this could thereby influence its composition and surface reactivity. The Mono model also failed to reproduce SRHA datasets (Kappeler, 2006; Lenoble et al., 2015). Since the occurrence of $H_2AsO_3^-$ was expected for most data, only five points of both datasets could be used for fitting. The RMSE depended on the number of extrapolated points. For large datasets, the RMSE is expected to be lower than for small datasets. Moreover, a high discrepancy was observed between Kappeler (2006) and Lenoble et al. (2015) datasets. Lenoble et al. (2015) showed that between 30 to 80% of As(III) was bound to SRHA versus 0.11 to 23.9% for Kappeler (2006) for equivalent experimental conditions (at pH = 8.4, DOC = 50 mg L^{-1}, $[As(III)]_{tot}$ = 0.134 µmol L^{-1}, As(III) bound = 8.87% and pH = 8, DOC = 15 mg L^{-1} and $[As(III)]_{tot}$ = 0.16 µmol L^{-1}, As(III) bound = 38%, respectively). So far, we have no explanations for these observed differences. The RMSE were high for both Mono and Tri

models. These RMSE corresponded to the average of the RMSE calculated for the 5 tested n_S in the calculation of which S_{tot} had the same values for each PAHA and each AHA samples, (%S = 2.33% and 4.2% for PAHA and AHA, respectively). However, considering the date of the various published studies, HA were probably provided from different lots. Moreover, for PAHA, the purification had probably modified S_{tot} and thiol % in the HA sample. Therefore, modeling calculations should only be considered as estimations and they had to be improved with the true S_{tot} and thiol %.

The As(III)-thiol HA binding parameter log K_{MS} is equal to 2.91 ± 0.04. Log K_{MS} was determined for protonated HA (see Eq. 4), in contrast to cation binding in PHREEQC-Model VI and Model VI. For deprotonated species, log K_{MS} is equal to = -5.38, which is very low compared to the log K_{MA} and log K_{MB} of cations (log K_{MA} (Ba) = -0.2 < log K_{MA} (Model VI) < log K_{MA}(Dy) = 2.9). This indicates that the capacity of HA to bind As(III) is much lower than the capacity of HA to bind cations. This is not surprising in terms of the global negative charge of HA and the neutral charge of As(III) which had to lose one OH in order to be bound to the negative charged-thiol group in HA.

In Figure I. 9 were plotted the log β relative to the number of coordinated thiols in the complexes formed between As(III) and thiol-containing organic molecules. It is important to note that Rey et al.'s (2004) log β values are much higher than the log β values determined by other workers, as previously noted (Spuches et al., 2005a). Log β increased with the increasing number of coordinated thiols. The binding of As(III) to dithiol molecules (e.g. dimercaptosuccinic acid - DMSA) leads to the formation of a ring stabilizing the complex. Few data for monodentate 1:1 complexes between As(III) and thiol-containing molecules are available in the literature. Thiol groups are strongly reactive regards to As(III) and As(III) is therefore often bound to 2 or 3 thiols, as bi- or tridentate complexes. The log K_{MS} (here, log K_{MS} = log K) of 2.91 extrapolated for the Mono model was within the log β range of the 1:1 complexes (Figure I. 9). Moreover, for aryl arsinous acid ($ArAs(CH_3)OH$), in which only OH is available for binding, Liang and Drueckhammer (2014) determined a log β of 2.80 with

mercaptoethane, which was close to log K determined in this work. The extrapolated log K_{MS} confirmed thereby the low affinity of As(III) for HA.

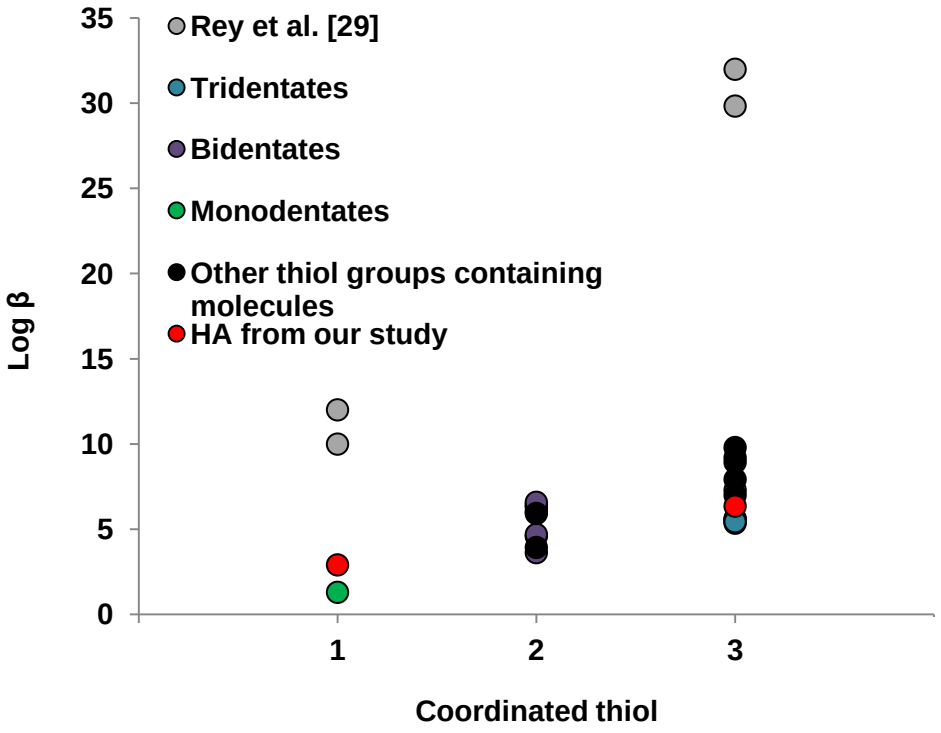

Figure I. 9: Comparison between log β of thiol-containing organic molecules and As(III) and log K_{MS} relative to the number of coordinated thiols in the complexes (Cavanillas et al., 2012; Gaber and Fluharty, 1972; Hoffmann et al., 2014; Rey et al., 2004; Spuches et al., 2005b; Spuches and Wilcox, 2008; Starý and Růzicka, 1968; Zahler and Cleland, 1968; Zhao et al., 2012).

For, the Tri model, extrapolated log K_{MS} was 2.02 and corresponded to log k ≈ 3 * log K_{MS} = 6.06. This calculated log k was in the range of the log β of the 3 coordinated thiol-As (III) complexes. Among this group, the binding mechanism can occur through 1:3, 1:2, 1:1 complexes. The Tri model corresponded, here, to the formation of tridentate 1:1 complexes. The log β of the tridentate 1:1 complexes of the group of the 3 coordinated thiols were lower than those of the Tri model (Figure I. 9).

If the formation of tridentates is efficient for As(III) binding by peptides, proteins, organic ligands or thiol-resin (Cavanillas et al., 2012; Hoffmann et al., 2014; Kitchin and Wallace, 2008; Rey et al., 2004; Spuches et al., 2005a; Starý and Růzicka, 1968; Zhao et al., 2012), the present results did not provide evidence that in HA, the formation of tridentates is

promoted. In organic ligand or thiol-resin, there was a high density of thiol groups compared to HA, in which phenolic and carboxylic groups predominate (n_A > 12 x n_S in the present study). Moreover, in Hoffmann et al. (2012), although the HA samples were grafted with thiols, only monodentates were formed, as evidenced by the spectroscopic analyses. Thus, the thiol concentrations are not the only controlling factor for monodentates or tridentates formation. Numerous organic ligands formed 1:3 (e.g. cysteine, glutathione) or 1:2 complexes (e.g. Sp1-zf2 f565-595 protein) with As(III) (Figure Intr. 9). Many of them are aliphatic and carry two or more thiol sites that are thus close to each other (e.g. dithiothreitol, dimercaptosuccinic acid). Spuches et al. (2005a) provided evidence that entropic factors are important in constraining the stability of the complex formed between As(III) proteins. Therefore proteins, in which the vicinity of the cysteine residue (i.e. the thiol groups) are conformably constrained (entropic advantage) and favorably positioned, are expected to form a high denticity complex (max 3) with As(III). Moreover, some peptides and proteins are flexible in solution, which allows As(III) to bind several thiol groups despite the distances between the thiol sites, subsequently modifying the geometry of the molecules (Kitchin and Wallace, 2008). In contrast to what occurs with peptides and proteins, HA are complex moieties that are strongly rigidified by the presence of aromatic rings. This rigidity combined with the low thiol density and subsequent high distances between the thiol groups prevent the formation of tridendate complexes with As(III).

4.3 Implications of the direct binding mechanism evidenced

The present study further demonstrated the ability of HA to directly bind As(III) via their thiol functional groups. However, the calculated binding parameters are low, suggesting a global weak affinity of As(III) for HA even though this affinity could be high for a few specific sites as suggested by the high value of the distribution term, ΔpK_S. The binding of As(III) by HA will therefore probably play a minor role in the fate of As in organic-rich waters. However, if the available database indicates that the amount of As(III) bound to HA should be low in most cases, this amount will depend on the abundance of the thiol functional groups in HA.

Since thiol % were not determined for the whole datasets, the thiol concentration had to be tested within the range expected from spectroscopic analyses (n_S = 10, 20, 30, 40 and 50% * S_{tot}). The obtained RMSE decreased with the increasing thiol concentrations, which provided evidence of a strong dependency between the amounts of bound As(III) and the thiol groups. The thiol abundance will be the major controlling factor with regards to the direct binding of As(III) to HA. Therefore, the composition and structure of HA will influence the amount of As on the surface of the humic colloids or particles. The sulfur concentrations in organic matter, especially in humic substances, vary a lot; for example, among the humic substances sold by IHSS, the sulfur concentrations vary from 0.36% (Waskish Peat reference HA) to 3.03% (Pony Lake fulvic acid). The first HA is sourced in deep, very poorly drained organic soils and consist of decomposed bogs, whereas Pony Lake fulvic acid comes from a saline coastal pond from Antartica and is composed of purely microbially-sourced fulvic acid. This microbial composition should explain the high concentration of sulfur found in this fulvic acid. Moreover, the only S_{tot} amount was not sufficient to determine the thiol concentrations in humic substances. The concentrations of thiol groups varied from from 1 to 46.9% (Dong et al., 2010; Haitzer et al., 2003; Jiang et al., 2015; Manceau and Nagy, 2012; Qian et al., 2002; Rao et al., 2014; Xia et al., 1998). To better understand the binding of As(III) to thiol groups, it is therefore absolutly necessary to determine thiol concentrations. If XAS techniques allow to estimate exocyclic S and thiol concentrations, its sensibility is low and this technique requires high concentrations of thiol (Rao et al., 2014). Recently, Rao et al. (2014), proposed a new titration methode based on the use of ThioGlo-1 as thiol groups complexing agent. These type of method had to be developed to systematically determine thiol concentrations and better estimated the As(III) amount bound to organic matter.

Since thiol groups are good potential binding sites for As(III), reduced peatland environments (in the absence of sulfurs that can precipitate As) with potentially high S(-II)-HA concentrations, will thus be favorable environments for the binding of As(III) to HA. In contrast, in oxidized environments with the development of Fe(III) species, As(III, V) is expected to be strongly bound to OM via ternary complexes with Fe(III) as cationic or

(nano)oxides bridges (Mikutta et al., 2010; Mikutta and Kretzschmar, 2011; Ritter et al., 2006; Sharma et al., 2010). Under reducing conditions, where Fe(III) is reduced to Fe(II), this mechanism will not be activated and the binding of As(III) to OM will thus predominantly occur through the direct binding of As(III) by thiol groups. However, in organic-rich environments such as wetland soils, Fe(II) is strongly bound to OM (Catrouillet et al., 2014; Rose and Waite, 2003; Schnitzer and Skinner, 1966; Theis and Singer, 1974). Therefore, several questions can be raised regarding the binding of As to OM in these environments, such as: can the Fe(II) bound to OM modify the As binding? Is it possible to form ternary complexes between As(III), Fe(II) and OM? If so, what is the dominant mechanism that binds As(III) to OM in these types of environments: As(III)-Fe(II)-HA or to As(III)-S(-II)-HA?

Conclusion and perspectives

We provided experimental data for As(III) binding by Leonardite that has either been grafted or not with thiol groups. Titrations of both HAs were used to calculate the protonation/deprotonation parameters of each thiol site defined in our modified PHREEQC-Model VI model. In a second step, As(III)-HA experimental sorption isotherms were fitted to determine the binding parameters of the As(III)-thiol HA complexes. Two binding hypotheses were tested, the establishment of monodentate complexes (the Mono model) and the formation of tridentate complexes (the Tri model). To test each of these models, the extrapolated binding parameter sets of the Mono and Tri models were used to fit several experimental datasets available in the literature. This procedure could be used to validate the Mono model, i.e. the monodentate hypothesis, in terms of its ability to predict As(III) binding by HA. Extrapolated log K_{MS} was equal to 2.91 ± 0.04. When the amount of bound As(III) to HA was low (around 5-10% of As(III) bound to HA in these experimental conditions), they were strongly dependent on the thiol density. The formation of monodentate complexes rather than tridentate ones could be explained by the combination of the low thiol density and the relative rigidity of HA forming molecules conferred by their abundance in aromatic rings, in contrast to flexible peptides or proteins, which are able to bind As(III) through tridentate

complexes with thiol functions. These results therefore highlighted the necessity to determine the concentration of S and more specifically the concentration of the thiol groups in the different organic matters, which is currently not easily determined. It could also be interesting to study the binding of As(III) by fulvic acids, which have a smaller aromatic nucleus and a long aliphatic chain, to better constrain the fate of As(III) in organic-rich environments. Moreover, the binding by Fe through ternary complexes should be better defined to determine the competition between both mechanisms in the different redox states of As and Fe.

Chapitre II : Complexation du Fe(II) par les substances humiques : apport de la modélisation

Dans la première partie de ce manuscrit, j'ai montré que l'As(III) pouvait se complexer par un mécanisme direct sur la matière organique via ses groupements thiols. Cependant, cette complexation reste faible en raison de la faible densité en sites thiols. Il existe cependant un autre mécanisme qui propose une complexation indirecte via un pont métallique. Dans ce travail, nous nous intéresserons à la possibilité que ce pont soit un pont de Fe(II). Il n'existe cependant que très peu d'information sur la complexation du Fe(II) par la matière organique que ce soit des données expérimentales ou des constantes de stabilité. Dans ce deuxième chapitre, nous allons donc nous intéresser aux mécanismes et aux paramètres de complexation du Fe(II) sur la MO à partir de résultats expérimentaux et du modèle PHREEQC-Model VI.

Ce chapitre correspond à un article publié dans la revue "Chemical Geology": Geochemical modeling of Fe(II) binding to humic and fulvic acids, Charlotte Catrouillet, Mélanie Davranche, Aline Dia, Martine Bouhnik-Le Coz, Rémi Marsac, Olivier Pourret, Gérard Gruau (Chemical Geology, Elsevier, 2014, 372, pp.109-118, DOI 10.1016/j.chemgeo.2014.02.019)

Geochemical modeling of Fe(II) binding to humic and fulvic acids

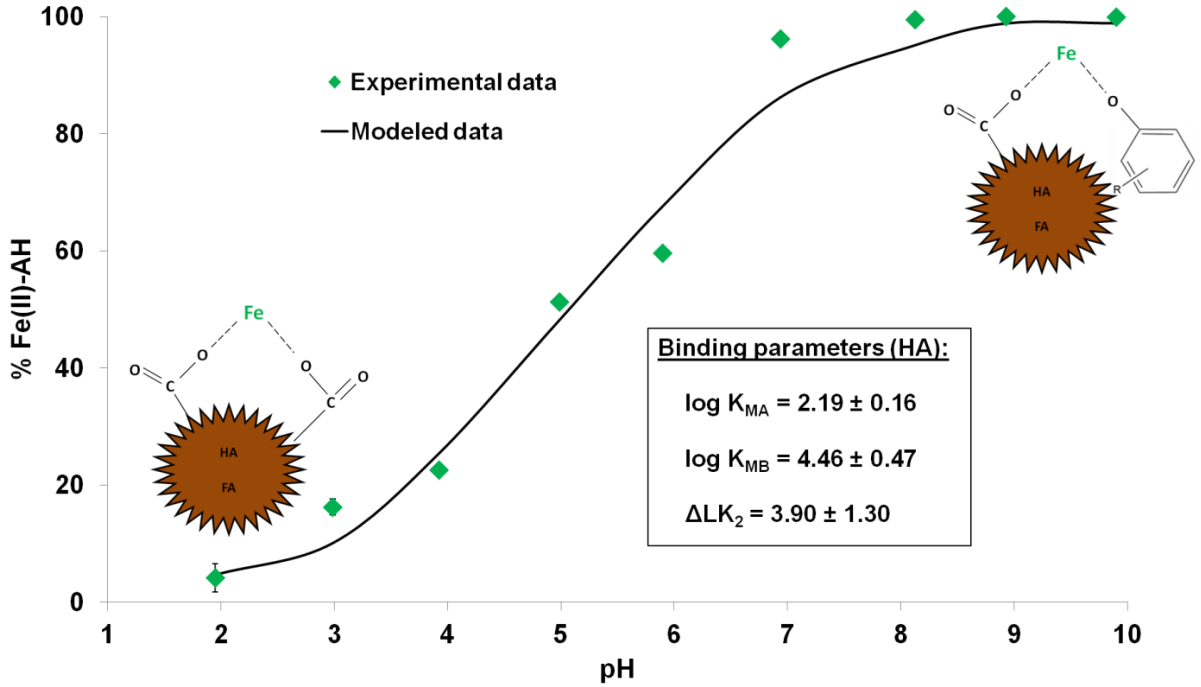

Pourcentage de Fe(II) complexé par les acides humiques en fonction du pH : faible complexation à pH acides et forte complexation à pH basiques - Fe(II) percentage of complexation by humic acid according to pH: weak complexation at acidic pH and strong complexation at basic pH

RESUME

La complexation du Fe(II) par la matière organique (MO) et plus spécialement par les acides humiques (AH) reste peu décrite dans la littérature. Dans cette étude, des expériences de complexation Fe(II)-AH ont été réalisées sur une gamme de pH de 1.95 à 9.90. Les concentrations de Fe(II) adsorbées aux AHs sont fortes et dépendent du pH. Les données expérimentales ont ensuite été utilisées afin de quantifier et paramétrer les mécanismes, par modélisation à l'aide d'un couplage entre PHREEPLOT et PHREEQC-Model VI. Les paramètres de complexation (log K_{MA} = 2.19 ± 0.16, log K_{MB} = 4.46 ± 0.47 and ΔLK_2 = 3.90 ± 1.30) ont été validés en utilisant la méthode de LFER (linear free energy relationship) et les données d'adsorption entre le Fe(II) et l'acide fulvique Suwannee River (AFSR) de la littérature (Rose et Waite, 2003). Ces paramètres de complexation ont permis de déterminer la distribution du Fe(II) sur les groupements fonctionnels de AH. Le Fe(II) forme majoritairement des complexes bidentates, et peu de complexes tridentates et monodentates avec les AHs. Il est également majoritairement adsorbé sur les groupements carboxyliques à pH acides et neutres et carboxy-phénoliques et phénoliques à pH basiques. L'espèce majoritaire adsorbée sur les groupements fonctionnels des AHs est Fe^{2+}, $Fe(OH)^{+}$ n'apparaissant qu'à pH basiques (de pH 8.13 à 9.9). La MO peut donc fortement influencer la spéciation et la biodisponibilité du Fe(II) dans les tourbières et les zones humides en période de réduction (hautes eaux).

ABSTRACT

The complexation of Fe(II) with organic matter (OM) and especially with humic acids (HA) remains poorly characterized in the literature. In this study, batch experiments were conducted on a pH range varying from 1.95 to 9.90 to study HA-mediated Fe(II) binding. The results showed that high amounts of Fe(II) are complexed with HA depending on the pH. Experimental data were used to determine a new set of binding parameters by coupling PHREEPLOT and PHREEQC-Model VI. The new binding parameters (log K_{MA} = 2.19 ± 0.16, log K_{MB} = 4.46 ± 0.47 and ΔLK_2 = 3.90 ± 1.30) were validated using the LFER (linear free

energy relationship) method and published adsorption data between Fe(II) and Suwannee River fulvic acid (SRFA) (Rose and Waite, 2003). They were then put in PHREEQC-Model VI to determine the distribution of Fe(II) onto HA functional groups. It was shown that Fe(II) forms mainly bidentate complexes, some tridentate complexes and only a few monodentate complexes with HA. Moreover, Fe(II) is mainly adsorbed onto carboxylic groups at acidic and neutral pH, whereas carboxy-phenolic and phenolic groups play a major role at basic pH. The major species adsorbed onto HA functional groups is Fe^{2+}; $Fe(OH)^{+}$ appears at basic pH (from pH 8.13 to 9.9). The occurrence of OM and the resulting HA-mediated binding of Fe(II) can therefore influence Fe(II) speciation and bioavailability in peatlands and wetlands, where seasonal anaerobic conditions prevail. Furthermore, the formation of a cationic bridge and/or the dissolution of Fe(III)-(oxy)hydroxides by the formation of Fe(II)-OM complexes can influence the speciation of other trace metals and contaminants such as As.

1 Introduction

Natural organic matter (NOM) derives from the biological and chemical degradation/transformation of plant and animal residues (Piccolo, 1996). The most refractory and reactive fraction with regards to metal binding is composed of humic substances (HS). Humic substances can be divided into three operational fractions: humic acids (HA) soluble under alkaline conditions, fulvic acids (FA) soluble over the entire pH range and humins, the insoluble fraction. Humic substances, and especially HA and FA, are considered to exert a major control on metal mobility and bioavailability in the environment (Buffle et al., 1998; Sposito, 1986; Tipping et al., 2002). They are renowned for their ability to bind a large range of metals and metalloids including possibly toxic elements such as REE, Al(III), Pb(II), Ca(II), Mn(II), Mg(II), Fe(III) and smaller amounts of As(V) (Bauer and Blodau, 2006; Buschmann et al., 2006; Kar et al., 2011; Lin et al., 2004; Redman et al., 2002; Ritter et al., 2006; Thanabalasingam and Pickering, 1986), As(III) (Buschmann et al., 2006; Liu et al., 2011; Thanabalasingam and Pickering, 1986; Warwick et al., 2005), Sb(V) (Filella and Williams, 2012; Pilarski et al., 1995; Tighe et al., 2005) and Sb(III) (Buschmann and Sigg, 2004; Filella

and Williams, 2012; Pilarski et al., 1995; Tella and Pokrovski, 2009). The high binding capacity of HS is usually attributed to the large surface density of oxygen-containing functional groups (carboxylic, phenolic, carbonyl) and, to a lesser extent, nitrogen- or sulfur-containing functional groups (Evangelou and Marsi, 2001). The binding ability of metals to HS has been intensively studied, notably through experimental and modeling studies (Christl et al., 2000; Fukushima et al., 1996, 1992; Milne et al., 2003; Mota et al., 1994; Nuzzo et al., 2013; Pinheiro et al., 1994; Tipping, 1998; Town and Powell, 1993). However, whereas HS binding with Fe(III) and Fe(III)-oxyhydroxides has been intensively studied (Morris and Hesterberg, 2012; van Schaik et al., 2008; Weber et al., 2006) only very few works have been dedicated to the understanding of Fe(II)-HS complexation mechanisms (Rose and Waite, 2003; Schnitzer and Skinner, 1966; Van Dijk, 1971; Yamamoto et al., 2010).

A better understanding and the quantification of Fe(II)-HS binding is crucial in the case of reduced waters, such as those occurring in peatlands, wetlands or anoxic sediments. As iron(II), the reduced species of Fe is much more soluble than Fe(III), Fe(II) concentrations are generally high (i.e. several mg L^{-1}) in these waters (Buffle et al., 1989; Davison, 1993; Dia et al., 2000; Olivie-Lauquet et al., 2001; Ponnamperuma, 1972). In such environments, where soils or sediments are periodically flooded and water-saturated, the organic matter (OM) is slightly degraded. High content of soluble, colloidal or particulate OM, and notably HS, are therefore encountered in these soils and soil solutions. The combination of these two features along with the high metal binding capacity of HS suggests that HS could be an important parameter in these waters, controlling not only the solubility, mobility and bioavailabity of Fe(II), but also the kinetics of Fe(II) oxidation and the type of Fe(III) oxides formed during reoxidation (Pédrot et al., 2011).

Another more indirect reason to study the binding of Fe(II) by HS is that this binding could have major implications regarding groundwater contamination by As. Recent studies have shown that reduced, organic-rich sediments from flood plains could be an important source of As for underlying aquifers (Fendorf, 2010; Harvey et al., 2006; Kocar, 2008; Polizzotto et al., 2008). It has been shown in an oxic environment that Fe(III), through the

formation of ternary complexes with HS, allows the binding of As(V) as an oxyanion to OM (Mikutta and Kretzschmar, 2011; Sharma et al., 2010). In this type of organic-rich environment, As(V) sorption onto OM seems to be a controlling factor for As speciation in contrast with previous studies which suggested that Fe-oxyhydroxides control the fate of As. Is it possible that similar complexes are formed between dissolved organic matter (DOM) and As(III) and As(V) in reduced, organic-rich waters, using Fe(II) as a cationic bridge between DOM and As species? Do these complexes enhance the mobility of As in flood plain sediments and to what extent are they involved in the contamination of underlying aquifers by As?

To better understand the potential role of HS with regards to Fe(II) and As mobility in reduced waters, a first step consists of describing and quantifying Fe(II)-HS binding. However, very few studies have been conducted to date with this purpose. It is necessary to identify which binding mechanisms are the prevailing ones and to estimate the stability constants of Fe(II) with HA and/or FA. Several attempts have been made to do this, but their results are contradictory. Schnitzer and Skinner (1966) established that Fe(II)-FA binding increases with increasing FA concentrations (from 0 to 1 g L^{-1}) and pH (from 3.5 to 5) with a maximum complexation at 57% of Fe(II) for pH = 3.5, $[Fe(II)]_{tot}$ = 100 mg L^{-1} and DOC = 553 mg L^{-1}. Van Dijk (1971) proposed from titration experiments that HA complexes Fe(II) through the formation of bidentate complexes. More recently, Rose and Waite (2003), who studied the kinetics of Fe(II) binding with 12 different NOMs in coastal waters, showed that Fe(II) binding with soil OM differs from one OM to another. Jackson et al. (2012) and Miller et al. (2012, 2009) studied the ability of OM to delay Fe(II) oxidation in an aerobic environment. Miller et al. (2012) proposed two mechanisms for Fe(II) oxidation in the presence of OM: first, a one-ligand model with two different oxidation mechanisms; second, they proposed a two-ligand model, where Fe(II) is first complexed with an OM strong binding site, and then with an OM weak binding site. Few datasets are therefore available concerning Fe(II)-HS binding.

These limited datasets could not be used to perform extensive modeling studies on Fe(II)-HS binding. Based on only one dataset (Van Dijk, 1971), Tipping (1998) reported the

following Fe(II)-HA binding parameters: log K_{MA} = 1.28 and ΔLK_2 = 0.81 using Model VI. For the NICA-Donnan model, Milne et al. (2003) did not use Van Dijk's (1971) dataset because this dataset corresponds to pH data. They simply estimated the Fe(II)-HA binding parameters using the LFERs (linear free energy relationship) between their binding parameters and log K_{OH}, the first hydrolysis constant. Concerning Fe(II)-FA complexation, they used Schnitzer and Skinner (1966) experimental datasets to determine their values for the binding parameters.

The aims of this study were to describe and quantify Fe(II)-HA complexation. Batch experiments involving complexation between Fe(II) and Leonardite HA were performed. This new experimental dataset was obtained through the coupling of an experimental approach combining ultrafiltration and Inductively Coupled Plasma Mass Spectrometry (ICP-MS) measurements. PHREEPLOT-PHREEQC-Model VI was then used to model the binding of Fe(II) to HS using our new dataset and to determine the binding parameters of Fe(II). A validation of these values for the binding parameters was then performed using the LFER method and by reproducing published data using PHREEQC-Model VI. Speciation on the different sites was then determined, providing complexation mechanisms of Fe(II) to HA.

2 Experimental, analytical and modeling methods

2.1 Reagents and materials

All aqueous solutions were prepared with analytical grade Milli-Q water (Millipore). The Fe(II) stock solutions were prepared with iron chloride tetrahydrate ($FeCl_2.4H_2O$) from Acros Organics. NaOH, HCl and HNO_3, all sub-boiling ultrapure grade, came from Fisher Chemical, Merck and VWR, respectively. Ammonium acetate, hydroxyammonium chloride and dimethyl-2,9 phenanthroline-1,10 chlorhydrate were obtained from Fisher Scientific, Merck and VWR Prolabo, respectively.

The HA used was the standard HA Leonardite from the International Humic Substance Society (IHSS). Prior to the experiments, HA molecules < 10 kDa were removed

using a Labscale TFF system equipped with a Pellicon XL membrane (PGCGC10, Millipore^{TM}). After acidic digestion, blank Fe, Mn and Mg concentrations occurring in HA were determined by ICP-MS. The average concentrations were 206.6 µg L^{-1}, 1 µg L^{-1} and 13.4 µg L^{-1} for Fe, Mn and Mg, respectively.

All materials were soaked in 10% HNO_3 and then rinsed with deionized water twice overnight. All experiments were conducted in a Jacomex isolator glove box (< 10 ppm of O_2) to prevent the oxidation of Fe(II) to Fe(III).

2.2 Setup of the binding experiments

A standard batch equilibrium technique was used. Three series of Fe(II)-HA complexation experiments were conducted in triplicate. Firstly, the pH was monitored and kept constant during 24 h with a multi-parameter Consort C830 analyzer combined with an electrode from Bioblock Scientific (combined Mettler InLab electrode). Calibrations were performed with WTW standard solutions (pH = 4.01 and 7.00 at 25°C). The accuracy of the pH measurements is ± 0.05 pH units. An isotherm adsorption experiment was carried out relative to the increasing Fe(II) concentration (0.61 to 8.55 mg L^{-1}). The average concentration of dissolved organic carbon (DOC) was 48.9 mg L^{-1}. The pH was fixed at 5.9 with ultrapure HCl and NaOH. Secondly, a pH sorption edge experiment was performed over a pH range from 1.95 to 9.90 with DOC and Fe(II) concentrations of 48.8 and 3.03 mg L^{-1}, respectively. Finally, a pH sorption-edge experiment was carried out over a pH range from 2.95 to 8.89 with DOC and Fe(II) concentrations of 76.5 mg L^{-1} and 3.15 mg L^{-1}, respectively. The $[Fe(II)]_{tot}$, pH and DOC concentrations used in these experiments are representative of the concentrations that can be found in wetland waters (Dia et al., 2000; Olivie-Lauquet et al., 2001; Ponnamperuma, 1972; Reddy and Patrick, 1977). The ionic strength of all experiments was fixed at 0.05 M with NaCl electrolyte solution. Experimental solutions were stirred for 24 h to reach equilibrium. At equilibrium, 15 mL of solution was sampled and ultrafiltrated at 5 kDa (Vivaspin VS15RH12, Sartorius) by centrifugation at 2970 g for 30 min.

under N_2 atmosphere. Ultracentrifugation cells were previously washed with 0.15 N HCl and Milli-Q water to obtain a DOC concentration below 1 mg L^{-1} in the ultrafiltrate.

2.3 Chemical analyses

Dissolved organic carbon (DOC) concentrations were determined using an organic carbon analyzer (Shimadzu TOC-V CSH). The accuracy of the DOC measurements was estimated at ± 5% for all samples using a standard solution of potassium hydrogen phtalate. Iron concentrations were determined by ICP-MS using an Agilent Technologies 7700x at Rennes 1 University. The samples were previously digested twice with 14.6 N HNO_3 at 90°C, evaporated to complete dryness and then resolubilized with HNO_3 at 0.37 mol L^{-1} to avoid any interferences with DOC during the analysis. ICP-MS analyses were carried out introducing He gas into collision cell to suppress any interference from Ar. The iron interference ($^{40}Ar^{16}O/^{56}Fe$) was properly reduced by using He gas into collision cell to reach a low detection limit for Fe analysis (LD Fe: 0.07 µg L^{-1}) (Instrumental and data acquisition parameters can be found in ANNEXE 1). Quantitative analyses were performed using a conventional external calibration procedure (7 external standard multi-element solutions - Inorganic Venture, USA). A mixed solution of rhodium-rhenium at a concentration level of 300 ppb was injected on-line with the sample in the nebulizer. This solution was used as an internal standard for all measured samples to correct instrumental drift and matrix effects. Calibration curves were calculated from the intensity ratios between the internal standard and the analyzed elements. A SLRS-5 water standard was used to check the accuracy of the measurement procedure, and the instrumental error on the Fe analysis is < 5%. Chemical blanks of Fe were below the detection limit (0.07 µg L^{-1}), and were thus negligible.

Concentrations of Fe(II) in the ultrafiltrate ($[Fe(II)]_{UF)}$ were determined with the 1.10-phenantroline colorimetric method (AFNOR, 1982) at 510 nm using a UV-visible spectrophotometer (UV/VIS Spectrometer "Lambda 25" from Perkin Elmer). Total Fe concentrations in the mixed HA-Fe(II) solutions were only measured by ICP-MS using the procedure described above. Indeed, the absorbance of Leonardite HA measured at 50 mg L^{-}

[1] of DOC is high (more than twice the absorbance of Fe(II)). The error of the $[Fe(II)]_{UF}$ and $[Fe(II)]_{tot}$ measurements was estimated at less than 5% above a concentration of Fe(II) of 0.85 mg L^{-1} (7% for a concentration of Fe(II) of 0.6 mg L^{-1}). Iron (II) concentrations in the ultrafiltrates were assumed to be inorganic Fe(II), whereas Fe(II) bound to HA (Fe(II)-HA) was considered to be the retentate fraction > 5 kDa. The fraction of Fe(II) bound to HA was calculated as $[Fe(II)\text{-}AH] = [Fe(II)]_{tot} - [Fe(II)]_{UF}$, with $[Fe(II)]_{tot}$ representing the Fe content of the mixed HA-Fe(II) solutions prior to ultrafiltration and $[Fe(II)]_{UF}$ the Fe concentration determined in the ultrafiltrate by ICP-MS.

2.4 Determination of the PHREEQC-Model VI binding parameters

2.4.1 PHREEQC-Model VI

In this study, Model VI was coupled with PHREEQC as has been previously done (Marsac et al., 2012). It was used to calculate the partitioning of ions between the various complexing sites available on HS. PHREEQC-Model VI assumes that the complexation of ions by HS occurs through eight discrete sites: four weak sites, named A sites (usually assumed to be carboxylic groups), and four strong sites, named B sites (usually assumed to be phenolic groups). The abundance of type A and B sites are respectively named n_A (mol g^{-1}) and $n_B = 0.5 * n_A$ (mol g^{-1}). The intrinsic proton dissociation constants for type A and B sites and their distribution term are pK_A, pK_B, ΔpK_A and ΔpK_B, respectively. The fractions of proton sites that can make bidentate sites and tridentate sites are named f_B and f_T, respectively. Ion adsorption by humic and fulvic substances is described by a specific complexation parameter log K_{MA} and log K_{MB} for carboxylic and phenolic sites, respectively. The abundance of type A and B sites, their distribution term and the fraction of sites that can form bidentates and tridentates sites differ from HA to FA. The values of these constants are presented in Table II. 1 (from Tipping et al., 2002).

Table II. 1: PHREEQC-Model VI parameters for the humic and fulvic acids (Tipping, 1998)

Parameter	Description	HA	FA
n_A	Abundance of type A sites (mol g^{-1})	0.0033	0.0048
n_B	Abundance of type B sites (mol g^{-1})	0.00165	0.0024
pK_A	Intrinsic proton dissociation constant for type A sites	4.1	3.2
pK_B	Intrinsic proton dissociation constant for type B sites	8.8	9.4
ΔpK_A	Distribution term that modifies pK_A	2.1	3.3
ΔpK_B	Distribution term that modifies pK_B	3.6	4.9
f_B	Fraction of proton sites that can make bidentate sites	0.5	0.42
f_T	Fraction of proton sites that can make tridentate sites	0.065	0.03
Log K_{MA}	Intrinsic equilibrium constant for metal binding at type A sites	Fitted from experimental data	
Log K_{MB}	Intrinsic equilibrium constant for metal binding at type B sites	Fitted from experimental data	
ΔLK_{1A}	Distribution term that modifies log K_{MA}	-0.7	0.5
ΔLK_{1B}	Distribution term that modifies log K_{MB}	0.8	2.1
ΔLK_2	Distribution term that modifies the strength of bidentate and tridentate sites	Fitted from experimental data	

Tipping (1998) established a linear relationship between log K_{MA} and log K_{MB}: log K_{MB} = 3.39 * log K_{MA} - 1.15 (R^2 = 0.80) to constrain the number of parameters set. This was deleted in PHREEQC-Model VI by Marsac et al. (2011), who determined the binding parameters of the rare earth elements (REE) with HA. The interaction between one site and one ion is characterized by the complexation constant log K. These eight sites can therefore form monodentate, bidentate or tridentate complexes with a given ion. The log K values are calculated from (1) log K_{MA} and ΔLK_{1a} for a monodentate carboxylic site, (2) log K_{MB} and ΔLK_{1b} for a monodentate phenolic site, (3) log K of the two monodentate sites for a weak bidentate site, (4) log K of the two monodentate sites and $1*\Delta LK_2$ (9% of the sites) and $2*\Delta LK_2$ (0.9% of the sites) for a strong bidentate site, (5) log K of the three monodentate sites for a weak tridentate site and (6) log K of the three monodentate sites and $1.5*\Delta LK_2$ (9% of the sites) and $3*\Delta LK_2$ (0.9% of the sites) for a strong tridentate site. Eighty binding equations are then defined. An electrical double layer is involved in the electrostatic interaction. The thickness of the electrical double layer corresponds to $1/\kappa$, where κ is the Debye-Hückel parameter. The ion distribution between the diffuse layer and the solution volume is calculated by a simple Donnan model.

2.4.2 PHREEPLOT

PHREEPLOT is a software used to create graphical output and to fit data using PHREEQC. The 80 complexation equilibria defined in PHREEQC-Model VI for HA and FA were added in the "minteq.v4" database. The humic and fulvic acids were defined as SOLUTION_MASTER_SPECIES, SOLUTION_SPECIES and PHASES. The 160 (80*2) types of sites defined in PHREEQC-Model VI were added as SURFACE_MASTER_SPECIES in the "minteq.v4" database. The aim of the modeling process was to determine the value of log K_{MA} and log K_{MB} for Fe(II) by fitting the concentration of Fe(II) bound to HA from experimental data with those calculated by PHREEPLOT. A nonlinear relationship between log K_{MA} and log K_{MB} was used as previously performed by Marsac et al. (2011). The specific PHREEQC-Model VI binding parameters, namely log K_{MA}, log K_{MB}, ΔLK_{2C} and ΔLK_{2P}, were defined in PHREEPLOT as fitting parameters. Their values were determined by extrapolation of the present experimental Fe(II)-HA dataset. Binding parameters were optimized using the weighted sum of squares of the residuals. The stability constants of all sites defined in PHREEQC-Model VI were calculated from log K_{MA} and log K_{MB}. The reactions necessary for PHREEPLOT calculation were added in the SURFACE_SPECIES section of PHREEPLOT using a different name for each constant. The 80 equations defined in PHREEQC-Model VI were added using their SURFACE_SPECIES nomenclature in the PHREEPLOT input as "numericTags".

2.5 LFER linear free energy relationship

The PHREEQC-Model VI type A sites represent carboxylic groups of HA or FA. Acetic acid (CH_3COOH) can be used as a molecular model of HA carboxylic groups. Pourret et al. (2007) determined a linear relationship (LFER) between log K_{MA} and log K(M-AA), the stability constant of a metal M with acetic acid:

$$\log K_{MA} = 1.03 * \log K(M\text{-}AA) - 0.43 \; ; \qquad R^2 = 0.80 \qquad (1)$$

Another LFER between log K_{MA} and the first hydrolysis constant of a metal M log K(M-OH) has been suggested by the same authors (Pourret et al., 2007):

$$\log K_{MA} = 0.24 * \log K(M\text{-}OH) + 0.32 ; \quad R^2 = 0.78 \qquad (2)$$

Marsac et al. (2011) showed that the linear relationship between log K_{MA} and log K_{MB} established by Tipping (1998) could not account for the binding of REE with HA. These authors estimated log K_{MB} using the LFER method based on log K_{MB} and the metal catechol stability constant (log K(M-catechol)):

$$\log K_{MB} = 0,37 * \log K(M\text{-catechol}) + 0,86 \quad (R^2 = 0.95) \qquad (3)$$

3 Results

3.1 Experimental results

$Fe(II)_{UF}$ and $Fe(II)_{tot}$ concentrations (data presented in the supplementary information) determined using the phenanthroline method showed that no oxidation of Fe(II) occurred during any of the experiments. The quantification limit (QL) of the phenanthroline method is 0.5 mg L^{-1} of $Fe(II)_{UF}$ which is x5000 the QL of the ICP-MS method (0.12 µg L^{-1}). The iron(II) concentrations used in this work were therefore those determined by ICP-MS.

3.1.1 Adsorption isotherm

Figure II. 1 presents log [Fe(II)-HA] according to log $[Fe(II)]_{UF}$. At low $[Fe(II)]_{UF}$ concentrations (log $[Fe(II)]_{UF}$ = -6.2), log [Fe(II)-HA] was approximately -5.0 and increased progressively to reach -4.28 for the maximum log $[Fe(II)]_{UF}$ value used (log $[Fe(II)]_{UF}$ = -4.00). The lack of any plateau suggests that the saturation of HA complexation sites was not reached.

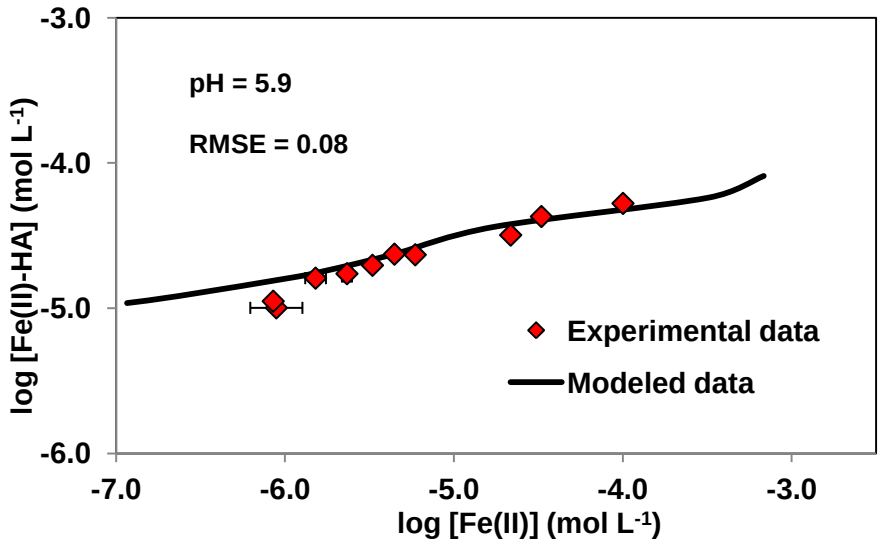

Figure II. 1: Adsorption isotherm: experimental and modeled data

3.1.2 pH sorption edge

pH sorption edge experiments are very useful to better constrain the values of the binding parameters. Indeed, at acidic pH, the HA sites are protonated and only strong sites are able to bind cations. At basic pH, all sites are deprotonated and able to bind cations. Figure II. 2a displays the proportion of Fe(II) bound to HA in the pH range 1.95 to 9.90 (DOC = 48.5 mg L^{-1}). At pH = 1.95, only 4.1% of the total Fe(II) was complexed with HA. The adsorbed Fe(II) percentage then increased progressively with increasing pH to reach 51.3% at pH = 4.99 and > 99% at pH > 8.13. Figure II. 2b displays the adsorbed Fe(II) percentage at DOC = 76.5 mg L^{-1} in the pH range 2.95 to 8.89. 17.6% of the total Fe(II) was bound to HA at pH = 2.95, with this amount reaching 62.9% and > 99% for pH values = 4 and 8.89, respectively. Both pH sorption edge experiments exhibited the same trend, but the percentages increased with the increasing DOC concentration.

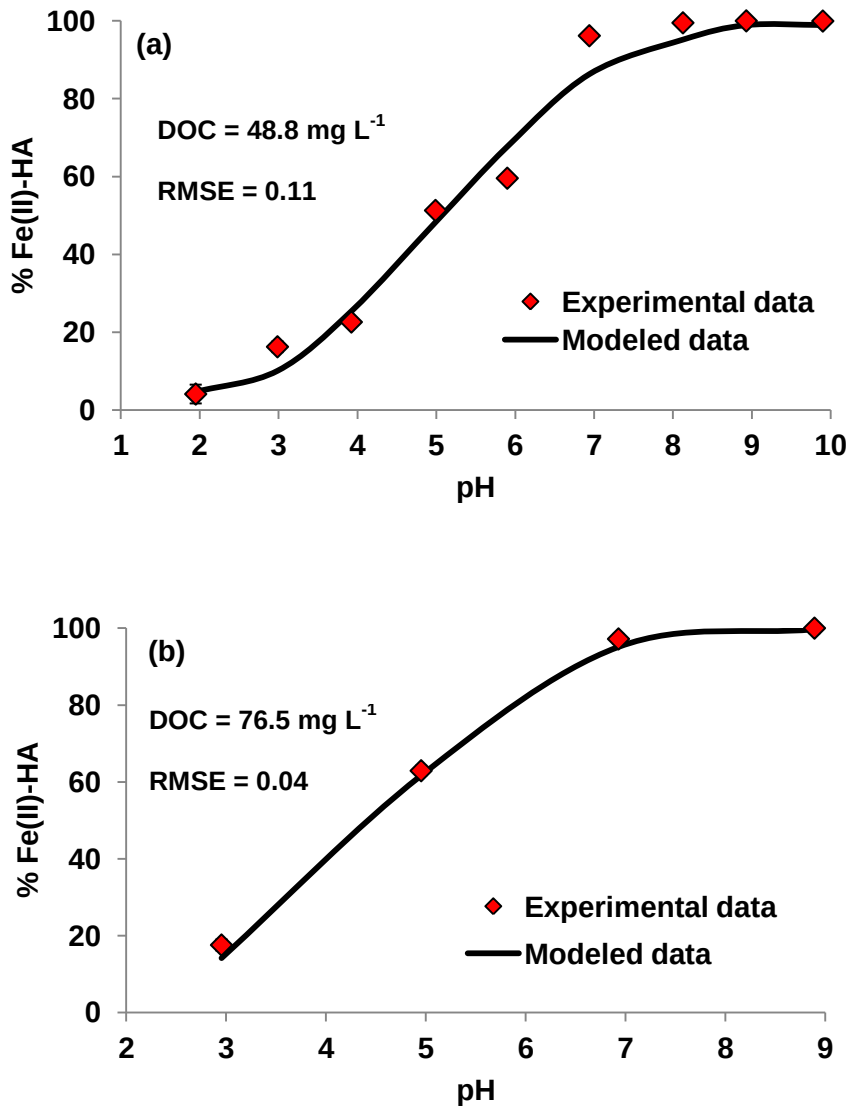

Figure II. 2: (a) pH adsorption edge - DOC = 50 mg L^{-1} (b) pH adsorption edge - DOC = 76 mg L^{-1} (the error bars calculated from the triplicated experiments are within the symbols.). As each experiment was performed in triplicate, each point represents the average of the triplicates. The error bars represent the standard deviation (in log or percentage, depending on the data) calculated from the triplicated experimental data.

3.2 Model results

As explained in section II.2.4, we used the coupling PHREEPLOT-PHREEQC-Model VI to simultaneously fit all our datasets. We determined the following values for the Fe(II) binding parameters (without the linear relationship between log K_{MA} and log K_{MB}): log K_{MA} = 2.19 ± 0.16, log K_{MB} = 4.46 ± 0.47 and ΔLK_2 = 3.90 ± 1.31 with R^2 = 0.97.

3.2.1 Adsorption isotherm

The root-mean-square error (RMSE) was calculated as $\mathrm{RMSE} = \sqrt{\mathrm{mean}(\log v_{exp} - \log v_{calc})^2}$ where v_{exp} and v_{calc} are the amounts of Fe bound to HA per gram of DOC for the experimental and modeled data, respectively. The modeled data were plotted as a solid line in Figure II. 1, 2a and 2b. The fit goodness of the adsorption isotherm was validated by the RMSE value of 0.09. Log [Fe(II)-AH] and log $[Fe(II)]_{UF}$ increased as the [Fe(II)] total concentration increased (Figure II. 1). The modeled data were close to the experimental data as shown by the RMSE equal to 0.08 for this dataset. In Figure II. 1, the first points, log [Fe(II)-HA] = -4.95 and -5, were both far from the modeled data compared to the other points. Despite the fact that the fit appears to be visually poor at low concentrations, the RMSE is good. This can be explained by the scale used here (log[Fe(II)]), which reinforces the differences. We tried to improve the fit for the points at low concentrations using the new parameters, but the fits for the global pH adsorption edge were worse. Furthermore, these parameters did not involve any modifications of the Fe(II) speciation on the HA sites. Therefore, we chose the set of binding parameters that provided the best RMSE.

3.2.2 pH adsorption edge

The percentage of adsorbed Fe(II) increased with increasing pH in both experiments (DOC concentration = 48.8 mg L^{-1}, Figure II. 2a and 76.5 mg L^{-1}, Figure II. 2b). The RMSE for the first dataset (DOC = 48.8 mg L^{-1}, Figure II. 2a) is equal to 0.11. The experimental percentage of adsorbed Fe(II) was higher than in the simulation at pH = 6.94 and 8.13, but lower than in the simulation at pH = 5.90 and 2.99, explaining this high RMSE. For the second dataset (DOC = 76.5 mg L^{-1}, Figure II. 2b) the RMSE is much lower (0.06) indicating a better fit between the modeled and experimental data. In both cases, the pH adsorption edge showed low Fe(II) complexation by HA (< 20%) at acidic conditions (pH ≤ 3), the complexation becoming instead nearly quantitative (> 90%) at pH > 7.

3.3 Fe(II) speciation onto HA binding sites

Speciation was calculated from the fit of the experimental data using PHREEQC-Model VI. PHREEQC-Model VI is able to calculate the proportions of Fe(II) bound to each site defined in the model: phenolic (sum of Fe(II) bound to phenolic monodentate, pheno-phenolic bidentate and pheno-pheno-phenolic tridentate groups), carboxylic (sum of Fe(II) bound to carboxylic monodentate, carboxy-carboxylic bidentate and carboxy-carboxy-carboxylic tridentate groups), carboxy-phenolic (sum of Fe(II) bound to carboxy-phenolic bidentate, carboxy-carboxy-phenolic and carboxy-pheno-phenolic tridentate groups), etc. The complex denticity was also determined: monodentates correspond to the sum of Fe(II) bound to carboxylic and phenolic groups, bidentates to the sum of Fe(II) bound to carboxy-phenolic, pheno-phenolic and carboxy-carboxylic groups and tridentates to the sum of Fe(II) bound to carboxy-carboxy-carboxylic, carboxy-pheno-phenolic and pheno-pheno-phenolic groups.

3.3.1 Adsorption isotherm

The majority of Fe(II) (between 73.1 and 83.9% of Fe(II)) was bound to HA by bidentates. The remaining Fe(II) was mainly bound through tridendate sites (20%), as the amount of Fe(II) bound through tridentate sites is insignificant (< 1%, Figure II. 3a). Moreover, the proportions of Fe(II) bound to carboxylic, carboxy-phenolic and phenolic functional groups were 50%, 40% and 10%, respectively (Figure II. 3b). All Fe(II) bound to HA was in the form of Fe^{2+} (Figure II. 3c).

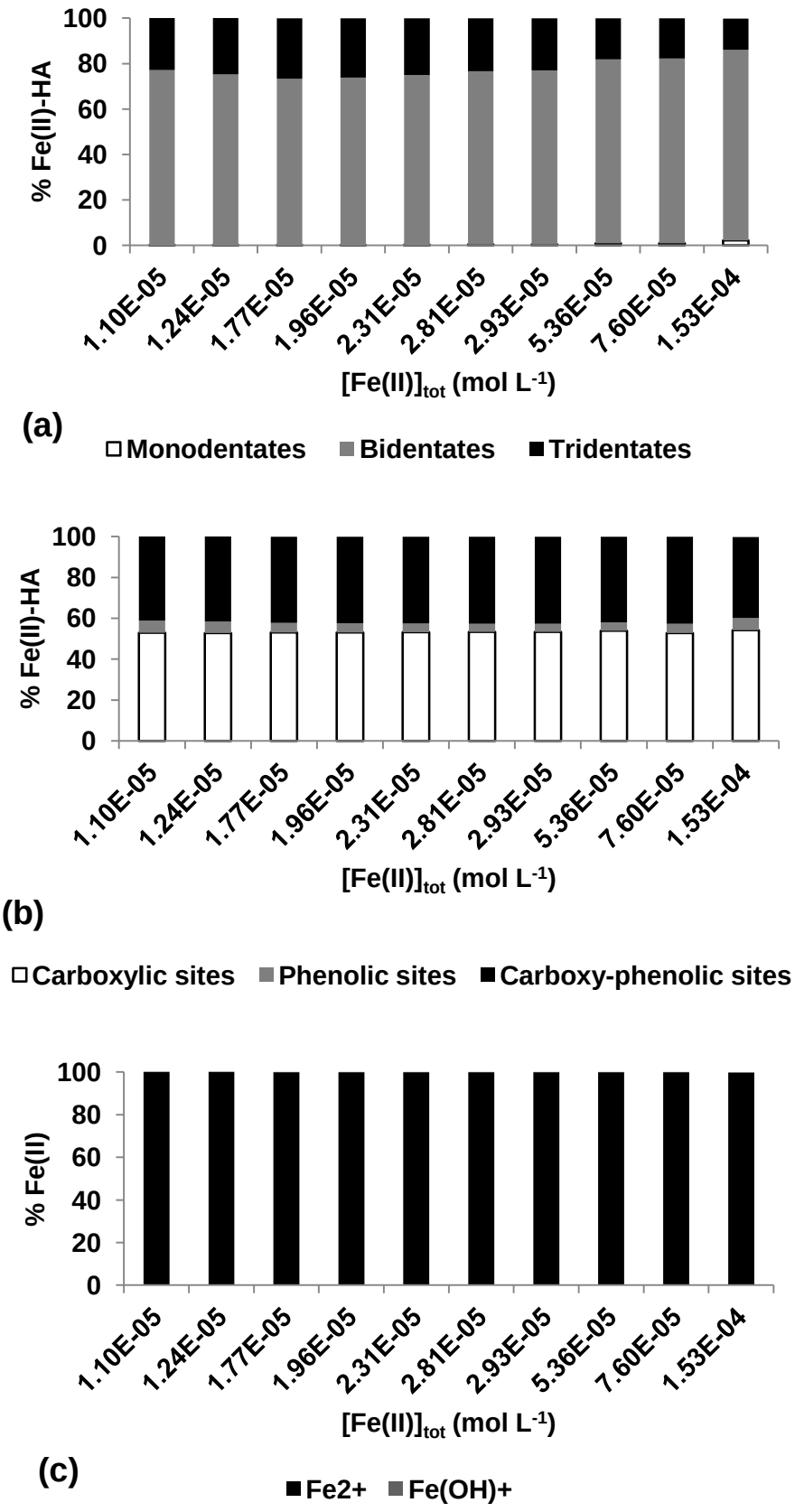

Figure II. 3: Fe(II) speciation onto the binding sites - adsorption isotherm (a) Denticity (b) Type of site (c) Form of adsorbed Fe(II).

3.3.2 pH adsorption edge

In the experiment conducted with a DOC concentration of 48.8 mg L^{-1}, more than 80% of Fe(II) bound to HA formed bidentates and approximately 15% formed tridentates. The number of monodentate sites was insignificant in this experiment (< 1%, Figure II. 4a). The pH did not influence their distribution, but strongly controlled the nature of the functional groups involved. Thus, the proportion of carboxylic groups decreased from > 80% at pH = 1.95 to < 10% at pH = 9.90 (Figure II. 4b), which was compensated by an increased role of carboxy-phenolic sites, which accounted for between 20 and 60% of the Fe(II) binding with increasing pH. Some phenolic sites were also involved (up to 20% at pH = 9.90), but only at high pH. From acidic to neutral pH conditions, all Fe(II) bound to HA occurred as Fe^{2+} (Figure II. 4c). The Fe-OH^{+} species appeared only from pH = 8.13 (1.35% of Fe(II) bound to HA), with the proportions of this species then increasing with increasing pH to reach 38.5% at pH = 9.90.

In the experiment conducted with a DOC concentration of 76.5 mg L^{-1}, considering the nature and proportion of the functional groups involved, the evolution with regards to the pH was quite similar to that observed in the previous experiment. Approximately 80% (from 78.8 to 86.7%) of Fe(II) was bound to HA as bidentates (Figure II. 5a) and approximately 20% as tridentates. The proportions of Fe(II) bound as monodentates were insignificant (< 1%). At acidic pH (2.95 and 4.95), 66% of Fe(II) was bound to carboxylic groups, approximately 30% to carboxy-phenolic groups and approximately 1% to phenolic groups (Figure II. 5b). At pH = 6.93, 52.3% of Fe(II) was bound to carboxy-phenolic groups, 33.5% to carboxylic groups and 14.2% to phenolic groups. At basic pH (8.89), Fe(II) was more bound to carboxy-phenolic groups (59.6%), than to phenolic (21.8%) or carboxylic groups (18.6%). At acidic and neutral pH (pH 2.95, 4.95 and 6.93), Fe(II) was completely bound to HA as Fe^{2+} (Figure II. 5c), whereas at basic pH (8.89), 6% of Fe(II) bound to HA occurred as $Fe(OH)^{+}$.

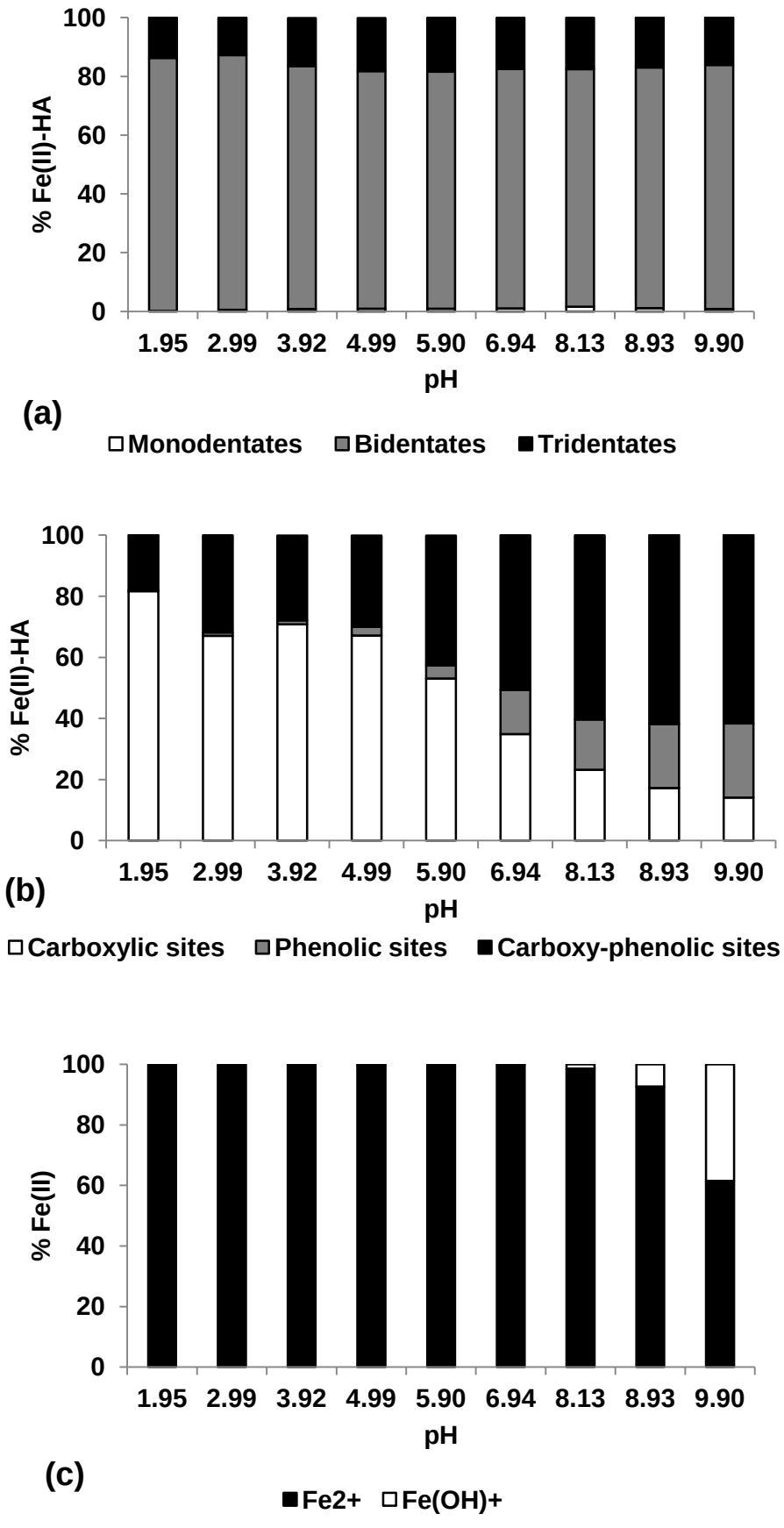

Figure II. 4: Fe(II) speciation onto the binding sites - pH adsorption edge - DOC = 50 mg L^{-1} (a) Denticity, (b) Type of site, (c) Form of adsorbed Fe(II).

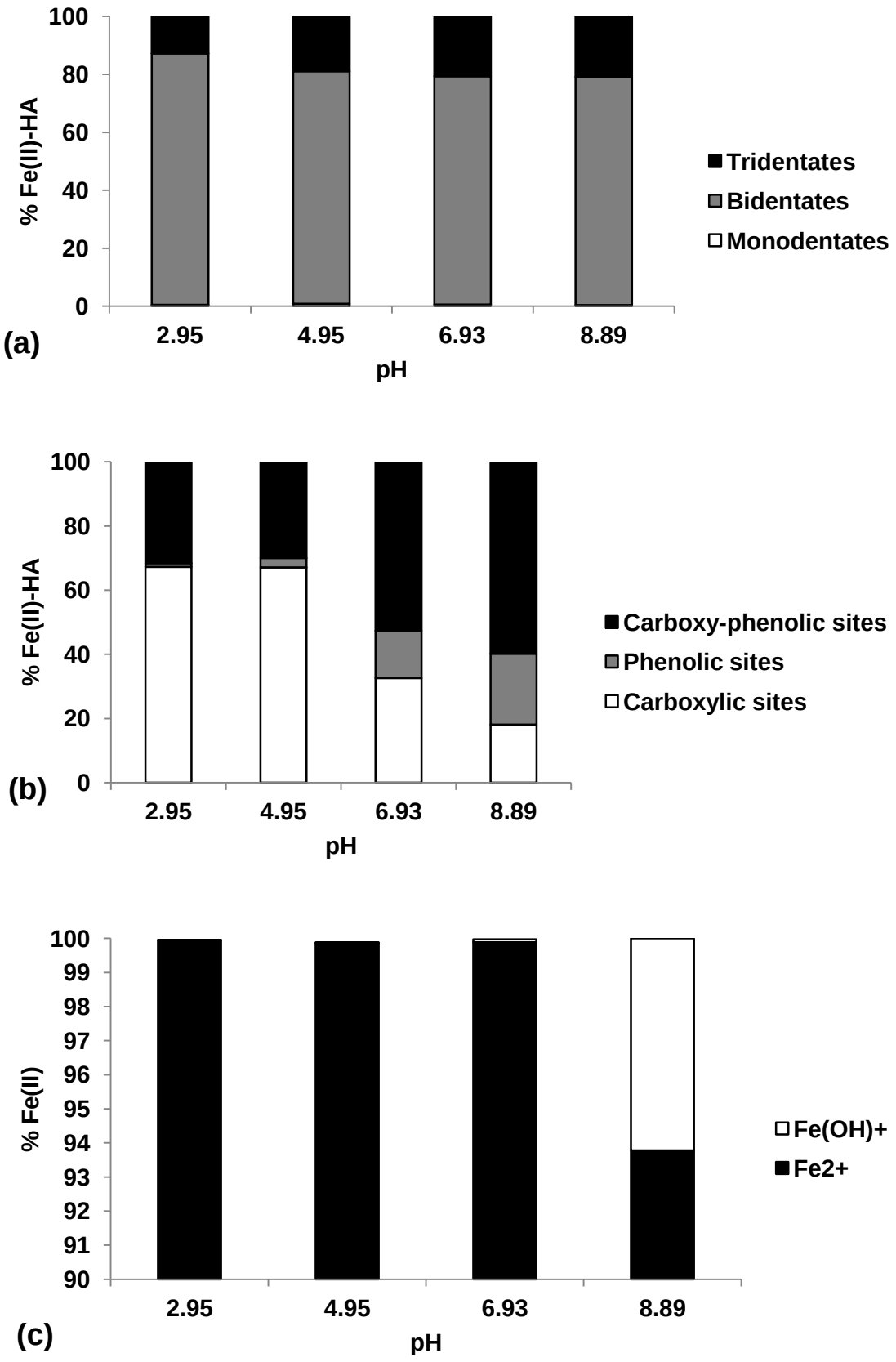

Figure II. 5: Fe(II) speciation onto the binding sites - pH adsorption edge - DOC = 76 mg L^{-1} (a) Denticity, (b) Type of site, (c) Form of adsorbed Fe(II).

4 Discussion

4.1 Validation of the set of binding parameters

Two strategies were used to validate the new estimated binding parameters (log K_{MA} and log K_{MB}). They were first compared with the parameters estimated by the LFER technique. Second, the conditions of the previously published experimental studies were put into PHREEQC-Model VI to calculate the expected Fe(II)-HS proportions; the calculated proportions were then compared with the proportions determined experimentally.

The binding parameters determined in the present work are different from those determined by Tipping (1998) due to (1) the deletion of the linear relationship between log K_{MA} and log K_{MB} as performed by Marsac et al. (2011) and (2) the experimental dataset used for fitting. Tipping (1998) only used the criticized Van Dijk (1971) dataset. Van Dijk (1971) studied Fe(II) binding with HA through titrations and consequently only provided pH data.

The specific log K_{MA} and log K_{MB} parameters can be estimated using the linear relationship existing between these parameters and the acid acetic (log K_{MA}), first hydrolysis (log K_{MA}), and catechol (log K_{MB}) stability constants. The stability constant of Fe(II) with acetic acid (log K(Fe(II)-AA)) and the first hydrolysis constant of Fe^{2+} (log K(Fe(II)-OH)) are log K(Fe(II)-AA) = 3.32 and log K(Fe(II)-OH) = 7.72 (IUPAC). Using these values, the LFERs determined by Pourret et al. (2007) and Marsac et al. (2011) resulted in the following estimates for the log K_{MA} and log K_{MB} values: 1.57 < log K_{MA} < 2.35 (acetic acid LFER, R^2 = 0.80) and 1.69 < log K_{MA} < 2.65 (first hydrolysis LFER, R^2 = 0.78); 3.70 < log K_{MB} < 4.09 (catechol LFER, R^2 = 0.95). As can be seen, there is a full agreement between the log K_{MA} value determined experimentally in this study (2.19) and the log K_{MA} values estimated using the LEFR method. For log $K_{MB,}$ the experimentally determined value (4.46) is bigger than the LFER estimate. However, the shift remains limited, as it was only 15%.

An attempt to experimentally determine the binding constants of Fe(II) by FA was made by Schnitzer and Skinner (1966) using an ion-exchange method. Two sets of experiments were performed with the same concentration of Fe(II) (1.79 10^{-3} mol L^{-1}): one at

pH 3.5 with 201, 402, 603, 804 and 1005 mg L^{-1} of FA, and one at pH = 5 with 100.5, 120.6, 160.8, 201 and 241.2 mg L^{-1} of FA (Figure II. 6). They showed that Fe(II) binding with FA was only slightly affected by pH. Schnitzer and Skinner's (1966) dataset was calculated using our new Fe(II)-HA binding parameters with PHREEQC-Model VI. For this purpose, we used the relationship between log K_{MA}(HA) and log K_{MA}(FA) established by Tipping (1998): log K_{MA}(HA) = 0.64 * log K_{MA}(FA) + 0.79 (R^2 = 0.84). We also used this relationship to determine the binding parameters for FA: log K_{MA} = 2.19 ; log K_{MB} = 4.46 and ΔLK_2 = 3.89. At pH = 3.5, the modeled partitioning of Fe(II) between free species and FA complexes was close to the experimental one, with a low RMSE value of 0.04, but the fit was not as good at pH = 5 as the RMSE value was much higher (RMSE = 0.26) (Figure II. 6). Thus, the new set of binding parameters failed to reproduce Schnitzer and Skinner's data (1966) over the entire pH range. It is to be noticed, however, that Tipping (1998) himself did neither use Schnitzer and Skinner's (1966) dataset in his estimation of Fe(II)-FA binding parameters, nor for the other metals studied by these authors. Tipping and Hurley (1992) justified this by noting that the log K_{MA} value of Fe(II)-FA calculated from Schnitzer and Skinner's (1966) dataset did not rank properly when compared to the log K_{MA} values determined for the other cations. The Fe(II) log K_{MA} obtained using Schnitzer and Skinner's (1966) dataset was intermediate between Pb^{2+} and Cu^{2+} log K_{MA}, in contradiction with the findings of Martell and Smith (1989), who established that Fe^{2+} stability constants should be lower than those for Pb^{2+} and Cu^{2+} binding constants with mono- and di-carboxylic acids. This dataset was also criticized by Milne et al. (2003) who attributed it a poor score when trying to fit it using the NICA-Donnan model. They could not simply extrapolate the calculated data from Schnitzer and Skinner (1966) experimental data and had to constrain the second site distribution values using LFER between their binding parameters and log KOH. According to Tipping and Hurley (1992) it is possible that in the experimental conditions used by Schnitzer and Skinner (1966), part of the Fe(II) was oxidized into Fe(III), and that this oxidation caused the observed shift between the calculated and expected log K_{MA} values.

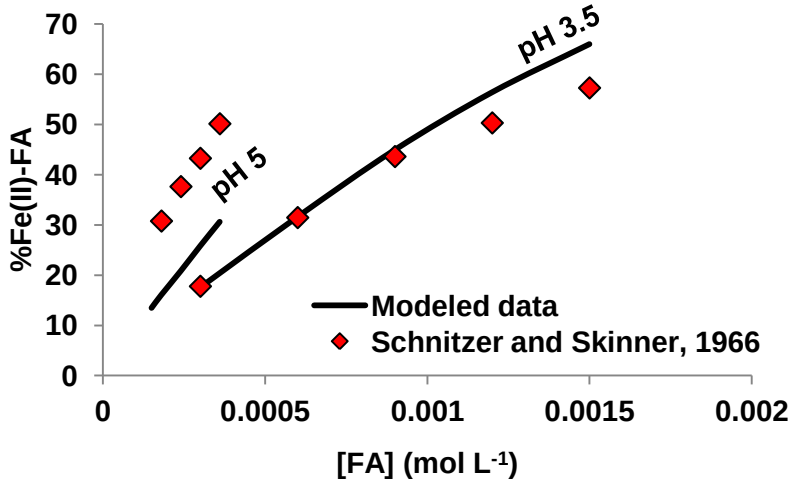

Figure II. 6: Schnitzer and Skinner's (1966) dataset: experimental and modeled % of Fe(II) adsorbed onto FA.

Yamamoto et al. (2010) estimated the binding capacities of HS with Fe(II) using a colorimetric method. Yamamoto et al. (2010) used HA and FA extracted from compost with a HA concentration of 1 mg L^{-1} and determined the Fe(II) concentrations using the ferrozine colorimetric method. As with Schnitzer and Skinner's (1966) data, the new binding parameters obtained here failed to model these data (RMSE > 1). This failure is thought to be due to an analytical bias in the dataset, related to the colorimetric method. Jackson et al. (2012) emphasized the poor reliability of the colorimetric methods to determine the Fe(II) concentration bound to HS.

Rose and Waite (2003) studied the kinetics of Fe(II) complexation with NOMs. They used 12 different NOMs recovered from the soil leaf litter layer and one fulvic acid stock solution: Suwannee River FA (SRFA). Binding experiments were performed in seawater with a nominal salinity of 36 (ionic strength ≈ 1.7 M) at pH 8.1. Three Fe(II) concentrations were used: 0.25, 0.5 and 1 µmol L^{-1} with a total organic carbon concentration of 1 mg L^{-1}. All of the data used for the calculations were equilibrium concentrations (i.e. concentrations determined at the end of the kinetics). The amount of Fe(II) adsorbed at equilibrium differed from one NOM to another. For example, for $[Fe(II)]_{tot}$ = 1 µmol L^{-1}, the percentages of experimentally adsorbed Fe(II) varied from 5 to 100% depending on the NOM sample considered. This variability could not be reproduced by PHREEQC-Model VI (Figure II. 7a),

suggesting that some important properties of the NOM samples used were not taken into account by the model. In fact, the NOM samples used by Rose and Waite (2003) in their experiments were extracted from soil leaf litter, which were probably different in composition from the HS structure considered in PHREEC-Model VI. The situation is obviously much different for the SRFA sample used by Rose and Waite (2003), which has a structure that is typical for a HS. Interestingly, a reasonably good fit (RMSE = 0.03) was obtained with the new binding parameters for the data (SRFA) published by Rose and Waite (2003) (Figure II. 7b). Note that data from Van Dijk's dataset (1971) were not used for the purpose of a validation test considering, as Milne et al. (2003) did, that the measurement of the pH values was not sufficiently precise in this study.

Thus the new binding parameters obtained here were able to model the Fe(II) adsorption onto both HA and FA reasonably well. The new set of parameters satisfactorily reproduced Rose and Waite's (2003) experimental data for SRFA (RMSE = 0.03) and the present data. It is interesting to see that previously determined binding parameters used a linear relationship between log K_{MA} and log K_{MB} (Tipping, 1998). In fact, the present data cannot be modeled if this relationship is imposed. As Marsac et al. (2012) did, we had to remove this constraint to satisfactorily model our data. When Marsac et al. (2012) tried to model their data using the linear relationship, REE patterns were identical for weak and strong sites, which is impossible with regards to their stability constants with single organic ligands, such as acetate (weak sites) or EDTA (strong sites) (Marsac et al., 2011). To reproduce correctly REE patterns binding to strong sites, the authors had to delete this linear relationship. Consequently, log K_{MB} values decreased and were compensated by higher values of ΔLK_{2C} and ΔLK_{2P}. Most likely, this explains why we also obtained a high ΔLK_2 value (3.90). Despite the use of a glovebox, part of the Fe(II) might be oxidized into Fe(III) which might explain the strong Fe adsorption at acidic pH and the subsequent high value of ΔLK_2.

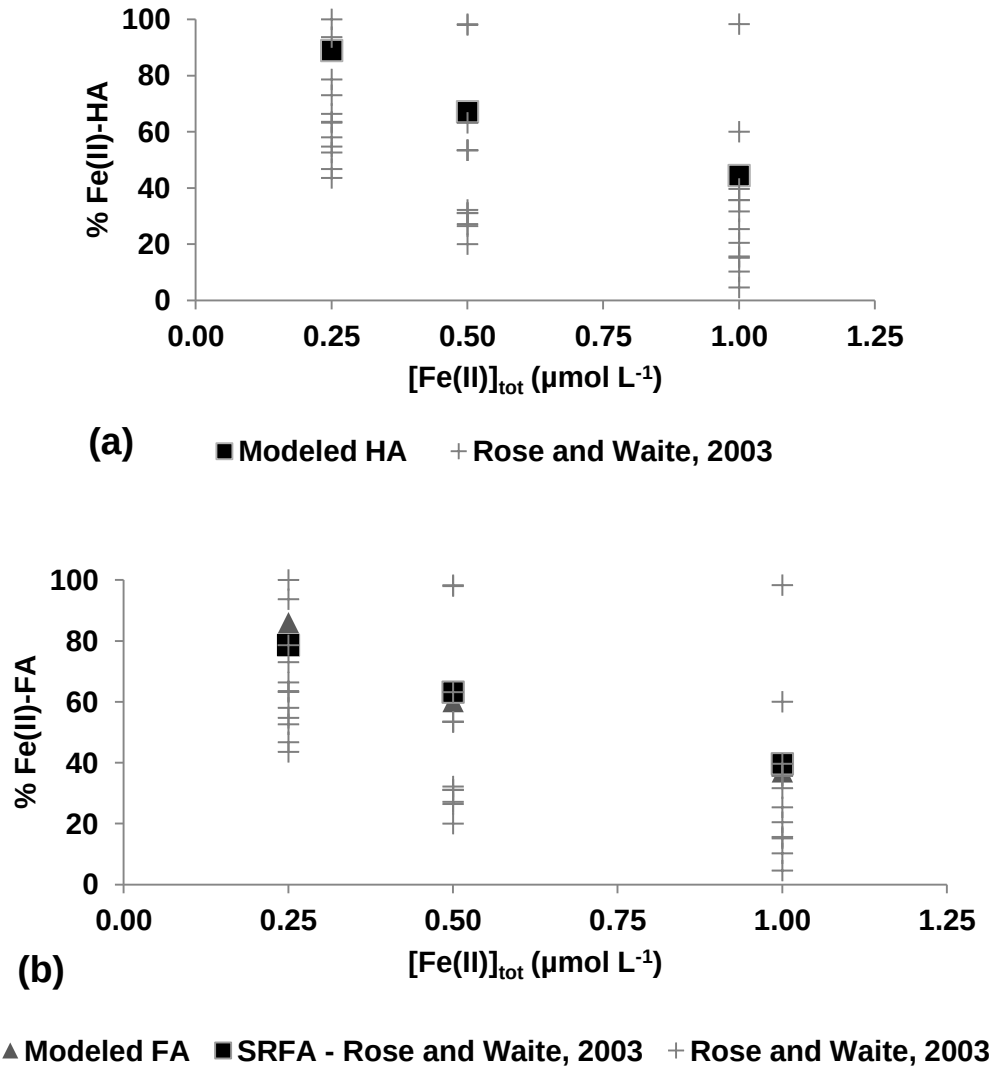

Figure II. 7: Rose and Waite's (2003) dataset: (a) Comparison % of Fe(II) adsorbed onto twelve different natural organic matters through an experimental approach and HA modeled data, (b) Experimental (SRFA)-mediated and modeled % of Fe(II) adsorbed onto FA.

However, humic substances are expected to delay the oxidation of Fe (Kleber et al., 2005; Miller et al., 2009; Weber et al., 2006; Wolthoorn et al., 2004) and no Fe(III) was measured in the ultrafiltrated solution. Indeed, Weber et al. (2006) performed sorption experiments of Fe(III) (50 and 30 µM) with organic matter (1.8 g L^{-1}). They showed that for the lowest total Fe concentrations, a fraction of Fe can be reduced by humic substances. The concentrations of Fe(II) used in the present study were from 11 to 56 µM, within the range of Weber et al.'s (2006) experiments. Weber et al.'s (2006) study suggests therefore that OM

tends to reduce Fe(III) into Fe(II) and not to oxidize it. So, oxidation of Fe(II) into Fe(III) seems unlikely in the experimental conditions used in the present study.

However at any rate, the high ΔLK_2 value obtained here is lower than the ΔLK_2 of 4.0 reported by Marsac et al. (2012; 2013) for the binding of Fe(III) by HS (Table II. 2), which is rather consistent given that Fe(III) species are known to form stronger complexes with HS than Fe(II) species (Ou et al., 2009). The new binding parameters determined in the present study (log K_{MA} = 2.19, log K_{MB} = 4.46 and ΔLK_2 = 3.90) are therefore in accordance with the Fe(III) binding parameters of Marsac et al. (2013).

Table II. 2: log K_{MA}, log K_{MB}, ΔLK_{2C} and ΔLK_{2P} values of the different species of Fe from Tipping (1998) (1) from this study (2), and from Marsac et al., 2013 (3).

Parameter	Fe^{2+} / $FeOH^{+}$ (1)	Fe^{2+} / $Fe(OH)^{+}$ (2)	Fe^{3+} / $FeOH^{2+}$ (1)	Fe^{3+} / $FeOH^{2+}$ (3)
log K_{MA}	1.3	2.19	2.5	3.5
log K_{MB}	3.257	4.46	7.325	6.9
ΔLK_{2C}	0.81	3.9	2.2	4 / 0
ΔLK_{2P}	0.81	3.9	2.2	4 / 0

4.2 Fe(II) speciation onto HA binding sites

Although several extended X-ray absorption fine structure (EXAFS) analyses concerning the binding of Fe to OM have been performed for Fe(III) (Gustafsson et al., 2007; Morris and Hesterberg, 2012; van Schaik et al., 2008), no spectroscopic data are currently available for Fe(II)-OM binding. Therefore, the validation of the speciation results obtained here for Fe(II)-HS binding using PHREEQC-Model VI can only be achieved through comparison with the case of Fe(III). Gustafsson et al. (2007) analyzed the binding of Fe(III) to organic soils using EXAFS spectroscopy. They determined that Fe(III) bound to organic soils seems to occur through dimeric and trimeric complexes, where Fe ions are connected by µ-oxo bridges. Using scanning electron microscopy (SEM) images, Ou et al. (2009) suggested that Fe(III) is bound to HA as oligomeric species (not as single ions). These results differ from the EXAFS studies performed on the binding of Fe(III) with FA (van Schaik et al., 2008), peat humic acid (Karlsson and Persson, 2010) and organic soils (Karlsson and Persson,

2010), which have shown the formation of mononuclear complexes between Fe(III) and organic functional groups. This reveals that mononuclear Fe species are likely the dominant species involved in the binding of Fe(III) by HS. The PHREEQC-Model VI binding hypothesis considers that Fe(II) is bound to HS as mononuclear species, which appears consistent with the spectroscopic data obtained for Fe(III). Moreover, Gustafsson et al. (2007), Morris and Hesterberg (2012) and van Schaik et al. (2008) suggested that the functional groups involved in the binding of Fe(III) are phenolate and carboxylate groups, while Weber et al. (2006) argued for a dominant role of carboxylic groups. They tested two models for Fe(III)-HA binding with or without a contribution from the phenolic groups. With phenolic groups, the adsorbed Fe(III) with phenolate was negligible. Using Fourier transform infrared spectroscopy (FTIR), Ou et al. (2009) suggested that Fe(III) is mainly bound to HA carboxylate and carboxylic groups via monodentate and bidentate sites, whereas binding with HA phenolate and carboxy-phenolate groups would occur mainly through monodentate and bidentate sites, respectively. The results of the modeling calculations performed in this study indicated that Fe(II) could bind to HA by carboxylic and phenolic groups as suggested by Gustafsson et al. (2007), van Schaik et al. (2008) and Morris and Hesterberg (2012) for Fe(III). Moreover, modeling calculations revealed that Fe(II) was bound with HA mainly through bidentate complexes with a subordinate participation of tridentate sites. At basic to neutral pH, Fe(II) was bound to carboxylic groups, which is consistent with the results obtained for Fe(III) by Weber et al. (2006) and Ou et al. (2009). By contrast, as suggested by Ou et al. (2009) for Fe(III), Fe(II) was mainly bound to carboxy-phenolic groups.

4.3 Environmental implications

These new data provided the assessment that Fe(II) could be strongly bound to HA. Iron(II) complexation with HA or OM therefore put strong constraints on the observed dissolved Fe(II) concentrations and the possible transfer of Fe(II) within waters and hydrosystems enriched in OM. For example, in a coastal environment, Fe occurs mainly as insoluble Fe-oxyhydroxides (Rose and Waite, 2003). Bioavailable Fe is therefore relatively

scarce in such environments. However, any Fe(II) binding by OM can largely increase its solubility by preventing its hydrolysis/oxidation, therefore forming mobile soluble organic complexes (Miller et al., 2012, 2009; Rose and Waite, 2003). These studies showed that Fe(II)-OM binding forms strong complexes, which can have a significant effect on its solubility in coastal waters.

Another major environmental implication concerns the behavior of Fe(II) within wetlands. When reductive conditions develop in wetlands during the flooding season, high amounts of dissolved Fe(II), DOC and trace elements can be released in the soil solution (Dia et al., 2000; McBride, 1994; Olivie-Lauquet et al., 2001; Ponnamperuma, 1972). In such conditions, with regards to the strong affinity of Fe(II) for OM, Fe(II) will be mainly bound to DOC thus preventing its precipitation as a secondary mineral such as magnetite or green rust. As the formation of Fe-rich secondary minerals is limited, Fe-associated trace elements are not taken up and thereby remain highly mobile. Such processes have been previously suggested by Davranche et al. (2013) from kinetic modeling. These authors showed that organic-mediated Fe(II) complexation is a major controlling factor of Fe reactivity in wetland soils.

Moreover, the presence of other cations can change the quantities of Fe(II) bound to HA. The values of the binding parameters for some cations (e.g. Mg(II), Ca(II), Mn(II), Co(II), Ni(II), Zn(II), Sr(III), Cd(II), Ba(II)) are smaller than those of Fe(II), which means that the presence of these cations would only have minor consequences on the quantities of Fe(II) bound to HA or FA. By contrast, some other cations (Al(III), Cr(III), Fe(III), Pb(II), REE) have binding parameters values that are higher than those of Fe(II) and can therefore strongly compete with Fe(II) for HA binding if they are present in sufficient concentrations.

Finally, several authors have shown that Fe(III), through the formation of ternary complexes with HS, allows the binding of As(V) as oxyanion to OM (Sharma et al., 2010) and HS (Mikutta and Kretzschmar, 2011). In anoxic environments, as Fe(II) is the dominant species, such ternary associations are thus expected to be formed binding Fe(II), HS and As(III) or As(V). In this context, the present study and the new set of binding parameters

suggested that such ternary associations with Fe(II) may be relatively important in wetlands and floodplains. Thus these data constitute a first step for studying the formation of a cationic bridge between As(III, V), Fe(II) and HA and therefore the involved processes controlling As mobility at the soil-water interface within organic-rich environments undergoing redox alternations.

Conclusions

Iron(II) adsorption experiments onto humic acid (HA) were designed to study the binding of Fe(II) by organic matter. The experimental results showed that Fe(II) was strongly bound to HA as previously observed by several authors (Rose and Waite, 2003; Schnitzer and Skinner, 1966; Tipping, 1998; Van Dijk, 1971; Yamamoto et al., 2010). Coupling PHREEPLOT and PHREEQC-Model VI, a new set of specific binding parameters was calculated for Fe(II)-HA complex (log K_{MA} = 2.19 ± 0.16, log K_{MB} = 4.46 ± 0.47 and ΔLK_2 = 3.90 ± 1.31). These binding parameters are higher than those previously calculated by Tipping (1998) using only Van Dijk's dataset (1971). The new set of Fe(II)-HA binding parameters was used to test and validate the model using the relationship between the HA and FA parameters. They reasonably reproduced Rose and Waite's data (2003) on the adsorption kinetics of Fe(II) with SRFA. The RMSE between the calculated and experimental data was low (0.03), validating the newly determined set of binding parameters as well as the experimental and modeling approaches used in this study. This new dataset of binding parameters implies a higher complexation between Fe(II) and humic substances than that previously suggested, and shows that OM is of major importance in the fate and bioavailability of Fe(II) and possibly associated trace metals such as As within the environment.

Chapitre III : L'As(III) est-il capable de former des complexes ternaires avec la matière organique via Fe(II) et Fe(III) ionique?

Dans le 1er chapitre, j'ai démontré que l'As(III) pouvait se complexer aux sites thiols de la matière organique mais que les pourcentages adsorbés étaient faibles (entre 5 et 10%). Dans un deuxième temps, je souhaitais tester l'hypothèse d'un deuxième mécanisme indirect faisant intervenir un pont cationique de Fe(II) pour les milieux anoxiques et de Fe(III) pour les conditions d'oxydoréduction intermédiaires. Seulement, il a fallu avant cela quantifier la complexation du Fe(II) seul par la MO puisque peu de données étaient disponibles dans la littérature. J'ai donc montré que le Fe(II) se complexe fortement à la matière organique via ses groupements carboxyliques et phénoliques. Dans cette dernière partie, je vais m'intéresser à la possibilité de former ou non des complexes ternaires As(III)-Fe(II, III)-MO. Les complexes Fe-(II)-MO sont-il capables de complexer à leur tour l'As(III)? Ces complexes sont-il plus favorablement formés à partir de Fe(III) dans les milieux redox intermédiaires?

Ce chapitre correspond à un article soumis dans Environmental Science & Technology : Does As(III) interact with Fe(II), Fe(III) and organic matter through ternary complexes?, Charlotte Catrouillet, Mélanie Davranche, Aline Dia, Martine Bouhnik-Le Coz, Edwige Demangeat, Gérard Gruau

Does As(III) interact with Fe(II), Fe(III) and organic matter through ternary complexes?

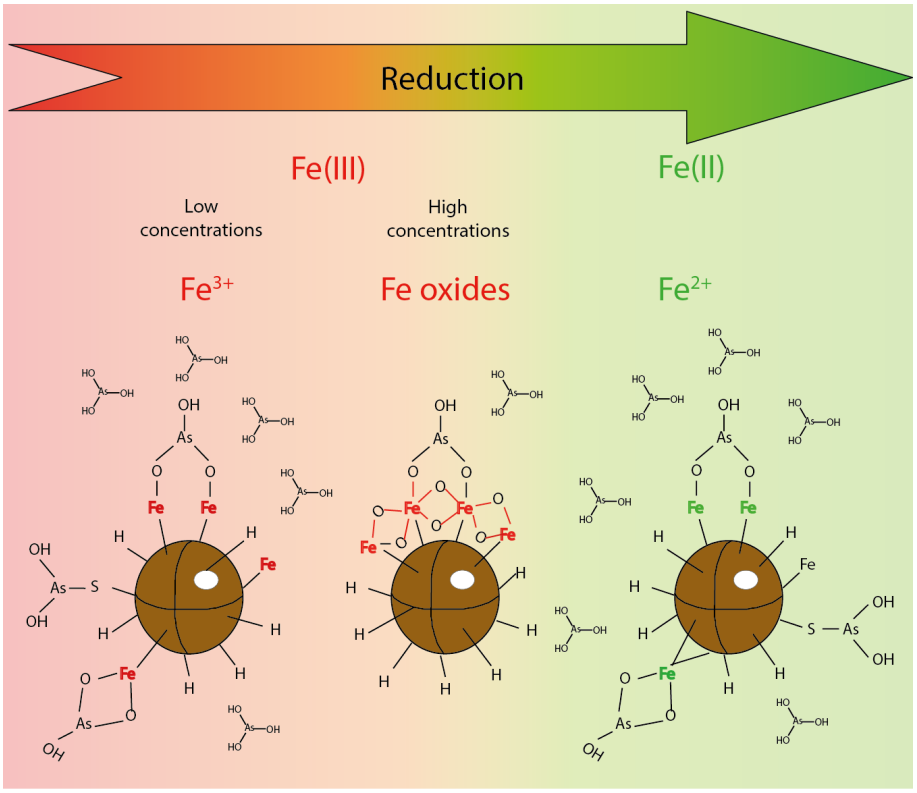

Modèle schématique décrivant les différents types de complexe pouvant se former entre l'As(III), le Fe(II) ou le Fe(III) et la matière organique dissoute en fonction des conditions d'oxydo-réduction et des concentrations du Fe

RESUME

Contrairement à l'As(V), seul un petit nombre d'études s'est intéressé à la complexation de l'As(III) par la matière organique (MO) via des ponts cationiques de Fe(III), et de Fe(II) (aucune étude actuellement). Des isothermes de complexation ont donc été réalisées entre l'As(III) et un acide humique (AH) (Leonardite) en présence de Fe(II) ou de Fe(III) pour des concentrations proches de celles retrouvées dans les zones humides. Les données produites ont ensuite été modélisées afin de déterminer et paramétrer les mécanismes mis en jeu. PHREEQC/Model VI, tenant compte des sites thiols de la MO, permet de reproduire les données en présence de Fe(III) mais pas de Fe(II) suggérant un autre mécanisme de complexation. Pour tester les hypothèses de formation de complexes ternaires entre l'As(III) et la MO via des ponts de Fe(II), PHREEQC/Model VI a été modifié afin de tenir compte de différentes conformations de complexes possibles. Ces dernières ont été déduites de données de spectroscopie de la littérature. La complexation de l'As(III) sous forme de complexe bidentate mononucléaire sur un complexe bidentate de Fe(II)-AH permet de reproduire au mieux les données expérimentales. Cependant, le modèle PHREEQC/Model VI doit être amélioré car la distribution des sites bidentates n'est pas réaliste en comparaison des données spectroscopiques qui proposent la complexation de l'As(III) sur des monodentates binucléaires de Fe. En présence de Fe(III), nos conditions expérimentales ne permettaient pas de détecter la formation de complexes ternaires. L'As(III) était lié aux groupements thiols plus compétitifs que les sites Fe(III)-AH formés. Ces nouvelles données ont permis de proposer un schéma général décrivant les conditions d'oxydoréduction et concentrations en Fe(II, III) dans lesquelles ces différents complexes peuvent être formés et se succéder.

ABSTRACT

Up until now, only a small number of studies have been dedicated to the binding processes of As(III) with organic matter (OM) via ionic Fe(III) bridges; none was interested in Fe(II). Complexation isotherms were carried out with As(III), Fe(II) or Fe(III) and Leonardite

humic acid (HA). Although PHREEQC/Model VI, implemented with OM thiol groups, reproduced the experimental datasets with Fe(III), the poor fit between the experimental and modeled Fe(II) data suggested another binding mechanism for As(III) to OM. PHREEQC/Model VI was modified to take various possible As(III)-Fe(II)-OM ternary complex conformations into account. The complexation of As(III) as a mononuclear bidentate complex to a bidentate Fe(II)-HA complex was evidenced. However, the model needed to be improved since the distribution of the bidentate sites appeared to be unrealistic with regards to the published XAS data. In the presence of Fe(III), As(III) was bound to thiol groups which are more competitive with regards to the low density of formed Fe(III)-HA complexes. Based on the new data and previously published results, we propose a general scheme describing the various As(III)-Fe-MO complexes that are able to form in Fe and OM-rich waters.

1 Introduction

Arsenic (As) is a strong contaminant of water and soil worldwide (Word Health organization), mainly as arsenite - As(III) - or arsenate - As(V) - depending on the redox conditions (Plant et al., 2004). Iron (Fe) speciation exerts a strong control on the As fate in the environment, as oxidized Fe species are known for their capacity to bind high concentrations of As(III,V) (Dixit and Hering, 2003; Dzombak and Morel, 1990). Organic matter (OM) seems to be an important direct and indirect controlling factor, especially in floodplains and wetlands where As concentrations can be high (Anawar et al., 2003; Kalbitz and Wennrich, 1998; Tseng et al., 1968). Organic matter act (i) as a source of C for bacterial metabolic activity, especially Fe(III) and As(V) reducing-bacteria, (ii) as a sorbent of Fe(III,II)/Fe(III)-oxyhydroxides (Catrouillet et al., 2014; Karlsson and Persson, 2010; Marsac et al., 2013; Sjöstedt et al., 2013; Van Dijk, 1971), and as an As(III, V) competitor for its binding to Fe(III)-oxyhydroxides (Bauer and Blodau, 2006; Grafe et al., 2001; Martin et al., 2009; Shipley et al., 2010; Wang and Mulligan, 2008). More recently, several studies demonstrated that OM may directly bind As(III,V). Different mechanisms were put forward to describe As-OM binding, including As(III,V) complexation with OM carboxylic and phenolic

groups (Buschmann et al., 2006; Lenoble et al., 2015), or As(III) binding with OM thiol groups (Catrouillet et al., 2015; Hoffmann et al., 2012; Langner et al., 2011a). However, most of the As bound to OM generally occurs as As-Fe-OM ternary complexes. The high affinity of As for Fe(III)-oxyhydroxides and of Fe(III)/Fe(III)-oxyhydroxides for OM explains this behavior (Bauer and Blodau, 2006; Ko et al., 2004; Lin et al., 2004; Liu et al., 2011; Mikutta and Kretzschmar, 2011; Ritter et al., 2006; Sharma et al., 2011). These studies were predominantly performed under oxidizing conditions and therefore concerned As(V). The situation is much less clear regarding the possible predominance of As(III)-Fe-OM ternary complexes. Using SEC-ICP-MS coupling and ultrafiltration, some authors provided evidence that As(III) could also form ternary complexes with OM via Fe(III) bridges, even though they failed to identify the nature of the Fe(III) bridges: Fe(III) ions or Fe(III)-oxyhydroxides (Liu et al., 2011). Hoffmann et al. (2013) who studied the As(III) binding to natural peat via ionic Fe(III) showed an increasing binding with increasing Fe(III) concentrations. Using EXAFS records, they suggested that As(III) binding could occur either through mononuclear bidentate or binuclear monodentate complexes with Fe(III). They argued that the stability constants for ternary complexes were probably lower than those for the direct As(III) binding to peat thiol groups. However, the high experimental concentrations required for the XAS measurements were quite far off from those generally expected in the environment, especially ionic Fe(III) concentrations which generally precipitate in such conditions. Finally, no study were interested in potential As(III) binding to OM via Fe(II), although these bridges are expected to be dominant in anoxic conditions, notably in wetlands and floodplains where OM, Fe and As concentrations are high (Davranche et al., 2013).

The aim of this study was to evaluate the potentiality to form As(III)-Fe-OM ternary complexes via ionic Fe(II) and Fe(III) bridges at concentrations prevailing in natural waters. As a result, we developed a combined experimental and modeling approach to (i) discriminate between the controlling binding mechanisms involved in the formation of As(III)-Fe-OM ternary complexes and (ii) provide stability constants to quantify which of these mechanisms are likely to be dominant in natural waters.

2 Experimental section

2.1 Experimental setup

All of the aqueous solutions were prepared with analytical grade Milli-Q water. The As(III), Fe(II) and Fe(III) stock solutions were prepared with sodium arsenite ($NaAsO_2$), iron chloride tetrahydrate ($FeCl_2.4H_2O$) and iron nitrate nonahydrate ($Fe(NO_3)_3.9H_2O$), respectively. The used humic acid (HA) was the standard HA Leonardite from the International Humic Substance Society. It was purified by removing the HA molecules < 10kDa using a Labscale TFF system equipped with a Pellicon XL membrane. All binding experiments (except Fe(III), see below) were conducted in a Jacomex isolator glove box (< 5 ppm of O_2) to prevent the oxidation of As(III) and Fe(II). The ionic strength was fixed at 0.05 M with NaCl for all experiments.

As(III)-Fe(II)-HA experiments. Three adsorption isotherm experiments were carried out at 50 mg L^{-1} DOC (dissolved organic carbon). The first adsorption isotherm was performed at pH 6 with 50 µg L^{-1} of As(III) and 0.8-12 mg L^{-1} of Fe(II). The second and third isotherms were carried out at pH 6 and 5, respectively, with 5-50 µg L^{-1} of As(III) and 5-6 mg L^{-1} of Fe(II). Solutions were stirred for 48 h to reach equilibrium.

As(III)-Fe(III)-HA experiments. Three standard batch equilibrium experiments were carried out with DOC and Fe^{3+} concentrations of 50 and 0.5 mg L^{-1}, respectively. The Fe(III) stock solution was prepared at pH 1.5 and the Fe^{3+} concentration used was adjusted to prevent oxyhydroxide precipitation. Using PHREEQC-Model VI and the minteq.v4 database modified with respect to Fe(III)-HA binding (Marsac et al., 2013, 2011), the model showed that precipitation was only expected to occur for Fe(III) concentrations > 1.2 mg L^{-1}. The pH was fixed at 4, 5 and 6 with sub boiling HCl and NaOH for the three isotherms, respectively. Experimental solutions were stirred for 24h to reach equilibrium between Fe^{3+} and HA. Arsenic(III) was added at concentrations ranging from 5 to 50 µg L^{-1} in a glove box to prevent oxidation. Experimental solutions were then stirred for 48h to reach equilibrium.

Sampling. For all experiments, 15 mL of solution was sampled and ultrafiltrated at 5 kDa (Vivaspin VS15RH12, Sartorius) under N_2 atmosphere. Ultracentrifugation cells were previously washed with Milli-Q water until DOC concentration in the ultrafiltrate was < 1 mg L^{-1}. All experiments were conducted in duplicate.

2.2 Chemical analyses

All measurements were performed at Géosciences Rennes, France. DOC concentrations were measured using an organic carbon analyzer (Shimadzu TOC-V CSH). Arsenic and Fe concentrations were determined using an ICP-MS. Instrumental and data acquisition parameters can be found in the ANNEXE I. To ensure that no oxidation occurred during the experiments, the concentrations of As(III) and As(V) were monitored using a HPLC-Agilent 1260 Infinity coupled to an Agilent G3154-65001 and Fe_{TOT} was compared to the Fe(II) measured in the ultrafiltrate ($Fe(II)_{UF}$) using the 1.10-phenanthroline colorimetric method (AFNOR, 1982). Because the absorbance of Leonardite at 50 mg L^{-1} is high, the Fe(II) concentration in the Fe(II)-HA solution was not checked. Arsenic(III) and Fe in the ultrafiltrates were assumed to be inorganic whereas As(III) and Fe bound to HA were considered to be in the fraction > 5 kDa.

2.3 Modeling

2.3.1 Model description

Because As(III) can bind to OM thiol groups, the modeling calculations were performed using a modified version of the PHREEQC/Model VI allowing this particular binding to be taken into account (Catrouillet et al., 2015). In the modified PHREEQC-Model VI, the ions complexation occurs through 12 discrete sites: four carboxylic groups (sites A), four phenolic groups (sites B) and four thiol groups (sites S). The abundances, intrinsic acidity constant for A, B and S sites and their distribution term are denoted as n_A, n_B, n_S, pK_A, pK_B, pK_S, ΔpK_A, ΔpK_B and ΔpK_S, respectively. Only monodentate complexes of As(III) with thiols are defined (Catrouillet et al., 2015). The fraction of proton sites that can form bidentate

and tridentate complexes are named f_B and f_T, respectively (Tipping, 1998). All values of the parameters used for modeling calculations are given in Table III. 1. The strength of the interaction between one site and one ion is defined by the complexation constant log K. Considering the 12 sites that can generate bidentates and tridentates, 84 equations are needed to describe the interaction between one ion and the 84 HA sites (further information is given in ANNEXE II). The specific complexation parameters for the carboxylic, phenolic and thiol groups are log K_{MA}, log K_{MB} and log K_{MS}, respectively. The CCM model was used to model the electrostatic interactions. Ion accumulation in the vicinity of HA is calculated with the Donnan model. Further information can be found elsewhere (Catrouillet et al., 2015).

Table III. 1: Summary of the different parameters of Model VI modified (from Catrouillet et al., 2015).

	A site carboxylic sites	**B site phenolic sites**	**S site thiol sites**
n (g mol^{-1})	1.96 10^{-3}	0.5*n_A	1.29.10^{-4}
pK	4.28	7.11	5.82
ΔpK	2.13	3.52	6.12
ΔLK_1	-0.7	0.8	0.8
f_B		0.5	
f_T		0.065	

2.3.2 Binding parameters and modeling strategy

Binary complexes. The binding parameters describing As(III) complexation by HA were previously determined using modified PHREEQC/Model VI including As(III)-thiol complexes (Catrouillet et al., 2015). The binding parameters used for the Fe(II)-HA binary complexes were determined using an earlier PHREEQC/Model VI version without thiol groups implementation (Catrouillet et al., 2014). These parameters therefore had to be re-evaluated using the present dataset and the new model version. To keep same proportions of monodentates, bidentates and tridentates the ΔLK_2 value used and the relationship between log K_{MA} and log K_{MB} were the same as those previously used (Catrouillet et al., 2014), ΔLK_2 = 3.90 and $\log K_{MA} = 0.49 * \log K_{MB}$. All binding parameters calculated here are presented in Table III. 2. All equations describing Fe(II) binding with each OM site were described in a previous study (Catrouillet et al., 2014).

Table III. 2: Binding parameters of Fe(II) (Catrouillet et al., 2014) and $As(OH)_3$ (Catrouillet et al., 2015) with HA.

Element	Log K_{MA}	Log K_{MB}	ΔLK_2	Log K_{MS}
Fe(II)*	2.19	4.46	3.90	-
Fe(II)**	0.49*log K_{MB}	fitted	3.90	-
$As(OH)_3$***	-	-	-	2.91*

*Biding parameters of Fe(II) using PHREEQC-Model VI
** Biding parameters of Fe(II) using PHREEQC-Model VI modified
*** note that $As(OH)_3$ complexation to HA is not written with the same writing than for cations (see Catrouillet et al., 2015 and present study).

Ternary complexes. The experimental data were fitted using the PHREEPLOT program coupled with the modified version of PHREEQC/Model VI (Catrouillet et al., 2014). The 84 sites, their acidity constants and the binding parameters for Fe(II) and As(III) were added into the "minteq.v4" database. No previous study exists on the binding of As(III) to Fe(II)-HA complexes. The nature of the complexes formed had to be deduced from our experimental dataset and/or literature data. Only one study was dedicated to the characterization of the binding mechanisms of As(III) to Fe(III) as ion bound to peat (Hoffmann et al., 2013). Using EXAFS records, this study showed that for low Fe(III) concentrations, As(III) bound with Fe(III) as mononuclear bidentate complexes, whereas for high Fe(III) concentrations, As(III) bound with Fe(III) either as mononuclear bidentate complexes or as binuclear monodentate complexes. Jönsson and Sherman (2008) suggested the formation of binuclear monodentate complexes for As(III) binding to green rust, fougerite and magnetite. However, Ona-Nguema et al. (2009) rejected this hypothesis and proposed the formation of As(III) polymers. Thoral et al. (2005) suggested that As(III) might form binuclear monodentate complexes with $Fe(OH)_2$ oxides under anoxic conditions. With respect to Fe(II), the modeling calculations performed earlier showed that Fe(II) bound with OM mainly through bidentate complexes (Catrouillet et al., 2014), confirming this spectroscopic data (Hoffmann et al., 2013).

Based on these proposed mechanisms, the modified PHREEQC/Model VI was first tested without Fe ternary complexes. They were implemented only when the model failed to reproduce the experimental datasets. From the spectroscopic data, six O atoms are bound to

both Fe(II) and Fe(III) as FeO_6 octahedra (Ona-Nguema et al., 2009, 2005). Furthermore, the distance between As(III) and Fe(III) when As(III) is bound to Fe(III) oxides as corner-sharing bidentate complexes is between $d_{As(III)-Fe(III)}$ = 3.4-3.58 Å and $d_{As(III)-Fe(II)}$ = 3.51 Å for $Fe(OH)_2$ (Ona-Nguema et al., 2009, 2005). All the complex conformations for As(III)-Fe(II) were thus deduced from the As(III)-Fe(III) spectroscopic datasets. The complexation of As(III) to monodentate Fe(II)-OM complexes was described either as mononuclear bidentate complexes (Eq. 1) or as binuclear bidentate complexes (Eq. 2). With regards to the As(III) binding to bidentate Fe(II)-OM complexes, As(III) complexation was described either as mononuclear bidentate complexes (Eq. 3) or as binuclear bidentate complexes (Eq. 4). Although Fe(III)-OM tridentate complexes were calculated in Model VI, the possibility to form complexes with As(III) was low considering their negative charge.

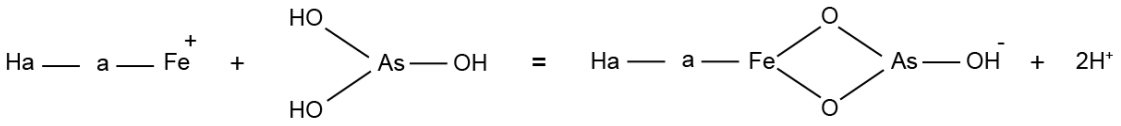

Eq. 1

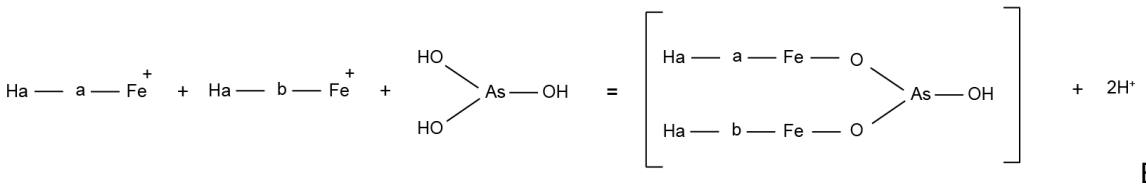

Eq. 2

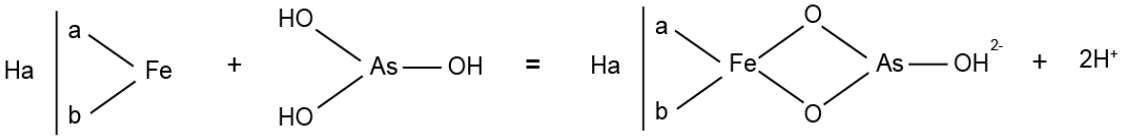

Eq. 3

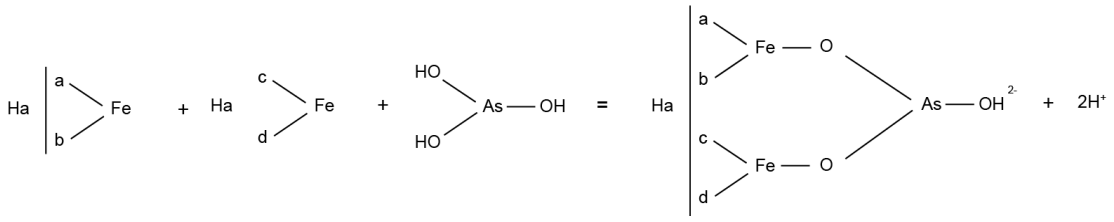

Eq. 4

All of these equations were first tested separately, then by pairs (i.e. Eqs. 1+2, or Eqs. 3+4), and last all together. All runs were finally compared to each other using their RMSE (Root Mean Square Deviation) calculated as $\sqrt{\text{mean}((\log\mu(\text{exp}) - \log\mu(\text{cal}))^2}$, with logμ(exp)

and logμ(cal) representing the logarithm of the measured and modeled As(III) bound concentrations, respectively.

3 Results

3.1 As(III)-Fe(II)-HA experimental and modelling data

No Fe(II) and As(III) oxidation occurred in the experiments. The binding parameters log K_{MA} (2.34) and log K_{MB} (4.78) for Fe(II) binding to HA, determined by fitting the experimental datasets using the modified PHREEQC/Model VI, were close to the log K_{MA} (2.19) and log K_{MB} (4.46) determined without the thiol sites implementation (Catrouillet et al., 2014). Since the relationship between log K_{MA}, log K_{MB} and ΔLK_2 was kept, the same proportions of monodentate, bidentate and tridentate complexes were calculated than previously (Catrouillet et al., 2014). Bidentates were the most abundant complexes formed between Fe(II) and HA. The experimental and modeled adsorption isotherm of Fe(II) binding to HA are presented in Figure III. 1.

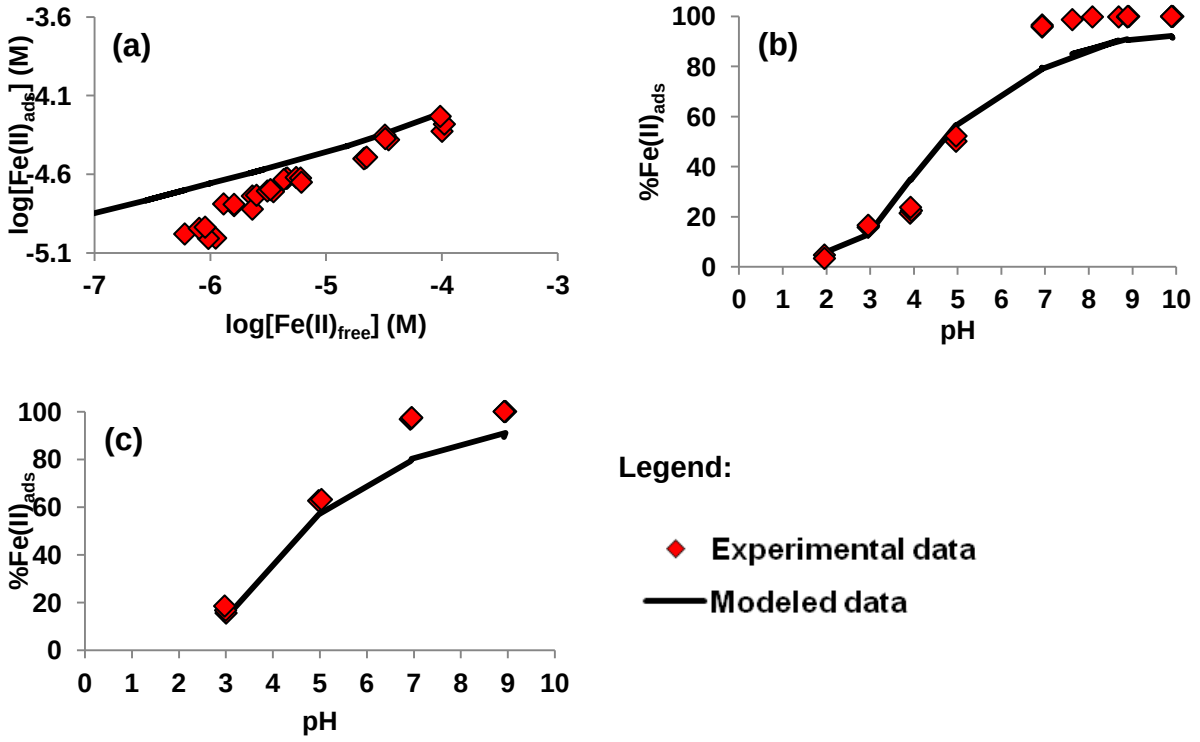

Figure III. 1: (a) Experimental and modeled adsorption isotherm of Fe(II) to HA (b) pH adsorption edge — DOC = 50 mg L^{-1}, (c) pH adsorption edge — DOC = 76 mg L^{-1}.

The adsorption isotherms of As(III) by Fe(II)-HA (log[As(III)-HA] relative to log[$As(III)_{UF}$]) are displayed in Figure III. 2a, b and c. Figure III. 2a showed that, for the same As(III) concentrations but increasing Fe(II) concentrations, the amount of bound As(III) increased. For adsorption isotherms at pH 5 and 6, no plateau was reached, i.e. no saturation was obtained (Figure III. 2b and c). The model that did not take ternary complexes into account (e.g. As(III)-S-HA complexes) could not reproduce the experimental datasets (RMSE = 0.87). Therefore, the presence of Fe(II) modified the binding behavior of As(III) to HA and had to be taken into account in the model hypothesis. No Fe(II) oxides precipitated as evidenced by the saturation index calculated using PHREEQC/Model VI. Therefore, As(III) speciation was mainly controlled by direct As(III)-S-HA and indirect As(III)-Fe(II)-HA complexes.

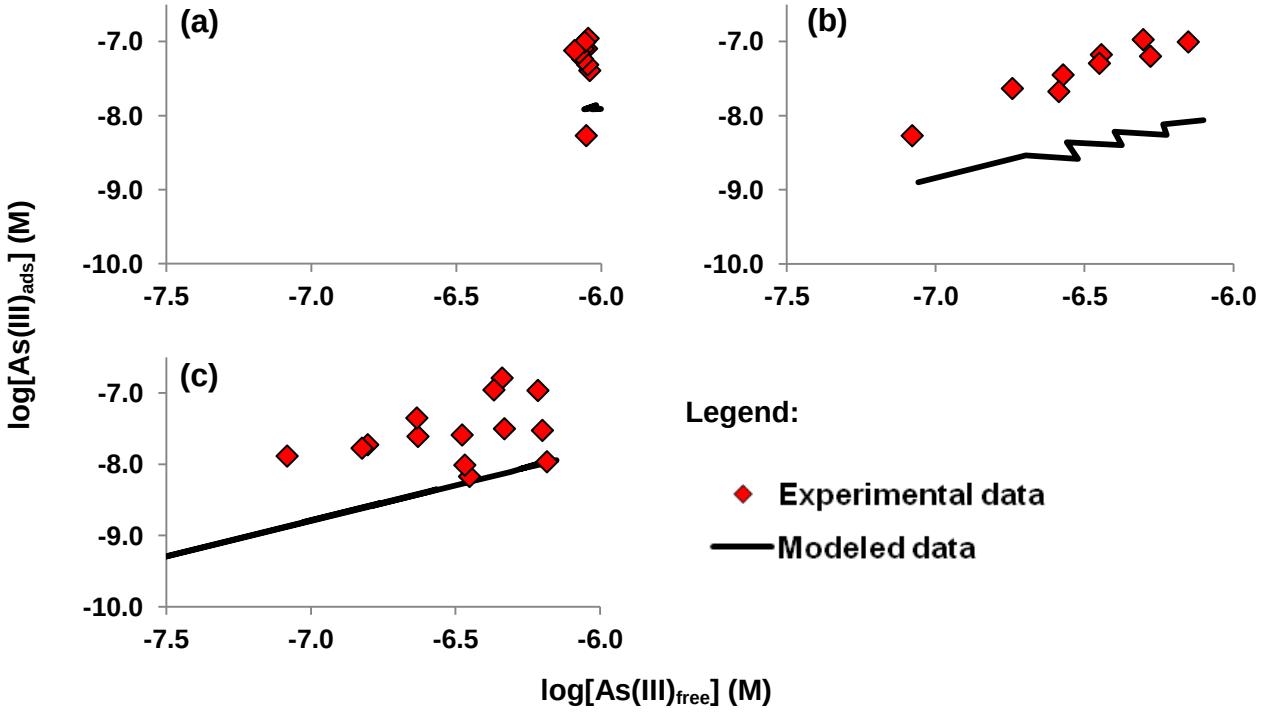

Figure III. 2: As(III)-Fe(II)-HA binding experiments and modeled data using only thiol binding parameters (a) according to the [Fe(II)] concentration, (b) at pH 6, (c) pH 5.

Model fits obtained using one or more of the four equations described in section 2.3.2 are displayed in ANNEXE III 1-10. When only one equation was used, Eqs. 3 and 4 were the most reliable as shown by the low RMSE (RMSE = 0.18 and 0.19 respectively, Table III. 3

and ANNEXES III 6 and 8). When a pair of equations were used (Eq. 1 + Eq. 2 or Eq. 3 + Eq. 4), the equation that yielded the smallest RMSE obtained in the single model (i.e. one equation) dominated the binding mechanism (Table III. 3). This result can be explained by the fact that the fitting program works based on the smallest statistical parameters. When Fe(II) binding to HA was considered to occur via monodentate complexes, Eq. 1 dominated over Eq. 2, leading to a comparatively much higher log K: log K = 4.15 for Eq. 3 versus -1.33 for Eq. 2. Note that the log K obtained for Eq. 1 was similar to the one obtained with Eq. 1 only (Table III. 3). For the models that used both Eqs 3 and Eqs 4 (RMSE = 0.18, Table III. 3) and all equations together (Figure III. 3), the dominant equation was Eq. 3 (mononuclear bidentate complexation of As(III) with bidentate Fe(II)-HA complexes), with RMSE = 0.18.

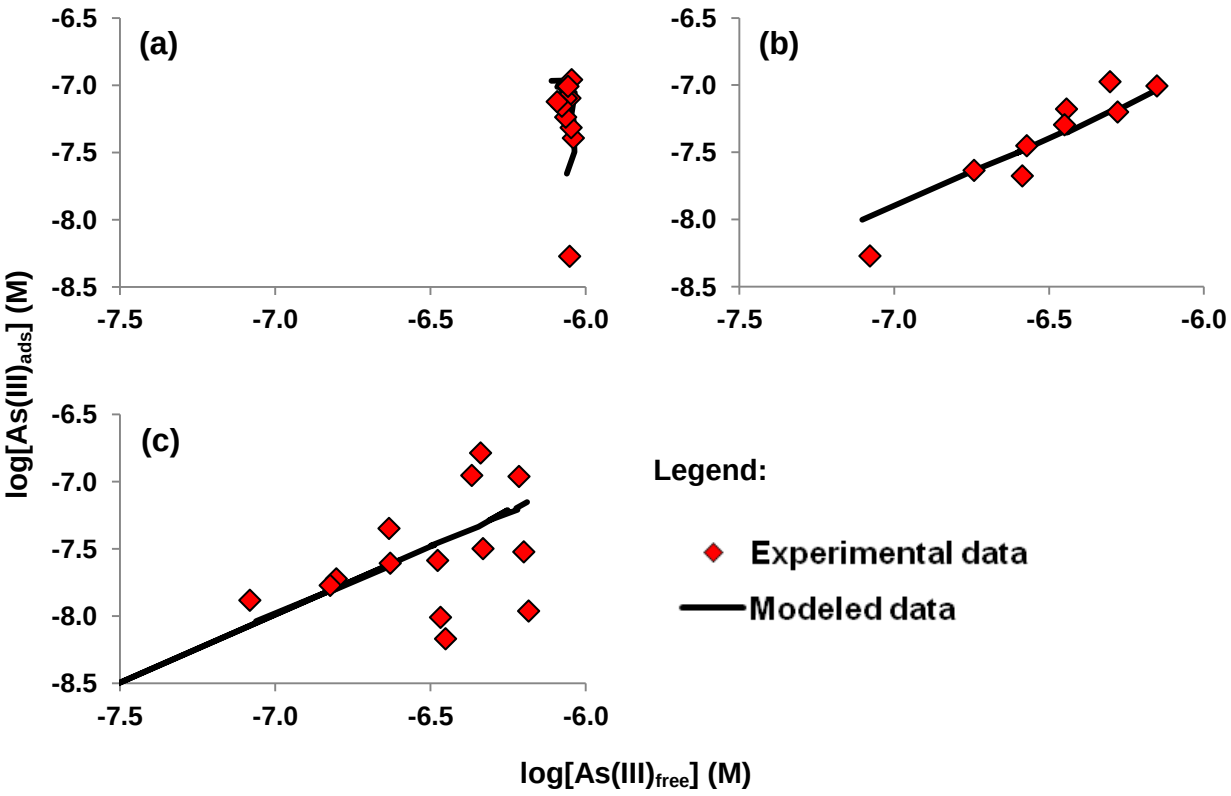

Figure III. 3: Sum of Eq.3 + Eq. 4 + Eq.5 + Eq. 6 (a) isotherm with increasing Fe(II) concentrations at pH 6, (b) isotherm with increasing As(III) concentrations at pH 6, (c) isotherm with increasing Fe(II) concentrations at pH 5.

Table III. 3: Binding parameters and RMSE for the different tested mechanisms.

Mechanism	Log k				RMSE
Eq. 3	4.15				0.38
Eq. 4	4.33				0.58
Eq. 5	3.39				0.18
Eq. 6	2.27				0.19
Eq. 3 + Eq. 4	4.15		-1.33		0.38
Eq. 5 + Eq. 6	3.39		-1.94		0.18
Eq. 3 + Eq. 4+ Eq. 5 + Eq. 6	-1.56	-1.32	3.39	-2.09	0.18

3.2 As(III)-Fe(III)-AH experimental and modeling data

The adsorption isotherms of As(III) to Fe(III)-HA (log[As(III)-HA] relative to $\log[As(III)_{UF}]$) are displayed in Figure III. 4d, e and f. No plateau was reached at pH 5 and 6 (Figure III. 4e and f), by contrast with pH 4 (Figure III. 4d). The proportion of bound As(III) at the different pH was similar, suggesting a minor role of pH in As(III) binding. The model that only considered the binding of As(III) to thiol groups correctly reproduced the experimental data (Figure III. 4d, e and f and total RMSE = 0.52). The high RMSE was due to the dispersion of the experimental points. In our experimental conditions, Fe(III) did not seem to influence the binding of As(III) to HA.

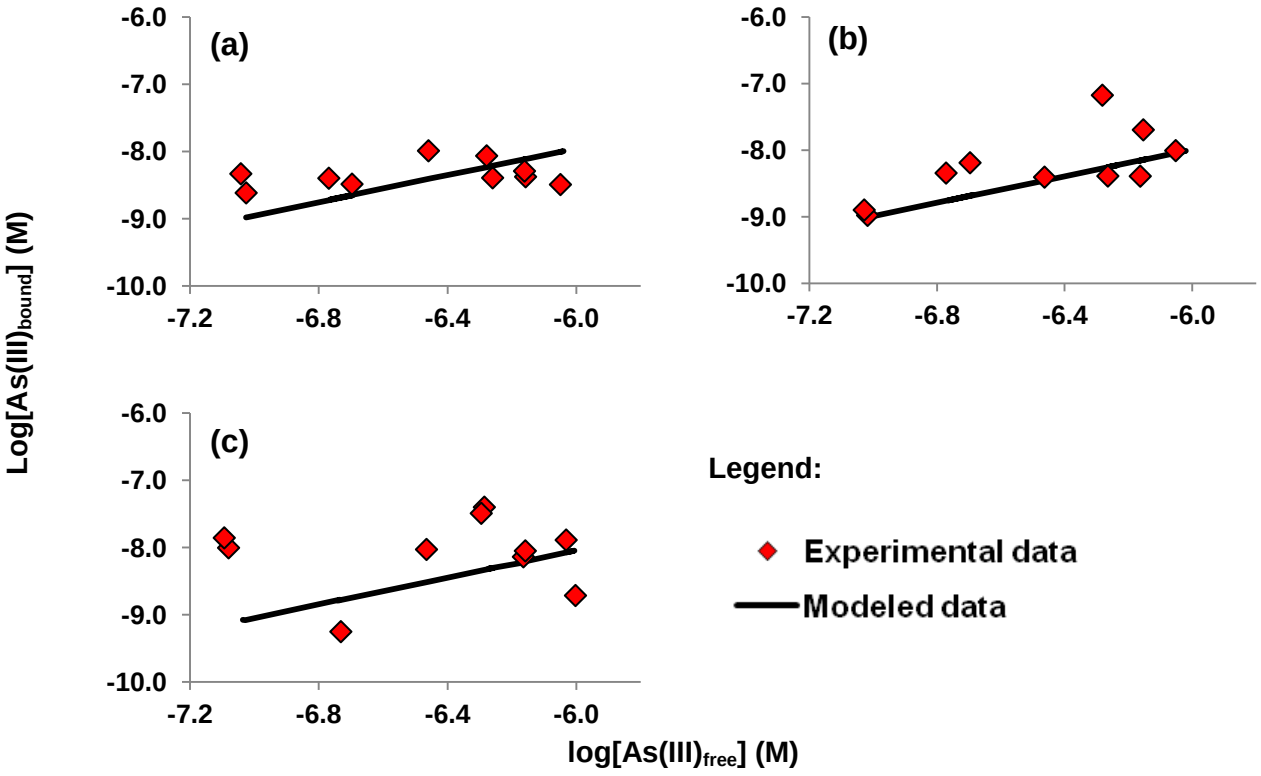

Figure III. 4: As(III)-Fe(III)-HA binding experiments and modeled data using only thiol binding parameters at (a) pH 4, (b) pH 5, (c) pH 6.

4 Discussion

4.1 Monodentate or bidentate Fe(II)-HA sites: which ones complex As(III) most efficiently?

As shown by their lowest RMSE, Eqs. 3 and 4 better fit the experimental dataset (RMSE = 0.18 and 0.19, Table III. 3). However in PHREEQC/Model VI, the fraction of sites that can make bidentate Fe(II)-OM complexes was determined from the geometry of the OM molecules. The minimal distance between two sites was fixed at 0.3 nm for a sphere with a radius of 0.8 nm. If the distance between two sites ranged between 0.3 and 0.45 nm, the sites were defined as bidentate sites (Tipping and Hurley, 1992). In our simulations, Eq. 4 represents the binding of As(III) to two Fe atoms, each forming bidentate complexes with OM. The distance between each Fe atom was $d_{Fe\text{-}Fe} \approx (0.3\text{-}0.45)*2 = 0.6\text{-}0.9$ nm = 6-9 Å (Figure III. 5a). Spectroscopic data demonstrated that the distance between As and the neighbor O ($d_{As\text{-}O}$) varied from 1.70 to 1.79 Å (Hoffmann et al., 2013; Ona-Nguema et al., 2009; ThomasArrigo et al., 2014; Thoral et al., 2005). The distance between Fe(III) and O atoms ($d_{Fe\text{-}O}$) varied from 1.94 to 1.99 Å (Hoffmann et al., 2013; ThomasArrigo et al., 2014) and from 1.99 to 2.14 Å for Fe(II)-O and Fe(II)-As(III) systems (Echigo and Kimata, 2008; Ona-Nguema et al., 2009; Thoral et al., 2005). The maximal distance between As and Fe bound via an O ($d_{As\text{-}O\text{-}Fe}$) was therefore equal to $d_{As\text{-}O\text{-}Fe}max = d_{As\text{-}O}max + d_{Fe\text{-}O}max = 1.79 + 2.14 = 3.93$ Å which was << 6-9 Å ($d_{Fe\text{-}Fe}$ for two bidentate sites). Thus, the binding of As to Fe through O with distances of 6-9 Å between two Fe atoms seemed impossible (Figure III. 5a). Therefore, although PHREEQC/Model VI allowed the binding of As(III) to HA through Fe(II) bidentate sites, for geometrical reasons, in experimental and natural conditions, this possibility was expected only when Fe dimer and trimer appeared (Hoffmann et al., 2013; Mikutta and Kretzschmar, 2011; van Schaik et al., 2008; Vilgé-Ritter et al., 1999).

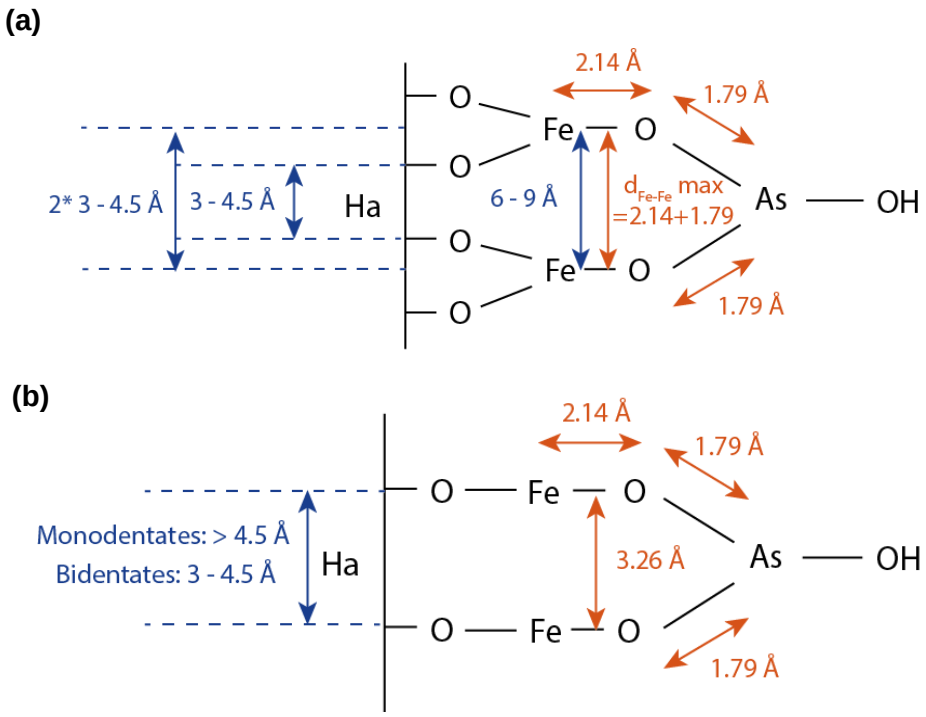

Figure III. 5: Complexes formed with (a) Eq. 6 and (b) Eq. 4. Fe-O and As-O distances (in red) were determined from the $Fe(OH)_2$ oxides and $As(OH)_3$, respectively (Ona-Nguema et al., 2009). The distances in blue are defined in PHREEQC-Model VI (Tipping, 1998).

Equation 2, which assumed the As(III) binding to two Fe(II)-MO monodentates, poorly reproduced the experimental datasets (RMSE = 0.58, SI Table III. 3). The fit was poor (RMSE = 0.71, ANNEXE III 4) for the isotherm at pH 5. According to PHREEQC-Model VI, the abundance of the Fe(II)-OM monodentate complexes would be quite low, ranging between 0.02 and 18% versus 74 and 83% for the Fe(II)-OM monodentate and bidentate complexes, respectively. This low abundance of the Fe(II)-OM monodentate complexes likely explained why Eq. 2 failed to satisfactorily reproduce the experimental data. A critical point was that in PHREEQC-Model VI, monodentate sites were assumed to be separated from each other by more than 4.5 Å whereas in the $Fe(OH)_2$ oxides, when As(III) was bound to Fe, d_{Fe-Fe} was smaller at 3.26 Å (Figure III. 5b). Therefore, Eq. 2 was impossible with the common hypothesis used in PHREEQC/Model VI. Hoffmann et al. (2013) showed that As(III) could form binuclear monodentates with Fe(III) complexed to HA. As discussed above, the complexation of As(III) by bidentate Fe(II)-OM complexes was not reliable for geometrical reasons and as a result, only Fe(II)-OM monodentate could bind As(III). These observations suggested that a part of the bidentate sites, defined in the model as spaced apart by 3 to 4.5

Å, possibly bound Fe(II) in a monodentate mode (e.g. Ha-ab$(Fe)_2$ versus Ha-abFe) (Figure III. 6).

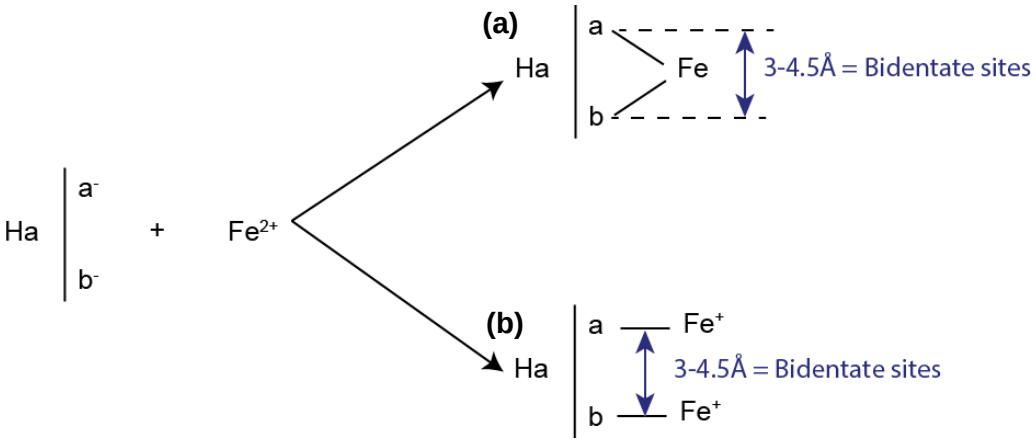

Figure III. 6: Bidentate sites defined in (a) a bidentate mode (actual definition in PHREEQC-Model VI) and (b) a monodentate mode (new definition).

Hoffmann et al. (2013) showed that As(III) was bound as binuclear monodentate complexed to Fe(III)-OM. Using PHREEQC/Model VI and their experimental conditions, we calculated that Fe(III) was able to recover between 0.75 and 5.95% of the HA sites. The coupling of the spectroscopic (Hoffmann et al., 2013) and modeled datasets demonstrated that As(III) binuclear monodentate complexes were formed from a recovery of 5.95%. In our experiments, the surface recovery by Fe(II) ranged between 5 and 38% which support our hypothesis that As(III) binding to HA mainly occurred through binuclear monodentate Fe(II)-HA complexes.

Although Eq. 1 better reproduced the experimental datasets than Eq. 2, the calculated RMSE was smaller than for Eqs. 3 and 4 (Table III. 3). Considering only the atomic distances, the binding of As(III) to only one Fe(II)-HA complex is thought to be plausible, but in addition, for example, to Eq. 3.

As seen previously, when several equations were used together, the model chose the equation that provided the smallest RMSE and attributed a negative log K to the other equations. With regards to the Fe(II) recovery on HA, and the spectroscopic data in the literature, mononuclear bidentate and binuclear monodentate complexes seemed to be the

most reliable mechanisms involved in As(III) binding by Fe(II)-HA. Used together Eqs. 1 and 2 described the As(III) binding to Fe(II)-HA monodentate complexes. Regarding the low density of Fe(II)-HA monodentates, the model should be able to determine the log K for both equations. When Eqs. 3 and 4 were used together, enough Fe(II) bidentate complexes were formed. However, none of these coupled equations reasonably fit the experimental datasets. In fact, the model was not able to assess the respective weight of each equation. Some constraints had to be implemented in PHREEQC/Model VI to improve the quantification of each equation relative to the other ones. PHREEQC/Model VI was able to accurately discriminate the binding of one ion to the carboxylic and phenolic sites and to determine the corresponding binding parameters. In this case, the constraints were imposed by the acidity constants which control the density of each site relative to the pH and by the imposed linear relationship between the log K_{MA} and log K_{MB} values (log K_{MB} = 3.39 * log K_{MA}) (Tipping, 1998).

4.2 Instructions to better model As(III)-Fe(II)-HA interactions

To improve the modeling of the data using Eq. 2 – the most probable equation with regards to the spectroscopic data (Hoffmann et al., 2013) - we modified PHREEQC/Model VI by identifying the proportion of bidentate sites that can potentially bind two Fe (2-monodentate mode). In Model VI, the bidentate Fe(II) sites are distributed between weak, strong, and very strong bidentate sites. The differences between each site are defined by the site abundance and the ion binding parameters (log K_{MA}, log K_{MB} and ΔLK_2). The strong and very strong bidentate sites are 10.01 and 100.11 times less abundant, respectively, than the weak bidentate site. The log K value for the strong bidentate sites is equal to that of the weak bidentate sites plus ΔLK_2, the distribution term that modified the strength of the bidentate and tridentate sites. Log K for the very strong bidentate sites are equal to those for weak bidentate sites plus $2*\Delta LK_2$. In a bidentate complex, two sites bind one Fe, whereas in the 2-monodentate mode, for each monodentate site, one site binds Fe. In the 2-monodentate mode, log K will be lower than the bidentate log K. Therefore, the 2-monodentate could only

be developed from the weak bidentate group, as strong and very strong bidentate sites have higher binding constants. In PHREEQC/Model VI, the binding constant for the weak bidentate group was defined as the sum of two monodentate sites; however, the mechanism had to be modified to correspond to the required 2-monodentate mode. Equation 5 corresponds to the classical equation and Eq. 6 to the equation for the 2-monodentate mode.

$Ha\_ab^{2-} + Fe^{2+} = Ha\_abFe$ $\log k = \log k(a) + \log k(b)$ (Eq. 5)

$Ha\_ab^{2-} + 2Fe^{2+} = Ha\_abFe_2^{+2}$ $\log k = \log k(a) + \log k(b)$ (Eq. 6)

With regards to the abundance of the sites, it cannot be assumed that all of the weak bidentate sites are involved in the 2-monodentate mode. It was also difficult to quantify the exact proportion of weak bidentate sites that could bind Fe(II) in the 2-monodentate mode. Consequently, tests were performed with a proportion of these weak bidentate sites varying from 5 to 90%. When the proportion was 5%, 5% of the weak bidentate sites bound Fe following Eq. 2 and 95% following Eq. 3 when fitting the experimental data (Table III. 4). This procedure was applied to Eqs. 2 and 3 simultaneously, which corresponded to a new modeling configuration. The model was not able to determine the log K for the proportions ranging from 5 to 80%. However, for 90% of the bidentate sites that used Eq. 3, the fitted log K were equal to 2.86 and 3.95, respectively. Because As(III) was only bound to one Fe following this equation versus two Fe in Eq. 2, the log K for Eq. 2 should be lower than for Eq. 3; 90% of the bidentate sites that used the 2-monodentate mode were therefore too large. Thus, it is necessary to experimentally/analytically determine the proportions of Fe(II) among the bidentate sites that could possibly be involved in the 2-monodentate mode (e.g. using spectroscopy). Then, log K between As(III) and the Fe(II)-HA complexes should be determined using both binding mechanisms.

Table III. 4: Fit of log K using Eq. 4 defined as weak bidentate sites and Eq. 5 the rest of weak and strong and very strong bidentate sites. First percentage represents the percentage of weak sites of Eq. 4, the second represents the percentage of weak site of Eq. 5.

	mononuclear bidentate log k	binuclear monodentate log k	RMSE
5%-95%	-0.11	3.38	0.18
10%-90%	-0.38	3.40	0.18
20%-80%	-0.68	3.43	0.18
30%-70%	-0.81	3.48	0.17
40%-60%	-0.87	3.53	0.17
50%-50%	-0.93	3.58	0.17
60%-40%	-0.91	3.65	0.18
70%-30%	-0.80	3.73	0.18
80%-20%	-0.37	3.83	0.18
90%-10%	2.86	3.95	0.18

4.3 Interpretation of As(III)-Fe(III)-AH data

The model using thiol groups only reproduced our experimental datasets reasonably well. The presence of Fe(III) did not seem to influence the binding of As(III) to the thiol groups, suggesting that (i) no competition for thiol groups occurred and (ii) no or negligible ternary complexes were formed. However, for their experimental conditions, Hoffmann et al.(2013) clearly observed this type of ternary associations between As(III), Fe(III) and peat. The reason was that the concentrations used were much higher (in Hoffmann et al., 2013 13 g L^{-1}, 20-200 mg L^{-1} and 22.5 mg L^{-1} of DOC, Fe(III) and As(III), respectively versus, here, 50 mg L^{-1}, 0.6 mg L^{-1} and 5-50 µg L^{-1} of DOC, Fe(III) and As(III), respectively), and the pH was different (pH 7, 8.4 and 8.8 in Hoffmann et al., 2013 versus 4, 5 and 6 here). At pH 8.4 and 8.8, As(III) occurred as $H_2AsO_3^-$ implying the formation of new complex. The negative charge caused by the higher pH increased the binding of As(III) as ternary complexes via Fe(III) bridges as shown by the comparison of the isotherms performed for similar Fe(III) and As(III) concentrations but different pH in Hoffmann et al. (Figure 2A in Hoffmann et al., 2013). Although the DOC/Fe ratios were equivalent (65-650 for Hoffmann et al., 2013 and 83 here), the As/Fe ratios were different (1.1-0.11 for Hoffmann et al., 2013 versus 0.0083-0.001 here). Moreover, the Fe(III) concentrations used here were chosen to avoid any Fe(III) precipitation.

The S content of the peat used by Hoffmann et al. (2013) was also very low and did not allow the binding of As(III) to peat through thiol sites, by contrast, with the here used HA as previously shown (Catrouillet et al., 2015). Thus, the thiol sites were able to compete with the Fe(III)-HA complexes, in low amounts, for As(III) binding. At circumneutral pH and intermediate As/C ratio, Hoffmann et al. (2013) observed that the log Kd (distribution coefficient of As(III) on organic carbon) was higher for As(III) bound to peat thiol sites than for As(III) bound to Fe(III)-peat complexes. In our experiments, As(III) bound to Fe(III)-HA was probably not present in high enough amounts to be detected, particularly in comparison with As(III) bound to S-HA. However, higher concentrations of Fe(III) should induce precipitation and the mechanism would be then performed with particulate or colloidal Fe(III) oxyhydroxides, which was not the purpose of the present study. It is important to note that the experimental conditions used by Hoffmann et al. (2013) were developed to specifically promote the formation of ternary complexes via ionic Fe(III) and to allow the detection of As(III) and Fe(III) using the XAS technique.

4.4 Environmental implications

In floodplains and wetlands, the speciation of the elements depends strongly on the redox conditions. In such environments, when the soils are flooded and become water saturated, O_2 is consumed by bacteria, creating anoxic conditions, whereas when the soils are not saturated, oxic conditions prevailed. Under reducing conditions, As is mainly as As(III) and Fe as Fe(II), while under moderately reducing conditions As(III), As(V), Fe(II) and Fe(III) species can coexist. The speciation of Fe(III) depends on the amount of Fe(III) and on the physico-chemical conditions (pH, Eh, OM, competitors, etc.). For high Fe(III) concentrations, Fe occurs mostly as particulate or colloidal oxyhydroxides (lepidocrocite, ferrihydrite, goethite, etc.) generally bound to OM in organic-rich environments (Pédrot et al., 2011). Iron(III) oxyhydroxides are the main sorbent of As(III) and As(V) in the environment. These systems are well documented and log K estimates can be found (Hfo_sOH + H_3AsO_3 = Hfo_sH_2AsO_3 + H_2O, log k = 5.41, 5.74 or 4.02 (Dixit and Hering, 2003; Dzombak and

Morel, 1990; Swedlund and Webster, 1999). In organic-rich environments, As(III) is expected to either compete with OM molecules for its binding to Fe(III) oxyhydroxydes, which could strongly limit its complexation (Grafe et al., 2001), or to be complexed by Fe(III) oxyhydroxides which are themselves bound to OM (Figure III. 7) (Grafe et al., 2001; Ko et al., 2004; Liu et al., 2011; Sharma et al., 2011). For low Fe(III) concentrations, no precipitation occurred and Fe occurs as Fe^{3+}, $Fe(OH)^{2+}$ and $Fe(OH)_2^{+}$, depending on the pH. In organic-rich environments, Fe(III) as ion can be bound by the carboxylic and phenolic groups of OM (Karlsson and Persson, 2010; Marsac et al., 2013; Sjöstedt et al., 2013; Vilgé-Ritter et al., 1999), mostly as bidentate complexes. Hoffmann et al. (2013) showed that at high concentrations of Fe(III), As(III) and OM, ternary complexes can be produced via ionic Fe(III) (Figure III. 7). However, these results were strongly dependent on their experimental conditions performed to specifically promote this binding mechanism. In environmental conditions, for high amounts of Fe(III) such as those used by Hoffmann et al. (2013) Fe(III) precipitated as Fe(III) oxyhydroxides and thus sorbed As(III) (high log K). In this case, we can consider that the ternary complex occurred through Fe(III) oxides or nano-oxides. In our studies, for higher OM thiol amounts and low Fe(III) concentrations, As(III)-Fe(III)-OM ternary complexes via ionic Fe(III) were not detected. Therefore, for an environmental level of Fe(III), ternary complexes via ionic Fe(III) does not seem possible even in organic-rich waters (Allard et al., 2004; Olivie-Lauquet et al., 1999; Pédrot et al., 2011; Pokrovsky et al., 2005), notably when there is a sufficient number of thiol sites on OM to bind As(III) (Catrouillet et al., 2015; Hoffmann et al., 2012). If the S% in OM does not totally correspond to thiol, much of the dissolved OM should contain a sufficiently high number of thiol groups to efficiently outcompete As(III) complexation by ternary Fe(III)-HA complexes. The competition between thiol binding and ternary complexes via ionic Fe(III) probably always occurs in natural OM-mediated interactions.

In waterlogged floodplains and wetlands, ferric-reducing bacteria reductively dissolved Fe(III) oxyhydroxides, thereby releasing Fe(II) into the solution. In such environments, high OM concentrations are produced. Catrouillet et al. (2014) demonstrated

that OM can strongly bind Fe^{2+} and $Fe(OH)^{+}$, especially at neutral and basic pH. Here, we showed that As(III) might be indirectly bound as ternary complexes to OM via ionic Fe(II) (Figure III. 7) and directly bound through OM thiol sites. The dynamics of the As(III) bound to OM is therefore controlled by the own OM dynamic. However, in the present work, we estimated that As(III) bound to OM by direct and indirect mechanisms could vary from 5% to 26% of the total As(III). We performed speciation calculations to test the studied mechanism in reduced water produced by the anoxic incubation of an organic-rich wetland soil (unpublished data). Arsenic(III), Fe(II) and DOC concentrations were measured in the colloidal fraction which corresponded to the concentrations measured by ultrafiltration in the > 3 kDa fraction, and the truly dissolved concentrations which corresponded to the concentrations measured by HPLC-ICP-MS in the < 3kDa fraction. In these calculations, we considered that the As(III) measured by HPLC-ICP-MS occurred as free species. This experimental dataset was used to test the present model using the following assumptions: DOC was only composed of HA (for which the proportion of reactive and non-reactive DOM was not known), the thiol groups concentration was equal to that of the Leonardite (0.13 mmol g^{-1}) and the binding of As(III) to Fe(II)-HA complexes was calculated using only Eq. 2, with log K = 3.39. We calculated that 1.2% of As(III) was bound to S-OM and 22.7% to Fe(II)-OM. These calculations were close to the proportion determined from the analytical techniques, i.e. 32% of As(III) bound to OM. The experimental proportions corresponded to the difference between As_{TOT} (determined by ICP-MS) and free As(III) concentrations (determined by HPLC-ICP-MS). Therefore, the binding of As(III) with OM as ternary complexes via ionic Fe(II) seemed to be potentially important in anoxic environments such as floodplains and wetlands, even if the mechanisms and binding constants used for this calculation had to be improved. As long as reducing conditions prevail, a large proportion (this study > 24-32%) of As(III) was in the solution as labile species, possibly transferred to the underlying aquifers.

Note that all of these complex conformations investigated in this study were described for the $As(OH)_3$ species. However, for pH > 8, As(III) is expected to occur as a negatively

charged species, namely $As(OH)_3O$. Hoffmann et al. (2013) showed that with increasing pH, As(III) speciation change should result in a higher proportion of As(III) bound to OM through ternary complexes. However, although the binding of ternary complexes seems to be favored for $As(OH)_2O^-$, few natural waters have pH > 8 and high enough OM and Fe concentrations. This is why these mechanisms were not presented in (Figure III. 7). All these results, now, raise the question of the fate of this As(III) that occurs as labile species or when is bound to OM when the conditions become oxidized?

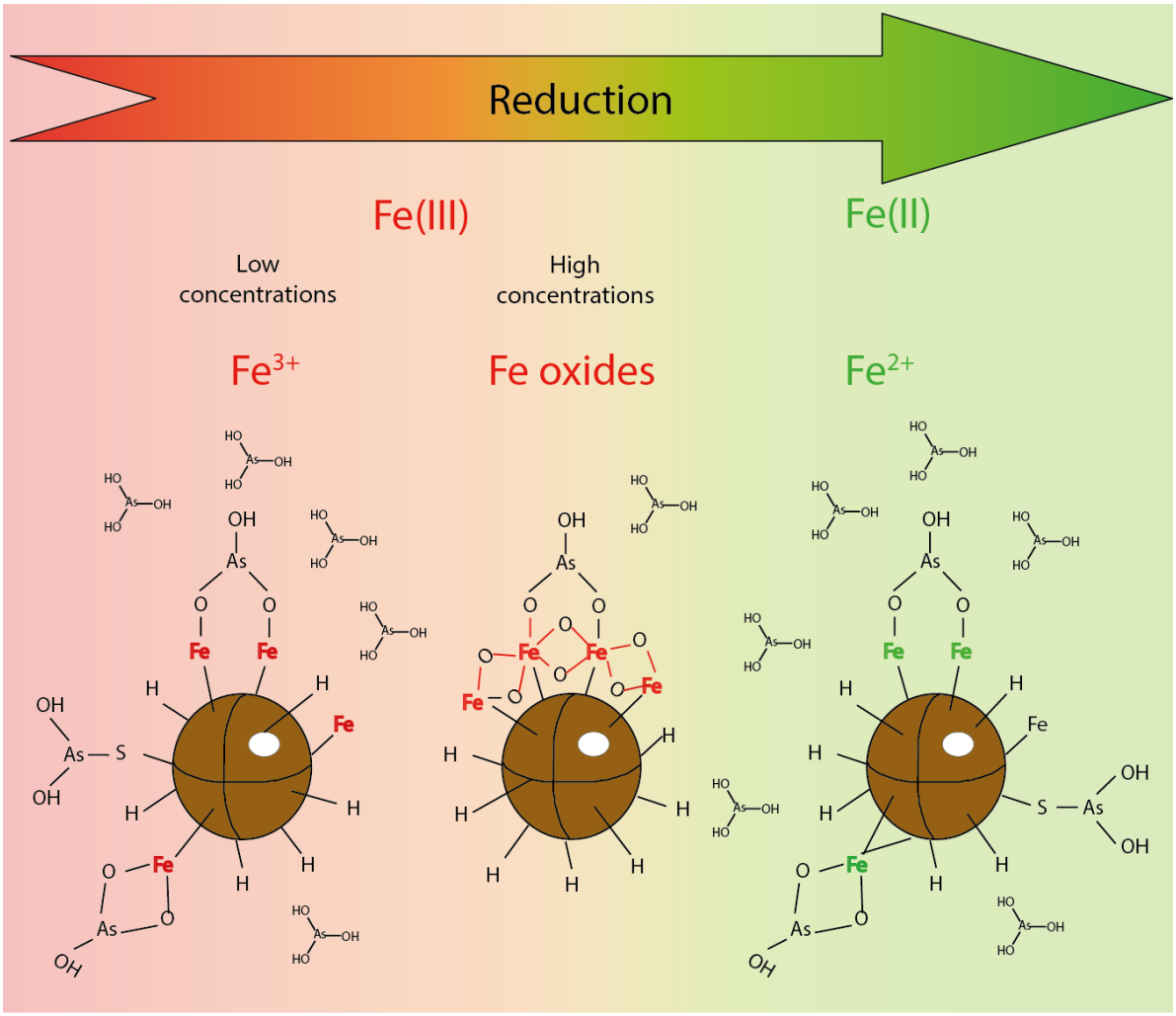

Figure III. 7: Schematic model describing the different complex types that may form between As(III) Fe(II) and /or Fe(III) and dissolved organic matter (DOM), depending on the redox status of Fe, and on Fe and DOM concentrations. This general scheme may apply to what happens in floodplain and wetland waters (Catrouillet et al., 2015; Hoffmann et al., 2013; Mikutta and Kretzschmar, 2011).

Conclusions

et

perspectives

1 Conclusions

La contamination des eaux et des sols par l'arsenic (As) est un problème majeur à travers le monde puisqu'il est responsable de l'une des plus grande morbidité et mortalité à l'échelle du globe (Smith et al., 2000). La compréhension des mécanismes géochimiques gouvernant sa dynamique dans l'environnement est donc indispensable. Cependant, si ces mécanismes ont été bien étudiés en milieu oxydant, il existe une vraie carence de connaissances en milieu réduit. Les processus de réduction sont pourtant largement actifs à la surface de la Terre, notamment dans les zones humides en période de hautes eaux, dans les tourbières ou les aquifères profonds. Les eaux souterraines sont par ailleurs utilisées comme eaux de boisson dans de nombreux pays et il est donc important de comprendre les mécanismes mis en jeu dans ces milieux. En milieu anoxique, la biodissolution réductrice des oxydes de Fe porteurs d'As entraine une libération de Fe(II) et d'As(III, V) dans la solution. Cette bioréduction nécessite un apport de carbone organique indispensable au développement et aux activités métaboliques des bactéries ferro-réductrices impliquées. De plus, la plupart de ces milieux sont naturellement très riches en matières organiques, à l'exception des aquifères profonds. Cependant, peu d'études se sont intéressées aux interactions possibles entre l'As(III), le Fe(II) et la matière organique (MO) en milieu anoxique. Ce travail de doctorat a donc consisté à mieux comprendre les interactions chimiques potentielles entre l'As(III), le Fe(II, III) et la MO en milieu anoxique. Cette étude a été décomposée en trois volets. La première partie de notre analyse portait sur les interactions directes entre l'As(III) et la MO. La deuxième partie a porté sur la complexation du Fe(II) par la MO. Enfin, le dernier volet a porté sur la possible formation de complexes ternaires d'As(III)-Fe(II,III)-MO.

1.1 La complexation directe d'As(III) par la MO est-elle possible?

Plusieurs mécanismes de complexation de l'As(III) par la MO ont été suggérés soit, via des groupements carboxyliques et phénoliques (Buschmann et al., 2006; Lenoble et al., 2015) ou via des complexes ternaires métalliques (Fe, Al, Mg, etc) (Hoffmann et al., 2013;

Liu et al., 2011; Redman et al., 2002; Warwick et al., 2005). Plus récemment, des données de spectroscopies ont montré que les sites thiols de la MO étaient impliqués dans la complexation de l'As(III) (Hoffmann et al., 2012; Langner et al., 2011a). Malgré la forte affinité de l'As(III) pour les sites thiols, notamment des protéines (Cavanillas et al., 2012; Gaber and Fluharty, 1972; Hoffmann et al., 2014; Rey et al., 2004; Spuches et al., 2005b; Spuches and Wilcox, 2008; Starý and Růzicka, 1968; Zahler and Cleland, 1968; Zhao et al., 2012), seulement deux études ont été menées sur les MO naturelles (Hoffmann et al., 2012; Langner et al., 2011a).

Sur la base de ces premiers résultats de la littérature, j'ai réalisé des expériences de complexation d'As(III) par des acides humiques (AH) greffés ou non en sites thiols (SH). Les jeux de données ainsi obtenus ont ensuite été modélisés à l'aide de PHREEQC-Model VI dans lequel j'ai introduit les sites thiols afin de déterminer les paramètres de complexation de As(III) par un AH. Les paramètres ont été ensuite validés avec les jeux de données de la littérature. Les principaux résultats peuvent être résumés comme suit :

Les concentrations d'As(III) complexées par un AH sont faibles. Quel que soit l'AH utilisé, les concentrations en As(III) liées à la MO sont faibles (de 5 à 10%). Cependant, les concentrations en As(III) liées aux AH greffés en sites thiols sont plus importantes que pour les AH non greffés.

La concentration en As(III) complexée dépend de la concentration en sites thiols. Les concentrations en As(III) complexé aux AH, obtenues à la fois dans notre étude et dans la littérature, augmentent avec l'augmentation de la concentration en sites thiols. Afin de déterminer la part d'As(III) lié aux AH, il est donc absolument nécessaire de déterminer avec précision les concentrations en thiols dans les MO.

Les complexes formés sont des complexes monodentates As(III)-S-AH. Le modèle PHREEQC/Model VI a été modifié afin de tenir compte des sites thiols des AH. Il a ensuite été utilisé pour déterminer les paramètres de complexation entre l'As(III) et les sites thiols des AH. La modélisation de nos données expérimentales et de celles de la littérature à l'aide de différentes hypothèses de mécanismes de complexation ont permis de valider la

complexation monodentate de l'As(III) par un seul site thiol de AH comme étant le mécanisme efficient.

1.2 La MO est-elle réellement un fort complexant du Fe(II)?

Si de nombreuses études se sont intéressées à la complexation du Fe(III) par la MO (Karlsson and Persson, 2010; Marsac et al., 2013; Morris and Hesterberg, 2012; van Schaik et al., 2008; Vilgé-Ritter et al., 1999; Weber et al., 2006), peu se sont intéressées aux interactions entre le Fe(II) et la MO (Rose and Waite, 2003; Schnitzer and Skinner, 1966; Van Dijk, 1971; Yamamoto et al., 2010). Pourtant, dans les zones humides, en période de hautes eaux, la biodissolution réductrice des oxydes de Fe par les bactéries ferro-réductrices entraine la libération de fortes concentrations en Fe(II) dans le milieu. Il est donc important de mieux comprendre les interactions potentielles entre le Fe(II) et les substances humiques en milieu anoxique, d'autant que la spéciation du Fe dans de tels milieux pourrait fortement influencer la spéciation de métaux et métalloïdes comme l'As. Dans cette étude, des expériences de complexation du Fe(II) par un AH ont été menées afin de déterminer les paramètres de complexation entre le Fe(II) et les substances humiques.

Le Fe(II) est fortement complexé par AH. Cette étude a montré la forte complexation du Fe(II) par les AH et les acides fulviques (AF). A pH acides, lorsque les groupements carboxyliques et phénoliques sont protonés, le Fe(II) reste largement en solution. En revanche, plus le pH augmente, plus le pourcentage de Fe(II) lié aux AH et AF est important. Pour des concentrations en Fe(II) et carbone organique dissous (COD), respectivement d'environ 3 mg L^{-1} et 50 mg L^{-1}, le pourcentage de Fe(II) lié aux AH atteint 100% à partir de pH 7.

Le Fe(II) est complexé majoritairement sous forme de complexes bidentates carboxyliques, carboxy-phénoliques et phénoliques. Les constantes de complexation déterminées à l'aide de PHREEPLOT-PHREEQC-Model VI ont été calculées à partir des trois paramètres de complexation log K_{MA} (associé aux sites A), log K_{MB} (associé aux sites B) et ΔLK_2 (le terme de distribution qui modifie la force des sites bidentates et tridentates). Ces

valeurs obtenues sont fortes (log K_{MA} = 2.19 ± 0.16, log K_{MB} = 4.46± 0.47 et ΔLK_2 = 3.90 ± 1.30). La valeur de ΔLK_2 suggère une complexation dominante du Fe(II) sur les sites bidentates des substances humiques. Au contraire, peu de Fe(II) est complexé aux sites monodentates. Par ailleurs, à pH acides, la majorité du Fe(II) est complexée aux sites carboxyliques, dont le pKa est plus faible que les sites B. A pH basiques, au contraire, le Fe(II) se lie majoritairement aux sites carboxy-phénoliques, puis aux sites phénoliques et enfin aux sites carboxyliques. Ceci est en accord avec l'hypothèse que les sites phénoliques sont plus complexants que les sites carboxyliques.

1.3 Est-il possible de former des complexes ternaires As(III)-Fe(II, III) ionique-MO?

En milieu oxydant, de nombreuses études ont montré la formation de complexes ternaires entre l'As(V), le Fe(III) et la MO (Bauer and Blodau, 2006; Ko et al., 2004; Mikutta and Kretzschmar, 2011; Redman et al., 2002; Ritter et al., 2006; Sharma et al., 2010). En revanche, peu de données sont disponibles concernant l'As(III). La formation de complexes ternaires entre l'As(III) et le Fe(III) ionique ou sous forme d'oxyhydroxydes a été démontrée (Hoffmann et al., 2013; Liu et al., 2011). Cependant, dans ces études, les concentrations en As(III), Fe(III) ionique et AH utilisées, bien qu'adaptées aux conditions analytiques exigées par le XAS, étaient peu représentatives des conditions environnementales. Enfin, aucune expérience n'a été réalisée avec Fe(II), forme prépondérante du Fe en milieu anoxique. Dans cette dernière partie, je me suis donc intéressée à la formation de complexes ternaires entre l'As(III) et la MO via des ponts de Fe(II) et de Fe(III) ionique. Les concentrations en Fe(II) et Fe(III) ont donc été choisies afin que ces derniers ne puissent précipiter.

La formation de complexes ternaires As(III)-Fe(II)-MO est possible. Les expériences de complexation d'As(III) par AH en présence de Fe(II) ont montré que l'As(III) était complexé aux AH. Les données expérimentales ont mis en évidence une augmentation de la complexation d'As(III) aux AH en présence de Fe(II). PHREEQC-Model VI modifié (prise en compte des sites thiols et des complexes ternaires) a permis de montrer que

l'As(III) est non seulement lié aux sites thiols des AH mais aussi, sous forme de complexes ternaires d'As(III)-Fe(II)-AH.

Les complexes ternaires As(III)-Fe(III)-MO n'ont pas pu être identifiés. Si les résultats expérimentaux ont montré que l'As(III) se liait à la MO en présence de Fe(III), la modélisation montrent que l'As(III) est lié aux sites thiols des AH. Aucun complexe ternaire n'a donc été détecté. Les concentration en Fe(III) adsorbées par les AH sont trop faibles dans nos conditions expérimentales pour permettre la formation de complexes ternaires. L'As(III) n'est donc complexé que par les sites thiols de AH.

Les complexes ternaires As(III)-Fe(II)-AH pourraient être des complexes bidentates mononucléaires d'As(III) liés à des complexes bidentates de Fe(II)-AH. En faisant l'hypothèse que les mécanismes de complexation de l'As(III) sur les complexes de Fe(II)-AH sont les mêmes que ceux de la complexation de l'As(III) sur les complexes de Fe(III)-AH, quatre modèles de complexation ont été proposés. Parmi tous ces mécanismes, deux mécanismes permettent de reproduire correctement les données expérimentales. L'un considère la complexation d'As(III) sous forme de complexes bidentates mononucléaires sur Fe(II), lui même lié sous forme de complexes bidentates à AH. L'autre considère la complexation d'As(III) sous forme de complexes monodentates binucléaires sur Fe(II), lui-même lié sous forme de complexes bidentates à AH. Cependant, pour que ce deuxième mécanisme puisse avoir lieu, les deux atomes de Fe doivent être suffisamment proches et l'abondance de tels sites est faible. Ce mécanisme n'est donc pas favorisé. L'écriture actuelle du modèle n'est pas adaptée à la modélisation des complexes ternaires As(III)-Fe(II)-AH, et doit donc être modifiée.

1.4 Dynamique de l'As en solution dans les zones humides

Les processus physiques et chimiques activés pendant l’altération des roches conduisent à leur désagrégation et à la destruction des réseaux des minéraux primaires. Si les processus purement mécaniques conduisent à la production de particules sédimentaires de même composition que les roches primaires, l’altération chimique via notamment

l’hydrolyse permet la libération puis, la précipitation subséquente des cations métalliques ou métalloïdes sous forme de minéraux néoformés. Si l’on se focalise sur la phase solide (l’altération produit aussi des phases dissoutes) l’ensemble des constituants issus de ces processus physiques et chimiques d’altération constitue les sédiments. La composition chimique des sédiments ainsi créés va donc être fortement dépendante de la nature des roches mères et des processus d'altération. Ces sédiments peuvent notamment comprendre des oxyhydroxydes de Fe porteurs de métaux et de métalloïdes (Figure Concl 2, processus 1). Ces sédiments sont transportés par les rivières et les fleuves et le cas-échéant peuvent être déposés, lors des épisodes de crue, dans les plaines d'inondation ou les zones humides ripariennes. Celles-ci sont des écosystèmes très complexes qui sont gouvernés par des processus physiques, chimiques et biologiques majeurs impactant fortement les cycles des éléments traces métalliques. En effet, dans nos latitudes, à la période hivernale, les précipitations sont importantes et les zones humides sont alors saturées en eau suite à des phénomènes de crues ou par remontée de la nappe de subsurface. Au contraire, à la période chaude (été), les précipitations sont faibles, voire inexistantes ; les rivières sont en étiage et les niveaux des nappes sont bas, les zones humides sont désaturées en eaux et s'assèchent. Ces périodes de hautes eaux ou basses eaux sont des facteurs de contrôle majeurs de la dynamique des éléments chimiques et notamment du Fe et de l'As, puisqu'elles régulent les conditions d'oxydoréduction du milieu. En période de basses eaux, les conditions sont oxydantes, le Fe et l'As sont sous forme de Fe(III) et d'As(V). En période de basses eaux, les conditions sont réductrices, le Fe et l'As sont sous les formes réduites de Fe(II) et d'As(III). Les zones humides sont riches en matières organiques particulaires, colloïdales et dissoutes provenant de la mauvaise dégradation des plantes et organismes par les microorganismes, au regard des conditions plus ou moins périodiques de saturation en eau. L'un des composants de cette MO : les substances humiques, s’avère particulièrement réactif, notamment vis-à-vis du Fe qu'il soit ionique ou sous forme d'oxydes de Fe(III) colloïdale ou particulaire.

Milieu anoxique. Les processus redox dans les zones humides sont catalysés par les bactéries, en grande partie hétérotrophes, qui oxydent le C organique pour croitre et, en échange, réduisent divers accepteurs d'électrons en fonction de leur rendement énergétique. Elles réduisent donc l'oxydant le plus fort, O_2, puis, lorsque tout l'O_2 est consommé, NO_3, MnO_2, $Fe(OH)_3$, SO_4 jusqu'à la fermentation et la méthanogenèse. En fonction du temps de saturation et/ou de la profondeur, une stratification des conditions d'oxydoréduction peut se produire. En surface, les conditions sont plus oxydantes (l'oxygène dissous est en équilibre avec l'atmosphère) mais plus en profondeur, des conditions réductrices se mettent en place, en partie régulées par la dynamique bactérienne (Figure Concl 1 et Figure Concl 2 processus 2).

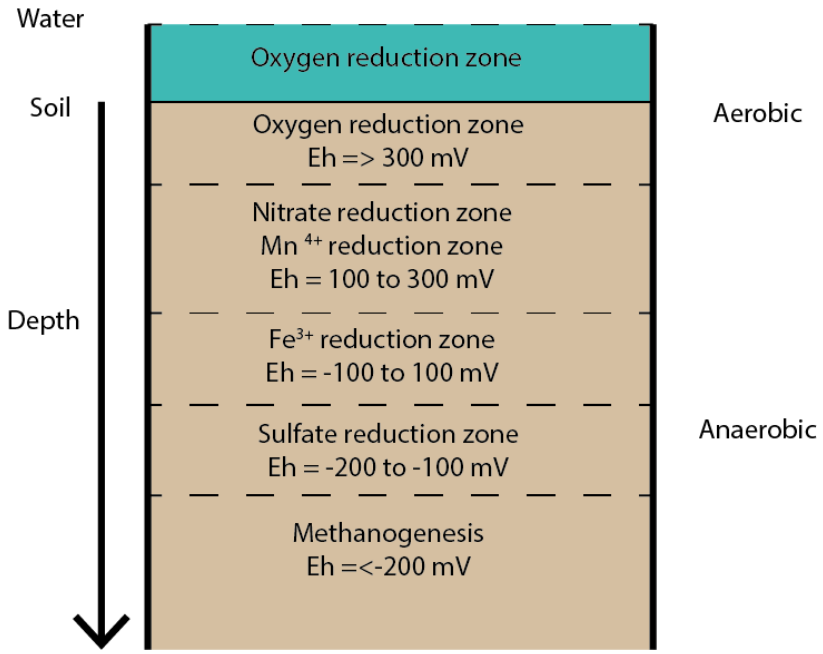

Figure Concl 1 : Distribution verticale de la gamme des espèces électrons accepteurs dans le sol d'une zone humide (Reddy and DeLaune, 2008)

La dissolution réductrice des oxyhydroxydes de Fe intervient sur une gamme d'Eh comprise entre 100 et -100 mV qualifiée de moyennement réductrice. Elle provoque la solubilisation des divers éléments traces associés, dont l'As. Ce travail a montré qu'une partie de l'As pouvait former des complexes colloïdaux dits ternaires, As(III)-Fe(II)-MO, dans ces conditions anoxiques (Figure Concl 2, processus 4). Si les mécanismes de complexation

ne sont pas clairement établis, ces complexes ternaires ne sont pas à négliger, notamment à fortes concentrations en Fe(II). Ce résultat est cependant à nuancer en présence de CO_3 et de S, conditions dans lesquelles la précipitation du Fe(II) en sidérite ou en pyrite devient possible si les conditions de saturation l'autorisent (Bowell et al., 2014). De plus, la sidérite est capable de former des complexes de sphère interne avec l'As(V) et des complexes de sphère externe avec l'As(III) (Jönsson and Sherman, 2008). Cependant, à faibles concentrations en carbonates et S, le Fe(II) reste majoritairement complexé à la MO. J'ai ainsi estimé à l'aide de PHREEQC/Model VI que dans une solution réduite de sol de zone humide environ 32% d'As(III) était lié à la MO dont 24% sous forme de complexes As(III)-Fe(II)-MO. Les sites thiols de la MO ne complexent, quant à eux, qu'1% de l'As(III) total. Même si ces calculs sont basés sur plusieurs hypothèses, ils montrent que la complexation de l'As(III) via les complexes ternaires peut être un mécanisme non négligeable en milieu anoxique. Pour autant, de nombreux éléments chimiques présents dans le milieu peuvent avoir une incidence sur la complexation de l'As(III) et du Fe(II) sur la MO. Ils peuvent soient être en compétition avec le Fe(II) à la surface de la MO ou avec l'As(III) à la surface du Fe(II), soit, au contraire, augmenter la concentration en As(III) complexé à la MO en formant de nouveaux types de complexes ternaires (éventuellement Al, Cu, voir dans la section perspectives). Les concentrations en As(III) complexé à la MO sont également très dépendantes de la densité en sites thiols. La nature de la MO pourrait donc être un facteur de contrôle non négligeable de la dynamique de l'As(III) en milieu anoxique. La densité en sites thiols peut être également en partie influencée par les conditions d'oxydoréduction du milieu. Lorsque les conditions sont suffisamment réductrices, les sulfates en solution peuvent être réduits en thiol, SH^-, qui peuvent ensuite s'adsorber à la surface de la MO et donc augmenter leur abondance (Hoffmann et al., 2012 et Matériel et méthodes de la 1ère partie du manuscrit).

La vitesse du transfert de l'As jusque dans les aquifères sous-jacents va dépendre non seulement, de sa spéciation (As libre, As complexé à la MO, co-précipité ou adsorbé à la surface de solides), de la densité, de la taille et de la composition chimique des sédiments

traversés mais aussi, de la vitesse d'écoulement. Si la porosité des sédiments traversés permet le passage des complexes As(III)-Fe(II)-MO, ceux-ci, peu adsorbés aux sédiments, migreront rapidement jusqu'aux aquifères sous-jacents (McCarthy and Zachara, 1989). Au contraire, si la porosité des sédiments est trop faible pour laisser passer la MO, celle-ci va s'agréger dans les pores et l'As(III) libre arrivera plus rapidement dans les aquifères que sa forme complexée (McCarthy and Zachara, 1989). Si les sédiments traversés sont composés de carbonates ou de S, l'As(III) pourra précipiter et être immobilisé dans les sédiments sous forme de sidérite ou de pyrite. Enfin, suivant la stabilité du complexe As(III)-Fe(II)-MO, une partie de l'As(III) complexé peut être remobilisée dans d'autres réactions chimiques (précipitation ou complexation) ou biologique (absorption) en fonction de la nature, de la chimie et du biota présent dans l'aquifère.

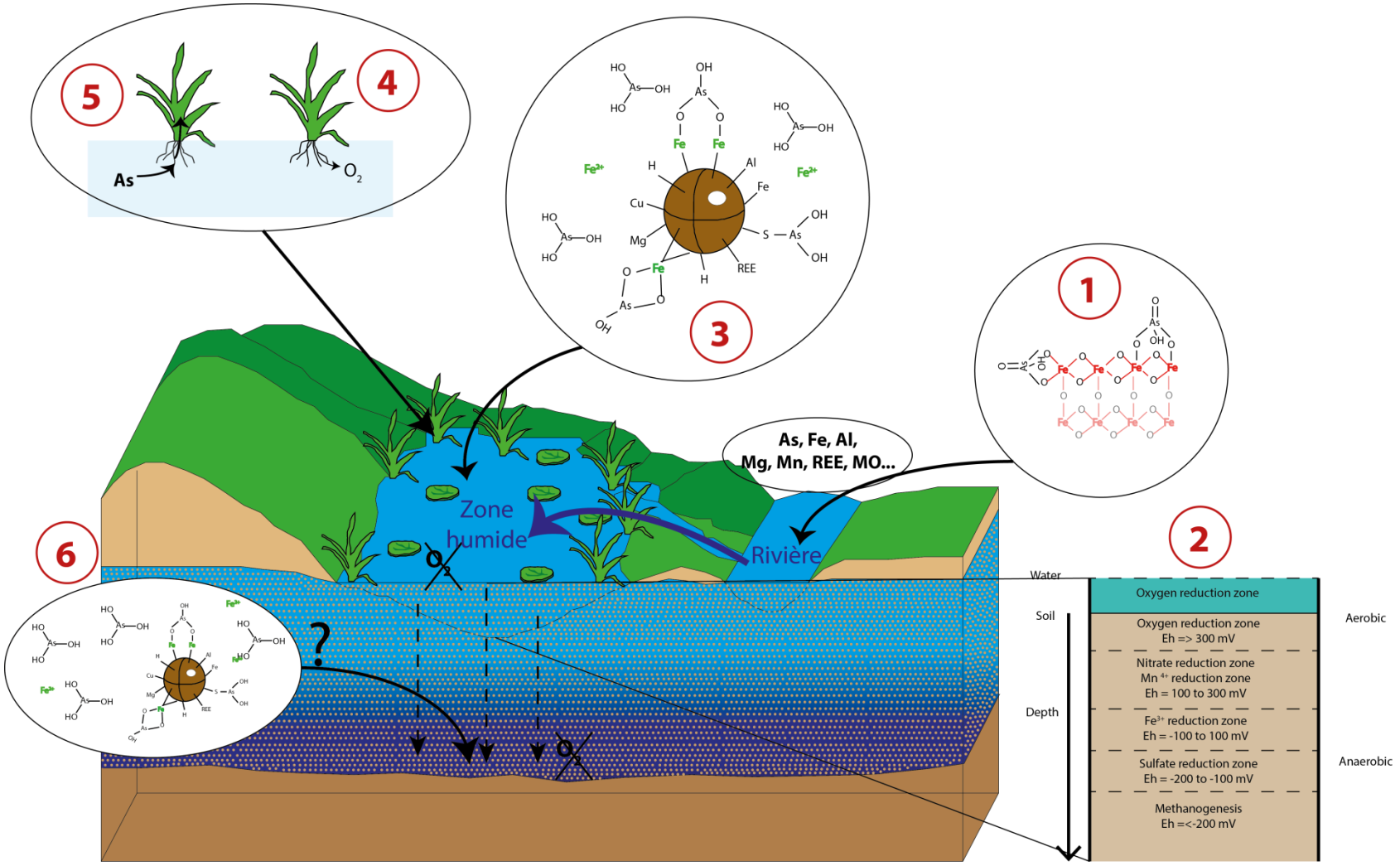

Figure Concl 2 : Récapitulatif des différents processus gouvernant la spéciation de l'As et du Fe en milieu anaérobie : 1) complexation de l'As sur les oxyhydroxydes de Fe(III), 2) réduction progressive de la colonne d'eau jusqu'à la réduction des oxydes de Fe porteurs d'As et libération de Fe^{2+} et As(III), 3) complexation de l'As(III) sur les sites thiols et les complexes ternaires As(III)-Fe(II)-MO, 4) production d'O_2 par les plantes et 5) possible absorption d'As par les plantes 6) possible transfert jusque dans les aquifères sous-jacents

Milieu oxique. Au contraire, en période de basses eaux, la zone humide est soit dépourvue d'eau en surface, soit peu alimentée par les nappes (Neubauer et al., 2013). Le Fe est sous forme oxydée, soit sous forme d'oxyhydroxydes de Fe précipités ou sous forme de complexes Fe(III)-MO (Neubauer et al., 2013). L'As est, quant à lui, présent sous forme d'As(V), lié aux oxyhydroxydes de Fe (Dixit and Hering, 2003; Grafe et al., 2001; Manning et al., 1998; Ona-Nguema et al., 2009). Si la MO dissoute peut être en compétition avec les oxyanions tels que l'As(V) pour leur complexation à la surface des oxydes de Fe(III), elle est aussi plus souvent impliquée dans la formation de complexes ternaires As(V)-Fe(III)-MO (Grafe et al., 2001; Ko et al., 2004; Redman et al., 2002). Des analyses NanoSIMS des produits de réoxydation d'une zone humide riparienne ont démontré des co-localisations majeures entre l'As, les oxydes de Fe et la MO et quelques associations minoritaires entre As-S-MO (Al-Sid-Cheikh et al., 2015). Dans ces conditions oxiques, l'As est donc sous forme colloïdale, ou particulaire et son transfert dans le réseau hydrographique de surface ne se produira que lors d'événements pluvieux de courte durée, ne provoquant pas la mise en place de conditions réductrices, tels que des orages (Neubauer et al., 2013) ou en tout début de reprise des écoulements avant ennoiement et saturation en eau des sols.

Milieu intermédiaire. A la reprise des écoulements, en début de saturation en eaux, des conditions redox intermédiaires se développent avec une coexistence dans la colonne d'eau et de sol d'As(III, V) et de Fe(II,III). Des complexes ternaires d'As(III)-oxyhydroxydes de Fe(III)-MO ou As(III)-Fe(III) ionique-MO pourraient se former (Hoffmann et al., 2013; Liu et al., 2011). Cependant, pour de faibles concentrations en Fe(III), proches de celles rencontrées dans le milieu naturel, ce travail a montré que ces complexes n'étaient pas détectables, remettant en cause l'impact d'un tel mécanisme sur le devenir de l'As(III). Dans de telles conditions, l'As(III) complexé, l'est donc majoritairement aux associations oxyhydroxydes de Fe(III)-MO qui persiste dans ces conditions d'oxydoréduction intermédiaires. Son transfert dans le réseau hydrographique de surface ou souterrain dépendra donc uniquement du comportement des particules ou colloïdes sur lesquels il est fixé.

2 Perspectives

Au delà des nouvelles contraintes ci-dessus déclinées et apportées via notre approche de modélisation sur la caractérisations des interactions Fe, As, MO, ces travaux nous suggèrent de nouvelles perspectives d'études.

2.1 Perspectives analytiques

Il apparaît nécessaire de connaitre la concentration exacte en sites thiols dans les MO afin de correctement déterminer la spéciation de l'As(III) par modélisation. En effet, s'il est actuellement relativement simple de mesurer la concentration en S dans une MO par une analyse élémentaire CHNS, seule une partie du S est présent sous la forme thiol. Actuellement, les concentrations en sites thiols dans les MO sont généralement mesurées par analyses XAS, mais ces analyses demandent de grandes quantités de matière. Or, sur le terrain, il est difficile de récupérer assez de solution pour ce type d'analyse. De plus, les concentrations mesurées ne sont pas les concentrations exactes en sites thiols mais les concentrations en S sous forme de cycles exocycliques (Manceau and Nagy, 2012). Une autre méthode décrite par Rao et al. (2014) propose la détermination des sites thiols par titration à l'aide d'un complexant spécifique aux sites thiols. Cependant, cette méthode a été développée récemment et il convient de vérifier sa validité notamment en présence de métaux et métalloïdes, ce qui est le cas dans les zones humides.

La spéciation du Fe a une très forte influence sur la spéciation de l'As(III). Il est donc nécessaire de pouvoir correctement la déterminer; notamment dans les milieux à fortes concentrations en MO. La méthode colorimétrique utilisée dans ce travail n'a malheureusement pas permis de déterminer la spéciation du Fe lorsqu'il était lié à la Leonardite. En effet, l'absorbance de l'AH recouvre l'absorbance du complexe Fe(II)-phénanthroline. Si les eaux de terrain ne présentent toutefois pas des absorbances aussi fortes que nos solutions expérimentales, une erreur analytique non négligeable reste cependant à déplorer. De plus, concernant le Fe(III), il peut être sous forme cationique et/ou d'oxyhydroxydes. La détermination de la proportion relative de ces deux formes en présence

de MO est difficile, d'autant que la MO est capable de complexer le Fe(III) sous ses deux formes. Les analyses XAS peuvent déterminer ces formes mais de grandes quantités de matières solides sont nécessaires, ce qui est difficile pour des objets naturels de terrain. Il serait donc intéressant de pouvoir déterminer la spéciation via des analyses *in situ* afin de ne pas changer la spéciation des éléments entre le prélèvement et l'analyse. Il serait nécessaire de supprimer la MO par exemple en faisant une première étape d'extraction du Fe complexé à la MO suivie d'une analyse de la spéciation par colorimétrie. Une autre possibilité serait de développer un complexant colorimétrique de Fe(II) dont l'absorbance ne recouvre pas celle de la MO.

Enfin, il a été montré dans cette étude que le Fe(II) pouvait se complexer à la MO et former des complexes ternaires avec l'As(III) mais les mécanismes de complexation n'ont pas été déterminés au préalable par mesure XAS. Ainsi, les mécanismes proposés dans cette étude ont été déterminés à partir des mécanismes de complexation de l'As(III) sur les complexes de Fe(III)-AH. Il conviendrait de déterminer, non seulement, les mécanismes de complexation du Fe(II) sur la MO mais aussi, les mécanismes de complexation de l'As(III) sur le Fe(II) complexé à la MO. S'il est vrai que les concentrations d'As(III), Fe(II) et MO nécessaires pour effectuer des mesures XAS sont fortes, c'est néanmoins le seul moyen actuel pour déterminer les mécanismes exactes de complexation. Il faut cependant être vigilant à conserver la spéciation de l'As et du Fe sous la forme réduite et veiller à employer des rapports de concentrations As(III)/Fe(II) et Fe(II)/MO qui représentent les rapports de concentrations retrouvées dans le milieu naturel. Enfin, il faut veiller à ce que le Fe(II) ne précipite pas en sidérite et en pyrite en se plaçant dans un milieu dépourvu de S et carbonates.

2.2 Modèle de complexation à la surface des AH

Dans la 3ème partie du manuscrit, la proportion de chaque mécanisme de formation des complexes ternaires As(III)-Fe(II)-AH n'a pas pu être clairement définie par modélisation. Des données XAS sont nécessaires pour déterminer ces proportions. De plus, il a été

montré que le modèle actuellement utilisé (PHREEQC-Model VI modifié) ne permettait pas de modéliser la complexation de monodentates de Fe(II) suffisamment proches pour former des monodentates binucléaires avec l'As(III). Ainsi, il est nécessaire de déterminer la contribution relative de sites bidentates dans PHREEQC-Model VI formant deux monodentates de Fe(II) pour modéliser la complexation de l'As(III) sur ces sites. Les données XAS du Fe(II) pourraient permettre de déterminer cette proportion. La difficulté repose sur la conservation de la spéciation du Fe qui doit nécessairement rester stable pendant le transport des échantillons et l'analyse sous le faisceau de rayons X.

2.3 Compétition ou formation d'autres complexes ternaires?

Peu de données sont actuellement disponibles concernant la formation de complexes en solution d'As(III) avec d'autres métaux. Or, la formation ou non de complexes en solution peut être un indice concernant l'affinité par exemple de l'As(III) avec les autres métaux. Marini and Accornero (2007) ont répertorié les constantes de destruction des complexes en solution d'As(III) avec Na, Ag, Mg, Ca, Sr, Ba, Cu, Pb, Al et Fe(III). Les constantes de ces complexes en solution recalculées dans l'ordre de formation sont par ordre croissant : Al > Fe(III) > Cu > Pb > Mg > Ca > Ba > Ag > Sr > Na. Comme l'As(III) forme des complexes ternaires avec Fe(III), cet ordre laisse suggérer que l'As(III) pourrait former des complexes ternaires avec Al(III) au contraire des résultats obtenus par Buschmann et al. (2006). Les concentrations en Al et COD utilisées dans les expériences de Buschmann et al. (2006) sont plus faibles que les concentrations retrouvées dans une solution de réduction de sol d'un horizon de surface de la zone humide de Kervidy-Naizin (Tableau Concl 1). Or, une concentration plus forte en COD complexera des concentrations en Al plus importantes. En cas de formation de complexes ternaires, l'As(III) aura alors plus de chance de former ces complexes. Des expériences doivent donc être réalisées avec des concentrations plus importantes en COD et en Al.

Tableau Concl 1 : Comparaison des concentrations en Al, As et COD dans les expériences conduites par Buschmann et al. (2006) et dans celles d'une solution correspondant à une réduction de sol de zone humide.

	Al (µmol L^{-1})	As (µmol L^{-1})	COD (mg L^{-1})
Buschmann et al. (2006)	0-15	0.4	30
	0-4	0.0134	93
Solution de réduction de sol de zone humide	21	0.4	104

Le Cu est également fortement complexé à la MO (Tipping, 1998) et pourrait également aussi potentiellement former des complexes ternaires avec l'As(III). De même, les terres rares (REE) se complexent très fortement à la MO (Marsac et al., 2011, 2010; Pourret et al., 2007). Or, des expériences en laboratoire (données non publiées) ont montré qu'elles pouvaient former des complexes en solution avec l'As(V) en présence de MO avec un changement du spectre des REE (REE lourdes) par rapport au spectre généralement caractéristique d'eaux riches en MO. Les concentrations naturelles en REE complexées aux AH sont cependant faibles par rapport à un élément majeur comme le Fe (% complexé plus important mais concentrations complexées plus faibles) et ne pourront vraisemblablement pas complexer l'As en grande quantité. La forme du spectre des REE est cependant un traceur intéressant des éléments complexés aux AH (Marsac et al., 2013, 2012). Ainsi, en présence d'Al ou de Fe, le spectre des REE (REE lourdes) est modifié. Ce changement de spectre observé en présence d'As pourrait être un traceur de la présence d'As. Enfin, l'As se complexe à la surface des oxydes de Mn, mais les valeurs des paramètres de complexation du Mn à la surface des HA sont faibles (log K_{MA} = 0.6) ; ce qui suggère que si des complexes ternaires avec le Mn pouvaient exister, les concentrations complexées seraient faibles.

Cependant, tous ces mécanismes de complexation ne tiennent pas compte des autres éléments chimiques présents dans le milieu. Or, dans les zones humides, de nombreux éléments chimiques sont potentiellement en compétition à la surface de la MO. Les phénomènes décrits ci-dessus, sont vraisemblablement plus complexes dans le milieu naturel. En tout état de fait, leur déconvolution est sans doute moins aisée. Par ailleurs, les zones humides sont des écosystèmes dans lequel le "compartiment" vivant (flore,

macrofaune, microfaune) joue un rôle majeur, notamment dans sa capacité à jouer sur la spéciation métaux et métalloïdes par des réactions d'absorption (Figure Concl 2, processus 5), contrôle du pH, libération de ligands organiques... De nombreux, champignons et algues sont capables de réduire ou d'oxyder l'As dans les zones humides (Reddy and DeLaune, 2008). Les bactéries sont également capables de réduire les oxydes de Fe en Fe(II) mais aussi de réduire l'As(V) en As(III) par des réactions de détoxification (Páez-Espino et al., 2009). Toute cette microfaune et microflore n'est pas prise en compte dans les modèles proposés malgré son fort impact dans le milieu naturel. Le développement d'un modèle pouvant prendre en compte son impact accroitrait significativement sa capacité à appréhender la diversité des mécanismes réellement mis en jeu dans le milieu naturel. Les bactéries utilisent généralement la MO comme des donneurs d'électrons et le Fe ou l'As comme des accepteurs d'électrons. Klüpfel et al. (2014) ont ainsi décrit la capacité de la MO à capter ou à donner des électrons en milieu réduit ou oxydant. Ces mécanismes pourraient ainsi être décrits comme un échange d'électrons entre la MO et le Fe ou l'As. Le modèle nécessite de définir une surface correspondant à une partie de la MO avec une capacité d'échange d'électrons. Cependant, dans PHREEQC-Model VI, deux surfaces utilisées en même temps sont difficiles à gérer par le modèle, notamment pour les calculs de complexation des espèces dans la double couche. Il est donc nécessaire de pallier ces problèmes pour être capable de modéliser une partie plus importante des mécanismes mis en jeu dans les zones humides.

ANNEXES

ANNEXE I: Instrumentation

Determination of total As concentrations.

As (isotope 75) concentrations were determined using a 7700 Agilent Technologies ICP-MS at Rennes 1 University. Normal plasma conditions were used with a collision cell (He). The instrumental parameters are listed in Table 1.

	Normal Plasma
RF Power	1550 W
Plasma gas	15L/min
Auxiliary gas	1.0 L/min
Carrier gas	1.15 L/min
Nebulizer	Micro mist
Spray Chamber T°	2°C
Collision Cell	0.45ml/mn He
Quantitative analysis	0.5 sec/mass
CeO^+/Ce^+	0.9%
Ce^{++}/Ce^+	1.5%

Table 1: Instrumental and data acquisition parameters.

Quantitative analyses were performed using a conventional external calibration procedure (seven external standard multi-element solutions - Inorganic Venture, USA). Rhodium-Rhenium was added on-line as internal standard at a concentration level of 300 ppb to correct for instrumental drift and possible matrix effects. The calibration curves were calculated from the intensity ratios of the internal standard and the analyzed elements. SLRS-5 water standard was used to control the “concentration accuracy.”, the instrumental error on As analysis was below 3%. Chemical blanks of As were all lower than detection limit (0.003 µg L^{-1} for As), and were thus negligible.

Determination of Arsenic As(V) and As(III) concentrations by LC-ICP-MS

An Agilent 7700x ICP-MS was coupled to an Agilent HPLC Infinity 1260. Separation of As(V) and As(III) species was conducted using an Agilent arsenic speciation column and guard column G3154A. The mobile phase consisted of 2.0 mmol L^{-1} PBS, 0.2 mmol L^{-1}

EDTA, 10 mmol L^{-1} CH_3COONa, 3.0 mmol L^{-1} $NaNO_3$ and 1% EtOH at pH 11 adjusted with NaOH. The method used was described in “As speciation Analysis Handbook” (G3154-90011- Rev.A) Agilent technologies, 2010 USA. Tellurium solution was added on-line as internal standard. Quantitative analyses were performed using external calibration by analyzing standard solutions of As(III) and As(V) (Inorganic Venture, USA) between 0.1 to 20 µg L^{-1}. Typical limit of detection was 0.1-0.2 µg L^{-1}. The instrument operating conditions are displayed in Table 2.

ICP-MS	**Normal Plasma**
Mode	Time Resolved Mode (TRA)
Acquired Mass	75 (As), 35(Cl), 125 (Te)
Integration time	0.5 s for As; 0.1 s for Cl; 0.05s for Te
Acquisition Time	780s
RF Power	1550 W
Plasma gas	15L min^{-1}
Auxiliary gas	1.0 L min^{-1}
Carrier gas	0.72 L min^{-1}
Makeup gas	0.42L min^{-1}
Nebulizer	Micro mist
Spray Chamber T°	2°C
Sampling depth	9 mn
Peristaltic pump speed	0.3 rps
HPLC	**Acquisition parameters**
Mobile phase flow rate	1.0 ml mn^{-1}
Injection volume	20 µL
Acquisition Time	800 s
Mobile phase	2.0 mmol L^{-1} PBS 0.2 mmol L^{-1} EDTA 10 mmol L^{-1} CH_3COONa 3.0 mmol L^{-1} $NaNO_3$ 1% EtOH pH = 11 with NaOH

Table 2: Instrumental and data acquisition parameters for ICP-MS and HPLC.

ANNEXE II: Definition of PHREEQC-Model VI modified

II.1. Abundances of the sites

Annexe II 3: Abundance of the 84 different sites describing the HA (Mono model).

PHREEQC name	Chemical nature	Abundance (mol gHA^{-1})
Ha_a	C	$(1-f_B-f_T)*n_A/4$
Ha_b	C	$(1-f_B-f_T)*n_A/4$
Ha_c	C	$(1-f_B-f_T)*n_A/4$
Ha_d	C	$(1-f_B-f_T)*n_A/4$
Ha_e	P	$(1-f_B-f_T)*n_B/4$
Ha_f	P	$(1-f_B-f_T)*n_B/4$
Ha_g	P	$(1-f_B-f_T)*n_B/4$
Ha_h	P	$(1-f_B-f_T)*n_B/4$
Ha_i	S	$n_S/4$
Ha_j	S	$n_S/4$
Ha_k	S	$n_S/4$
Ha_l	S	$n_S/4$
Ha_ab	CC	$n_A*f_B*0.901/6$
Ha_cd	CC	$n_A*f_B*0.901/6$
Ha_ae	CP	$n_A*f_B*0.901/(6*rpsite_B)$
Ha_bf	CP	$n_A*f_B*0.901/(6*rpsite_B)$
Ha_cg	CP	$n_A*f_B*0.901/(6*rpsite_B)$
Ha_dh	CP	$n_A*f_B*0.901/(6*rpsite_B)$
Ha_ef	PP	$n_A*f_B*0.901/(6*rpsite_B^2)$
Ha_gh	PP	$n_A*f_B*0.901/(6*rpsite_B^2)$
Ha_abx	CC	$n_A*f_B*0.09/6$
Ha_cdx	CC	$n_A*f_B*0.09/6$
Ha_aex	CP	$n_A*f_B*0.09/(6*rpsite_B)$
Ha_bfx	CP	$n_A*f_B*0.09/(6*rpsite_B)$
Ha_cgx	CP	$n_A*f_B*0.09/(6*rpsite_B)$
Ha_dhx	CP	$n_A*f_B*0.09/(6*rpsite_B)$
Ha_efx	PP	$n_A*f_B*0.09/(6*rpsite_B^2)$
Ha_ghx	PP	$n_A*f_B*0.09/(6*rpsite_B^2)$
Ha_abxx	CC	$n_A*f_B*0.009/6$
Ha_cdxx	CC	$n_A*f_B*0.009/6$
Ha_aexx	CP	$n_A*f_B*0.009/(6*rpsite_B)$
Ha_bfxx	CP	$n_A*f_B*0.009/(6*rpsite_B)$
Ha_cgxx	CP	$n_A*f_B*0.009/(6*rpsite_B)$
Ha_dhxx	CP	$n_A*f_B*0.009/(6*rpsite_B)$
Ha_efxx	PP	$n_A*f_B*0.009/(6*rpsite_B^2)$
Ha_ghxx	PP	$n_A*f_B*0.009/(6*rpsite_B^2)$
Ha_abc	CCC	$n_A*f_B*0.901/3^3$
Ha_abd	CCC	$n_A*f_B*0.901/3^3$
Ha_acd	CCC	$n_A*f_B*0.901/3^3$
Ha_bcd	CCC	$n_A*f_B*0.901/3^3$
Ha_abe	CCP	$n_A*f_B*0.901/(3^2*rpsite_B)$
Ha_cdf	CCP	$n_A*f_B*0.901/(3^2*rpsite_B)$
Ha_acg	CCP	$n_A*f_B*0.901/(3^2*rpsite_B)$
Ha_bdh	CCP	$n_A*f_B*0.901/(3^2*rpsite_B)$

C, P and S are the carboxylic, phenolic and thiol groups, respectively; $rpsite_B = n_A/n_B$

PHREEQC name	Chemical nature	Abundance (mol gHA^{-1})
Ha_aef	CPP	$n_A*f_B*0.901/(3^2*rpsite_{B^2})$
Ha_bgh	CPP	$n_A*f_B*0.901/(3^2*rpsite_{B^2})$
Ha_ceg	CPP	$n_A*f_B*0.901/(3^2*rpsite_{B^2})$
Ha_dfh	CPP	$n_A*f_B*0.901/(3^2*rpsite_{B^2})$
Ha_efg	PPP	$n_A*f_B*0.901/(3^2*rpsite_B^3)$
Ha_efh	PPP	$n_A*f_B*0.901/(3^2*rpsite_B^3)$
Ha_egh	PPP	$n_A*f_B*0.901/(3^2*rpsite_B^3)$
Ha_fgh	PPP	$n_A*f_B*0.901/(3^2*rpsite_B^3)$
Ha_abcy	CCC	$n_A*f_B*0.09/3^3$
Ha_abdy	CCC	$n_A*f_B*0.09/3^3$
Ha_acdy	CCC	$n_A*f_B*0.09/3^3$
Ha_bcdy	CCC	$n_A*f_B*0.09/3^3$
Ha_abey	CCP	$n_A*f_B*0.09/(3^2*rpsite_B)$
Ha_cdfy	CCP	$n_A*f_B*0.09/(3^2*rpsite_B)$
Ha_acgy	CCP	$n_A*f_B*0.09/(3^2*rpsite_B)$
Ha_bdhy	CCP	$n_A*f_B*0.09/(3^2*rpsite_B)$
Ha_aefy	CPP	$n_A*f_B*0.09/(3^2*rpsite_{B^2})$
Ha_bghy	CPP	$n_A*f_B*0.09/(3^2*rpsite_{B^2})$
Ha_cegy	CPP	$n_A*f_B*0.09/(3^2*rpsite_{B^2})$
Ha_dfhy	CPP	$n_A*f_B*0.09/(3^2*rpsite_{B^2})$
Ha_efgy	PPP	$n_A*f_B*0.09/(3^2*rpsite_B^3)$
Ha_efhy	PPP	$n_A*f_B*0.09/(3^2*rpsite_B^3)$
Ha_eghy	PPP	$n_A*f_B*0.09/(3^2*rpsite_B^3)$
Ha_fghy	PPP	$n_A*f_B*0.09/(3^2*rpsite_B^3)$
Ha_abcyy	CCC	$n_A*f_B*0.009/3^2$
Ha_abdyy	CCC	$n_A*f_B*0.009/3^2$
Ha_acdyy	CCC	$n_A*f_B*0.009/3^2$
Ha_bcdyy	CCC	$n_A*f_B*0.009/3^2$
Ha_abeyy	CCP	$n_A*f_B*0.009/(3^2*rpsite_B)$
Ha_cdfyy	CCP	$n_A*f_B*0.009/(3^2*rpsite_B)$
Ha_acgyy	CCP	$n_A*f_B*0.009/(3^2*rpsite_B)$
Ha_bdhyy	CCP	$n_A*f_B*0.009/(3^2*rpsite_B)$
Ha_aefyy	CPP	$n_A*f_B*0.009/(3^2*rpsite_B^2)$
Ha_bghyy	CPP	$n_A*f_B*0.009/(3^2*rpsite_B^2)$
Ha_cegyy	CPP	$n_A*f_B*0.009/(3^2*rpsite_B^2)$
Ha_dfhyy	CPP	$n_A*f_B*0.009/(3^2*rpsite_B^2)$
Ha_efgyy	PPP	$n_A*f_B*0.009/(3^2*rpsite_B^3)$
Ha_efhyy	PPP	$n_A*f_B*0.009/(3^2*rpsite_B^3)$
Ha_eghyy	PPP	$n_A*f_B*0.009/(3^2*rpsite_B^3)$
Ha_fghyy	PPP	$n_A*f_B*0.009/(3^2*rpsite_B^3)$

C, P and S are the carboxylic, phenolic and thiol groups, respectively; $rpsite_B = n_A/n_B$

Annexe II 4: Calculations of the abundances of the thiol sites for the Tri model.

PHREEQC name	Chemical nature	Abundance (mol gHA^{-1})
Ha_i	S	$(1-f_T)*n_S/4$
Ha_j	S	$(1-f_T)*n_S/4$
Ha_k	S	$(1-f_T)*n_S/4$
Ha_l	S	$(1-f_T)*n_S/4$
Ha_ijk	SSS	$n_S*f_T/3^3$
Ha_ijl	SSS	$n_S*f_T/3^3$
Ha_ikl	SSS	$n_S*f_T/3^3$
Ha_jkl	SSS	$n_S*f_T/3^3$

II.2. Protonation/deprotonation and complexation constants of the sites

Annexe II 5: Deprotonation reaction and associated pK for the 12 monodentate sites.

Reactions	pK
Ha_aH = Ha_a$^-$ + H$^+$	$\mathrm{pK(a)} = \mathrm{pK_A} - \frac{\Delta \mathrm{pK_A}}{2}$
Ha_bH = Ha_b$^-$ + H$^+$	$\mathrm{pK(b)} = \mathrm{pK_A} - \frac{\Delta \mathrm{pK_A}}{6}$
Ha_cH = Ha_c$^-$ + H$^+$	$\mathrm{pK(c)} = \mathrm{pK_A} + \frac{\Delta \mathrm{pK_A}}{6}$
Ha_dH = Ha_d$^-$ + H$^+$	$\mathrm{pK(d)} = \mathrm{pK_A} + \frac{\Delta \mathrm{pK_A}}{2}$
Ha_eH = Ha_e$^-$ + H$^+$	$\mathrm{pK(e)} = \mathrm{pK_B} - \frac{\Delta \mathrm{pK_B}}{2}$
Ha_fH = Ha_f$^-$ + H$^+$	$\mathrm{pK(f)} = \mathrm{pK_B} - \frac{\Delta \mathrm{pK_B}}{6}$
Ha_gH = Ha_g$^-$ + H$^+$	$\mathrm{pK(g)} = \mathrm{pK_B} + \frac{\Delta \mathrm{pK_B}}{6}$
Ha_hH = Ha_h$^-$ + H$^+$	$\mathrm{pK(h)} = \mathrm{pK_B} + \frac{\Delta \mathrm{pK_B}}{2}$
Ha_iH = Ha_i$^-$ + H$^+$	$\mathrm{pK(i)} = \mathrm{pK_S} - \frac{\Delta \mathrm{pK_S}}{2}$
Ha_jH = Ha_j$^-$ + H$^+$	$\mathrm{pK(j)} = \mathrm{pK_S} - \frac{\Delta \mathrm{pK_S}}{6}$
Ha_kH = Ha_k$^-$ + H$^+$	$\mathrm{pK(k)} = \mathrm{pK_S} + \frac{\Delta \mathrm{pK_S}}{6}$
Ha_lH = Ha_l$^-$ + H$^+$	$\mathrm{pK(l)} = \mathrm{pK_S} + \frac{\Delta \mathrm{pK_S}}{2}$

Annexe II 6: Complexation reaction and associated log k between As and the four monodentate and tridentate thiol groups of HA.

Mono model	
Reaction	**Log k**
$Ha\_iH + As(OH)_3 = Ha\_iAs(OH)_2 + H_2O$	$\log K(i) = \log K_{MS} - \frac{\Delta LK_{1S}}{2}$
$Ha\_jH + As(OH)_3 = Ha\_jAs(OH)_2 + H_2O$	$\log K(j) = \log K_{MS} - \frac{\Delta LK_{1S}}{6}$
$Ha\_kH + As(OH)_3 = Ha\_kAs(OH)_2 + H_2O$	$\log K(k) = \log K_{MS} + \frac{\Delta LK_{1S}}{6}$
$Ha\_lH + As(OH)_3 = Ha\_lAs(OH)_2 + H_2O$	$\log K(l) = \log K_{MA} + \frac{\Delta LK_{1B}}{2}$
Tri model	
Reaction	**Log k**
$Ha\_ijkH_3 + As(OH)_3 = Ha\_ijkAs + 3\ H_2O$	$\log K(ijk) = 3*\log K_{MS} - \frac{\Delta LK_{1S}}{2}$
$Ha\_ijlH_3 + As(OH)_3 = Ha\_ijlAs + 3\ H_2O$	$\log K(ijl) = 3*\log K_{MS} - \frac{\Delta LK_{1S}}{6}$
$Ha\_iklH_3 + As(OH)_3 = Ha\_iklAs + 3\ H_2O$	$\log K(ikl) = 3*\log K_{MS} + \frac{\Delta LK_{1S}}{6}$
$Ha\_jklH_3 + As(OH)_3 = Ha\_jklAs + 3\ H_2O$	$\log K(jkl) = 3*\log K_{MS} + \frac{\Delta LK_{1S}}{2}$

ANNEXE III: Equations and results of As(III) complexation through As(III)-Fe(II)-HA complexes

ANNEXE III 1: Chemical equations of Fe(II) monodentate and As(III) mononuclear bidentate complexes

Equations of Fe(II) monodentate and As(III) mononuclear bidentate complexes					Log k
Ha_aFe^{+}	+	H_3AsO_3	=	$Ha\_aFeH_3AsO_3^{+}$	Log_k_1
Ha_bFe^{+}	+	H_3AsO_3	=	$Ha\_bFeH_3AsO_3^{+}$	Log_k_1
Ha_cFe^{+}	+	H_3AsO_3	=	$Ha\_cFeH_3AsO_3^{+}$	Log_k_1
Ha_dFe^{+}	+	H_3AsO_3	=	$Ha\_dFeH_3AsO_3^{+}$	Log_k_1
Ha_eFe^{+}	+	H_3AsO_3	=	$Ha\_eFeH_3AsO_3^{+}$	Log_k_1
Ha_fFe^{+}	+	H_3AsO_3	=	$Ha\_fFeH_3AsO_3^{+}$	Log_k_1
Ha_gFe^{+}	+	H_3AsO_3	=	$Ha\_gFeH_3AsO_3^{+}$	Log_k_1
Ha_hFe^{+}	+	H_3AsO_3	=	$Ha\_hFeH_3AsO_3^{+}$	Log_k_1

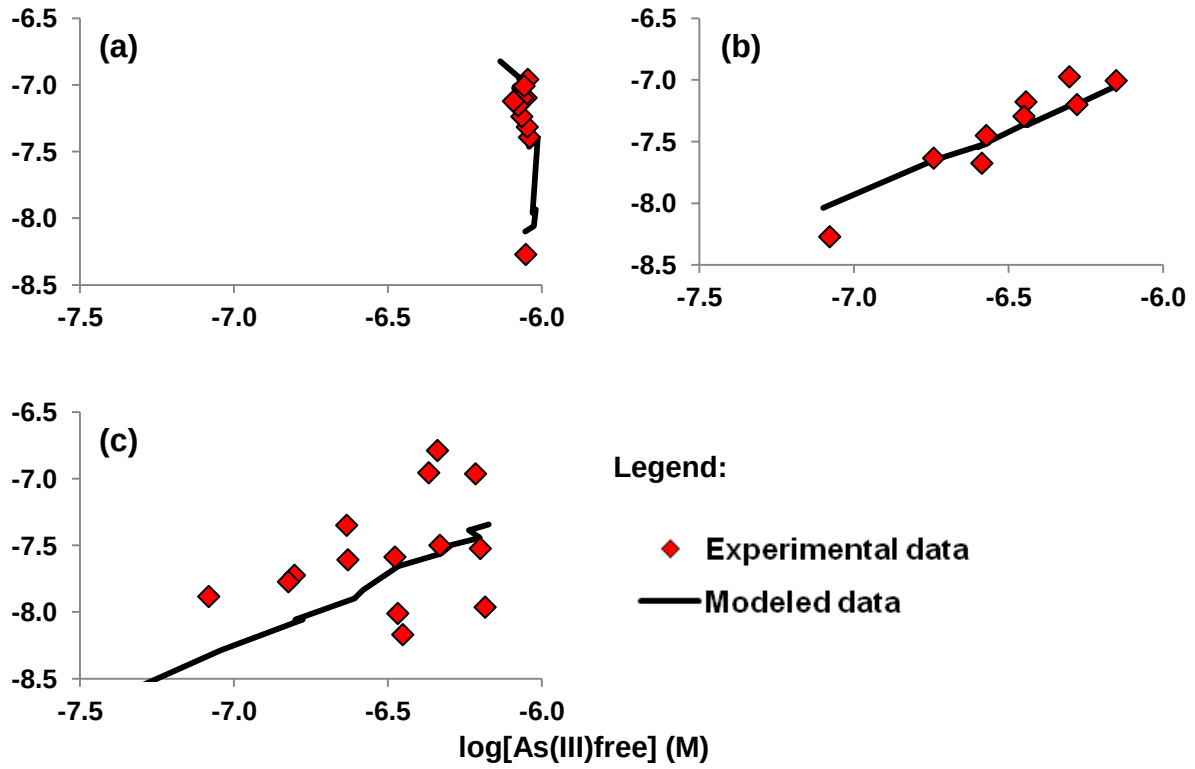

ANNEXE III 2: Formation of As(III) mononuclear bidentate to Fe(II) monodentate with OM (a) isotherm with increasing Fe(II) concentrations at pH 6, (b) isotherm with increasing As(III) concentrations at pH 6, (c) isotherm with increasing Fe(II) concentrations at pH 5.

ANNEXE III 3: Chemical equations of Fe(II) monodentate and As(III) binuclear monodentate complexes

Equations of Fe(II) monodentate and As(III) binuclear monodentate complexes							Log k
Ha_aFe^{+}	+	Ha_bFe^{+}	+	H_3AsO_3	=	$Ha\_aFeH_3AsO_3Ha\_bFe^{+2}$	Log_k_1
Ha_aFe^{+}	+	Ha_cFe^{+}	+	H_3AsO_3	=	$Ha\_aFeH_3AsO_3Ha\_cFe^{+2}$	Log_k_1
Ha_aFe^{+}	+	Ha_dFe^{+}	+	H_3AsO_3	=	$Ha\_aFeH_3AsO_3Ha\_dFe^{+2}$	Log_k_1
Ha_aFe^{+}	+	Ha_eFe^{+}	+	H_3AsO_3	=	$Ha\_aFeH_3AsO_3Ha\_eFe^{+2}$	Log_k_1
Ha_aFe^{+}	+	Ha_fFe^{+}	+	H_3AsO_3	=	$Ha\_aFeH_3AsO_3Ha\_fFe^{+2}$	Log_k_1
Ha_aFe^{+}	+	Ha_gFe^{+}	+	H_3AsO_3	=	$Ha\_aFeH_3AsO_3Ha\_gFe^{+2}$	Log_k_1
Ha_aFe^{+}	+	Ha_hFe^{+}	+	H_3AsO_3	=	$Ha\_aFeH_3AsO_3Ha\_hFe^{+2}$	Log_k_1
Ha_bFe^{+}	+	Ha_cFe^{+}	+	H_3AsO_3	=	$Ha\_bFeH_3AsO_3Ha\_cFe^{+2}$	Log_k_1
Ha_bFe^{+}	+	Ha_dFe^{+}	+	H_3AsO_3	=	$Ha\_bFeH_3AsO_3Ha\_dFe^{+2}$	Log_k_1
Ha_bFe^{+}	+	Ha_eFe^{+}	+	H_3AsO_3	=	$Ha\_bFeH_3AsO_3Ha\_eFe^{+2}$	Log_k_1
Ha_bFe^{+}	+	Ha_fFe^{+}	+	H_3AsO_3	=	$Ha\_bFeH_3AsO_3Ha\_fFe^{+2}$	Log_k_1
Ha_bFe^{+}	+	Ha_gFe^{+}	+	H_3AsO_3	=	$Ha\_bFeH_3AsO_3Ha\_gFe^{+2}$	Log_k_1
Ha_bFe^{+}	+	Ha_hFe^{+}	+	H_3AsO_3	=	$Ha\_bFeH_3AsO_3Ha\_hFe^{+2}$	Log_k_1
Ha_cFe^{+}	+	Ha_dFe^{+}	+	H_3AsO_3	=	$Ha\_cFeH_3AsO_3Ha\_dFe^{+2}$	Log_k_1
Ha_cFe^{+}	+	Ha_eFe^{+}	+	H_3AsO_3	=	$Ha\_cFeH_3AsO_3Ha\_eFe^{+2}$	Log_k_1
Ha_cFe^{+}	+	Ha_fFe^{+}	+	H_3AsO_3	=	$Ha\_cFeH_3AsO_3Ha\_fFe^{+2}$	Log_k_1
Ha_cFe^{+}	+	Ha_gFe^{+}	+	H_3AsO_3	=	$Ha\_cFeH_3AsO_3Ha\_gFe^{+2}$	Log_k_1
Ha_cFe^{+}	+	Ha_hFe^{+}	+	H_3AsO_3	=	$Ha\_cFeH_3AsO_3Ha\_hFe^{+2}$	Log_k_1
Ha_dFe^{+}	+	Ha_eFe^{+}	+	H_3AsO_3	=	$Ha\_dFeH_3AsO_3Ha\_eFe^{+2}$	Log_k_1
Ha_dFe^{+}	+	Ha_fFe^{+}	+	H_3AsO_3	=	$Ha\_dFeH_3AsO_3Ha\_fFe^{+2}$	Log_k_1
Ha_dFe^{+}	+	Ha_gFe^{+}	+	H_3AsO_3	=	$Ha\_dFeH_3AsO_3Ha\_gFe^{+2}$	Log_k_1
Ha_dFe^{+}	+	Ha_hFe^{+}	+	H_3AsO_3	=	$Ha\_dFeH_3AsO_3Ha\_hFe^{+2}$	Log_k_1
Ha_eFe^{+}	+	Ha_fFe^{+}	+	H_3AsO_3	=	$Ha\_eFeH_3AsO_3Ha\_fFe^{+2}$	Log_k_1
Ha_eFe^{+}	+	Ha_gFe^{+}	+	H_3AsO_3	=	$Ha\_eFeH_3AsO_3Ha\_gFe^{+2}$	Log_k_1
Ha_eFe^{+}	+	Ha_hFe^{+}	+	H_3AsO_3	=	$Ha\_eFeH_3AsO_3Ha\_hFe^{+2}$	Log_k_1
Ha_fFe^{+}	+	Ha_gFe^{+}	+	H_3AsO_3	=	$Ha\_fFeH_3AsO_3Ha\_gFe^{+2}$	Log_k_1
Ha_fFe^{+}	+	Ha_hFe^{+}	+	H_3AsO_3	=	$Ha\_fFeH_3AsO_3Ha\_hFe^{+2}$	Log_k_1
Ha_gFe^{+}	+	Ha_hFe^{+}	+	H_3AsO_3	=	$Ha\_gFeH_3AsO_3Ha\_hFe^{+2}$	Log_k_1

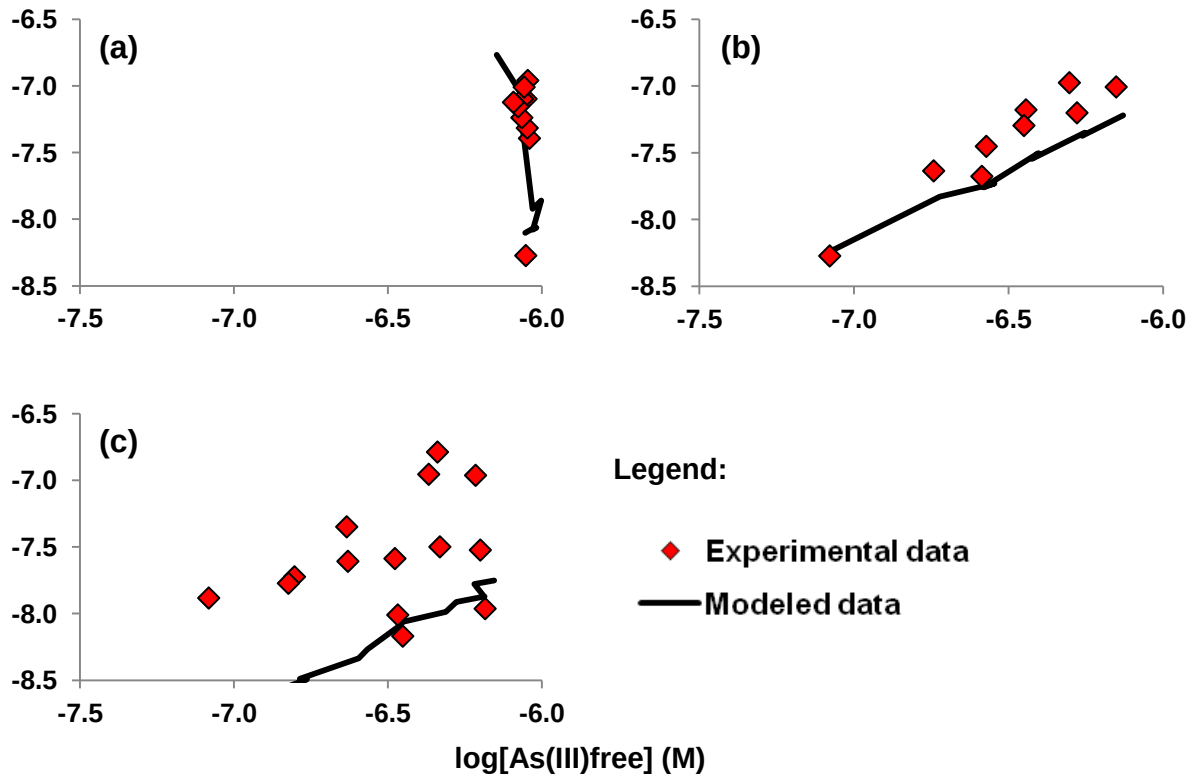

ANNEXE III 4: Formation of As(III) binuclear monodentate to Fe(II) monodentate with OM (a) isotherm with increasing Fe(II) concentrations at pH 6, (b) isotherm with increasing As(III) concentrations at pH 6, (c) isotherm with increasing Fe(II) concentrations at pH 5.

ANNEXE III 5: Chemical equations of Fe(II) bidentate and As (III) mononuclear bidentate complexes

Equations of Fe(II) bidentate and As (III) mononuclear bidentate complexes					Log k
Ha_abFe	+	H_3AsO_3	=	Ha_abFeH_3AsO_3	Log_k_3
Ha_cdFe	+	H_3AsO_3	=	Ha_cdFeH_3AsO_3	Log_k_3
Ha_aeFe	+	H_3AsO_3	=	Ha_aeFeH_3AsO_3	Log_k_3
Ha_bfFe	+	H_3AsO_3	=	Ha_bfFeH_3AsO_3	Log_k_3
Ha_cgFe	+	H_3AsO_3	=	Ha_cgFeH_3AsO_3	Log_k_3
Ha_dhFe	+	H_3AsO_3	=	Ha_dhFeH_3AsO_3	Log_k_3
Ha_efFe	+	H_3AsO_3	=	Ha_efFeH_3AsO_3	Log_k_3
Ha_ghFe	+	H_3AsO_3	=	Ha_ghFeH_3AsO_3	Log_k_3
Ha_abxFe	+	H_3AsO_3	=	Ha_abxFeH_3AsO_3	Log_k_3
Ha_cdxFe	+	H_3AsO_3	=	Ha_cdxFeH_3AsO_3	Log_k_3
Ha_aexFe	+	H_3AsO_3	=	Ha_aexFeH_3AsO_3	Log_k_3
Ha_bfxFe	+	H_3AsO_3	=	Ha_bfxFeH_3AsO_3	Log_k_3
Ha_cgxFe	+	H_3AsO_3	=	Ha_cgxFeH_3AsO_3	Log_k_3
Ha_dhxFe	+	H_3AsO_3	=	Ha_dhxFeH_3AsO_3	Log_k_3

Equations of Fe(II) bidentate and As (III) mononuclear bidentate complexes					Log k
Ha_efxFe	+	H_3AsO_3	=	Ha_efxFeH_3AsO_3	Log_k_3
Ha_ghxFe	+	H_3AsO_3	=	Ha_ghxFeH_3AsO_3	Log_k_3
Ha_abxxFe	+	H_3AsO_3	=	Ha_abxxFeH_3AsO_3	Log_k_3
Ha_cdxxFe	+	H_3AsO_3	=	Ha_cdxxFeH_3AsO_3	Log_k_3
Ha_aexxFe	+	H_3AsO_3	=	Ha_aexxFeH_3AsO_3	Log_k_3
Ha_bfxxFe	+	H_3AsO_3	=	Ha_bfxxFeH_3AsO_3	Log_k_3
Ha_cgxxFe	+	H_3AsO_3	=	Ha_cgxxFeH_3AsO_3	Log_k_3
Ha_dhxxFe	+	H_3AsO_3	=	Ha_dhxxFeH_3AsO_3	Log_k_3
Ha_efxxFe	+	H_3AsO_3	=	Ha_efxxFeH_3AsO_3	Log_k_3
Ha_ghxxFe	+	H_3AsO_3	=	Ha_ghxxFeH_3AsO_3	Log_k_3

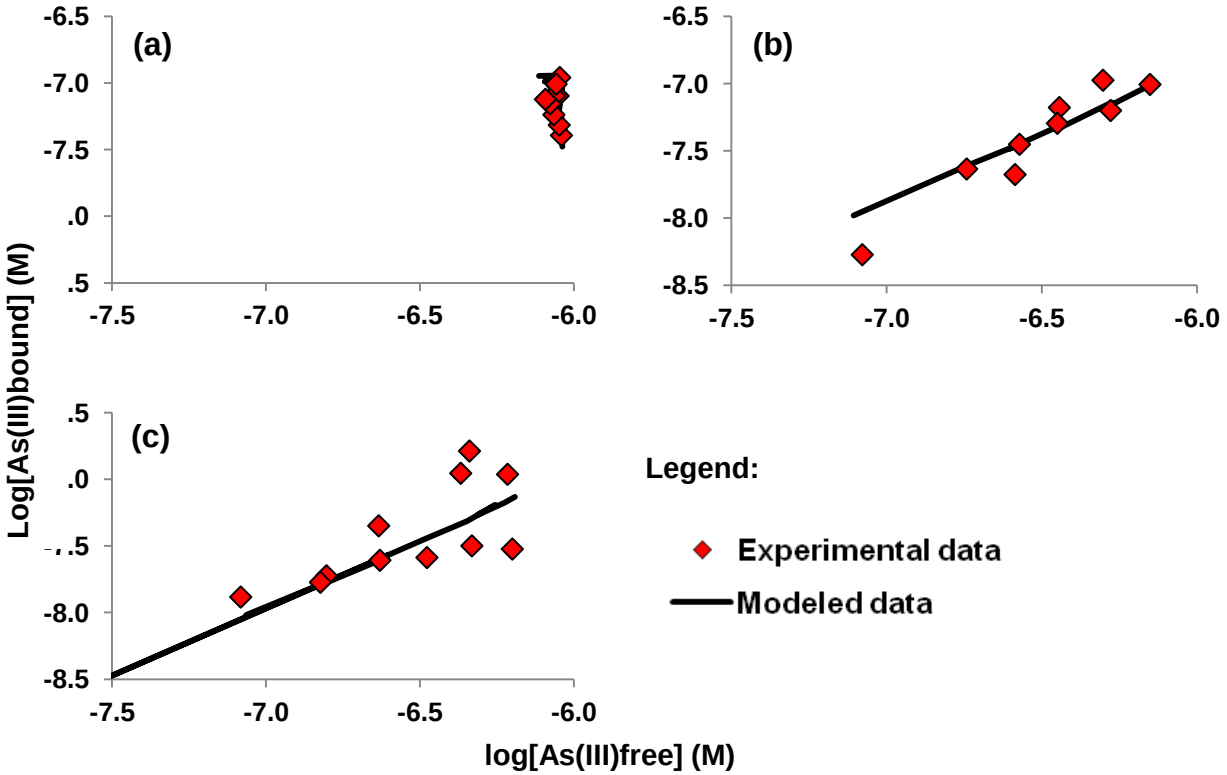

ANNEXE III 6: Formation of As(III) mononuclear bidentate to Fe(II) bidentate with OM (a) isotherm with increasing Fe(II) concentrations at pH 6, (b) isotherm with increasing As(III) concentrations at pH 6, (c) isotherm with increasing Fe(II) concentrations at pH 5.

ANNEXE III 7: Chemical Equations of Fe(II) bidentate and As(III) binuclear monodentate complexes

Equations of Fe(II) bidentate and As(III) binuclear monodentate complexes							Log k
Ha_abFe	+	Ha_cdFe	+	H_3AsO_3	=	Ha_abFeH_3AsO_3Ha_cdFe	Log_k_4
Ha_abFe	+	Ha_aeFe	+	H_3AsO_3	=	Ha_abFeH_3AsO_3Ha_aeFe	Log_k_4
Ha_abFe	+	Ha_bfFe	+	H_3AsO_3	=	Ha_abFeH_3AsO_3Ha_bfFe	Log_k_4
Ha_abFe	+	Ha_cgFe	+	H_3AsO_3	=	Ha_abFeH_3AsO_3Ha_cgFe	Log_k_4
Ha_abFe	+	Ha_dhFe	+	H_3AsO_3	=	Ha_abFeH_3AsO_3Ha_dhFe	Log_k_4
Ha_abFe	+	Ha_efFe	+	H_3AsO_3	=	Ha_abFeH_3AsO_3Ha_efFe	Log_k_4
Ha_abFe	+	Ha_ghFe	+	H_3AsO_3	=	Ha_abFeH_3AsO_3Ha_ghFe	Log_k_4
Ha_abFe	+	Ha_cdxFe	+	H_3AsO_3	=	Ha_abFeH_3AsO_3Ha_cdxFe	Log_k_4
Ha_abFe	+	Ha_aexFe	+	H_3AsO_3	=	Ha_abFeH_3AsO_3Ha_aexFe	Log_k_4
Ha_abFe	+	Ha_bfxFe	+	H_3AsO_3	=	Ha_abFeH_3AsO_3Ha_bfxFe	Log_k_4
Ha_abFe	+	Ha_cgxFe	+	H_3AsO_3	=	Ha_abFeH_3AsO_3Ha_cgxFe	Log_k_4
Ha_abFe	+	Ha_dhxFe	+	H_3AsO_3	=	Ha_abFeH_3AsO_3Ha_dhxFe	Log_k_4
Ha_abFe	+	Ha_efxFe	+	H_3AsO_3	=	Ha_abFeH_3AsO_3Ha_efxFe	Log_k_4
Ha_abFe	+	Ha_ghxFe	+	H_3AsO_3	=	Ha_abFeH_3AsO_3Ha_ghxFe	Log_k_4
Ha_abFe	+	Ha_cdxxFe	+	H_3AsO_3	=	Ha_abFeH_3AsO_3Ha_cdxxFe	Log_k_4
Ha_abFe	+	Ha_aexxFe	+	H_3AsO_3	=	Ha_abFeH_3AsO_3Ha_aexxFe	Log_k_4
Ha_abFe	+	Ha_bfxxFe	+	H_3AsO_3	=	Ha_abFeH_3AsO_3Ha_bfxxFe	Log_k_4
Ha_abFe	+	Ha_cgxxFe	+	H_3AsO_3	=	Ha_abFeH_3AsO_3Ha_cgxxFe	Log_k_4
Ha_abFe	+	Ha_dhxxFe	+	H_3AsO_3	=	Ha_abFeH_3AsO_3Ha_dhxxFe	Log_k_4
Ha_abFe	+	Ha_efxxFe	+	H_3AsO_3	=	Ha_abFeH_3AsO_3Ha_efxxFe	Log_k_4
Ha_abFe	+	Ha_ghxxFe	+	H_3AsO_3	=	Ha_abFeH_3AsO_3Ha_ghxxFe	Log_k_4
Ha_cdFe	+	Ha_aeFe	+	H_3AsO_3	=	Ha_cdFeH_3AsO_3Ha_aeFe	Log_k_4
Ha_cdFe	+	Ha_bfFe	+	H_3AsO_3	=	Ha_cdFeH_3AsO_3Ha_bfFe	Log_k_4
Ha_cdFe	+	Ha_cgFe	+	H_3AsO_3	=	Ha_cdFeH_3AsO_3Ha_cgFe	Log_k_4
Ha_cdFe	+	Ha_dhFe	+	H_3AsO_3	=	Ha_cdFeH_3AsO_3Ha_dhFe	Log_k_4
Ha_cdFe	+	Ha_efFe	+	H_3AsO_3	=	Ha_cdFeH_3AsO_3Ha_efFe	Log_k_4
Ha_cdFe	+	Ha_ghFe	+	H_3AsO_3	=	Ha_cdFeH_3AsO_3Ha_ghFe	Log_k_4
Ha_cdFe	+	Ha_aexFe	+	H_3AsO_3	=	Ha_cdFeH_3AsO_3Ha_aexFe	Log_k_4
Ha_cdFe	+	Ha_bfxFe	+	H_3AsO_3	=	Ha_cdFeH_3AsO_3Ha_bfxFe	Log_k_4
Ha_cdFe	+	Ha_cgxFe	+	H_3AsO_3	=	Ha_cdFeH_3AsO_3Ha_cgxFe	Log_k_4
Ha_cdFe	+	Ha_dhxFe	+	H_3AsO_3	=	Ha_cdFeH_3AsO_3Ha_dhxFe	Log_k_4
Ha_cdFe	+	Ha_efxFe	+	H_3AsO_3	=	Ha_cdFeH_3AsO_3Ha_efxFe	Log_k_4
Ha_cdFe	+	Ha_ghxFe	+	H_3AsO_3	=	Ha_cdFeH_3AsO_3Ha_ghxFe	Log_k_4
Ha_cdFe	+	Ha_aexxFe	+	H_3AsO_3	=	Ha_cdFeH_3AsO_3Ha_aexxFe	Log_k_4
Ha_cdFe	+	Ha_bfxxFe	+	H_3AsO_3	=	Ha_cdFeH_3AsO_3Ha_bfxxFe	Log_k_4

Equations of Fe(II) bidentate and As(III) binuclear monodentate complexes							Log k
Ha_cdFe	+	Ha_cgxxFe	+	H_3AsO_3	=	Ha_cdFeH_3AsO_3Ha_cgxxFe	Log_k_4
Ha_cdFe	+	Ha_dhxxFe	+	H_3AsO_3	=	Ha_cdFeH_3AsO_3Ha_dhxxFe	Log_k_4
Ha_cdFe	+	Ha_efxxFe	+	H_3AsO_3	=	Ha_cdFeH_3AsO_3Ha_efxxFe	Log_k_4
Ha_cdFe	+	Ha_ghxxFe	+	H_3AsO_3	=	Ha_cdFeH_3AsO_3Ha_ghxxFe	Log_k_4
Ha_aeFe	+	Ha_bfFe	+	H_3AsO_3	=	Ha_aeFeH_3AsO_3Ha_bfFe	Log_k_4
Ha_aeFe	+	Ha_cgFe	+	H_3AsO_3	=	Ha_aeFeH_3AsO_3Ha_cgFe	Log_k_4
Ha_aeFe	+	Ha_dhFe	+	H_3AsO_3	=	Ha_aeFeH_3AsO_3Ha_dhFe	Log_k_4
Ha_aeFe	+	Ha_efFe	+	H_3AsO_3	=	Ha_aeFeH_3AsO_3Ha_efFe	Log_k_4
Ha_aeFe	+	Ha_ghFe	+	H_3AsO_3	=	Ha_aeFeH_3AsO_3Ha_ghFe	Log_k_4
Ha_aeFe	+	Ha_bfxFe	+	H_3AsO_3	=	Ha_aeFeH_3AsO_3Ha_bfxFe	Log_k_4
Ha_aeFe	+	Ha_cgxFe	+	H_3AsO_3	=	Ha_aeFeH_3AsO_3Ha_cgxFe	Log_k_4
Ha_aeFe	+	Ha_dhxFe	+	H_3AsO_3	=	Ha_aeFeH_3AsO_3Ha_dhxFe	Log_k_4
Ha_aeFe	+	Ha_efxFe	+	H_3AsO_3	=	Ha_aeFeH_3AsO_3Ha_efxFe	Log_k_4
Ha_aeFe	+	Ha_ghxFe	+	H_3AsO_3	=	Ha_aeFeH_3AsO_3Ha_ghxFe	Log_k_4
Ha_aeFe	+	Ha_bfxxFe	+	H_3AsO_3	=	Ha_aeFeH_3AsO_3Ha_bfxxFe	Log_k_4
Ha_aeFe	+	Ha_cgxxFe	+	H_3AsO_3	=	Ha_aeFeH_3AsO_3Ha_cgxxFe	Log_k_4
Ha_aeFe	+	Ha_dhxxFe	+	H_3AsO_3	=	Ha_aeFeH_3AsO_3Ha_dhxxFe	Log_k_4
Ha_aeFe	+	Ha_efxxFe	+	H_3AsO_3	=	Ha_aeFeH_3AsO_3Ha_efxxFe	Log_k_4
Ha_aeFe	+	Ha_ghxxFe	+	H_3AsO_3	=	Ha_aeFeH_3AsO_3Ha_ghxxFe	Log_k_4
Ha_bfFe	+	Ha_cgFe	+	H_3AsO_3	=	Ha_bfFeH_3AsO_3Ha_cgFe	Log_k_4
Ha_bfFe	+	Ha_dhFe	+	H_3AsO_3	=	Ha_bfFeH_3AsO_3Ha_dhFe	Log_k_4
Ha_bfFe	+	Ha_efFe	+	H_3AsO_3	=	Ha_bfFeH_3AsO_3Ha_efFe	Log_k_4
Ha_bfFe	+	Ha_ghFe	+	H_3AsO_3	=	Ha_bfFeH_3AsO_3Ha_ghFe	Log_k_4
Ha_bfFe	+	Ha_cgxFe	+	H_3AsO_3	=	Ha_bfFeH_3AsO_3Ha_cgxFe	Log_k_4
Ha_bfFe	+	Ha_dhxFe	+	H_3AsO_3	=	Ha_bfFeH_3AsO_3Ha_dhxFe	Log_k_4
Ha_bfFe	+	Ha_efxFe	+	H_3AsO_3	=	Ha_bfFeH_3AsO_3Ha_efxFe	Log_k_4
Ha_bfFe	+	Ha_ghxFe	+	H_3AsO_3	=	Ha_bfFeH_3AsO_3Ha_ghxFe	Log_k_4
Ha_bfFe	+	Ha_cgxxFe	+	H_3AsO_3	=	Ha_bfFeH_3AsO_3Ha_cgxxFe	Log_k_4
Ha_bfFe	+	Ha_dhxxFe	+	H_3AsO_3	=	Ha_bfFeH_3AsO_3Ha_dhxxFe	Log_k_4
Ha_bfFe	+	Ha_efxxFe	+	H_3AsO_3	=	Ha_bfFeH_3AsO_3Ha_efxxFe	Log_k_4
Ha_bfFe	+	Ha_ghxxFe	+	H_3AsO_3	=	Ha_bfFeH_3AsO_3Ha_ghxxFe	Log_k_4
Ha_cgFe	+	Ha_dhFe	+	H_3AsO_3	=	Ha_cgFeH_3AsO_3Ha_dhFe	Log_k_4
Ha_cgFe	+	Ha_efFe	+	H_3AsO_3	=	Ha_cgFeH_3AsO_3Ha_efFe	Log_k_4
Ha_cgFe	+	Ha_ghFe	+	H_3AsO_3	=	Ha_cgFeH_3AsO_3Ha_ghFe	Log_k_4
Ha_cgFe	+	Ha_dhxFe	+	H_3AsO_3	=	Ha_cgFeH_3AsO_3Ha_dhxFe	Log_k_4
Ha_cgFe	+	Ha_efxFe	+	H_3AsO_3	=	Ha_cgFeH_3AsO_3Ha_efxFe	Log_k_4
Ha_cgFe	+	Ha_ghxFe	+	H_3AsO_3	=	Ha_cgFeH_3AsO_3Ha_ghxFe	Log_k_4

Equations of Fe(II) bidentate and As(III) binuclear monodentate complexes							Log k
Ha_cgFe	+	Ha_dhxxFe	+	H_3AsO_3	=	Ha_cgFeH_3AsO_3Ha_dhxxFe	Log_k_4
Ha_cgFe	+	Ha_efxxFe	+	H_3AsO_3	=	Ha_cgFeH_3AsO_3Ha_efxxFe	Log_k_4
Ha_cgFe	+	Ha_ghxxFe	+	H_3AsO_3	=	Ha_cgFeH_3AsO_3Ha_ghxxFe	Log_k_4
Ha_dhFe	+	Ha_efFe	+	H_3AsO_3	=	Ha_dhFeH_3AsO_3Ha_efFe	Log_k_4
Ha_dhFe	+	Ha_ghFe	+	H_3AsO_3	=	Ha_dhFeH_3AsO_3Ha_ghFe	Log_k_4
Ha_dhFe	+	Ha_efxFe	+	H_3AsO_3	=	Ha_dhFeH_3AsO_3Ha_efxFe	Log_k_4
Ha_dhFe	+	Ha_ghxFe	+	H_3AsO_3	=	Ha_dhFeH_3AsO_3Ha_ghxFe	Log_k_4
Ha_dhFe	+	Ha_efxxFe	+	H_3AsO_3	=	Ha_dhFeH_3AsO_3Ha_efxxFe	Log_k_4
Ha_dhFe	+	Ha_ghxxFe	+	H_3AsO_3	=	Ha_dhFeH_3AsO_3Ha_ghxxFe	Log_k_4
Ha_efFe	+	Ha_ghFe	+	H_3AsO_3	=	Ha_efFeH_3AsO_3Ha_ghFe	Log_k_4
Ha_efFe	+	Ha_ghxFe	+	H_3AsO_3	=	Ha_efFeH_3AsO_3Ha_ghxFe	Log_k_4
Ha_efFe	+	Ha_ghxxFe	+	H_3AsO_3	=	Ha_efFeH_3AsO_3Ha_ghxxFe	Log_k_4
Ha_abxFe	+	Ha_cdFe	+	H_3AsO_3	=	Ha_abxFeH_3AsO_3Ha_cdFe	Log_k_4
Ha_abxFe	+	Ha_aeFe	+	H_3AsO_3	=	Ha_abxFeH_3AsO_3Ha_aeFe	Log_k_4
Ha_abxFe	+	Ha_bfFe	+	H_3AsO_3	=	Ha_abxFeH_3AsO_3Ha_bfFe	Log_k_4
Ha_abxFe	+	Ha_cgFe	+	H_3AsO_3	=	Ha_abxFeH_3AsO_3Ha_cgFe	Log_k_4
Ha_abxFe	+	Ha_dhFe	+	H_3AsO_3	=	Ha_abxFeH_3AsO_3Ha_dhFe	Log_k_4
Ha_abxFe	+	Ha_efFe	+	H_3AsO_3	=	Ha_abxFeH_3AsO_3Ha_efFe	Log_k_4
Ha_abxFe	+	Ha_ghFe	+	H_3AsO_3	=	Ha_abxFeH_3AsO_3Ha_ghFe	Log_k_4
Ha_abxFe	+	Ha_cdxFe	+	H_3AsO_3	=	Ha_abxFeH_3AsO_3Ha_cdxFe	Log_k_4
Ha_abxFe	+	Ha_aexFe	+	H_3AsO_3	=	Ha_abxFeH_3AsO_3Ha_aexFe	Log_k_4
Ha_abxFe	+	Ha_bfxFe	+	H_3AsO_3	=	Ha_abxFeH_3AsO_3Ha_bfxFe	Log_k_4
Ha_abxFe	+	Ha_cgxFe	+	H_3AsO_3	=	Ha_abxFeH_3AsO_3Ha_cgxFe	Log_k_4
Ha_abxFe	+	Ha_dhxFe	+	H_3AsO_3	=	Ha_abxFeH_3AsO_3Ha_dhxFe	Log_k_4
Ha_abxFe	+	Ha_efxFe	+	H_3AsO_3	=	Ha_abxFeH_3AsO_3Ha_efxFe	Log_k_4
Ha_abxFe	+	Ha_ghxFe	+	H_3AsO_3	=	Ha_abxFeH_3AsO_3Ha_ghxFe	Log_k_4
Ha_abxFe	+	Ha_cdxxFe	+	H_3AsO_3	=	Ha_abxFeH_3AsO_3Ha_cdxxFe	Log_k_4
Ha_abxFe	+	Ha_aexxFe	+	H_3AsO_3	=	Ha_abxFeH_3AsO_3Ha_aexxFe	Log_k_4
Ha_abxFe	+	Ha_bfxxFe	+	H_3AsO_3	=	Ha_abxFeH_3AsO_3Ha_bfxxFe	Log_k_4
Ha_abxFe	+	Ha_cgxxFe	+	H_3AsO_3	=	Ha_abxFeH_3AsO_3Ha_cgxxFe	Log_k_4
Ha_abxFe	+	Ha_dhxxFe	+	H_3AsO_3	=	Ha_abxFeH_3AsO_3Ha_dhxxFe	Log_k_4
Ha_abxFe	+	Ha_efxxFe	+	H_3AsO_3	=	Ha_abxFeH_3AsO_3Ha_efxxFe	Log_k_4
Ha_abxFe	+	Ha_ghxxFe	+	H_3AsO_3	=	Ha_abxFeH_3AsO_3Ha_ghxxFe	Log_k_4
Ha_cdxFe	+	Ha_aeFe	+	H_3AsO_3	=	Ha_cdxFe H_3AsO_3Ha_aeFe	Log_k_4
Ha_cdxFe	+	Ha_bfFe	+	H_3AsO_3	=	Ha_cdxFeH_3AsO_3Ha_bfFe	Log_k_4
Ha_cdxFe	+	Ha_cgFe	+	H_3AsO_3	=	Ha_cdxFeH_3AsO_3Ha_cgFe	Log_k_4
Ha_cdxFe	+	Ha_dhFe	+	H_3AsO_3	=	Ha_cdxFeH_3AsO_3Ha_dhFe	Log_k_4

Equations of Fe(II) bidentate and As(III) binuclear monodentate complexes							Log k
Ha_cdxFe	+	Ha_efFe	+	H_3AsO_3	=	Ha_cdxFeH_3AsO_3Ha_efFe	Log_k_4
Ha_cdxFe	+	Ha_ghFe	+	H_3AsO_3	=	Ha_cdxFeH_3AsO_3Ha_ghFe	Log_k_4
Ha_cdxFe	+	Ha_aexFe	+	H_3AsO_3	=	Ha_cdxFeH_3AsO_3Ha_aexFe	Log_k_4
Ha_cdxFe	+	Ha_bfxFe	+	H_3AsO_3	=	Ha_cdxFeH_3AsO_3Ha_bfxFe	Log_k_4
Ha_cdxFe	+	Ha_cgxFe	+	H_3AsO_3	=	Ha_cdxFeH_3AsO_3Ha_cgxFe	Log_k_4
Ha_cdxFe	+	Ha_dhxFe	+	H_3AsO_3	=	Ha_cdxFeH_3AsO_3Ha_dhxFe	Log_k_4
Ha_cdxFe	+	Ha_efxFe	+	H_3AsO_3	=	Ha_cdxFeH_3AsO_3Ha_efxFe	Log_k_4
Ha_cdxFe	+	Ha_ghxFe	+	H_3AsO_3	=	Ha_cdxFeH_3AsO_3Ha_ghxFe	Log_k_4
Ha_cdxFe	+	Ha_aexxFe	+	H_3AsO_3	=	Ha_cdxFeH_3AsO_3Ha_aexxFe	Log_k_4
Ha_cdxFe	+	Ha_bfxxFe	+	H_3AsO_3	=	Ha_cdxFeH_3AsO_3Ha_bfxxFe	Log_k_4
Ha_cdxFe	+	Ha_cgxxFe	+	H_3AsO_3	=	Ha_cdxFeH_3AsO_3Ha_cgxxFe	Log_k_4
Ha_cdxFe	+	Ha_dhxxFe	+	H_3AsO_3	=	Ha_cdxFeH_3AsO_3Ha_dhxxFe	Log_k_4
Ha_cdxFe	+	Ha_efxxFe	+	H_3AsO_3	=	Ha_cdxFeH_3AsO_3Ha_efxxFe	Log_k_4
Ha_cdxFe	+	Ha_ghxxFe	+	H_3AsO_3	=	Ha_cdxFeH_3AsO_3Ha_ghxxFe	Log_k_4
Ha_aexFe	+	Ha_bfFe	+	H_3AsO_3	=	Ha_aexFeH_3AsO_3Ha_bfFe	Log_k_4
Ha_aexFe	+	Ha_cgFe	+	H_3AsO_3	=	Ha_aexFeH_3AsO_3Ha_cgFe	Log_k_4
Ha_aexFe	+	Ha_dhFe	+	H_3AsO_3	=	Ha_aexFeH_3AsO_3Ha_dhFe	Log_k_4
Ha_aexFe	+	Ha_efFe	+	H_3AsO_3	=	Ha_aexFeH_3AsO_3Ha_efFe	Log_k_4
Ha_aexFe	+	Ha_ghFe	+	H_3AsO_3	=	Ha_aexFeH_3AsO_3Ha_ghFe	Log_k_4
Ha_aexFe	+	Ha_bfxFe	+	H_3AsO_3	=	Ha_aexFeH_3AsO_3Ha_bfxFe	Log_k_4
Ha_aexFe	+	Ha_cgxFe	+	H_3AsO_3	=	Ha_aexFeH_3AsO_3Ha_cgxFe	Log_k_4
Ha_aexFe	+	Ha_dhxFe	+	H_3AsO_3	=	Ha_aexFeH_3AsO_3Ha_dhxFe	Log_k_4
Ha_aexFe	+	Ha_efxFe	+	H_3AsO_3	=	Ha_aexFeH_3AsO_3Ha_efxFe	Log_k_4
Ha_aexFe	+	Ha_ghxFe	+	H_3AsO_3	=	Ha_aexFeH_3AsO_3Ha_ghxFe	Log_k_4
Ha_aexFe	+	Ha_bfxxFe	+	H_3AsO_3	=	Ha_aexFeH_3AsO_3Ha_bfxxFe	Log_k_4
Ha_aexFe	+	Ha_cgxxFe	+	H_3AsO_3	=	Ha_aexFeH_3AsO_3Ha_cgxxFe	Log_k_4
Ha_aexFe	+	Ha_dhxxFe	+	H_3AsO_3	=	Ha_aexFeH_3AsO_3Ha_dhxxFe	Log_k_4
Ha_aexFe	+	Ha_efxxFe	+	H_3AsO_3	=	Ha_aexFeH_3AsO_3Ha_efxxFe	Log_k_4
Ha_aexFe	+	Ha_ghxxFe	+	H_3AsO_3	=	Ha_aexFeH_3AsO_3Ha_ghxxFe	Log_k_4
Ha_bfxFe	+	Ha_cgFe	+	H_3AsO_3	=	Ha_bfxFeH_3AsO_3Ha_cgFe	Log_k_4
Ha_bfxFe	+	Ha_dhFe	+	H_3AsO_3	=	Ha_bfxFeH_3AsO_3Ha_dhFe	Log_k_4
Ha_bfxFe	+	Ha_efFe	+	H_3AsO_3	=	Ha_bfxFeH_3AsO_3Ha_efFe	Log_k_4
Ha_bfxFe	+	Ha_ghFe	+	H_3AsO_3	=	Ha_bfxFeH_3AsO_3Ha_ghFe	Log_k_4
Ha_bfxFe	+	Ha_cgxFe	+	H_3AsO_3	=	Ha_bfxFeH_3AsO_3Ha_cgxFe	Log_k_4
Ha_bfxFe	+	Ha_dhxFe	+	H_3AsO_3	=	Ha_bfxFeH_3AsO_3Ha_dhxFe	Log_k_4
Ha_bfxFe	+	Ha_efxFe	+	H_3AsO_3	=	Ha_bfxFeH_3AsO_3Ha_efxFe	Log_k_4
Ha_bfxFe	+	Ha_ghxFe	+	H_3AsO_3	=	Ha_bfxFeH_3AsO_3Ha_ghxFe	Log_k_4

Equations of Fe(II) bidentate and As(III) binuclear monodentate complexes							Log k
Ha_bfxFe	+	Ha_cgxxFe	+	H_3AsO_3	=	Ha_bfxFeH_3AsO_3Ha_cgxxFe	Log_k_4
Ha_bfxFe	+	Ha_dhxxFe	+	H_3AsO_3	=	Ha_bfxFeH_3AsO_3Ha_dhxxFe	Log_k_4
Ha_bfxFe	+	Ha_efxxFe	+	H_3AsO_3	=	Ha_bfxFeH_3AsO_3Ha_efxxFe	Log_k_4
Ha_bfxFe	+	Ha_ghxxFe	+	H_3AsO_3	=	Ha_bfxFeH_3AsO_3Ha_ghxxFe	Log_k_4
Ha_cgxFe	+	Ha_dhFe	+	H_3AsO_3	=	Ha_cgxFeH_3AsO_3Ha_dhFe	Log_k_4
Ha_cgxFe	+	Ha_efFe	+	H_3AsO_3	=	Ha_cgxFeH_3AsO_3Ha_efFe	Log_k_4
Ha_cgxFe	+	Ha_ghFe	+	H_3AsO_3	=	Ha_cgxFeH_3AsO_3Ha_ghFe	Log_k_4
Ha_cgxFe	+	Ha_dhxFe	+	H_3AsO_3	=	Ha_cgxFeH_3AsO_3Ha_dhxFe	Log_k_4
Ha_cgxFe	+	Ha_efxFe	+	H_3AsO_3	=	Ha_cgxFeH_3AsO_3Ha_efxFe	Log_k_4
Ha_cgxFe	+	Ha_ghxFe	+	H_3AsO_3	=	Ha_cgxFeH_3AsO_3Ha_ghxFe	Log_k_4
Ha_cgxFe	+	Ha_dhxxFe	+	H_3AsO_3	=	Ha_cgxFeH_3AsO_3Ha_dhxxFe	Log_k_4
Ha_cgxFe	+	Ha_efxxFe	+	H_3AsO_3	=	Ha_cgxFeH_3AsO_3Ha_efxxFe	Log_k_4
Ha_cgxFe	+	Ha_ghxxFe	+	H_3AsO_3	=	Ha_cgxFeH_3AsO_3Ha_ghxxFe	Log_k_4
Ha_dhxFe	+	Ha_efFe	+	H_3AsO_3	=	Ha_dhxFeH_3AsO_3Ha_efFe	Log_k_4
Ha_dhxFe	+	Ha_ghFe	+	H_3AsO_3	=	Ha_dhxFeH_3AsO_3Ha_ghFe	Log_k_4
Ha_dhxFe	+	Ha_efxFe	+	H_3AsO_3	=	Ha_dhxFeH_3AsO_3Ha_efxFe	Log_k_4
Ha_dhxFe	+	Ha_ghxFe	+	H_3AsO_3	=	Ha_dhxFeH_3AsO_3Ha_ghxFe	Log_k_4
Ha_dhxFe	+	Ha_efxxFe	+	H_3AsO_3	=	Ha_dhxFeH_3AsO_3Ha_efxxFe	Log_k_4
Ha_dhxFe	+	Ha_ghxxFe	+	H_3AsO_3	=	Ha_dhxFeH_3AsO_3Ha_ghxxFe	Log_k_4
Ha_efxFe	+	Ha_ghFe	+	H_3AsO_3	=	Ha_efxFeH_3AsO_3Ha_ghFe	Log_k_4
Ha_efxFe	+	Ha_ghxFe	+	H_3AsO_3	=	Ha_efxFeH_3AsO_3Ha_ghxFe	Log_k_4
Ha_efxFe	+	Ha_ghxxFe	+	H_3AsO_3	=	Ha_efxFeH_3AsO_3Ha_ghxxFe	Log_k_4
Ha_abxxFe	+	Ha_cdFe	+	H_3AsO_3	=	Ha_abxxFeH_3AsO_3Ha_cdFe	Log_k_4
Ha_abxxFe	+	Ha_aeFe	+	H_3AsO_3	=	Ha_abxxFeH_3AsO_3Ha_aeFe	Log_k_4
Ha_abxxFe	+	Ha_bfFe	+	H_3AsO_3	=	Ha_abxxFeH_3AsO_3Ha_bfFe	Log_k_4
Ha_abxxFe	+	Ha_cgFe	+	H_3AsO_3	=	Ha_abxxFeH_3AsO_3Ha_cgFe	Log_k_4
Ha_abxxFe	+	Ha_dhFe	+	H_3AsO_3	=	Ha_abxxFeH_3AsO_3Ha_dhFe	Log_k_4
Ha_abxxFe	+	Ha_efFe	+	H_3AsO_3	=	Ha_abxxFeH_3AsO_3Ha_efFe	Log_k_4
Ha_abxxFe	+	Ha_ghFe	+	H_3AsO_3	=	Ha_abxxFeH_3AsO_3Ha_ghFe	Log_k_4
Ha_abxxFe	+	Ha_cdxFe	+	H_3AsO_3	=	Ha_abxxFeH_3AsO_3Ha_cdxFe	Log_k_4
Ha_abxxFe	+	Ha_aexFe	+	H_3AsO_3	=	Ha_abxxFeH_3AsO_3Ha_aexFe	Log_k_4
Ha_abxxFe	+	Ha_bfxFe	+	H_3AsO_3	=	Ha_abxxFeH_3AsO_3Ha_bfxFe	Log_k_4
Ha_abxxFe	+	Ha_cgxFe	+	H_3AsO_3	=	Ha_abxxFeH_3AsO_3Ha_cgxFe	Log_k_4
Ha_abxxFe	+	Ha_dhxFe	+	H_3AsO_3	=	Ha_abxxFe$_3AsO_3$Ha_dhxFe	Log_k_4
Ha_abxxFe	+	Ha_efxFe	+	H_3AsO_3	=	Ha_abxxFeH_3AsO_3Ha_efxFe	Log_k_4
Ha_abxxFe	+	Ha_ghxFe	+	H_3AsO_3	=	Ha_abxxFeH_3AsO_3Ha_ghxFe	Log_k_4
Ha_abxxFe	+	Ha_cdxxFe	+	H_3AsO_3	=	Ha_abxxFeH_3AsO_3Ha_cdxxFe	Log_k_4

Equations of Fe(II) bidentate and As(III) binuclear monodentate complexes							Log k
Ha_abxxFe	+	Ha_aexxFe	+	H_3AsO_3	=	Ha_abxxFeH_3AsO_3Ha_aexxFe	Log_k_4
Ha_abxxFe	+	Ha_bfxxFe	+	H_3AsO_3	=	Ha_abxxFeH_3AsO_3Ha_bfxxFe	Log_k_4
Ha_abxxFe	+	Ha_cgxxFe	+	H_3AsO_3	=	Ha_abxxFeH_3AsO_3Ha_cgxxFe	Log_k_4
Ha_abxxFe	+	Ha_dhxxFe	+	H_3AsO_3	=	Ha_abxxFeH_3AsO_3Ha_dhxxFe	Log_k_4
Ha_abxxFe	+	Ha_efxxFe	+	H_3AsO_3	=	Ha_abxxFeH_3AsO_3Ha_efxxFe	Log_k_4
Ha_abxxFe	+	Ha_ghxxFe	+	H_3AsO_3	=	Ha_abxxFeH_3AsO_3Ha_ghxxFe	Log_k_4
Ha_cdxxFe	+	Ha_aeFe	+	H_3AsO_3	=	Ha_cdxxFeH_3AsO_3Ha_aeFe	Log_k_4
Ha_cdxxFe	+	Ha_bfFe	+	H_3AsO_3	=	Ha_cdxxFeH_3AsO_3Ha_bfFe	Log_k_4
Ha_cdxxFe	+	Ha_cgFe	+	H_3AsO_3	=	Ha_cdxxFeH_3AsO_3Ha_cgFe	Log_k_4
Ha_cdxxFe	+	Ha_dhFe	+	H_3AsO_3	=	Ha_cdxxFeH_3AsO_3Ha_dhFe	Log_k_4
Ha_cdxxFe	+	Ha_efFe	+	H_3AsO_3	=	Ha_cdxxFeH_3AsO_3Ha_efFe	Log_k_4
Ha_cdxxFe	+	Ha_ghFe	+	H_3AsO_3	=	Ha_cdxxFeH_3AsO_3Ha_ghFe	Log_k_4
Ha_cdxxFe	+	Ha_aexFe	+	H_3AsO_3	=	Ha_cdxxFeH_3AsO_3Ha_aexFe	Log_k_4
Ha_cdxxFe	+	Ha_bfxFe	+	H_3AsO_3	=	Ha_cdxxFeH_3AsO_3Ha_bfxFe	Log_k_4
Ha_cdxxFe	+	Ha_cgxFe	+	H_3AsO_3	=	Ha_cdxxFeH_3AsO_3Ha_cgxFe	Log_k_4
Ha_cdxxFe	+	Ha_dhxFe	+	H_3AsO_3	=	Ha_cdxxFeH_3AsO_3Ha_dhxFe	Log_k_4
Ha_cdxxFe	+	Ha_efxFe	+	H_3AsO_3	=	Ha_cdxxFeH_3AsO_3Ha_efxFe	Log_k_4
Ha_cdxxFe	+	Ha_ghxFe	+	H_3AsO_3	=	Ha_cdxxFeH_3AsO_3Ha_ghxFe	Log_k_4
Ha_cdxxFe	+	Ha_aexxFe	+	H_3AsO_3	=	Ha_cdxxFeH_3AsO_3Ha_aexxFe	Log_k_4
Ha_cdxxFe	+	Ha_bfxxFe	+	H_3AsO_3	=	Ha_cdxxFeH_3AsO_3Ha_bfxxFe	Log_k_4
Ha_cdxxFe	+	Ha_cgxxFe	+	H_3AsO_3	=	Ha_cdxxFeH_3AsO_3Ha_cgxxFe	Log_k_4
Ha_cdxxFe	+	Ha_dhxxFe	+	H_3AsO_3	=	Ha_cdxxFeH_3AsO_3Ha_dhxxFe	Log_k_4
Ha_cdxxFe	+	Ha_efxxFe	+	H_3AsO_3	=	Ha_cdxxFeH_3AsO_3Ha_efxxFe	Log_k_4
Ha_cdxxFe	+	Ha_ghxxFe	+	H_3AsO_3	=	Ha_cdxxFeH_3AsO_3Ha_ghxxFe	Log_k_4
Ha_aexxFe	+	Ha_bfFe	+	H_3AsO_3	=	Ha_aexxFeH_3AsO_3Ha_bfFe	Log_k_4
Ha_aexxFe	+	Ha_cgFe	+	H_3AsO_3	=	Ha_aexxFeH_3AsO_3Ha_cgFe	Log_k_4
Ha_aexxFe	+	Ha_dhFe	+	H_3AsO_3	=	Ha_aexxFeH_3AsO_3Ha_dhFe	Log_k_4
Ha_aexxFe	+	Ha_efFe	+	H_3AsO_3	=	Ha_aexxFeH_3AsO_3Ha_efFe	Log_k_4
Ha_aexxFe	+	Ha_ghFe	+	H_3AsO_3	=	Ha_aexxFeH_3AsO_3Ha_ghFe	Log_k_4
Ha_aexxFe	+	Ha_bfxFe	+	H_3AsO_3	=	Ha_aexxFeH_3AsO_3Ha_bfxFe	Log_k_4
Ha_aexxFe	+	Ha_cgxFe	+	H_3AsO_3	=	Ha_aexxFeH_3AsO_3Ha_cgxFe	Log_k_4
Ha_aexxFe	+	Ha_dhxFe	+	H_3AsO_3	=	Ha_aexxFeH_3AsO_3Ha_dhxFe	Log_k_4
Ha_aexxFe	+	Ha_efxFe	+	H_3AsO_3	=	Ha_aexxFeH_3AsO_3Ha_efxFe	Log_k_4
Ha_aexxFe	+	Ha_ghxFe	+	H_3AsO_3	=	Ha_aexxFeH_3AsO_3Ha_ghxFe	Log_k_4
Ha_aexxFe	+	Ha_bfxxFe	+	H_3AsO_3	=	Ha_aexxFeH_3AsO_3Ha_bfxxFe	Log_k_4
Ha_aexxFe	+	Ha_cgxxFe	+	H3AsO3	=	Ha_aexxFeH_3AsO_3Ha_cgxxFe	Log_k_4
Ha_aexxFe	+	Ha_dhxxFe	+	H_3AsO_3	=	Ha_aexxFeH_3AsO_3Ha_dhxxFe	Log_k_4

Equations of Fe(II) bidentate and As(III) binuclear monodentate complexes							Log k
Ha_aexxFe	+	Ha_efxxFe	+	H_3AsO_3	=	Ha_aexxFeH_3AsO_3Ha_efxxFe	Log_k_4
Ha_aexxFe	+	Ha_ghxxFe	+	H_3AsO_3	=	Ha_aexxFeH_3AsO_3Ha_ghxxFe	Log_k_4
Ha_bfxxFe	+	Ha_cgFe	+	H_3AsO_3	=	Ha_bfxxFeH_3AsO_3Ha_cgFe	Log_k_4
Ha_bfxxFe	+	Ha_dhFe	+	H_3AsO_3	=	Ha_bfxxFeH_3AsO_3Ha_dhFe	Log_k_4
Ha_bfxxFe	+	Ha_efFe	+	H_3AsO_3	=	Ha_bfxxFeH_3AsO_3Ha_efFe	Log_k_4
Ha_bfxxFe	+	Ha_ghFe	+	H_3AsO_3	=	Ha_bfxxFeH_3AsO_3Ha_ghFe	Log_k_4
Ha_bfxxFe	+	Ha_cgxFe	+	H_3AsO_3	=	Ha_bfxxFeH_3AsO_3Ha_cgxFe	Log_k_4
Ha_bfxxFe	+	Ha_dhxFe	+	H_3AsO_3	=	Ha_bfxxFeH_3AsO_3Ha_dhxFe	Log_k_4
Ha_bfxxFe	+	Ha_efxFe	+	H_3AsO_3	=	Ha_bfxxFeH_3AsO_3Ha_efxFe	Log_k_4
Ha_bfxxFe	+	Ha_ghxFe	+	H_3AsO_3	=	Ha_bfxxFeH_3AsO_3Ha_ghxFe	Log_k_4
Ha_bfxxFe	+	Ha_cgxxFe	+	H_3AsO_3	=	Ha_bfxxFeH_3AsO_3Ha_cgxxFe	Log_k_4
Ha_bfxxFe	+	Ha_dhxxFe	+	H_3AsO_3	=	Ha_bfxxFeH_3AsO_3Ha_dhxxFe	Log_k_4
Ha_bfxxFe	+	Ha_efxxFe	+	H_3AsO_3	=	Ha_bfxxFeH_3AsO_3Ha_efxxFe	Log_k_4
Ha_bfxxFe	+	Ha_ghxxFe	+	H_3AsO_3	=	Ha_bfxxFeH_3AsO_3Ha_ghxxFe	Log_k_4
Ha_cgxxFe	+	Ha_dhFe	+	H_3AsO_3	=	Ha_cgxxFeH_3AsO_3Ha_dhFe	Log_k_4
Ha_cgxxFe	+	Ha_efFe	+	H_3AsO_3	=	Ha_cgxxFeH_3AsO_3Ha_efFe	Log_k_4
Ha_cgxxFe	+	Ha_ghFe	+	H_3AsO_3	=	Ha_cgxxFeH_3AsO_3Ha_ghFe	Log_k_4
Ha_cgxxFe	+	Ha_dhxFe	+	H_3AsO_3	=	Ha_cgxxFeH_3AsO_3Ha_dhxFe	Log_k_4
Ha_cgxxFe	+	Ha_efxFe	+	H_3AsO_3	=	Ha_cgxxFeH_3AsO_3Ha_efxFe	Log_k_4
Ha_cgxxFe	+	Ha_ghxFe	+	H_3AsO_3	=	Ha_cgxxFeH_3AsO_3Ha_ghxFe	Log_k_4
Ha_cgxxFe	+	Ha_dhxxFe	+	H_3AsO_3	=	Ha_cgxxFeH_3AsO_3Ha_dhxxFe	Log_k_4
Ha_cgxxFe	+	Ha_efxxFe	+	H_3AsO_3	=	Ha_cgxxFeH_3AsO_3Ha_efxxFe	Log_k_4
Ha_cgxxFe	+	Ha_ghxxFe	+	H_3AsO_3	=	Ha_cgxxFeH_3AsO_3Ha_ghxxFe	Log_k_4
Ha_dhxxFe	+	Ha_efFe	+	H_3AsO_3	=	Ha_dhxxFeH_3AsO_3Ha_efFe	Log_k_4
Ha_dhxxFe	+	Ha_ghFe	+	H_3AsO_3	=	Ha_dhxxFeH_3AsO_3Ha_ghFe	Log_k_4
Ha_dhxxFe	+	Ha_efxFe	+	H_3AsO_3	=	Ha_dhxxFeH_3AsO_3Ha_efxFe	Log_k_4
Ha_dhxxFe	+	Ha_ghxFe	+	H_3AsO_3	=	Ha_dhxxFeH_3AsO_3Ha_ghxFe	Log_k_4
Ha_dhxxFe	+	Ha_efxxFe	+	H_3AsO_3	=	Ha_dhxxFeH_3AsO_3Ha_efxxFe	Log_k_4
Ha_dhxxFe	+	Ha_ghxxFe	+	H_3AsO_3	=	Ha_dhxxFeH_3AsO_3Ha_ghxxFe	Log_k_4
Ha_efxxFe	+	Ha_ghFe	+	H_3AsO_3	=	Ha_efxxFeH_3AsO_3Ha_ghFe	Log_k_4
Ha_efxxFe	+	Ha_ghxFe	+	H_3AsO_3	=	Ha_efxxFeH_3AsO_3Ha_ghxFe	Log_k_4
Ha_efxxFe	+	Ha_ghxxFe	+	H_3AsO_3	=	Ha_efxxFeH_3AsO_3Ha_ghxxFe	Log_k_4

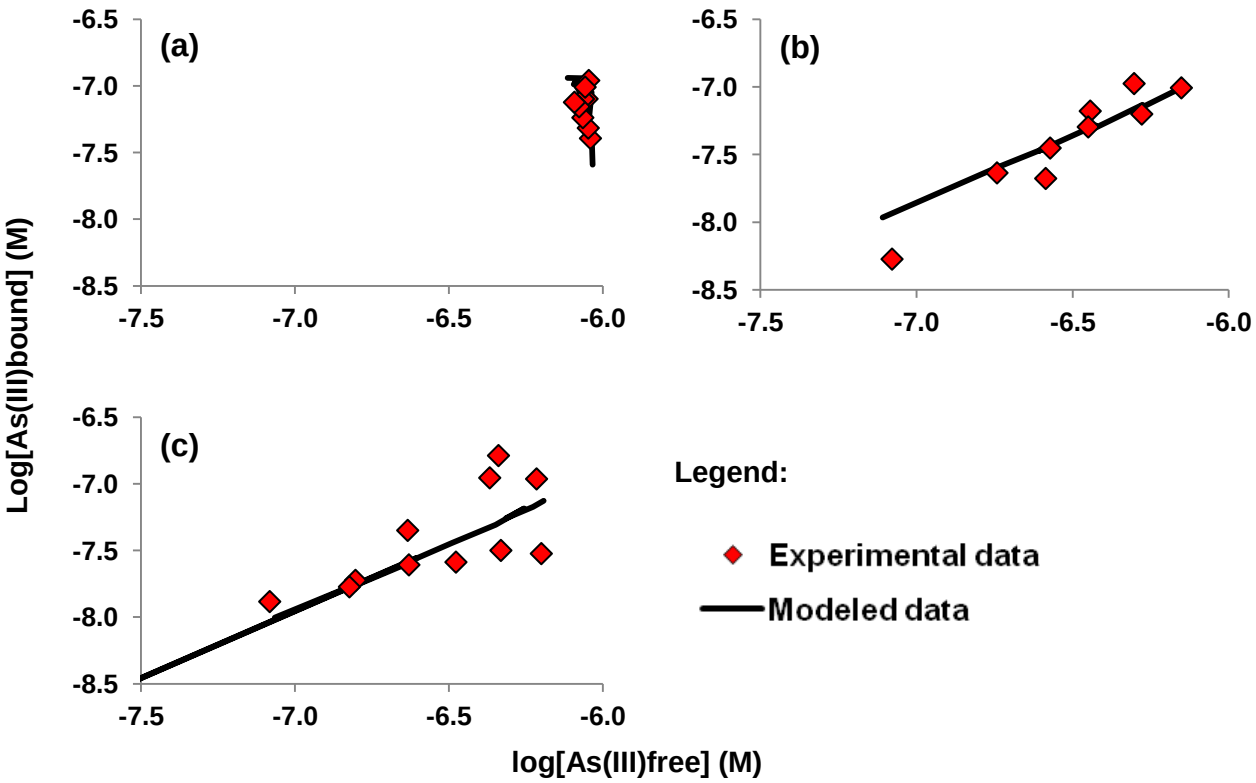

ANNEXE III 8: Formation of As(III) binuclear monodentate to Fe(II) bidentate with OM (a) isotherm with increasing Fe(II) concentrations at pH 6, (b) isotherm with increasing As(III) concentrations at pH 6, (c) isotherm with increasing Fe(II) concentrations at pH 5.

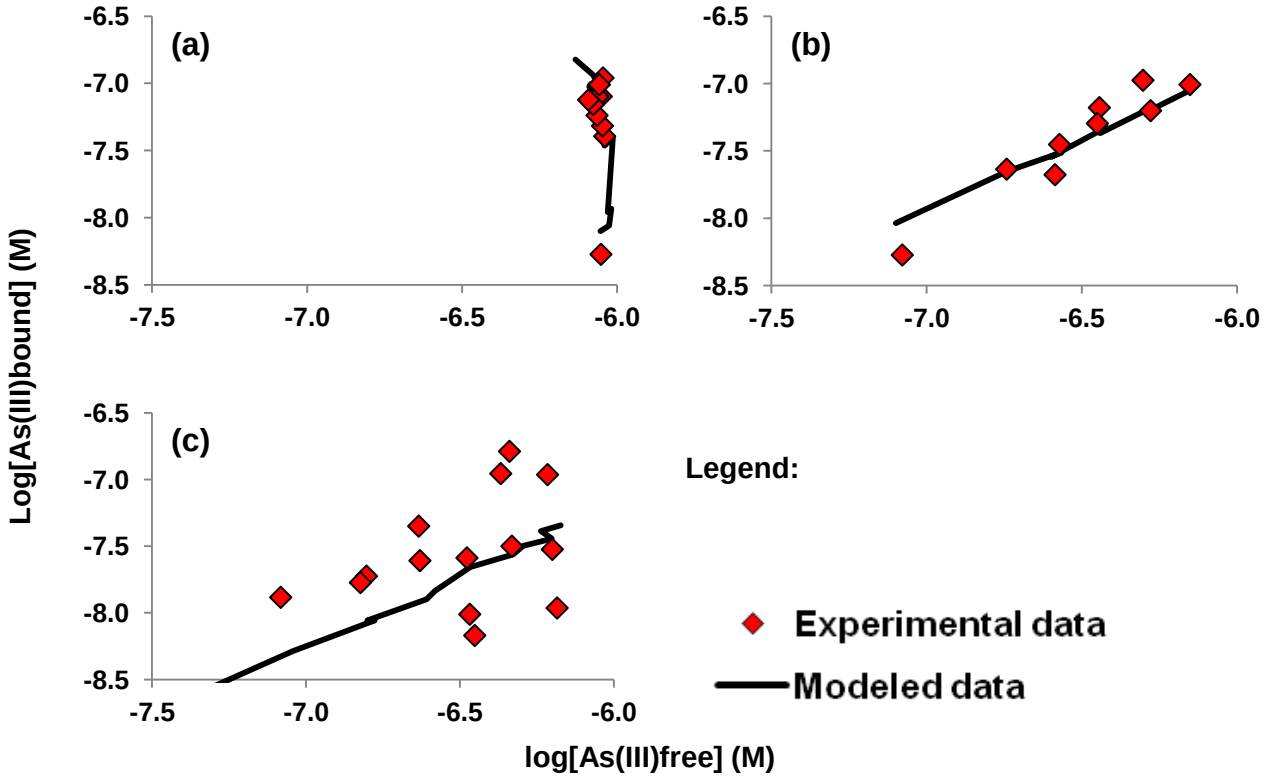

ANNEXE III 9: Sum of Eq.1 + Eq. 2 (a) isotherm with increasing Fe(II) concentrations at pH 6, (b) isotherm with increasing As(III) concentrations at pH 6, (c) isotherm with increasing Fe(II) concentrations at pH 5.

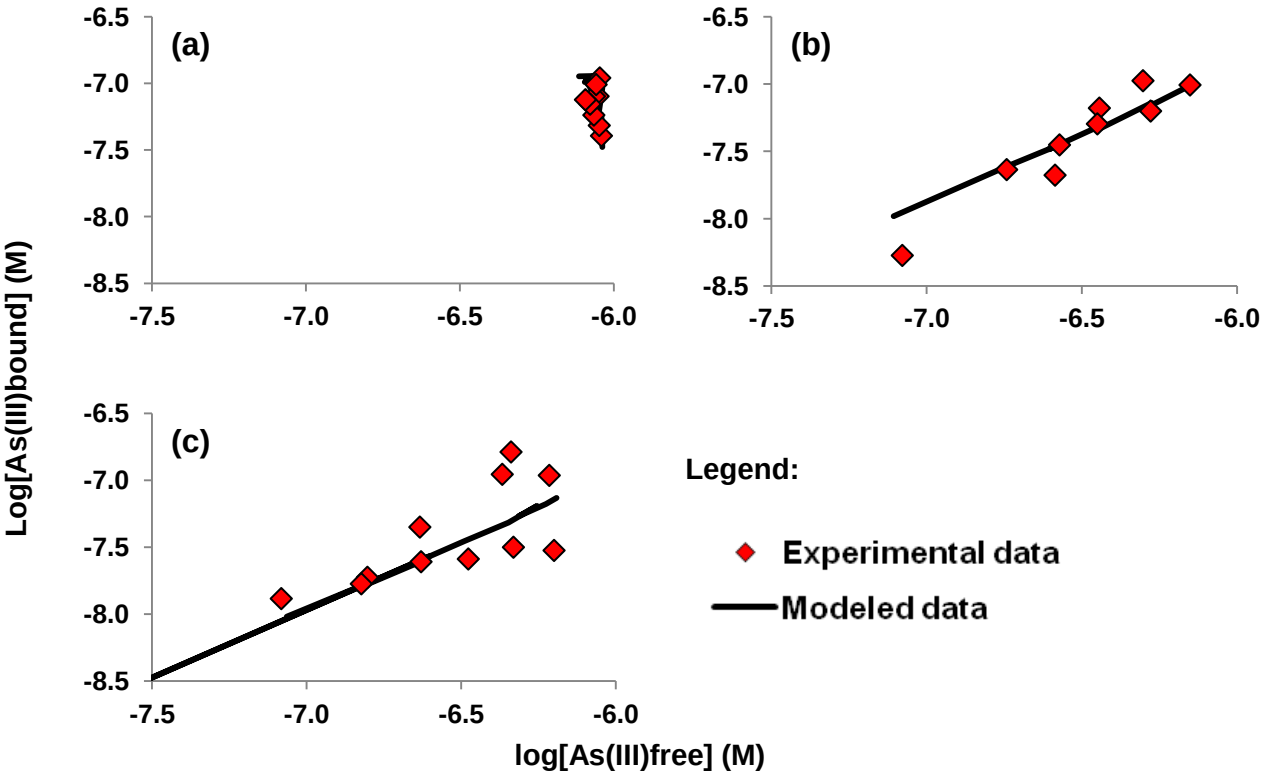

ANNEXE III 10: Sum of Eq.3 + Eq. 4 (a) isotherm with increasing Fe(II) concentrations at pH 6, (b) isotherm with increasing As(III) concentrations at pH 6, (c) isotherm with increasing Fe(II) concentrations at pH 5.

BIBLIOGRAPHIE

Abdullah, M., Shiyu, Z., Mosgren, K., 1995. Arsenic and selenium species inthe oxic and anoxic waters of the Oslofjord, Norway. Mar. Pollut. Bull. 31, 116–126.

AFNOR, 1982. Essais des eaux — Dosage du fer — Méthode spectrométrique à la phénantroline-1,10.

Akai, J., Izumi, K., Fukuhara, H., Masuda, H., Nakano, S., Yoshimura, T., Ohfuji, H., Md Anawar, H., Akai, K., 2004. Mineralogical and geomicrobiological investigations on groundwater arsenic enrichment in Bangladesh. Appl. Geochem. 19, 215–230. doi:10.1016/j.apgeochem.2003.09.008

Allan, R.J., Ball, A.J., 1990. An overview of toxic contaminants in water and sediments of the Great Lakes. Water Pollut. Res. J. Can. Part I, 387–505.

Allard, T., Menguy, N., Salomon, J., Calligaro, T., Weber, T., Calas, G., Benedetti, M., 2004. Revealing forms of iron in river-borne material from major tropical rivers of the Amazon Basin (Brazil). Geochim. Cosmochim. Acta 68, 3079–3094.

Al-Sid-Cheikh, M., Pédrot, M., Dia, A., Guenet, H., Vantelon, D., Davranche, M., Gruau, G., Delhaye, T., 2015. Interactions between natural organic matter, sulfur, arsenic and iron oxides in re-oxidation compounds within riparian wetlands: NanoSIMS and X-ray adsorption spectroscopy evidences. Sci. Total Environ. 515-516, 118–128. doi:10.1016/j.scitotenv.2015.02.047

Amini, M., Abbaspour, K.C., Berg, M., Winkel, L., Hug, S.J., Hoehn, E., Yang, H., Johnson, C.A., 2008. Statistical Modeling of Global Geogenic Arsenic Contamination in Groundwater. Environ. Sci. Technol. 42, 3669–3675. doi:10.1021/es702859e

Anawar, H.M., Akai, J., Komaki, K., Terao, H., Yoshioka, T., Ishizuka, T., Safiullah, S., Kato, K., 2003. Geochemical occurrence of arsenic in groundwater of Bangladesh: sources and mobilization processes. J. Geochem. Explor. 77, 109–131. doi:10.1016/S0375-6742(02)00273-X

Andreae, M., Andreae, T., 1989. Dissolved arsenic species in the Schelde estuary and watershed, Belgium. Estuar. Coast. Shelf Sci. 29, 421–433.

Andreae, M., Byrd, J., Froelich, P., 1983. Arsenic, antimony, germanium, and tin in the Tejo estuary, Portugal - Modeling a polluted estuary. Environ. Sci. Technol. 17, 731–737.

Andreae, M.O., 1980. Arsenic in Rain and the Atmospheric Mass Balance of Arsenic. Jounral Geophys. Res. 85, 4512–4518.

Appelo, C., Postma, D., 2005. Geochemistry, groundwater and pollution, Taylor & Francis. ed. New York.

Arnold, C., Ciani, A., Müller, S.R., Amirbahman, A., Schwarzenbach, R.P., 1998. Association of Triorganotin Compounds with Dissolved Humic Acids. Environ. Sci. Technol. 32, 2976–2983. doi:10.1021/es980114z

Arribére, M.A., Cohen, I.M., Ferpozzi, L.H., Kestelman, A.J., Casa, V.A., Guevara, S.R., 1997. Neutron activation analysis of soils and loess deposits, for the investigation of the origin of the natural arsenic-contamination in the Argentine Pampa. Radiochim. Acta 187–191.

Atalay, Y.B., Carbonaro, R.F., Di Toro, D.M., 2009. Distribution of Proton Dissociation Constants for Model Humic and Fulvic Acid Molecules. Environ. Sci. Technol. 43, 3626–3631. doi:10.1021/es803057r

Avena, M.J., Koopal, L.K., Van Riemsdijk, W.H., 1999. Proton Binding to Humic Acids: Electrostatic and Intrinsic Interactions. J. Colloid Interface Sci. 217, 37–48.

Azcue, J.M., Murdoch, A., Rosa, F., Hall, G.E.M., 1994. Effects of abandoned gold mine tailings on the arsenic concentrations in water and sediments of Jack of Clubs Lake, BC. Environ. Technol. 669–678.

Azcue, J.M., Nriagu, J.O., 1995. Impact of abandoned mine tailings on the arsenic concentrations in Moira Lake, Ontario. J. Geochem. Explor. 81–89.

Bauer, M., Blodau, C., 2009. Arsenic distribution in the dissolved, colloidal and particulate size fraction of experimental solutions rich in dissolved organic matter and ferric iron. Geochim. Cosmochim. Acta 73, 529–542. doi:10.1016/j.gca.2008.10.030

Bauer, M., Blodau, C., 2006. Mobilization of arsenic by dissolved organic matter from iron oxides, soils and sediments. Sci. Total Environ. 354, 179–190. doi:10.1016/j.scitotenv.2005.01.027

Baur, W.H., Onishi, B.-M.H., 1969. Arsenic. Handbook of Geochemistry, Wedepohl, K.H. ed. Springer-Verlag, Berlin.

Belkin, H.E., Zheng, B., Finkelman, R.B., 2000. Human Health effects of domestic combustion of coal in rural China: a causal factor for arsenic anf fluorine poisoning. Stanford University.

Benson, L.V., Spencer, R.J., 1983. A hydrochemical Reconnaissance Study of the Walker River Basin, California and Nevada. USGS Open File Rep., United States Geological Survey, Denver, pp. 83–740.

BGS, DPHE, 2001. Arsenic contamination of groundwater in Bangladesh. In: Kinniburgh, D.G., Smedley, P.L. (Eds.), British Geological Survey (Technical Report, WC/00/19. 4 volumes). British Geological Survey, Keyworth.

Bowell, R.J., Alpers, C.N., Jamieson, H.E., Nordstrom, D.K., Majzlan, J., 2014. Arsenic: Environmental Geochemistry, Mineralogy, and Microbiology, Reviews in Mineralogy & Geochemistry. Mineralogical Society of America Geochemical Society.

Boyle, R.W., Jonasson, I.R., 1973. The geochemistry of As and its use as an indicator element in geochemical prospecting. J. Geochem. Explor. 251–296.

Bright, D., Dodd, M., Reimer, K., 1996. Arsenic in subArtic lakes influenced by gold mine effluent: The occurrence of organoarsenicals and “hidden” arsenic. Sci. Total Environ. 180, 165–182.

Buffle, J., Vitre, R.R., Perret, D., Leppard, G.G., 1989. Physico-chemical characteristics of a colloidal iron phosphate species formed at the oxic-anoxic interface of a eutrophic lake. Geochim. Cosmochim. Acta 53, 399–408.

Buffle, J., Wilkinson, K.J., Stoll, S., Filella, M., Zhang, J., 1998. A generalized description of aquatic colloidal interactions: the three-colloidal component approach. Environ. Sci. Technol. 32, 2887–2899.

Buschmann, J., Kappeler, A., Lindauer, U., Kistler, D., Berg, M., Sigg, L., 2006. Arsenite and arsenate binding to dissolved humic acids: Influence of pH, type of humic acid, and aluminum. Environ. Sci. Technol. 40, 6015–6020.

Buschmann, J., Sigg, L., 2004. Antimony(III) Binding to Humic Substances: Influence of pH and Type of Humic Acid. Environ. Sci. Technol. 38, 4535–4541. doi:10.1021/es049901o

Caceres, L., Gruttner, E., Contreras, R., 1992. Water recycling in arid regions - Chilean case. Ambio 21, 138–144.

Catrouillet, C., Davranche, M., Dia, A., Bouhnik-Le Coz, M., Marsac, R., Pourret, O., Gruau, G., 2014. Geochemical modeling of Fe(II) binding to humic and fulvic acids. Chem. Geol. 372, 109–118. doi:10.1016/j.chemgeo.2014.02.019

Catrouillet, C., Davranche, M., Dia, A., Coz, M.B.-L., Pédrot, M., Marsac, R., Gruau, G., 2015. Thiol groups controls on arsenite binding by organic matter: New experimental and modeling evidence. J. Colloid Interface Sci. doi:10.1016/j.jcis.2015.08.045

Cavanillas, S., Chekmeneva, E., Ariño, C., Díaz-Cruz, J.M., Esteban, M., 2012. Electroanalytical and isothermal calorimetric study of As(III) complexation by the metal poisoning remediators, 2,3-dimercapto-1-propanesulfonate and meso-2,3-dimercaptosuccinic acid. Anal. Chim. Acta 746, 47–52. doi:10.1016/j.aca.2012.08.005

Christl, I., Knicker, H., Kögel-Knabner, I., Kretzschmar, R., 2000. Chemical heterogeneity of humic substances: characterization of size fractions obtained by hollow-fibre ultrafiltration. Eur. J. Soil Sci. 51, 617–625.

Cook, S.J., Levson, V.M., Giles, T.R., Jackaman, W., 1995. A comparison of regional lake sediment and till geochemistry surveys-a case-study from the Fawnie Creek area, Central British Columbia. Explor. Miner. Geol. 93–110.

Cronan, D.S., 1972. The mid-Atlantic Ridge near 45°N, XVII: Al, As, Hg, and Mn in ferriginous sediments from the median valley. Can. J. Earth Sci. 319–323.

Cullen, W., Reimer, K., 1989. Arsenic speciation in the environment. Chem. Rev. 89, 713–764.
Das, D., Chatterjee, A., Mandal, B., Samanta, G., Chakraborti, D., 1995. Arsenic in ground-water in 6 districts of West-Bengal, Indio - The biggest Arsenic calamity in the World. 2. Arsenic concentration in drinking-water, hair, nails, urine, skin-scale and liver-tissue (biopsy) of the affected people. Analyst 120, 9917–924.
Datta, D.K., Subramanian, V., 1997. Texture and mineralogy of sediments from the Ganges-Brahmaputra-Meghna river system in the Bengal basin, Bangladesh and their environmental implications. Environ. Geol. 181–188.
Davis, A., de Curnou, P., Eary, L.E., 1997. Discriminating between sources of arsenic in the sediments of a tidal waterway, Tacoma, Washington. Environ. Sci. Technol. 1985–1991.
Davison, W., 1993. Iron and mangagene in lakes. Earth-Sci. Rev. 34, 119–163.
Davranche, M., Dia, A., Fakih, M., Nowack, B., Gruau, G., Ona-nguema, G., Petitjean, P., Martin, S., Hochreutener, R., 2013. Organic matter control on the reactivity of Fe(III)-oxyhydroxides and associated As in wetland soils: A kinetic modeling study. Chem. Geol. 335, 24–35. doi:10.1016/j.chemgeo.2012.10.040
Delrazo, L., Arellano, M., Cebrian, M., 1990. The oxidation-states of arsenic in well-water from a chronic arsenicism area of Northern Mexico. Environ. Pollut. 64, 143–153.
Dia, A., Gruau, G., Olivié-Lauquet, G., Riou, C., Molénat, J., Curmi, P., 2000. The distribution of rare earth elements in groundwaters: assessing the role of source-rock composition, redox changes and colloidal particles. Geochim. Cosmochim. Acta 64, 4131–4151.
Dixit, S., Hering, J.G., 2003. Comparison of Arsenic(V) and Arsenic(III) Sorption onto Iron Oxide Minerals: Implications for Arsenic Mobility. Environ. Sci. Technol. 37, 4182–4189. doi:10.1021/es030309t
Dong, W., Liang, L., Brooks, S., Southworth, G., Gu, B., 2010. Roles of dissolved organic matter in the speciation of mercury and methylmercury in a contaminated ecosystem in Oak Ridge, Tennessee. Environ. Chem. 7, 94. doi:10.1071/EN09091
Dudas, M.J., 1984. Enriched levels of arsenic in post-active acid sulfate soils in Alberta. Soil Sci. Soc. Am. J. 1451–1452.
Dudas, M.J., Warren, Spiers, G.A., 1988. Chemistry of arsenic in acid sulfate soils of northern Alberta. Common Soil Sci. Plant Anal. 887–895.
Dzombak, D.A., Morel, F.M.M., 1990. Surface Complexation Modeling. New York.
Echigo, T., Kimata, M., 2008. Single-crystal X-ray diffraction and spectroscopic studies on humboldtine and lindbergite: weak Jahn–Teller effect of Fe2+ ion. Phys. Chem. Miner. 35, 467–475. doi:10.1007/s00269-008-0241-7
Edmunds, W.M., Cook, J.M., Kinniburgh, D.G., Miles, D.L., 1989. Trace-element Occurrence in British Groundwaters (British Geological Survey, Keyworth No. SD/89/3).
Edsall, J.T., Wyman, J., 1958. Biophysical Chemistry. Academic Press, New York.
Ellis, A.J., Mahon, W.A.J., 1977. Chemistry and Geothermal Systems. Academic Press, New York.
Evangelou, V.P., Marsi, M., 2001. Composition and metal ion complexation behavour of humic fractions derived from corn tissue. Plant Soil 229, 13–24.
Fakih, M., Davranche, M., Dia, A., Nowack, B., Morin, G., Petitjean, P., Châtellier, X., Gruau, G., 2009. Environmental impact of As(V)–Fe oxyhydroxide reductive dissolution: An experimental insight. Chem. Geol. 259, 290–303. doi:10.1016/j.chemgeo.2008.11.021
Fakour, H., Lin, T.-F., 2014. Experimental determination and modeling of arsenic complexation with humic and fulvic acids. J. Hazard. Mater. 279, 569–578. doi:10.1016/j.jhazmat.2014.07.039
Fendorf, S., 2010. Arsenic chemistry in soils and sediments. Lawrence Berkeley Natl. Lab.
Fendorf, S., Kocar, B.D., 2009. Chapter 3 Biogeochemical Processes Controlling the Fate and Transport of Arsenic, in: Advances in Agronomy. Elsevier, pp. 137–164.

Filella, M., Williams, P.A., 2012. Antimony interactions with heterogeneous complexants in waters, sediments and soils: A review of binding data for homologous compounds. Chem. Erde - Geochem. 72, 49–65. doi:10.1016/j.chemer.2012.01.006

Froelich, P., Kaul, L., Byrd, J., Andreae, M., Roe, K., 1985. aesenic, barium, germanium, tin, diméthylsulfide and nutrient biogeochemistry in Charlotte harbor, Florida, a phosphorus-enriched estuary. Estuar. Coast. Shelf Sci. 20, 239–264.

Fukushima, M., Hasebe, K., Taga, M., 1992. Effect of sodium dodecyl sulphate on the measurement of labile copper(II) species by anodic stripping voltammetry in the presence of humic acid. Anal. Chim. Acta 270, 153–159.

Fukushima, M., Tanaka, S., Nakamura, H., Ito, S., Haraguchi, K., Ogata, T., 1996. Copper(II) binding abilities of molecular weight fractionated humic acids and their mixtures. Anal. Chim. Acta 322, 173–185.

Gaber, B.P., Fluharty, A.L., 1972. Cadmium and Arsenite Binding by N-Dihydrolipoylaminoethoxydextran: A Model Study of Enzyme Dithiol Criteria. Bioinorg. Chem. 2, 135–148.

Gelova, G.A., 1977. Hydrogeochemistry of Ore Elements. Nedra, Moscow.

Gough, J.D., Gargano, J.M., Donofrio, A.E., Lees, W.J., 2003. Aromatic Thiol p K_a Effects on the Folding Rate of a Disulfide Containing Protein †. Biochemistry (Mosc.) 42, 11787–11797. doi:10.1021/bi034305c

Grafe, M., Eick, M.J., Grossl, P.R., 2001. Adsorption of arsenate (V) and arsenite (III) on goethite in the presence and absence of dissolved organic carbon. Soil Sci. Soc. Am. J. 65, 1680–1687.

Guo, H., Zhang, B., Zhang, Y., 2011. Control of organic and iron colloids on arsenic partition and transport in high arsenic groundwaters in the Hetao basin, Inner Mongolia. Appl. Geochem. 26, 360–370. doi:10.1016/j.apgeochem.2010.12.009

Gustafsson, J.P., 2001. Modeling the Acid–Base Properties and Metal Complexation of Humic Substances with the Stockholm Humic Model. J. Colloid Interface Sci. 244, 102–112. doi:10.1006/jcis.2001.7871

Gustafsson, J.P., Persson, I., Kleja, D.B., Van Schaik, J.W., 2007. Binding of iron (III) to organic soils: EXAFS spectroscopy and chemical equilibrium modeling. Environ. Sci. Technol. 41, 1232–1237.

Gustafsson, J.P., Tin, N.T., 1994. Arsenic and selenium in some Vietnamese acid sulfate soils. Sci. Total Environ. 153–158.

Haitzer, M., Aiken, G.R., Ryan, J.N., 2003. Binding of mercury (II) to aquatic humic substances: Influence of pH and source of humic substances. Environ. Sci. Technol. 37, 2436–2441.

Hale, J.R., Foos, A., Zubrow, J.S., Cook, J., 1997. Better characterization of arsenic and chromium in soils: a field-scale example. J. Soil Contam. 371–389.

Harvey, C.F., Ashfaque, K.N., Yu, W., Badruzzaman, A.B.M., Ali, M.A., Oates, P.M., Michael, H.A., Neumann, R.B., Beckie, R., Islam, S., Ahmed, M.F., 2006. Groundwater dynamics and arsenic contamination in Bangladesh. Chem. Geol. 228, 112–136. doi:10.1016/j.chemgeo.2005.11.025

Hoffmann, M., Mikutta, C., Kretzschmar, R., 2014. Arsenite Binding to Sulfhydryl Groups in the Absence and Presence of Ferrihydrite: A Model Study. Environ. Sci. Technol. 48, 3822–3831. doi:10.1021/es405221z

Hoffmann, M., Mikutta, C., Kretzschmar, R., 2013. Arsenite Binding to Natural Organic Matter: Spectroscopic Evidence for Ligand Exchange and Ternary Complex Formation. Environ. Sci. Technol. 47, 12165–12173. doi:10.1021/es4023317

Hoffmann, M., Mikutta, C., Kretzschmar, R., 2012. Bisulfide Reaction with Natural Organic Matter Enhances Arsenite Sorption: Insights from X-ray Absorption Spectroscopy. Environ. Sci. Technol. 46, 11788–11797. doi:10.1021/es302590x

Holleman, A.F., Wiberg, E., 1995. Lehrbuch der Anorganischen Chemie, 101st ed. W. deGruyter.

Howard, A., Apte, S., Comber, S., Morris, R., 1988. Biogeochemical control of the summer distribution and speciation of arsenic in the Tamar estuary. Estuar. Coast. Shelf Sci. 27, 427–443.

Hsu, K.H., Froines, J.R., Chen, C.J., 1997. Studies of arsenic ingestion from drinking water in northeastern Taiwan: chemical speciation and urinary metabolites. In: Abernathy, C.O., Calderon, R.L., Chappell, W.R. (Eds.), Arsenic Exposure and Health Effects. Chapman Hall, London, pp. 190–209.

Islam, F.S., Gault, A.G., Boothman, C., Polya, D.A., Charnock, J.M., Chatterjee, D., Lloyd, J.R., 2004. Role of metal-reducing bacteria in arsenic release from Bengal delta sediments. Nature 430, 68–71.

Jackson, A., Gaffney, J.W., Boult, S., 2012. Subsurface Interactions of Fe(II) with Humic Acid or Landfill Leachate Do Not Control Subsequent Iron(III) (Hydr)oxide Production at the Surface. Environ. Sci. Technol. 46, 7543–7550. doi:10.1021/es301084c

Jiang, T., Skyllberg, U., Wei, S., Wang, D., Lu, S., Jiang, Z., Flanagan, D.C., 2015. Modeling of the structure-specific kinetics of abiotic, dark reduction of Hg(II) complexed by O/N and S functional groups in humic acids while accounting for time-dependent structural rearrangement. Geochim. Cosmochim. Acta 154, 151–167. doi:10.1016/j.gca.2015.01.011

Jönsson, J., Sherman, D.M., 2008. Sorption of As(III) and As(V) to siderite, green rust (fougerite) and magnetite: Implications for arsenic release in anoxic groundwaters. Chem. Geol. 255, 173–181. doi:10.1016/j.chemgeo.2008.06.036

Kalbitz, K., Wennrich, R., 1998. Mobilization of heavy metals and arsenic in polluted wetland soils and its dependence on dissolved matter. Sci. Total Environ. 209, 27–39.

Kappeler, A., 2006. Arsenic binding to dissolved humic acids in aqueous solution. ETHZ.

Karlsson, T., Persson, P., 2010. Coordination chemistry and hydrolysis of Fe(III) in a peat humic acid studied by X-ray absorption spectroscopy. Geochim. Cosmochim. Acta 74, 30–40. doi:10.1016/j.gca.2009.09.023

Kar, S., Maity, J.P., Jean, J.-S., Liu, C.-C., Nath, B., Lee, Y.C., Bundschuh, J., Chen, C.-Y., Li, Z., 2011. Role of organic matter and humic substances in the binding and mobility of arsenic in a Gangetic aquifer. J. Environ. Res. Public Health 46, 1231–1238.

Kavanagh, P.J., Farago, M.E., Thornton, I., Braman, R.S., 1997. Bioavailability of arsenic in soil and mine wastes of the Tarmar Valley, SW England. Chem. Speciat. Bioavailab. 77–81.

Kim, J.-I., Buckau, G., Li, G.H., Duschner, H., Psarros, N., 1990. Characterization of humic and fulvic acids from Gorleben groundwater. Fresenius J. Anal. Chem. 338, 245–252.

Kinniburgh, D.G., van Riemsdijk, W.H., Koopal, L.K., Borkovec, M., Benedetti, M.F., Avena, M.J., 1999. Ion binding to natural organic matter: competition, heterogeneity, stoichiometry and thermodynamic consistency. Colloids Surf. Physicochem. Eng. Asp. 151, 147–166.

Kitchin, K.T., Wallace, K., 2008. The role of protein binding of trivalent arsenicals in arsenic carcinogenesis and toxicity. J. Inorg. Biochem. 102, 532–539. doi:10.1016/j.jinorgbio.2007.10.021

Kleber, R.J., Skrabal, S.A., Smith, B.J., Wiley, J.D., 2005. Organic Complexation of Fe(II) and Its Impact on the Redox Cycling of Iron in Rain. Environ. Sci. Technol. 39, 1576–1583.

Klüpfel, L., Piepenbrock, A., Kappler, A., Sander, M., 2014. Humic substances as fully regenerable electron acceptors in recurrently anoxic environments. Nat. Geosci. 7, 195–200. doi:10.1038/ngeo2084

Kocar, B.D., 2008. Soil-sediment processes perpetuating history's largest mass poisoning through release of arsenic to Asian groundwaters. ProQuest.

Ko, I., Kim, J.-Y., Kim, K.-W., 2004. Arsenic speciation and sorption kinetics in the As–hematite–humic acid system. Colloids Surf. Physicochem. Eng. Asp. 234, 43–50. doi:10.1016/j.colsurfa.2003.12.001

Langner, P., Mikutta, C., Kretzschmar, R., 2011a. Arsenic sequestration by organic sulphur in peat. Nat. Geosci. 5, 66–73. doi:10.1038/ngeo1329

Langner, P., Mikutta, C., Kretzschmar, R., 2011b. Arsenic sequestration by organic sulphur in peat. Nat. Geosci. 5, 66–73. doi:10.1038/ngeo1329
Leenheer, J.A., Wershaw, R.L., Reddy, M.M., 1995. Strong-acid, carboxyl-group structures in fulvic acid from the Suwannee River, Georgia. 2. Major structures. Environ. Sci. Technol. 29, 399–405.
Legeleux, F., Reyss, J.L., Bonte, P., Organo, C., 1994. Concomitant enrichments of uranium, molybdenum and arsenic in suboxic continental-margin sediments. Oceanol. Acta 417–429.
Lenoble, V., Dang, D.H., Loustau Cazalet, M., Mounier, S., Pfeifer, H.-R., Garnier, C., 2015. Evaluation and modelling of dissolved organic matter reactivity toward AsIII and AsV – Implication in environmental arsenic speciation. Talanta 134, 530–537. doi:10.1016/j.talanta.2014.11.053
Lerda, D., Prosperi, C., 1996. Water mutagenicity abd toxicology in Rio Tercero (Cordoba, Argentina). Water Res. 30, 819–824.
Liang, X., Drueckhammer, D.G., 2014. Arsinous acid as a thiol binding group: potential cysteine peptide tagging functionality that binds a single thiol. New J. Chem. 38, 1368. doi:10.1039/c3nj01462b
Lin, H.-T., Wang, M.., Li, G.-C., 2004. Complexation of arsenate with humic substance in water extract of compost. Chemosphere 56, 1105–1112. doi:10.1016/j.chemosphere.2004.05.018
Liu, D.J., Bruggeman, C., Maes, N., 2008. The influence of natural organic matter on the speciation and solubility of Eu in Boom Clay porewater. Radiochim. Acta 96. doi:10.1524/ract.2008.1557
Liu, G., Cai, Y., 2010. Complexation of arsenite with dissolved organic matter: Conditional distribution coefficients and apparent stability constants. Chemosphere 81, 890–896. doi:10.1016/j.chemosphere.2010.08.002
Liu, G., Fernandez, A., Cai, Y., 2011. Complexation of Arsenite with Humic Acid in the Presence of Ferric Iron. Environ. Sci. Technol. 45, 3210–3216. doi:10.1021/es102931p
Luo, Z.D., Zhang, Y.M., Ma, L., Zhang, G.Y., He, X., Wilson, R., Byrd, D.M., Griffiths, J.G., Lai, S., He, L., Grumski, K., Lamm, S.H., 1997. Chronic arsenicism and cancer in Inner Mongolia - consequences of well-water arsenic levels greater than 50 mg l-1 In Abernathy, C.O., Calderon, R.L., Chappell, W.R. (Eds.), Arsenic Exposure and Health Effects. Chapman Hall, London, pp. 55–68.
Lützenkirchen, J., 1999. The Constant Capacitance Model and Variable Ionic Strength: An Evaluation of Possible Applications and Applicability. J. Colloid Interface Sci. 217, 8–18.
Lützenkirchen, J., van Male, J., Leermakers, F., Sjöberg, S., 2011. Comparison of Various Models to Describe the Charge−pH Dependence of Poly(acrylic acid). J. Chem. Eng. Data 56, 1602–1612. doi:10.1021/je101253q
Manceau, A., Nagy, K.L., 2012. Quantitative analysis of sulfur functional groups in natural organic matter by XANES spectroscopy. Geochim. Cosmochim. Acta 99, 206–223. doi:10.1016/j.gca.2012.09.033
Manning, B.A., Fendorf, S.E., Goldberg, S., 1998. Surface structures and stability of arsenic (III) on goethite: spectroscopic evidence for inner-sphere complexes. Environ. Sci. Technol. 32, 2383–2388.
Marini, L., Accornero, M., 2007. Prediction of the thermodynamic properties of metal–arsenate and metal–arsenite aqueous complexes to high temperatures and pressures and some geological consequences. Environ. Geol. 52, 1343–1363. doi:10.1007/s00254-006-0578-5
Marsac, R., Banik, N.L., Marquardt, C.M., Kratz, J.V., 2014. Stabilization of polynuclear plutonium(IV) species by humic acid. Geochim. Cosmochim. Acta 131, 290–300. doi:10.1016/j.gca.2014.01.039
Marsac, R., Davranche, M., Gruau, G., Bouhnik-Le Coz, M., Dia, A., 2011. An improved description of the interactions between rare earth elements and humic acids by

modeling: PHREEQC-Model VI coupling. Geochim. Cosmochim. Acta 75, 5625–5637. doi:10.1016/j.gca.2011.07.009
Marsac, R., Davranche, M., Gruau, G., Dia, A., 2010. Metal loading effect on rare earth element binding to humic acid: Experimental and modelling evidence. Geochim. Cosmochim. Acta 74, 1749–1761. doi:10.1016/j.gca.2009.12.006
Marsac, R., Davranche, M., Gruau, G., Dia, A., Bouhnik-Le Coz, M., 2012. Aluminium competitive effect on rare earth elements binding to humic acid. Geochim. Cosmochim. Acta 89, 1–9. doi:10.1016/j.gca.2012.04.028
Marsac, R., Davranche, M., Gruau, G., Dia, A., Pédrot, M., Le Coz-Bouhnik, M., Briant, N., 2013. Effects of Fe competition on REE binding to humic acid: Origin of REE pattern variability in organic waters. Chem. Geol. 342, 119–127. doi:10.1016/j.chemgeo.2013.01.020
Martell, A.E., Smith, R.M., 1989. Critical Stability Constants.
Martin, J.-M., Whitfield, M., 1983. The significance of the river input of chemical elements to the ocean. In: Wong, C.S., Boyle, E., Bruland, K.W., Burton, J.D., Goldberg, E.D. (Eds.), Trace Metals in Seawater, Plenum Press. ed. TRace Metals in Seawater, New York.
Martin, M., Celi, L., Barberis, E., Violante, A., Kozak, L.M., Huang, P.M., 2009. Effect of humic acid coating on arsenic adsorption on ferrihydrite-kaolinite mixed systems. Can. J. Soil Sci. 89, 421–434.
McArthur, J.., Banerjee, D.., Hudson-Edwards, K.., Mishra, R., Purohit, R., Ravenscroft, P., Cronin, A., Howarth, R.., Chatterjee, A., Talukder, T., Lowry, D., Houghton, S., Chadha, D.., 2004. Natural organic matter in sedimentary basins and its relation to arsenic in anoxic ground water: the example of West Bengal and its worldwide implications. Appl. Geochem. 19, 1255–1293. doi:10.1016/j.apgeochem.2004.02.001
McArthur, J.M., Ravenscroft, P., Safiulla, S., Thirlwall, M.F., 2001. Arsenic in groundwater: Testing pollution mechanims for sedimentary aquifers in Bangladesh. Water Resour. Res. 37, 109–117.
McBride, M.B., 1994. Environmental Chesmitry of Soils, Oxford University Press. ed. New York.
McCarthy, J.F., Zachara, J.M., 1989. Subsurface transport of contaminants. Environ. Sci. Technol. 23, 496–502.
McCreadie, H., Blowes, D., 2000. Influence of reduction reactions and solid phase composition on porewater concentrations of arsenic. Environ. Sci. Technol. 34, 3159–3166.
McLaren, S., Kim, N., 1995. Evidence for a seasonal fluctuation of arsenic in New-Zealands longest river and the effect of treatment on concentrations in drinking-water. Environ. Pollut. 90, 67–73.
McSweeney, N.J., Forbes, L., 2014. Arsenic-interacting plant proteins as templates for arsenic specific flotation collectors? A review. Miner. Eng. 64, 67–77. doi:10.1016/j.mineng.2014.03.009
Meharg, A.A., Scrimgeour, C., Hossain, S.A., Fuller, K., Cruickshank, K., Williams, P.N., Kinniburgh, D.G., 2006. Codeposition of Organic Carbon and Arsenic in Bengal Delta Aquifers. Environ. Sci. Technol. 40, 4928–4935. doi:10.1021/es060722b
Mikutta, C., Frommer, J., Voegelin, A., Kaegi, R., Kretzschmar, R., 2010. Effect of citrate on the local Fe coordination in ferrihydrite, arsenate binding, and ternary arsenate complex formation. Geochim. Cosmochim. Acta 74, 5574–5592. doi:10.1016/j.gca.2010.06.024
Mikutta, C., Kretzschmar, R., 2011. Spectroscopic Evidence for Ternary Complex Formation between Arsenate and Ferric Iron Complexes of Humic Substances. Environ. Sci. Technol. 45, 9550–9557. doi:10.1021/es202300w
Miller, C.J., Rose, A.L., Waite, T.D., 2009. Impact of natural organic matter on H2O2-mediated oxidation of Fe(II) in a simulated freshwater system. Geochim. Cosmochim. Acta 73, 2758–2768. doi:10.1016/j.gca.2009.02.027

Miller, C.J., Vincent Lee, S.M., Rose, A.L., Waite, T.D., 2012. Impact of Natural Organic Matter on H_2O_2-Mediated Oxidation of Fe(II) in Coastal Seawaters. Environ. Sci. Technol. 46, 11078–11085. doi:10.1021/es3022792

Milne, C.J., Kinniburgh, D.G., Tipping, E., 2001. Generic NICA-Donnan model parameters for proton binding by humic substances. Environ. Sci. Technol. 35, 2049–2059.

Milne, C.J., Kinniburgh, D.G., Van Riemsdijk, W.H., Tipping, E., 2003. Generic NICA-Donnan model parameters for metal-ion binding by humic substances. Environ. Sci. Technol. 37, 958–971.

Moore, J.N., Ficklin, W.H., Johns, C., 1988. Partitioning of arsenic and metals in reducing sulfidic sediments. Environ. Sci. Technol. 432–437.

Morris, A.J., Hesterberg, D., 2012. Iron(III) coordination and phosphate sorption in peat reacted with ferric or ferrous iron. Soil Sci. Soc. Am. J. 76, 101–109.

Mota, A.M., Pinheiro, J.P., Gonçalves, M.L., 1994. Adsorption of humic acid on a mercury/aqueous solution interface. Water Res. 28, 1285–1296.

Nagorski, S.A., Moore, J.N., 1999. Arsenic mobilization in the hyporheic zone of a contaminated stream. Water Resour. Res. 3441–3450.

Navarro, M., Sanchez, M., Lopez, H., Lopez, M., 1993. Arsenic contamination levels in waters, soils, and sludges in southeast Spain. Bull. Environ. Contam. Toxicol. 50, 356–362.

Neubauer, E., Kammer, F. von der, Knorr, K.-H., Peiffer, S., Reichert, M., Hofmann, T., 2013. Colloid-associated export of arsenic in stream water during stormflow events. Chem. Geol. 352, 81–91. doi:10.1016/j.chemgeo.2013.05.017

Nicolli, H., Suriano, J., Peral, M., Ferpozzi, L., Baleani, O., 1989. Groundwater contamination with arsenic and other trace-elements in an area of the Pampa, province of Cordoba, Argentina. Environ. Geol. Water Sci. 14, 3–16.

Nimick, D., Moore, J., Dalby, C., Savka, M., 1998. The fate of geothermal arsenic in the Madison and Missouri Rivers, Mintana and Wyoming. Water Resour. Res. 34, 3051–3067.

Nordstrom, D.K., Alpers, C.N., 1999. Negative pH, efflorescent mineralogy, and consequences for environmental restoration at the Iron Mountain Superfund site, California. Proc. Natl. Acad. Sci. U. S. A. 96, 3455–3462.

Nuzzo, A., Sánchez, A., Fontaine, B., Piccolo, A., 2013. Conformational changes of dissolved humic and fulvic superstructures with progressive iron complexation. J. Geochem. Explor. 129, 1–5. doi:10.1016/j.gexplo.2013.01.010

Olivie-Lauquet, G., Allard, T., Benedetti, M., Muller, J.-P., 1999. Chemical distribution of trivalent iron in riverine material from a tropical ecosystem: a quantitative EPR study. Water Res. 33, 2726–2734.

Olivie-Lauquet, G., Gruau, G., Dia, A., Riou, C., Jaffrezic, A., Henin, O., 2001. Release of trace elements in wetlands: role of seasonal variability. Water Res. 35, 943–952.

Ona-Nguema, G., Morin, G., Juillot, F., Calas, G., Brown, G.E., 2005. EXAFS Analysis of Arsenite Adsorption onto Two-Line Ferrihydrite, Hematite, Goethite, and Lepidocrocite. Environ. Sci. Technol. 39, 9147–9155. doi:10.1021/es050889p

Ona-Nguema, G., Morin, G., Wang, Y., Menguy, N., Juillot, F., Olivi, L., Aquilanti, G., Abdelmoula, M., Ruby, C., Bargar, J.R., Guyot, F., Calas, G., Brown, G.E., 2009. Arsenite sequestration at the surface of nano-Fe(OH)2, ferrous-carbonate hydroxide, and green-rust after bioreduction of arsenic-sorbed lepidocrocite by Shewanella putrefaciens. Geochim. Cosmochim. Acta 73, 1359–1381. doi:10.1016/j.gca.2008.12.005

Onishi, H., Sandell, E.B., 1955. Geochemistry of arsenic. Geochim. Cosmochim. Acta 1–33.

Ou, X., Chen, S., Quan, X., Zhao, H., 2009. Photochemical activity and characterization of the complex of humic acids with iron(III). J. Geochem. Explor. 102, 49–55. doi:10.1016/j.gexplo.2009.02.003

Páez-Espino, D., Tamames, J., de Lorenzo, V., Cánovas, D., 2009. Microbial responses to environmental arsenic. BioMetals 22, 117–130. doi:10.1007/s10534-008-9195-y

Pédrot, M., Boudec, A.L., Davranche, M., Dia, A., Henin, O., 2011. How does organic matter constrain the nature, size and availability of Fe nanoparticles for biological reduction? J. Colloid Interface Sci. 359, 75–85. doi:10.1016/j.jcis.2011.03.067
Pédrot, M., Dia, A., Davranche, M., 2009. Double pH control on humic substance-borne trace elements distribution in soil waters as inferred from ultrafiltration. J. Colloid Interface Sci. 339, 390–403. doi:10.1016/j.jcis.2009.07.046
Piccolo, A., 1996. Humus and Soil Conservation, in: Piccilo, Humic Substances in Terrestrial Ecosystems, Elsevier. ed. Amsterdam.
Pilarski, J., Waller, P., Pickering, W., 1995. Sorption of antimony species by humic acid. Water. Air. Soil Pollut. 84, 51–59.
Pinheiro, J.P., Mota, A.M., Gonçalves, M.L., 1994. Complexation study of humic acids with cadmium(II) and lead(II). Anal. Chim. Acta 284, 525–537.
Plant, J.A., Kinniburgh, D.G., Smedley, P.L., Fordyce, F.M., 2004. Arsenic and Selenium, in: Treatise on Geochemistry. Elsevier, pp. 17–66.
Plumlee, M.L., Smith, K.S., Montour, M.R., Ficklin, W.H., Mosier, E.L., 1999. Chapter 17: Geologic controls on the composition of natural waters and mine waters draining diverse mineraldeposit types, in: Environmental Geochemistry of Mineral Deposits. Part B: Case Studies. pp. 373–432.
Pokrovsky, O.S., Schott, J., Dupré, B., 2005. Trace element fractionation and transport in boreal rivers and soil porewaters of permafrost-dominated basaltic terrain in Central Siberia. Geochim. Cosmochim. Acta 70, 3239–3260.
Polizzotto, M.L., Harvey, C.F., Sutton, S.R., Fendorf, S., 2005. Processes conducive to the release and transport of arsenic into aquifers of Bangladesh. Proc. Natl. Acad. Sci. U. S. A. 102, 18819–18823.
Polizzotto, M.L., Kocar, B.D., Benner, S.G., Sampson, M., Fendorf, S., 2008. Near-surface wetland sediments as a source of arsenic release to ground water in Asia. Nature 454, 505–508. doi:10.1038/nature07093
Ponnamperuma, F.N., 1972. The chemistry of submerged soils. Adv. Agron. 24, 29–96.
Pourret, O., Davranche, M., Gruau, G., Dia, A., 2007. Organic complexation of rare earth elements in natural waters: Evaluating model calculations from ultrafiltration data. Geochim. Cosmochim. Acta 71, 2718–2735. doi:10.1016/j.gca.2007.04.001
Qian, J., Skyllberg, U., Frech, W., Bleam, W.F., Bloom, P.R., Petit, P.E., 2002. Bonding of methyl mercury to reduced sulfur groups in soil and stream organic matter as determined by X-ray absorption spectroscopy and binding affinity studies. Geochim. Cosmochim. Acta 66, 3873–3885.
Rao, B., Simpson, C., Lin, H., Liang, L., Gu, B., 2014. Determination of thiol functional groups on bacteria and natural organic matter in environmental systems. Talanta 119, 240–247. doi:10.1016/j.talanta.2013.11.004
Reddy, K.J., Patrick, W.H., 1977. Effect of redox potential and pH on the uptake of cadmium and lead products in soil. Soil Sci. Soc. Am. J. 54, 67–71.
Reddy, K.R., DeLaune, R.D., 2008. Biogeochemistry of Wetlands: science and applications. CRC Press.
Redman, A.D., Macalady, D.L., Ahmann, D., 2002. Natural Organic Matter Affects Arsenic Speciation and Sorption onto Hematite. Environ. Sci. Technol. 36, 2889–2896. doi:10.1021/es0112801
Rey, N.A., Howarth, O.W., Pereira-Maia, E.C., 2004. Equilibrium characterization of the As(III)–cysteine and the As(III)–glutathione systems in aqueous solution. J. Inorg. Biochem. 98, 1151–1159. doi:10.1016/j.jinorgbio.2004.03.010
Riedel, F.N., Eikmann, T., 1986. Natural occurrence of arsenic and its compounds in soils and rocks. Wiss. Umw. 108–117.
Ritchie, J.D., Perdue, E.M., 2003. Proton-binding study of standard and reference fulvic acids, humic acids, and natural organic matter. Geochim. Cosmochim. Acta 67, 85–96.

Ritter, K., Aiken, G., R., Ranville, J.F., Bauer, M., Macalady, D.L., 2006. Evidence for the Aquatic Binding of Arsenate by Natural Organic Matter−Suspended Fe(III). Environ. Sci. Technol. 40, 5380–5387. doi:10.1021/es0519334

Robinson, B., Outred, H., Brooks, R., Kirkman, J., 1995. The distribution and fate of arsenic in the Waikato River System, North Island, New Zealand. Cehmical Speciat. Bioavailab. 7, 89–96.

Rose, A.L., Waite, T.D., 2003. Kinetics of iron complexation by dissolved natural organic matter in coastal waters. Mar. Chem. 84, 85–103. doi:10.1016/S0304-4203(03)00113-0

Schnitzer, M., Skinner, S.I.M., 1966. Organo-metallic interations in soils: 5. Stability constants of Cu++, Fe++, and Zn++-fulvic acid complexes. Soil Sci. 102, 361–365.

Scudlark, J., Church, T., 1988. The atmospheric deposition of arsenic and association with acid precipitation. Atmos. Environ. 22, 937–943.

Seyler, P., Martin, J., 1990. Distribution of arsenite and total dissolved arsenic in major franch estuaries - dependence on biogeochemical processes and anthropogenic inputs. Mar. Chem. 29, 277–294.

Seyler, P., Martin, J.-M., 1991. Arsenic and selenium in a pristine estuarine system - the KRKA (Yugoslavia). Mar. Chem. 34, 137–151.

Seyler, P., Martin, J.-M., 1989. Biogeochemical precesses affecting arsenic species distribution in a permanently stratified lake. Environ. Sci. Technol. 23, 1258–1263.

Sharma, P., Ofner, J., Kappler, A., 2010. Formation of Binary and Ternary Colloids and Dissolved Complexes of Organic Matter, Fe and As. Environ. Sci. Technol. 44, 4479–4485. doi:10.1021/es100066s

Sharma, P., Rolle, M., Kocar, B., Fendorf, S., Kappler, A., 2011. Influence of Natural Organic Matter on As Transport and Retention. Environ. Sci. Technol. 45, 546–553. doi:10.1021/es1026008

Shen, S., Li, X.-F., Cullen, W.R., Weinfeld, M., Le, X.C., 2013. Arsenic Binding to Proteins. Chem. Rev. 113, 7769–7792. doi:10.1021/cr300015c

Shipley, H.J., Yean, S., Kan, A.T., Tomson, M.B., 2010. A sorption kinetics model for arsenic adsorption to magnetite nanoparticles. Environ. Sci. Pollut. Res. 17, 1053–1062. doi:10.1007/s11356-009-0259-5

Sjöstedt, C., Persson, I., Hesterberg, D., Kleja, D.B., Borg, H., Gustafsson, J.P., 2013. Iron speciation in soft-water lakes and soils as determined by EXAFS spectroscopy and geochemical modelling. Geochim. Cosmochim. Acta 105, 172–186. doi:10.1016/j.gca.2012.11.035

Smedley, P.L., 1996. Arsenic in rural groundwater in Ghana. J. Afr. Earth Sci. 22, 459–470.

Smedley, P.L., Kinniburgh, D.G., 2002. A review of the source, behaviour and distribution of arsenic in natural waters. Appl. Geochem. 17, 517–568.

Smedley, P.L., Nicolli, H.B., Macdonald, D.M.J., Barros, A.J., Tullio, J.O., 2002. Hydrogeochemistry of arsenic and other inorganic constituents in groundwaters from La Pampa, Argentina. Appl. Geochem. 259–284.

Smedley, P.L., Zhang, M., Zhang, G., Luo, Z., 2001. Arsenic and other redox-sensitive elements in groundwater from the Huhhot Basin, Inner Mongolia. Water-Rock Interact. 1-2.

Smith, A.H., Lingas, E., Rahman, M., 2000. Contamination of drinking-water by arsenic in Bangladesh: a publi health emergency. Bull. World Health Organ. 78, 1093–1103.

Sonderegger, J., Ohguchi, T., 1988. Irrigation related arsenic contamination of a thin, alluvial aquifer, Madison River Valley, Montana, USA. Environ. Geol. Water Sci. 11, 153–161.

Sposito, G., 1986. Sorption of trace-metals by humicmaterials in soils and natural-waters. CRC Crit. Rev. Environ. Control 16, 193–229.

Spuches, A.M., Kruszyna, H.G., Rich, A.M., Wilcox, D.E., 2005a. Thermodynamics of the As(III)−Thiol Interaction: Arsenite and Monomethylarsenite Complexes with Glutathione, Dihydrolipoic Acid, and Other Thiol Ligands. Inorg. Chem. 44, 2964–2972. doi:10.1021/ic048694q

Spuches, A.M., Kruszyna, H.G., Rich, A.M., Wilcox, D.E., 2005b. Thermodynamics of the As(III)−Thiol Interaction: Arsenite and Monomethylarsenite Complexes with Glutathione, Dihydrolipoic Acid, and Other Thiol Ligands. Inorg. Chem. 44, 2964–2972. doi:10.1021/ic048694q

Spuches, A.M., Wilcox, D.E., 2008. Monomethylarsenite Competes with Zn^{2+} for Binding Sites in the Glucocorticoid Receptor. J. Am. Chem. Soc. 130, 8148–8149. doi:10.1021/ja802179p

Starý, J., Růzicka, J., 1968. Metal chelate exchange in the organic phase-II. Talanta 15, 505–514.

Sullivan, K., Aller, R., 1996. Diagenetic cycling of arsenic in Amazon shelf sediments. Geochim. Cosmochim. Acta 60, 1465–1477.

Swedlund, P.J., Webster, J.G., 1999. Adorption and Polymerisation of silicic acid on ferrihydrite, and its effect on arsenic adsorption. Water Res. 33, 3413–3422.

Tella, M., Pokrovski, G.S., 2009. Antimony(III) complexing with O-bearing organic ligands in aqueous solution: An X-ray absorption fine structure spectroscopy and solubility study. Geochim. Cosmochim. Acta 73, 268–290. doi:10.1016/j.gca.2008.10.014

Thanabalasingam, P., Pickering, W.F., 1986. Arsenic Sorption by Humic Acids. Environ. Pollut. 12, 233–246.

Theis, T.L., Singer, P.C., 1974. Complexation of iron (II) by organic matter and its effect on iron (II) oxygenation. Environ. Sci. Technol. 8, 569–573.

ThomasArrigo, L.K., Mikutta, C., Byrne, J., Barmettler, K., Kappler, A., Kretzschmar, R., 2014. Iron and Arsenic Speciation and Distribution in Organic Flocs from Streambeds of an Arsenic-Enriched Peatland. Environ. Sci. Technol. 48, 13218–13228. doi:10.1021/es503550g

Thoral, S., Rose, J., Garnier, J.M., Van Geen, A., Refait, P., Traverse, A., Fonda, E., Nahon, D., Bottero, J.Y., 2005. XAS study of iron and arsenic speciation during Fe (II) oxidation in the presence of As (III). Environ. Sci. Technol. 39, 9478–9485.

Thurman, E.M., 1985. Organic Geochemistry of Natural Waters.

Tighe, M., Lockwood, P., Wilson, S., 2005. Adsorption of antimony(v) by floodplain soils, amorphous iron(iii) hydroxide and humic acid. J. Environ. Monit. 7, 1177. doi:10.1039/b508302h

Tipping, E., 1998. Humic ion-binding model VI: an improved description of the interactions of protons and metal ions with humic substances. Aquat. Geochem. 4, 3–47.

Tipping, E., Hurley, M.A., 1992. A unifying model of cation binding by humic substances. Geochim. Cosmochim. Acta 56, 3627–3641.

Tipping, E., Rey-Castro, C., Bryan, S.E., Hamilton-Taylor, J., 2002. Al (III) and Fe (III) binding by humic substances in freshwaters, and implications for trace metal speciation. Geochim. Cosmochim. Acta 66, 3211–3224.

Town, M.R., Powell, H.K., 1993. Ion-selective electrode potentiometric studies on the complexation of copper(II) by soil-derived humic and fulvic acids. Anal. Chim. Acta 279, 221–233.

Tseng, W.P., Chu, H.M., How, S.W., Fong, J.M., Lin, C.S., Yeh, S., 1968. Prevalence of skin cancer in an endemic area of chronic arsenicism in Taiwan. J. Natl. Cancer Inst. 40, 453.

Tufano, K.J., Reyes, C., Saltikov, C.W., Fendorf, S., 2008. Reductive Processes Controlling Arsenic Retention: Revealing the Relative Importance of Iron and Arsenic Reduction. Environ. Sci. Technol. 42, 8283–8289. doi:10.1021/es801059s

Ure, A., Berrow, M., 1982. The elemental constituents of soils. Environmental Chemistry. Royal Society of Chemistry, London.

Van Dijk, H., 1971. Cation binding of humic acids. Geoderma 5, 53–67.

van Schaik, J.W.J., Persson, I., Kleja, D.B., Gustafsson, J.P., 2008. EXAFS Study on the Reactions between Iron and Fulvic Acid in Acid Aqueous Solutions. Environ. Sci. Technol. 42, 2367–2373. doi:10.1021/es072092z

Varsanyi, I., Fodre, Z., Bartha, A., 1991. Arsenic in drinking-water and mortality in the southern grat plain, Hungary. Environ. Geochem. Health 13, 14–22.

Vermeer, A.W.P., Van Riemsdijk, W.H., Koopal, L.K., 1998. Adsorption of humic acid to mineral particles. 1. Specific and electrostatic interactions. Langmuir 14, 2810–2819.
Vilgé-Ritter, A., Rose, J., Masion, A., Bottero, J.-Y., Lainé, J.-M., 1999. Chemistry and structure of aggregates formed with Fe-salts and natural organic matter. Colloids Surf. Physicochem. Eng. Asp. 147, 297–308.
Wang, S., Mulligan, C.N., 2008. Speciation and surface structure of inorganic arsenic in solid phases: A review. Environ. Int. 34, 867–879. doi:10.1016/j.envint.2007.11.005
Wang, S., Mulligan, C.N., 2006. Natural attenuation processes for remediation of arsenic contaminated soils and groundwater. J. Hazard. Mater. 138, 459–470. doi:10.1016/j.jhazmat.2006.09.048
Warwick, P., Inam, E., Evans, N., 2005. Arsenic's Interaction with humic Acid. Environ. Chem. 2, 119–124.
Waslenchuk, D., 1979. Geochemical controls on arsenic concentrations in southeastern united-states rivers. Chem. Geol. 24, 315–325.
Weber, T., Allard, T., Tipping, E., Benedetti, M.F., 2006. Modeling iron binding to organic matter. Environ. Sci. Technol. 40, 7488–7493.
Welch, A.H., Lico, M.S., Hughes, J.L., 1988. Arsenic in ground-water if the Western United States. Ground Water 333–347.
White, D.E., Hem, J.D., Waring, G.A., 1963. Chapter F. Data of Geochemistry, in: Chemical Composition of Sub-Surface Waters. M. Fleischer. US Geol. Surv. Prof. Pap. 440-F.
Widerlund, A., Ingri, J., 1995. Early diagenesis of arsenic in sediments of the Kalix-river estuary, northern Sweden. Chem. Geol. 125, 185–196.
Williams, M., Fordyce, F., Paijitprapapon, A., Charoenchaisri, P., 1996. Arsenic contamination in surface drainage and groundwater in part of the southeast Asian tin belt, Nakhon Si Thammarat Province, southern Thailand. Environ. Geol. 27, 16–33.
Williams, R., n.d. pKa Data Compiled [WWW Document]. URL http://research.chem.psu.edu/brpgroup/pKa_compilation.pdf (accessed 3.25.15).
Wilson, F., Hawkins, D., 1978. Arsenic in streams, stream sediments, and ground-water, fairbanks area, Alaska. Environ. Geol. 2, 195–202.
Wolthoorn, A., Temminghoff, E.J.M., Weng, L., van Riemsdijk, W.H., 2004. Colloid formation in groundwater: effect of phosphate, manganese, silicate and dissolved organic matter on the dynamic heterogeneous oxidation of ferrous iron. Appl. Geochem. 19, 611–622. doi:10.1016/j.apgeochem.2003.08.003
Xia, K., Weesner, F., Bleam, W.F., Bloom, P.R., Skyllberg, U.L., Helmke, P.A., 1998. XANES Studies of Oxidation States of Sulfur in Aquatic and Soil Humic Substances. Soil Sci. Soc. Am. J. 62, 1240–1246.
Yamamoto, M., Nishida, A., Otsuka, K., Komai, T., Fukushima, M., 2010. Evaluation of the binding of iron(II) to humic substances derived from a compost sample by a colorimetric method using ferrozine. Bioresour. Technol. 101, 4456–4460. doi:10.1016/j.biortech.2010.01.050
Zahler, W.L., Cleland, W.W., 1968. A specific and sensitive assay for disulfides. J. Biol. Chem. 243, 716–719.
Zhao, L., Chen, S., Jia, L., Shu, S., Zhu, P., Liu, Y., 2012. Selectivity of arsenite interaction with zinc finger proteins. Metallomics 4, 988. doi:10.1039/c2mt20090b
Zhu, B.J., Tabatabai, M.A., 1995. An alkaline oxidation method for determination of total arsenic and selenium in sewage sludges. J. Environ. Qual. 622–626.